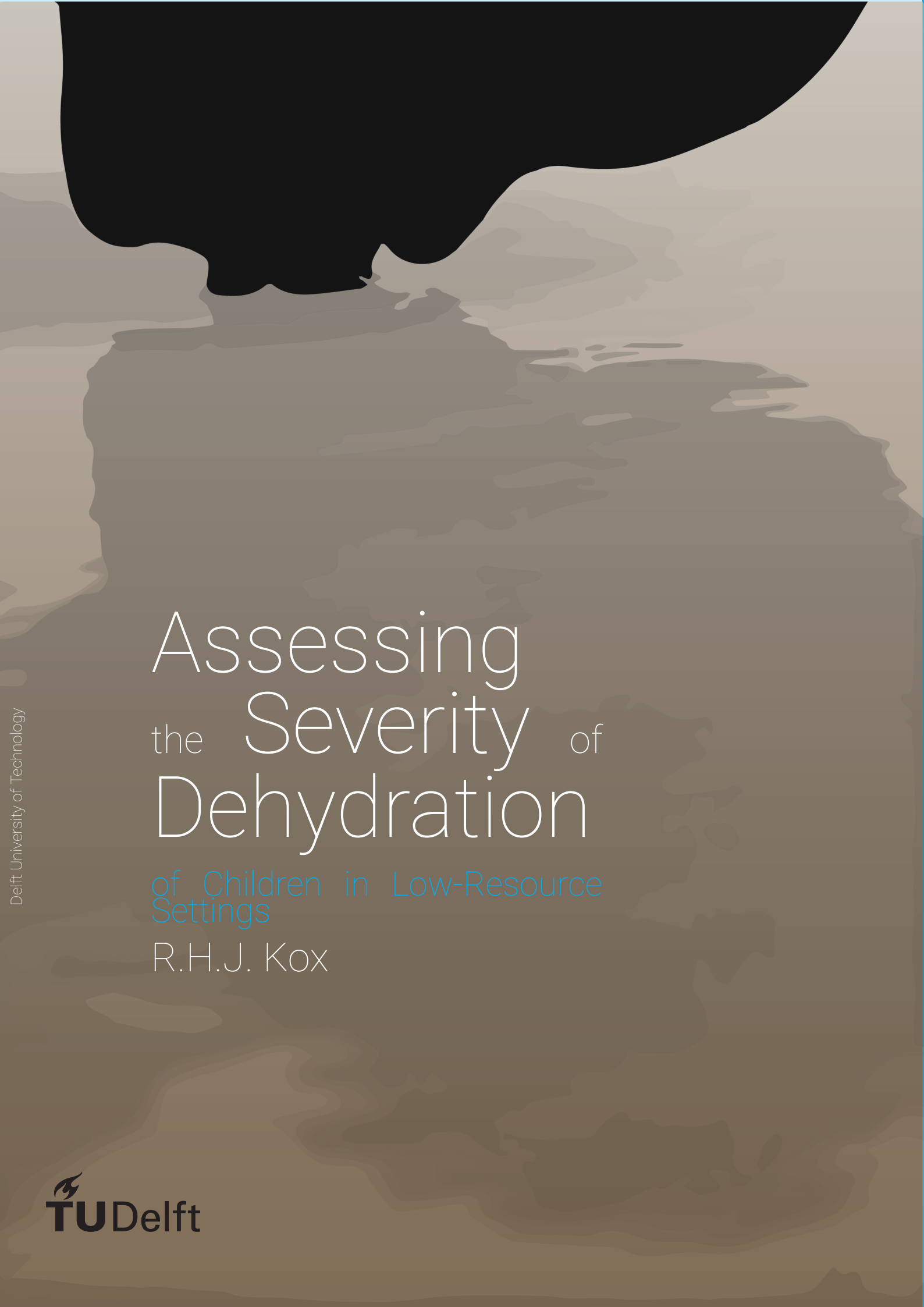

# Assessing the Severity of Dehydration

## of Children in Low-Resource Settings

R.H.J. Kox

Delft University of Technology

TU Delft

# Assessing the Severity of Dehydration

## of Children in Low-Resource Settings

by

R.H.J. Kox

to obtain the degree of Master of Science
at the Delft University of Technology,
to be defended publicly on Monday March 20th, 2017 at 3:30PM.

| | | |
|---|---|---|
| Student number: | 4088492 | |
| Project duration: | March 14, 2016 – March 20, 2017 | |
| Thesis committee: | Prof. dr. J. Dankelman, | TU Delft, supervisor |
| | Ir. R.M. Oosting, | TU Delft |
| | Dr. ir. W.L. Simonse, | TU Delft |
| | Dr. ir. P. Dadlani, | Philips Research, supervisor |

*This thesis is confidential and cannot be made public until March 20, 2022.*

An electronic version of this thesis is available at `http://repository.tudelft.nl/`.

TU Delft PHILIPS

*Due to the confidential nature of some of its contents, the appendix has been removed from this version of the thesis report.*

# Preface

Six and a half years feels like such a short time. But when I look back at all the lessons and experiences that I encountered within that time as a student, I find it hard to believe how much I've learned within that time. I started out with a bachelor in Industrial Design Engineering, determined to become a creative engineer, but shortly after finishing the bachelor programme I wanted to put my focus on more meaningful issues, such as healthcare. Biomedical Engineering was the perfect master programme for me, as it combined elements of Industrial Design Engineering, healthcare related topics, and technically challenging issues within one programme. I immediately felt at home.

During the master programme I learned that I wanted to take one more step further in focussing on meaningful issues, when I got the chance to experience the daily goings in an African hospital in Ghana. I saw the shortcomings that could be prevented by dedicated medical equipment for hospitals in a developing world setting. Because of this, I became highly motivated to use this experience together with my knowledge as a Biomedical Engineering student to solve these specific issues for healthcare in developing countries.

As a result, shortly after coming back to the Netherlands I was given the chance to put this drive into action at Philips Research, where I since than did two successive internships. The document in front of you is the reporting of the last of those two internships, where I was provided the chance to graduate on a very urgent topic, *dehydration*, which turned out to be among the main health risks among children in developing countries.

I am thankful to Philips Research for giving me the chance and the means to conduct this project. I want to thank every individual at Philips (in Eindhoven and in Nairobi) who supported me with their expertise on specific technical issues, and in particular I want to thank Pavan Dadlani for his guidance as my supervisor at Philips. In addition, I want thank Jenny Dankelman for being my supervisor at the TU Delft, as she was always available for feedback on my general proceedings.

*R.H.J. Kox*
*Eindhoven, February 2017*

# Summary


### Introduction

Diarrhoea is the second major cause of child mortality global, being responsible for an estimated 600000 deaths of children under the age of five per year. 80% of these deaths happen in Sub-Saharan Africa and South-East Asia. Among the majors risks with persistent diarrhoea is severe dehydration, which in fact is the main cause of death when talking about diarrhoea related mortality. One identified problem that may be causing this large rate of mortality is that currently there are no reliable ways of assessing the severity of dehydration, which leads to ineffective treatment of the condition. Current methods of assessing dehydration involves manual observations, such as the *capillary refill time* test and the *skin turgor* test. The main problems with these tests that cause inaccuracy are *subjectivity*, influence from *external factors* and lack of appropriate *training* of the health workers.

Health workers and clinicians working in rural settings in developing countries have identified the need for innovations regarding diagnosis of dehydration in children. The problems of subjectivity, external factors and lack of training could be solved with a diagnostic device, that could objectively measure and digitally analyse bio-markers which have been identified as diagnostic variables for dehydration. In this assignment the aim is to identify and validate a novel technological method for assessing the severity of dehydration in young patients. To achieve this, first most appropriate diagnostic variables and the most appropriate corresponding technological principles for measuring them have to be determined.

### Literature study

In order to make a well-substantiated choice for which *diagnostic variables* and *technological principles* would be most suitable for further investigation during this assignment, a clear overview of current standards and developments regarding these subjects has to be compiled first. This overview has been based on a literature research. After conducting a multi-criteria analysis it was concluded that *photoplethysmographic capillary refill time measurements* (PPG-CRT) and *digital assessment methods for skin turgor* (ST) would have the highest potential of becoming useful methods for assessing total body dehydration. This conclusion is based on (among other things) diagnostic performance of the manual tests, as well as anticipated cost-effectiveness of these methods and other user related requirements. It is therefore chosen to investigate these methods in further detail for the rest of the duration of this research.

### Validation Experiment

An in-depth desk research into the physiological and technological details regarding PPG-CRT and ST has been conducted. It was found how dehydration affects these variables, and how they are affected by other external factors such as for instance ambient- and body core temperature. Based on the learnings it was chosen to perform a validation experiment to test the correlation between the severity dehydration and these variables of interest. To measure capillary refill time, a prototype using green light photoplethysmography was built. To measure skin turgor, the Cutometer device was used since it is considered to standard in measuring bio-mechanical properties of the skin.

During this experiment subjects were stimulated to dehydrate up to a safe level, while measurements where made using the equipment as described above. Dehydration was stimulated by physical exercises in a warm room, while rehydration was prohibited. Also any external factors that might influence the measurements were monitored. The level of dehydration was directly measured by monitoring the loss of body mass of each subject during each run. Loss of body mass is considered the gold standard for monitoring dehydration, if the baseline (well-hydrated) body mass is known.

The collected data were processed and analysed in Matlab. A regression analysis was chosen as the method for determining how well PPG-CRT and ST would be able to estimate the level of dehydration. The *adjusted coefficient of determination* ($\bar{R}^2$), would in the end serve as the main differentiator, since this value would for each parameter indicate the variation in levels of dehydration accounted for by the dependent variable (being ST and PPG-CRT).

After processing and analysing all the data it was concluded that, apart from a few specific samples, no significant relations were found between dehydration and the dependent variables. It has however also been

found that this may be caused by considerable limitations to the experiment, regarding both the protocol and the equipment used. Most importantly, the levels of dehydration that were allowed/achieved in the subjects were considered to be too low to have significant effect on the parameters of interest. Also, some considerable limitations to the equipment that was used have been identified, especially with the PPG prototype for measuring CRT. This could have had a major contribution to the unexplainable variability in the data.

It was concluded that more extensive experiments need to be conducted with an improved set of prototypes on subjects that are more severely dehydrated. A recommendation is to build a set of high-quality functional prototypes, and perform a study in the field (in developing countries where dehydration is highly prevalent among young children) to collect data which than should be analysed for diagnostic performance.

### Prototype redesign

Based on the identified limitations of the validation experiment, it was decided that the first next step should be to build an improved prototype which could be used in future studies. It was chosen to focus on an improved version of the CRT-PPG prototype. This prototype would feature a fully automated CRT measurement protocol, integrated skin-temperature sensors, an improved signal-to-noise ratio, a higher and more stable sampling rate, and an integrated data pre-processing protocol.

The prototype was validated by performing a small experiment. Since it already found that the previous dehydration experiment would not lead to significant results, a different approach was chosen. It was already established that ambient temperature has a significant negatively proportional effect on CRT, meaning that CRT increases when ambient temperature decreases.

The results indicate a significant effect of different ambient temperatures on CRT ($F(1,35) = 6.15$, $p < .05$), and it can clearly be observed in the data that CRT indeed increases when temperature is low.

### Conclusions & Recommendations

despite having conducted an experiment that involved dehydration of subjects, no significant relations between the measured diagnostic variables and the degree of dehydration have yet been demonstrated. It is believed that this experiment was not representative to the situation of severely dehydrated children. Together with the limitations regarding the used equipment, the results of this experiment should be interpreted with care.

Based on the learnings, an improved PPG-CRT prototype has been developed, which has been experimentally validated. Having analysed the results, it is demonstrated that this prototype is indeed able to detect expected variations in CRT, and would therefore be suitable as a starting point for future versions of this prototype.

In the end it is recommended to build a set of high-quality prototypes next to this PPG-CRT prototype. Each prototype should be able to measure a different diagnostic variable, such as skin-turgor or more direct ways of measuring total body water content. A data-collection study in the areas where child-dehydration is frequent should be conducted, where these prototypes are tested in parallel to the usual activities of the health workers. The data collected by the devices should be analysed retrospectively for potential predictive models, which could be used as diagnostic models for future devices.

# Contents

# 1 Introduction

*The full content of this chapter (with exception of section 1.1.4) is directly based on the literature study report regarding this graduation assignment [54], which has already been submitted, assessed and graded.*

There can be no debate that water is vital in the support of life on earth. All known forms of life on earth rely on this substance. It facilitates many vital mechanisms in the human body, such as transport of gasses and nutrients and wastes, temperature regulation, lubrication of joints and it helps keeping vital chemical processes in the body going. Moreover, the total body water in humans is more than 73% in infants, and drops to about 45% in old age [59]. Despite the massive amounts of water that we carry around in our bodies, slight changes in the fluid balance of our body can have severe consequences, such as hypovolemic shock and (subsequently) death.

This assignment is granted by Philips Research Eindhoven and focusses on the detection of dehydration in children, who are located in rural areas in developing countries, from now on labelled as low-resource settings. The background for this assignment originates from conversations with *Community Health Workers* (CHW's), which are members of a community in low-resource settings with very minimal training in routine health check-ups of their fellow community members. Their main task is to diagnose any main health issues within their patients, provide some basic treatment up to a certain level and triage for further treatment from medical professionals whenever needed. They indicated that dehydration is very prevalent in their communities, but detecting dehydration can be very problematic, as they at this moment perform very unreliable methods manually to assess the severity of dehydration. This triggered the scientists at Philips Research who are working on *diagnostics for low-resource settings* to further investigate the problem of *dehydration in low-resource settings*, in particular the diagnostic part of it. It resulted in this graduation assignment.

Figure 1.1: A CHW in action. source:
`http://www.healthenvoy.org/new-financing-task-team-established-for-community-health-workers/`

## 1.1. Problem analysis: Diarrhoeal Disease

First a clear general definition of dehydration has to be established when analysing the problem. Dehydration occurs when the water output (along with any solutes) of the body is exceeded by the water input. It can have several causes, like haemorrhage, severe burns, prolonged vomiting or diarrhoea, intense sweating, lack of water intake, diuretic drug abuse or endocrine disturbances. [59]. In the Netherlands dehydration is generally regarded as a problem most prevalent for elderly or athletes. Yet, after a small desk research it was found that children under the age of five suffering from *gastroenteritis* (from now on labelled as *diarrhoea*), as a group actually seem have the highest numbers of mortality due to dehydration, as can be seen in figure 1.2. This observation will be further discussed in this section.

### 1.1.1. Burden

It has been established that one of the major causes of dehydration due to severe fluid loss is diarrhoea. Diarrhoea is defined as the passage of three or more loose or liquid stools per day. Diarrhoeal episodes result loss of water and electrolytes through liquid stools, vomit, sweat, urine and breathing, which causes dehydration if these electrolytes and water are not replaced rapidly. Most people who die from diarrhoea, actually die from severe dehydration. [13]

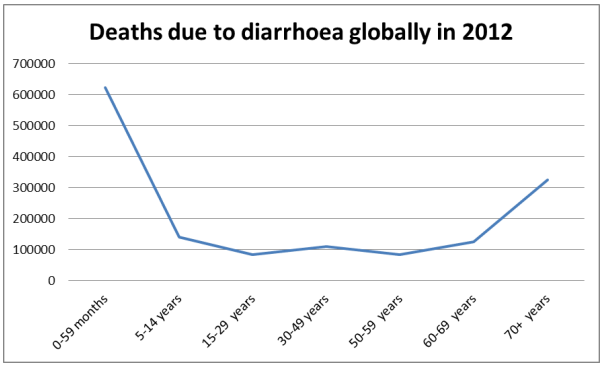


Figure 1.2: Global deaths due to diarrhoea in 2012, per age group. Data from WHO [12].

Infectious diarrhoea is usually caused by infection of the intestinal tract, which is caused by either bacteria, viruses or parasites. Most of these pathogens use similar mode of transmission: from stool to mouth, although there are differences in route and the amount of organisms needed to cause disease. It can for instance be spread directly from person-to-person, contaminated water and through foods. Hygiene and sanitation are thus key in preventing diarrhoea. Malnutrition (not getting enough-, or the right sort of nutrients) causes a vicious circle with diarrhoea: diarrhoea worsens malnutrition, while malnutrition makes the patient more vulnerable to diarrhoea. [76]

On a global scale there are yearly almost 1.7 billion cases of diarrhoeal disease [13]. Although in high-quality healthcare systems diarrhoea is considered nothing else than an unpleasant inconvenience (due to sufficient hygiene and proper management), in many parts of the world this disease can be life threatening. Especially children under the age of 5 are more at risk of dying from diarrhoeal disease, because water constitutes a greater proportion of their body weight and because they need more water due to their higher metabolic rates [76]. In 2012, nearly 1 500 000 people died of diarrhoea globally, as can be derived from figure 1.2. Among these deaths were an estimated 622 165 children under the age of 5. Also among these people were 452 059 elderly over the age of 60 (326 499 were 70+)[12]. Yet, as the number of deaths in the group of children under the age of five is significantly higher, and for the sake of focus, this group has been chosen as the *subject for this assignment.* In addition, WHO calls diarrhoea the second leading cause of death in children under 5 years old (after pneumonia), and a leading cause of malnutrition [13]. 80% of all these child deaths occur in Africa and South Asia, with India far on top of the list of countries with most child deaths [76]. This also substantiates the already predetermined choice to put focus on low-resource settings.

However, over the last decades, mortality and absolute number of deaths due to diarrhoea have dropped significantly (more than half since 2000) [12], as can be seen in figures 1.3a and 1.3b. This might be due to the Millennium Development Goals of the United Nations of reducing child mortality, where several actions to better prevent and treat dehydration have been set in place. It can also bee seen in figures 1.3c and 1.3d, that the percentage of deaths due to diarrhoea per age-group in relation to the total amount of deaths in that age-group has declined somewhat over the last years.

Despite the efforts that have been made in managing diarrhoea in this context, and the fact that mortality is already dropping, diarrhoea remains to be a substantial cause of mortality among children in low resource settings. When looking at the data, it also suggests that even with this trend of dropping mortality rates, it would still take many years for the management of this disease to be equally adequate in low-resource settings compared to more advanced healthcare systems. It suggests that in order to reduce mortality further, new approaches in improving management of diarrhoea need to be implemented.

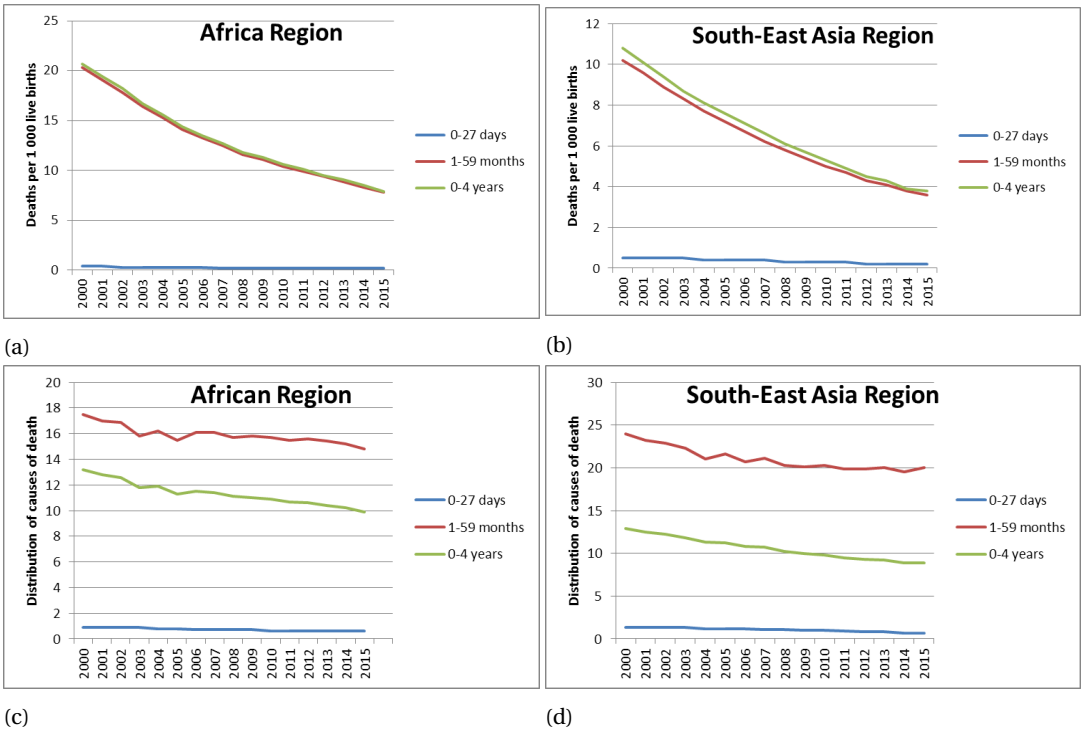


Figure 1.3: Figures 1.3a and 1.3b show yearly recorded diarrhoea related death rates in WHO regions Africa and South-East Asia (respectively) for different age groups. Simularly, figures 1.3c and 1.3d show the recorded percentage of deaths due to diarrhoea with respect to the total amount of deaths. Data from WHO [12].

### 1.1.2. Dehydration

As explained in section 1.1.1, dehydration is the most severe risk with diarrhoea, and is therefore accountable for 80% of all deaths related to diarrhoea. Before going straight into the ways diarrhoea and dehydration are managed currently in low-resource settings, this sections sets-out a concise explanation of dehydration of the human body from a physiological point of view.

Total body water (TBW) can be divided into two main compartments: *intracellular fluid* (ICF, $\frac{5}{8}$ of TBW) and *extracellular fluid* (ECF, $\frac{3}{8}$ of TBW). ECF can be subdivided into *interstitial fluid* (IF, 80% of ECF which accounts mostly for fluid in the microscopic spaces between tissue cells) and *plasma* (20% of ECF, fluid portion of blood) [59]. See figure 1.4.

Balance between these fluid compartments is mainly regulated by *osmosis* and *hydrostatic pressure*. Osmosis is the movement of water through a semi-permeable membrane up its osmotic gradient (from low-osmolality to high osmolality). Osmolality is defined by the amount of *electrolytes* (typically inorganic salts that dissociate into at least two ions when dissolved) in *osmoles* in one solution. A measure of indicating the difference in osmolality between two solutes is called *tonicity*. Non-electrolytes are solutes that do not dissociate, causing them to have much less osmotic power than electrolytes. Electrolytes therefore have the greatest ability to cause fluid shifts. Osmolalities of all fluids in the body are equal (except for the first few minutes after a sudden change occurs in one of the fluids), because water moves freely between compartments. So ECF solute concentration directly deter-

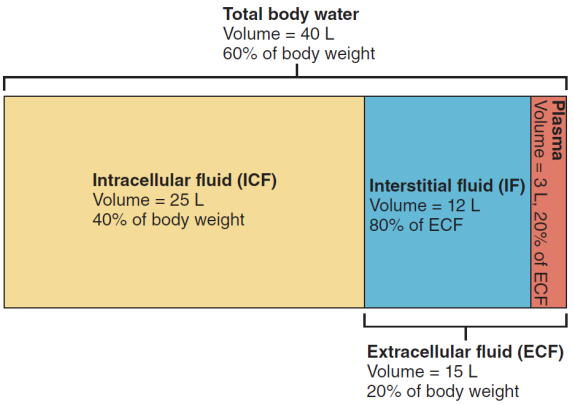


Figure 1.4: The major fluid compartments of the human body, based on a 70-kg male. [59]

mines ICF volume. The salts that play a central role in fluid- and electrolyte balance (and overall body homeostasis) are salts containing *sodium* ($Na^+$). Hydrostatic pressure also cause fluid shifts, for instance the diffusion of water from the blood across capillary walls into IF because of blood pressure/ capillary permeability [59].

In a healthy (well hydrated) human, water intake is equal in volume to water output. Water intake varies widely, but is typically about 2500ml a day in adults. 60% of all body intake is through beverages, 30% through foods and 10% through wat is produced in cellular metabolism. Water output is 60% urine, 28% goes through skin and lungs (also known as *insensible loss*), 8% through sweat and 4% through faeces (see figure 1.5). Water intake is regulated by the *thirst mechanism*, which is governed by the hypothalamic thirst centre. The last one is activated by various stimuli, such as: hypothalamic osmo-receptors, dry mouth and decreased blood volume/pressure. Thirst is quenched instantly when we drink water, making this mechanism very effective. In some situations it may be unreliable, for instance premature thirst quenching during athletic events, or confused people that don't recognise/heed the thirst signal [59].

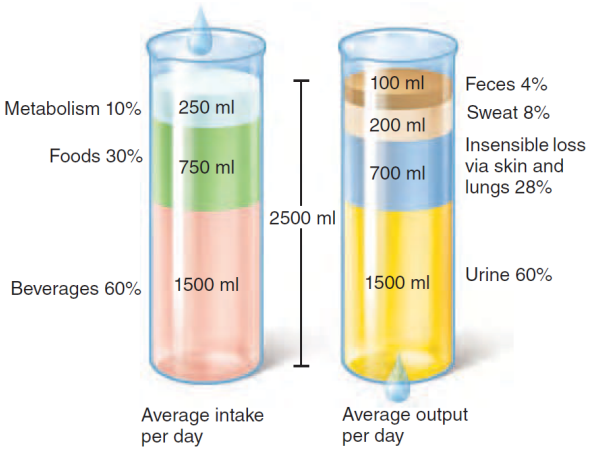


Figure 1.5: Major sources of water intake and output [59]

Fluid output consists partly of *obligatory water loss* (including insensible water loss, a daily minimum of 500ml in urine and water in faeces), and partly of urine loss that depends of fluid intake, diet and water loss via other avenues. Antidiuretic hormone (ADH, released from the posterior pituitary when triggered by hypothalamic osmo-receptors, baroreceptors and indirectly the renin-angiotensin-aldosterone mechanism when they sense a large decrease in blood pressure) controls the level of which plasma is drained out of the blood into the blather. Rising ADH levels results in more concentrated and a decreased output of urine [59].

It was already determined that *dehydration* occurs when water output is exceeded by water input. The first signs of (mild) dehydration include thirst, sticky oral mucosa, dry skin and decreased urine output. Prolonged (more severe) dehydration could lead to significant weight loss, fever and mental confusion. Decreased plasma volume is another potential consequence, and may lead to inadequate blood volume to maintain circulation, resulting in hypovolemic shock. This means that the heart becomes unable to pump enough blood around due to lack of blood volume, which may have fatal consequences.

Dehydration is often not just the loss of water, but the solutes (dissolved electrolytes and non-electrolytes) can also be lost, which than affects the tonicity of fluids within the body. If water and solutes are lost together without affecting tonicity of fluids inside the body (as in haemorrhage or in most cases of gastroenteritis), it is called *isotonic* (or *isonatremic*) dehydration. In this case the fluids and solutes lost have the same relative ratio as the fluids and salts than remain inside the body. Dehydraton is called *hyponatremic* or *hypotonic* if the relative proportion of lost solutes is bigger, causing fluids inside the body to decrease in osmolarity. If only water is lost (or more water than solutes, as in profuse sweating) than it is called *hypernatremic*, *hypertonic* or *hyperosmolar* (due to either increased sodium or glucose) [75]. In the case of hypernatremic dehydration, water moves osmotically into the ECF to equalize osmolality [59].

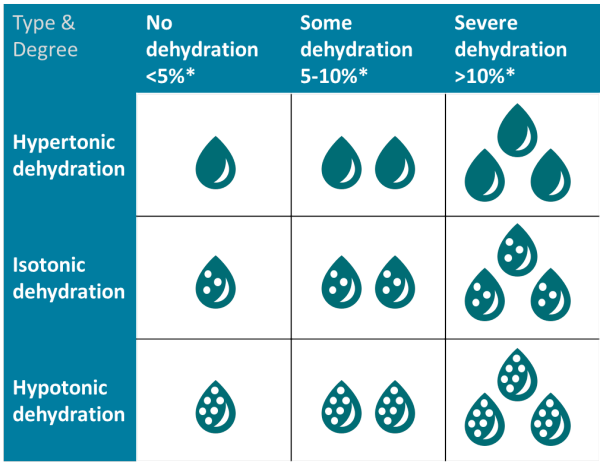


Figure 1.6: Types and degrees of dehydration, amount of droplets stand for lost amount of fluid, and amount of white dots stand for relative lost amount of electrolytes. *Percentage of body weight lost

The World Health Organisation (WHO) has defined three degrees of dehydration: *no dehydration*, *some dehydration* and *severe dehydration* [64]. The degree of dehydration is a measure of the amount of water lost

in terms of mass, relative to total body mass in percentages. See table 1.1.

| Assessment | Fluid deficit as % of body weight | Fluid deficit in ml/kg body weight |
|---|---|---|
| No dehydration | <5% | <50 ml/kg |
| Some dehydration | 5-10% | 50-100 ml/kg |
| Severe dehydration | >10% | >100 ml/kg |

Table 1.1: Degrees of dehydration as formulated by the WHO [64].

In summary, dehydration can thus be classified by type (tonicity, relative amount of electrolytes lost) and degree (amount of water lost). This is visualized in figure 1.6.

### 1.1.3. Current standards in management of diarrhoeal disease

Since dehydration is the most severe risk when a child suffers from diarrhoea, the *first priority* for the CHW is to manage the potential dehydration, before treating the diarrhoea itself. If a child is suspected by the CHW of suffering from dehydration, proper diagnostic tests should be done to assess the degree of dehydration. Accurately assessing the degree of dehydration is an important step in management of dehydration, since the outcome of the diagnosis be key in determining the most appropriate treatment plan.

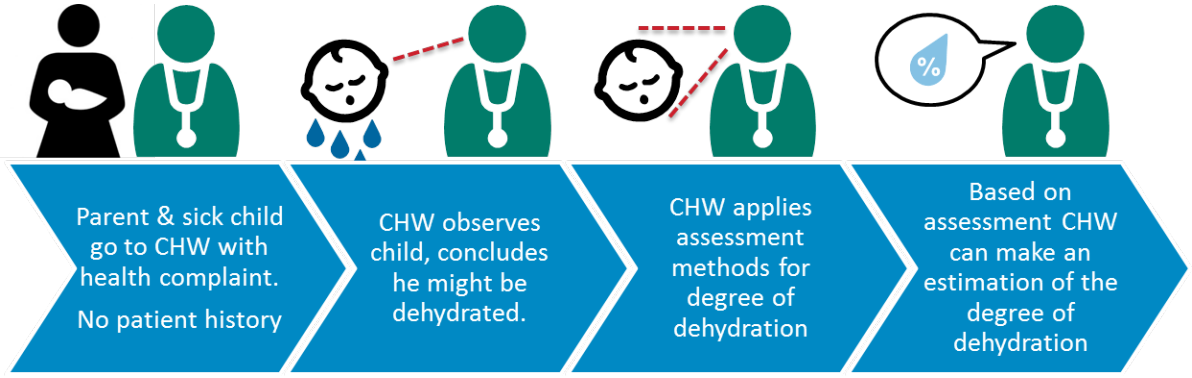


Figure 1.7: Dehydration assessment, the first step to undertake by the CHW when a child is presenting diarrhoea or other signs of potential dehydration.

Patients with *no signs of dehydration* (but who are still at risk) will be educated how to prevent dehydration with a home-therapy plan. With children who are at risk, the parents will be taught how to prevent dehydration at home by giving the child more fluid than usual and to continue feeding the child accordingly.

Patients with *some dehydration* should be treated with Oral Rehydration Therapy (ORT), by drinking an Oral Rehydration Salts (ORS) solution [64]. ORS is very cheap and can be bought in powder-form in little sachets, containing basically carbohydrates, sodium and potassium. When solved in drinking-water, it can be consumed to restore both fluid and electrolyte balance in the body. Patients who are also malnourished next to dehydrated often have different electrolyte imbalances than dehydrated patients without malnutrition. For them, to prevent cardiac failure due to inbalanced sodium to potassium ratio, another kind of ORS is available called *Rehydration Solution for Malnutrition* (ReSoMal), which is higher in potassium and lower in sodium than ORS [20][27]. If dehydration is caused by prolonged diarrhoea, there is an additional treatment available next to ORS. *Zinc supplementation* can be used to reduce severity of the diarrhoea, duration and risk of subsequent infections for 2-3 months [52]. Zinc supplementation however is not a direct treatment for dehydration itself.

Whenever the patient is *severely dehydrated*, rapid intravenous rehydration should be the preferred treatment. Intravenous rehydration should preferably be done with Ringer's Lactate Solution or normal (isotonic) saline (NaCl solution) [64]. ORS should be administered (via nasogastric tube if the patient refuses to drink) until the IV drip is running [27]. Rehydration using intravenous fluids is more expensive compared to ORS, as IV-fluids are more expensive and sparse in low-resource settings, and as this treatment requires close monitoring of health-workers and cannot be administered by the parent alone (such as with ORS). In practice it

means that a patient needs to be sent to a nearby health-care facility as soon as possible, which then should be able to provide the right resources and the right people to correctly rehydrate the patient.

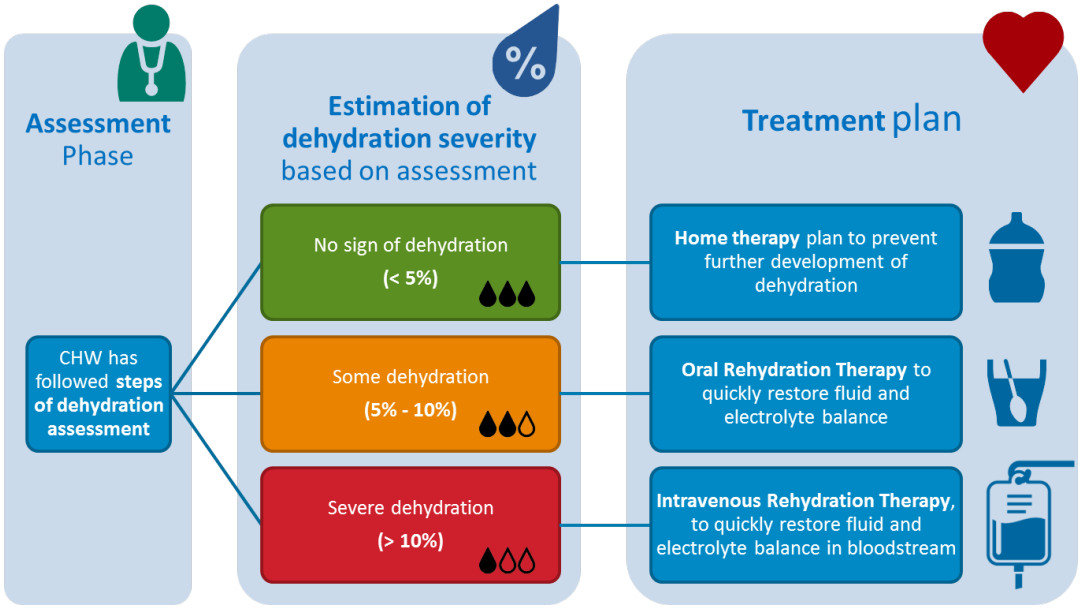


Figure 1.8: A visual representation of the outcomes of the assessment (figure 1.7) and corresponding treatment plans.

| **Diagnosis** | *No dehydration* | *Some dehydration* | *Severe dehydration* |
|---|---|---|---|
| **Treatment** | Home therapy plan to prevent the development of dehydration | Oral Rehydration Therapy | Intravenous Rehydration |
| **Cost** | **0**<br>No associated cost. No extra workload or treatment, just a "normal" routine of hydration | **+**<br>US$ 0.06 - 0.10*, treatment requires little workload from health worker | **+++**<br>Ringer's Lactate Solution or Saline are a lot more expensive, more invasive, and treatment requires close monitoring by well-trained healthcare worker. |

** Price per sachet good for 1 litre of solution. Based on WHO-formula and including shipping/import cost [79].*

Table 1.2: Indication of cost and workload for the CHW, per treatment plan

Providing the right treatment plan that corresponds to the patient's degree of dehydration is considered very important, since choosing the wrong treatment can either lead to over-utilisation of precious healthcare resources or harm to the patient. Providing intravenous fluids (IVF) to patients without severe dehydration is not only more expensive and human-resource intensive, but can also lead to seizures and death [58], although the scenario of overhydrating a patient is considered very unlikely (confirmed in interviews with clinicians and health-workers, see appendices A and B). On the other hand, providing a severely dehydrated patient with merely ORS could result in under-hydration and therefore death, although in most cases of severe dehydration the patient will refuse to drink at all [64]. Providing the correct diagnostic outcome is quite difficult. Even in high-quality healthcare systems about 40-80% of all diagnosed dehydration cases are not supported by laboratory data (which is, clinically, considered to be the most reliable diagnostic tool), due to varying criteria for diagnosis of dehydration, poor education about dehydration among many physicians and fiscal incentives to positively diagnose dehydration [75].

The assessment of dehydration in low-resource settings can be performed using several methods, often without using any devices or diagnostic tools. None of these manual methods have a diagnostic performance

that is good enough as individual tests. Therefore, a few diagnostic scales have been developed for the assessment of dehydration: the *WHO scale*, *Gorelick scale*, and *Clinical Dehydration Scale*. These scales consist of a combination of diagnostic tests, and a standardized method for interpreting the outcomes of these combined tests. Obviously this is meant to improve the cumulative diagnostic performance, although several studies cast doubt regarding the reliability of these scales.

The *WHO scale*, considered as the most accepted scale, has been found to actually be an unreliable clinical diagnostic method [50]. Moreover, its validation is largely based on expert opinion rather than being empirically derived and validated [58]. It even has recently been found that none of the current three popular scales are accurate in a developing world setting, and it is suggested that new scales or tools need to be developed specifically for resource-limited settings [66]. Accurate hydration status assessment in low/middle income settings is even more critical compared to other settings, since patients could travel for several hours before reaching a hospital and IV-fluids and hospital beds are often scarce. In these settings western models may also be less effective due to different disease patterns, patients presenting in a later stage of the disease and lack of specialized training of healthcare providers [66]. It is also shown that reliability of these models in predicting *severe* dehydration is suboptimal [66], yet severe dehydration is most critical to diagnose in these settings.

Adam C Levine et al. recently developed two diagnostic models (DHAKA Dehydration Tree and DHAKA Dehydration Score), focussing on resource-limited settings, that he derived empirically and validated internally and which seem to be more accurate than other models. Yet, external validation still needs to be executed in order to implement these models [58].

In the next paragraphs each of the three mentioned scales will be explained in terms of how they should be executed, and where problems with these scales arise.

**WHO Scale [64]** This scale is based on the detection and interpretation of clinical diagnostic variables by the observer. The variables to be observed are explained in table 1.3. The observations are scored which should lead to a decision. Notes to this method are that the difference should be seen between lethargic and sleepy. Also in some children *sunken eyes* can be their normal appearance, so this should be consulted with the parent. It is also found that assessing skin turgor (elasticity of the skin, measured with the *skin pinch test*) can be unreliable in children who are obese, malnourished (with marasmus or kwashiorkor, due to the loss of subcutaneous tissue) or when they have an oedema.

| | **A** | **B** | **C** |
|---|---|---|---|
| **Look at**: Condition | Well, alert | Restless, irritable | Lethargic or unconscious |
| Eyes | Normal | Sunken | Sunken |
| Thirst | Drinks normally, not thirsty | Thirsty, drinks eagerly | Drinks poorly, or not able to drink |
| **Feel**: Skin pinch | Goes back quickly | Goes back slowly | Goes back very slowly |
| **Decide**: | The patient has **no signs of dehydration** | if the patien has two or more signs in column **B**, there is **some dehydration** | If the patients has two or more signs in **C**, there is **Severe dehydration** |
| | The treatment plan is based on the degree of dehydration in the *"decide"* row. | | |

Table 1.3: Assessment for dehydration according to the *WHO scale* [64].

**Gorelick Scale [43][66]** This scale is also based on detecting clinical diagnostic variables, which are all stated in table 1.4. The third column stated how a variable would look like in the case of dehydration. The table can be looked at in 2 ways: you can either use all 10 signs for diagnosis, or only the top 4 (italic). The

first way is called the *10 point scale*, and requires to observe the patient for all 10 signs. If 3 or more signs are identified, the child suffers from some dehydration. If 7 or more signs are found, the child has severe dehydration. The second way, or the *4 point scale*, uses only the top 4 variables. If 2 of these signs are found, it means that the child has some dehydration. If 3 or 4 are found, the child is severely dehydrated.

| Characteristic | No or minimal dehydration | Moderate to severe dehydration |
|---|---|---|
| ***General appearance*** | *Alert* | *Restless, lethargic, unconscious* |
| ***Capillary refill time*** | *Normal* | *Prolonged or minima*l |
| ***Tears*** | *Present* | *Absent* |
| ***Mucous membranes*** | *Moist* | *Dry, very dry* |
| **Eyes** | Normal | Sunken; deeply sunken |
| **Breathing** | Present | Deep; deep and rapid |
| **Quality of pulses** | Normal | Thready; weak or impalpable |
| **Skin elasticity** | Instant recoil | Recoil slowly; recoil >2 s |
| **Heart rate** | Normal | Tachycardia |
| **Urine output** | Normal | Reduced; not passed in many hours |

Table 1.4: Assessment for dehydration according to the *Gorelick scale* [66][43].

**Clinical Dehydration Scale (CDS) [40][66][41]** The CDS is the only scale that has been prospectively validated against the currently accepted golden standard of percent weight change with dehydration in high-income countries (high quality healthcare systems), yet it still seems to be unreliable in resource limited settings [66]. Also the CDS is based on observation of diagnostic variables which could suggest dehydration, as shown in table 1.5. Note that the CDS handles another scale of dehydration degrees than stated in table 1.1, consisting of *no dehydration* (fluid deficit < 3% of bodyweight), *some dehydration* (3% ≤ fluid deficit < 6% of body weight), or *moderate/severe dehydration* (fluid deficit ≥ 6% of bodyweight). The scoring system based on observing all 4 signs, and determining their appearance as stated in table 1.5. Each appearance has its own score, which can be seen in the top row. After observing all the signs, the score is added up. a total score of 0 means *no dehydration*, a total score of 1-4 means *some dehydration*, and a total score of 5-8 means *moderate/severe dehydration*. Also note that the target group for the CDS are children of 1-36 months.

| Characteristic | 0 | 1 | 2 |
|---|---|---|---|
| **General appearance** | Normal | thirsty, restless, or lethargic but irritable when touched | Drowsy, limp, cold, sweaty and/or comatose |
| **Eyes** | Normal | Slightly sunken | Very sunken |
| **Mucous membranes (tongue)** | Moist | “Sticky” | Dry |
| **Tears** | Tears | Decreased tears | Absent tears |

Table 1.5: Assessment for dehydration according to the *CDS Scale* [40].

In conclusion it can be established that none of the mentioned scales is sufficiently reliable for diagnosing the degree of dehydration, especially in low-resource settings. The main identified problems that cause the low diagnostic performance are *external influences* on the assessment outcome, *subjectivity* of the methods used [66], and the lack of specialized *training* of the CHW. In chapter 2, a comprehensive investigation in all known clinical diagnostic methods and technologies will be performed. This will provide quantitative insights into the real diagnostic performance per test.

*Side note*: Hypertonic dehydration is known to account for 10% to 20% of all paediatric cases of dehydration due to diarrhoea, hypotonic dehydration 10% to 15%, and isotonic dehydration for most cases [48]. Besides the fact that most cases of dehydration due to diarrhoea are isotonic, WHO stated that testing the levels of serum electrolytes (body fluid osmolality) rarely changes management of children with diarrhoea in practice[64], except of course when this variable is used to assess the *degree* of dehydration directly. The

reason is that these values are often misinterpreted which could lead to inappropriate treatment. Knowing the dehydration status should be enough to determine the treatment plan. So for example, whether a patient suffers from for instance *hypertonic dehydration* or *hypotonic dehydration* does usually not make a difference in treatment when the degrees of dehydration are the same, as volume replenishment is much more critical compared to precisely replenishing the exact amount of lost electrolytes.

### 1.1.4. Learnings from interviews with local health workers around Nairobi, Kenya

A survey study has been performed by a team member who is stationed at Philips Research in Nairobi, with input for relevant questions from the team in Eindhoven (see appendix A). The main goal was to get a better grip on the real problems regarding dehydration in low-resource settings, and to validate the overall problem analysis, which was initially based on desk research.

The most important findings from these interviews will be summarized below:

- Most of the interviewed individuals confirm that there currently are problems with the assessment of the degree of dehydration, in terms of accuracy of current standard tests.
- The main causes of death according to the clinician is that severe dehydration is often identified too late. This can have two causes: The parent or guardian of the child could be too late with visiting the community health worker or clinician, or the community health worker accidentally misdiagnoses the severity of dehydration. In the latter case, the CHW often only assesses the severity of dehydration by asking the parent for the amount of diarrhoeal episodes per day, according to the interviewed individuals. This is not in compliance with the current standards regarding dehydration assessment as explained in section 1.1.3, meaning that in practice probably every CHW uses a different method. This often results in severe dehydration remaining unnoticed, and that causes the child to be hospitalized too late. Therefore a tool for the CHW to correctly assess dehydration could be a solution to this problem.
- Another problem is that ORS is often out of stock. This does not often lead to mortality, as the child would then receive intravenous fluids for rehydration, as this is always available for emergencies. It would however potentially be a major cost saver if ORS could be deployed more efficiently (only to the patients in need), which would be enabled by a tool with high diagnostic performance. This would save cost, as the use of intravenous fluids is much more expensive in terms of workload and treatment resources.
- The higher level specialists (clinical officer and paediatrist) indicate that a spot-check or bed-site electrolyte analyser would be very useful, as even in a hospital environment assessing dehydration can be unreliable. For accurate testing of hydration status the child is often send to the lab for fluid electrolyte level tests, as this is considered a very reliable method. Having a portable bed-site electrolyte tester would thus be preferred due to the high diagnostic performance, yet for this test obviously a fluid sample is needed.

## 1.2. Problem statement

Based on the learnings from the problem analysis, the problem statement can be defined. To help formulate the problem statement, first the *5 "W's* (who, what, when, where, and why) are established:

- **Who**: As described in section 1.1.1, a specific group that is affected by dehydration often are *children under the age of 5 suffering from diarrhoea. CHW's*, which are often poorly trained in these settings, will be the users of the solution. They want to be empowered to provide better services to their patients/community. Any solution should therefore be suitable for both groups.
- **What**: Current ways of diagnosing dehydration in low-resource settings are considered to be very unreliable. Result is that the degree of dehydration is often misdiagnosed, leading to ineffective decision-making for the most appropriate treatment plan. The main identified causes for the low diagnostic

performance of these tests are: *subjectivity* of the test, lack of *training* for the CHW, *external factors* that influence the reading. A tool or device that overcomes these problems could be a potential solution.

- **When**: The issue occurs in the stage of assessing the degree of dehydration in acute-care settings, which is the step prior to treatment of the patient.

- **Where**: Low-resource settings, so in low/middle income countries in rural areas. The mortality of gastroenteritis is largest in Sub-Saharan Africa and South-Asia, as explained in section 1.1.1. These areas will be the focus for now. Rural settings are regarded to be the starting point, as these settings are regarded to be most critical in terms of the consequential criteria to a device that should be able to function everywhere. This is regarded as a context where things such as unstable electricity, high ambient temperature and relative humidity, and mechanical stress on the device due to incautious handling could be prevalent.

- **Why**: Strategies for improved prevention and treatment resources have been focus points by global health authorities and have decreased mortality of diarrhoea significantly. Starting point of this research is that improving diagnosis could be the final factor to effectively reduce mortality of dehydration within the group of young children in low-resource settings. Improved diagnosis is believed to result in better decision making in terms of deployment of treatment resources per patient, which would enable not only more effective use of treatment resources, but also more efficient use in general by focussing treatment resources to patients really in need. In the end improving diagnostic performance would therefore potentially reduce child mortality while saving cost of treatment.

Now the problem statement can be defined:

- **Vision**: A new device or tool, such as but not limited to a digital device, that will significantly increase accuracy and objectivity of dehydration assessment for children under the age of 5 in low-resource settings, while mitigating the need of rigorous training for the CHW and the influence from external factors.

- **Problem statement**: Current standard diagnostic scales are found to be inaccurate due to subjectivity, lack of training and influencing factors, and are therefore unreliable for use in low-resource settings. It is hypothesized that this might be co-responsible for the mortality due to dehydration.

- **Method**: Validating a technological principle for a device that can be easily implemented in healthcare systems in low-resource settings, that will significantly increase diagnostic performance of dehydration assessment, and therefore enabling improved provision of treatment which in turn reduces child-mortality and lowers cost of treatment. A (digital) device is envisioned that has a high diagnostic performance, while mitigating the current problems of operator subjectivity, need of training and influence from external factors.

### 1.2.1. Scope of work

Before starting the assignment the scope has to be defined, which means setting clear boundaries for this research for the sake of focus. In order to define the scope, below a number of topics are discussed that are either included or excluded from the rest of this assignment.

#### Included in the Scope of Work

- **Point-of-care diagnosis**: In this research the focus is on patients that might be in need of acute care due to dehydration, which requires rapid diagnosis, triage and treatment. The setting should not be restricted to laboratory environments, but should include community (non-clinical) settings, as well as in-/outpatient departments within a hospital. Within these settings health workers are often found to be heavily overburdened. Therefore the focus is on *quick, easy and accurate clinical point-of-care diagnosis of dehydration status in acute care settings.*

- **Range of target groups**: The target group for this assignment will be children in developing countries, but if the results of this research is more widely applicable it should not be limited to this group. The results might for instance also be applicable to (or serve as an inspiration for) other groups of patients, such as elderly suffering from dehydration in high-quality healthcare systems, where assessing hydration status may also be expensive or challenging to the nursing staff. Applicability of the results to other groups should be studied with care in future iterations.

### Excluded from the Scope of Work

- **The collection of body fluid samples for diagnostic purposes**: The assessment of dehydration can be done using *clinical* diagnostic methods, which will be defined here as assessment methods based on diagnostic variables that can be measured/observed in an in-/outpatient or community environment by healthcare workers. Another way of assessing dehydration status is *laboratory* testing, which involves the acquisition and testing of fluids or other samples of the patients in a laboratory environment. This often involves time-consuming (and invasive) procedures and can often only be executed by highly trained staff, but it does often result in more objective and accurate diagnosis. Still it is chosen to exclude the use of extracted body fluids for diagnosis, as it involves either a lot of time or invasiveness. Also hygiene would play a big role, and it would probably require disposables. All this is very unwanted in the chosen context, and therefore the use of (invasive) methods requiring body fluids should be avoided.

- **Aetiology**: This research will focus on the clinical assessment of dehydration, so that in acute-care settings proper rehydration can be carried out immediately. This is chosen as in cases of dehydration, rehydration has first priority before further management of the causes of dehydration, such as profuse diarrhoea. Therefore, further investigation in the diagnosis of the aetiology (cause) of dehydration (or diarrhoea) is out of scope for this research.

- **Prevention**: Prevention of dehydration is mostly related to hygiene/lifestyle associated with the targeted environment, and is believed to be best addressed by proper education of the population at risk, together with vaccinations for certain pathogens related to diarrhoea. Also facilitating adequate hygiene and sanitation would significantly contribute to preventing gastroenteritis and therefore dehydration. As the methods for preventing diarrhoea are already quite well established, this literature study focusses on the relatively under-established diagnosis aspect of the problem of dehydration.

- **Treatment methods**: Although treatment plans for dehydration should be well understood, since clinical assessment of dehydration is key in the decision process for treatment, further detailed research into better methods of treatment is out of scope for this research. It is established what treatment for different types of dehydration is currently used, and it is understood how the outcome of this research could improve utilization of treatment resources.

- **Credibility of the CHW**: Additional challenges are the socio-cultural and individual factors that undermine the credibility of health-workers in resource-limited settings. Although the variety of cultures across Sub-Saharan Africa and South-Asia are impossible to generalize, it has been found that in some areas health-workers have a high authority, whereas in some other areas the assessment of such health-workers is often questioned by the health-receiver (or parent), which leads to over-subscription of unnecessary (or even damaging) treatment resources [47], while the use of ORS is often neglected since it is not seen as a sufficing treatment of gastroenteritis or dehydration by some parents [68]. The assumption is that by objectifying the assessment of dehydration, not only the precision and accuracy will be increased, but also trust in the assessment of the health-worker. Testing this assumption will not be a part of this study, but should be done in other parallel or subsequent studies.

- **Cultural context**: That also brings us to the challenge of having an adequate understanding the targeted context, including: environment, culture, system, work-flow, etc. This is important as it will have great influence on the success of a potential proposition at the end of this research. If the factor of context is not taken into account it could lead to for instance a lack of interest from the market, misuse, disuse or malfunction. This could in turn have severe consequences on the patient. Investigating the context in detail further to the knowledge of the researcher will not be a part of this study, but should be done in parallel or subsequent studies. Eventually the list of requirements should be fitting to the context.

## 1.3. Conclusion

Based on this exploration of the problem it is clear that there as a need for novel and cost-effective diagnostic devices that can quickly and accurately measure dehydration in children under the age of five in low-resource settings. Health workers and clinicians have identified the need, and it is in line with the available literature on the problem of dehydration assessment. Improving the diagnostic performance of dehydration assessment would likely result in reduced child mortality, as well as reduced cost of treatment due to more effective use of treatment resources. The problem statement of this assignment clearly states that a new technological principle should solve the issues of subjectivity, lack of training for performing diagnostic tests and influence from external factors. In order to treat this problem statement, a clear overview of all current standards and developments regarding this topic should be in place. In order to achieve this overview, an explorative literature study will be conducted in the next phase of this assignment.

# 2

# Literature Study

*The full content of this chapter is directly based on the literature study report regarding this graduation assignment [54], which has already been submitted, assessed and graded.*

As a base for further research into new methods and technological principles for diagnosing dehydration, a literature study was conducted. The objective was to have a clear overview of *diagnostic variables* or *biomarkers* that are currently known to be linked to the degree of dehydration, and an overview of proven or conceptual *technological principles* that use sensors (and digital processing) to automatically analyse the signal for the degree of dehydration. These two overviews also contain information on diagnostic performance of the individual methods, as currently known. Together with the results of a *multi-criteria analysis*, the interpretation of the researcher (in collaboration with the dehydration team at Philips Research) on the suitability based on requirements, all this data should converge into a clearly substantiated direction for further research. This should be in the form of a recommendation on which technological principles and diagnostic variables are most optimal to further investigate in this assignment. This chapter contains the summary of the literature study.

## 2.1. Method

A systematic literature search has been conducted. In this search scientific papers, patents and reports on diagnostic variables and (conceptual) technological principles where included according to strict inclusion and exclusion criteria. In the information extraction part of the study, a distinction has been made between quantitative data on diagnostic performance and qualitative information on usage of the concerning method and potentially its suitability for use in low-resource settings. All quantitative data, in particular *sensitivity* (true positives versus false negatives) and *specificity* (true negatives versus false positives), is summarized in tables 2.1 and 2.2. A final score on *diagnostic performance* is given per individual object in both tables in the fourth column, which is generated by taking the average of the sensitivity and specificity. This approach was chosen to come with a single number for diagnostic performance, and since sensitivity and specificity are regarded in this assignment for being equally important. This is because a new method should both

Figure 2.1: Source: `https://www.hampshire.edu/areas-of-study/literature`

ensure that patients in need would be entitled to the right treatment, while at the same time ensure that treatment resources are efficiently applied to only the patients in need to prevent shortage. Hence *sensitivity* and *specificity* are regarded to weigh fifty-fifty when generating the *diagnostic performance score*.

All qualitative information is also summarized. All data on technological principles will then be used to perform a multi-criteria analysis together with the supervisor at Philips Research and some team-members. This analysis consists of first defining a number of key requirements, and giving these requirements a weight-factor from 1 to 5 in terms of importance. Each technological principle will then be assessed in terms of these requirements, which should result in a final weighed score for each individual technological principle. The outcome of this analysis would serve as an input for the recommendation for further research within this assignment.

## 2.2. Results

In table 2.1 all non-invasive biomarkers are collected, together with their individual numbers for sensitivity and specificity. The same has been done for all collected technological principles in table2.2.

| *Diagnostic variable* | *Sensitivity (%)* | *Specificity (%)* | Diagnostic Performance Score (%) | *Sources* |
|---|---|---|---|---|
| **Skin turgor** | **58** | **76** | **67** | Colletti et al. [33]<br>Steiner et al. [72]<br>Andersson and Hedvall [18] |
| **Capillary refill time** | **34.6**,<br>**54**,<br>**60** | **92.3**,<br>**88**,<br>**85** | **69** | Colletti et al. [33]<br>Fleming et al. [39]<br>Shavit et al. [70]<br>Steiner et al. [72] |
| **Tears** | **63** | **68** | **65.5** | Colletti et al. [33]<br>Steiner et al. [72] |
| **Mucous membranes (mouth & tongue)** | **86** | **44** | **65** | Colletti et al. [33]<br>Steiner et al. [72] |
| **Thirst** | *na* | *na* | - | Colletti et al. [33] |
| **Mental status** | *na* | *na* | - | Colletti et al. [33] |
| **Cool extremities** | **10** | **93** | **51.5** | Colletti et al. [33]<br>Steiner et al. [72] |
| **Eyes** | **75** | **52** | **63.5** | Colletti et al. [33]<br>Steiner et al. [72] |
| **Breathing** | **43** | **79** | **61** | Colletti et al. [33]<br>Steiner et al. [72] |
| **Quality of Pulses (systolic blood pressure)** | **04** | **86** | **45** | Colletti et al. [33]<br>Steiner et al. [72] |
| **Heart rate** | **52** | **58** | **55** | Colletti et al. [33]<br>Steiner et al. [72] |
| **Sunken fontanelle** | **49** | **54** | **51.5** | Steiner et al. [72] |
| **Body weight change** | *na* | *na* | - | Baron et al. [22]<br>Cheuvront et al. [30]<br>Colletti et al. [33] |

Table 2.1: Collected diagnostic variables for assessing dehydration, with data on diagnostic performance. Simplified version from [54].

The two diagnostic variables that are considered to be most reliable in assessing dehydration, *skin turgor* and *capillary refill time*, will be shortly explained below based on the collected information from literature.

**Skin Turgor:** Also known as *skin recoil time*, skin turgor (ST) is examined by performing the *skin pinch test*: The examiner pulls a skinfold (of the patient's dorsum of the hand, or abdomen) up with his

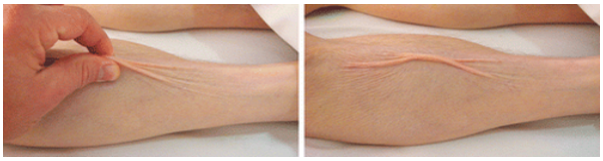

Figure 2.2: The skin pinch test. [36].

thumb and index finger, and then instantly releases it (see figure 2.2). The time it takes for the skin to return to its original state is indicative for the degree of dehydration. The skin pinch test is widely considered as a standard due to relatively high accuracy and quickness and ease of execution, which is why it is part of most standardized clinical dehydration assessment routines. Inaccuracy (the sensitivity is quite low: 58% [72]) might result from examiner subjectivity, and differences in pinching time/ pressure. When children present severe malnutrition symptoms (very little subcutaneous fat, marasmus or kwashiorkor), this test is found to be unreliable [64]. Also, the physiological relationship of this marker to dehydration is not understood very well. Formally, skin turgor is defined here as the speed or ability of the skin to return to its original state after being pinched for a few seconds. Some suggest that the phenomenon could be the result of water-lacking dermal elastic fibres (consisting of protein elastin), while others suggest that skin turgor is determined by fluid tension inside the skin-cells [38].

**Capillary refill time:** This biomarker is assessed by compressing a small part of the patients skin. The examiner presses thumb/index finger firmly against patient's finger pulp, nailbed or chest wall for up to five seconds, causing the skin to blanch. The examiner than releases the finger and measures time for skin to return to its original colour (see figure 2.3). Capillary refill time (CRT) is mostly determined by the perfusion of blood in the capillary beds in the dermis of the skin. As dehydration progresses, the total blood volume decreases. As total blood volume decreases, hypovolaemia and vasoconstriction cause perfusion in less-vital organs such as the dermis to drop [59]. Reduced perfusion is than easily observed by the colour of the skin returning to its original colour after applying pressure, which is the process of capillary blood in the dermis returning after being forced out of the distal capillary bed. The total time for this process is than called capillary refill time. This phenomenon is found to have a good correlation with the degree of dehydration in infants presenting with diarrhoea [65], although some inconsistency can be found in table 2.1. It is also found that fever has no clinically important effect on the observation of this variable [44]. Some data even show that CRT has the best clinical diagnostic performance (when examined by a human observer), with a sensitivity of .60 and a specificity of .85 [72]. Although these numbers are not yet very convincing of its potential diagnostic performance, it is hypothesized that the human factor of manually assessing CRT introduces a substantial amount of subjectivity to the examination. Also, external factors such as ambient light [26] have great influence on the observation. Skin and ambient temperature are also found to have significant effect on CRT [42]. Significant relations (statistically) have even been found between temperature and CRT. It has been found that CRT decreased 1.2% for every degree (Celsius) rise in ambient temperature (in adults) [17], an increase of .21 seconds per degree reduction of skin-temperature [42] and a decrease of 5% time for every increased degree of tympanic (or core) temperature (in adults) [17].

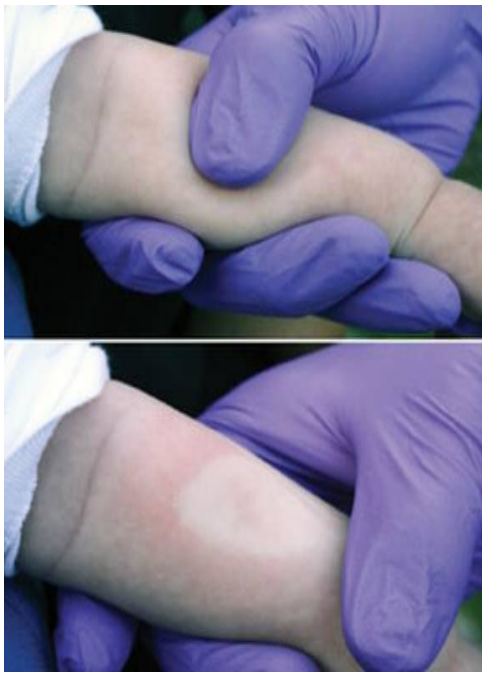

Figure 2.3: The Capillary Refill Time test. Source: *http://www.watersafetyguy.org/wp-content/uploads/2015/10/CapillaryRefill_Infant-218x300.jpg.*

A selection of a few promising technologies from table 2.2 (based on both any diagnostic performance data and application suitability) will be explained below. For the full explanation of all technologies be referred to [54].

**Camera based Digital Skin Turgor (DST):** *ST* was also noted as one of the best clinical diagnostic variables [72], which is still subjected to substantial amount of examiner variability. Therefore this diagnostic variable is quite interesting to objectify with technology to see if diagnostic performance would be improved. Hence, the *skin recoil time sensor* was prototyped [53]. The used resources are a camera, illumination and a video-processing unit (again a Raspberry-Pi). The device is placed on the sternum of the subject so that it

| *Technology* | *Sensitivity (%)* | *Specificity %* | Diagnostic Performance Score (%) | *Sources* |
|---|---|---|---|---|
| **Bioelectrical impedance analysis** | *na* | *na* | - | Baron et al. [22]<br>Dantas et al. [35] |
| **Ultrasound measurement of the Inferior Vena Cava Diameter** | **86**,<br>**67**,<br>**93** | **56**,<br>**71**,<br>**59** | **72** | Chen et al. [28]<br>Chen et al. [29]<br>Haines et al. [46]<br>Jauregui et al. [49]<br>Levine et al. [57] |
| **Ultrasound measurement of the Inferior Vena Cava Diameter** | **83**,<br>**93** | **42**,<br>**35** | **63.3** | Jauregui et al. [49]<br>Levine et al. [57] |
| **Camera based Digital Capillary Refill Time** | **100**,<br>**50** | **91**,<br>**50** | **72.8** | Shavit et al. [70]<br>Kieser et al. [53] |
| **Camera based Skin Turgor** | **80** | **84** | **82** | Kieser et al. [53] |
| **Skin Temperature Profile Sensor** | **68** | **59** | **63.5** | Kieser et al. [53] |
| **Infrared Spectroscopy of the Skin** | *na* | *na* | - | Visser et al. [77] |
| **Photoplethysmography based Capillary Refill Time** | *na* | *na* | - | A. Bordoley [14]<br>Messerges and Hutchinson [61]<br>Mcpherson et al. [60]<br>Pickard et al. [65]<br>Kviesis-Kipge et al. [55]<br>Blaxter et al. [25]<br>Karlen et al. [51]<br>Kviesis-Kipge et al. [56] |

Table 2.2: Collected technological principles for assessing dehydration, with data on diagnostic performance. Simplified version from [54].

could record a normal skin pinch test which the examiner would perform on the abdomen of the subject. The recording is yet to be analysed manually, not digitally by an algorithm.

Figure 2.4: [53] One of the prototypes built for measuring SRT.

**infrared spectrometry:** The use of *infrared spectrometry* is based on the estimation of water concentration in a tissue sample using near-infrared to short-wavelength infrared. It is based on the fact that light at certain (infrared) wavelengths has a higher water absorption coefficient. Using these wavelengths and sensing the transmitted/reflected light's intensity after it passed through the tissue, one can estimate the water content (or more precisely its chromophore concentration) within that part of the body [77].

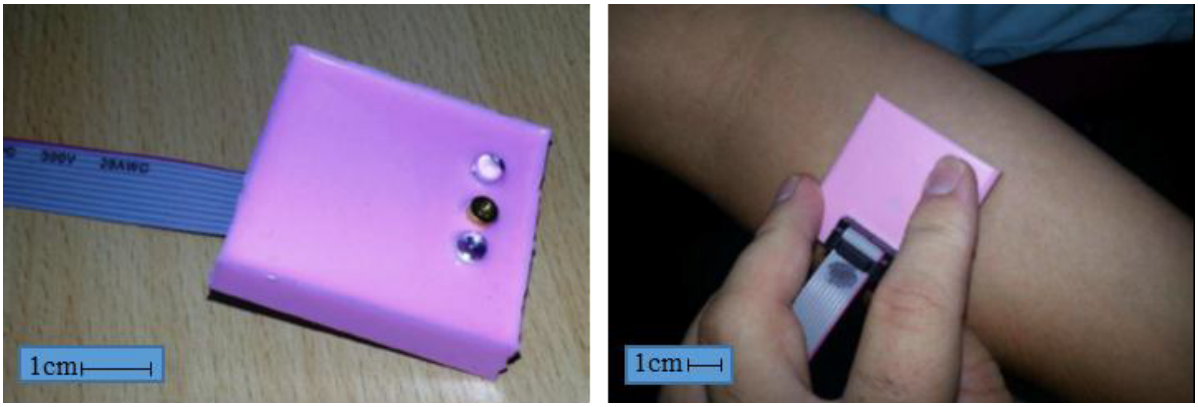


Figure 2.5: [53] Near-infrared spectrometry probe prototype to assess dehydration based on skin water-content.

**Photoplethysmographic Capillary Refill Time (PPG-CRT):** *Photoplethysmography* (PPG) is a relatively simple, and cost-effective optical technology which can detect blood volume changes in the capillary bed of tissues, and is often used non-invasively to make transcutaneous measurements of capillary blood-flow kinetics in tissues such as the dermis [16]. The general principle is based on the absorption of specific wavelengths of light by certain materials in the body, such as haemoglobin in the red blood-cells. So when a certain wavelength of light is applied on a part of the body, changes in reflected or transmitted light indicate volumetric changes of certain materials in that part of the body. There is a (nearly) static part of the PPG-signal (low-frequency), the DC-component, which is light being absorbed by "static" tissues such as skin, muscle, bone, etcetera. The short-term changes in the PPG-signal ("high"-frequency), the AC-component, would than consist of light being absorbed by fluid-material in the body, which in many body-parts mainly consists of blood. The AC-component therefore often shows pulses, due to the pulsating blood in the arteries and capillaries. The PPG signal is therefore potentially suitable to acquire capillary refilling data. Reflected or transmitted light can be measured with a photo-diode. A well-known and appreciated application of PPG is pulse-oximetry.


Figure 2.6: [14] A prototype for measuring temperature-adjusted CRT using PPG.

A way PPG can be used to assess dehydration, in theory, is more or less similar to DCRT as described before. Pressure has to be applied on a certain spot of the skin (standardized pressure and time), after which the PPG signal will be acquired of that spot which indicates the CRT. The sensor consists of a LED with an emission peak wave-length of 420 nm (which is violet, other wavelengths like the near-infrared spectrum or combinations are of course possible) and a photo detector next to it or opposed to it on the other side of the tissue of interest. PPG can also be used to measure backscattered/reflected or transmitted light.

A few concepts of PPG/CRT-based dehydration sensors have been found, without any quantitative data on diagnostic performance [65][55][25][51]. Also, some patents have been found that use PPG (in different ways) to assess dehydration and CRT [61][60]. One patent regards a wearable that assesses hydration status

by analysing the *plethysmographic waveforms* that are acquired from arteries or arterioles by using several algorithmic methods such as the first and second derivative, systolic peak-to-peak value and the crest factor, while using a motion sensor to compensate for any motion artefacts [60]. Another patent comprises a pulse-oximeter with an automated actuator that can pressurize a selected portion of the body to assess CRT from the photoplethysmographic waveform, adjusted by measurement of skin temperature by an integrated temperature detector [61]. Both patents can be used for spot-checks and monitoring. Another concept that was found uses PPG, skin temperature and a press for manual pressure application that measures temperature-adjusted CRT (figure 2.6) [14].

## 2.3. Discussion

First the two top diagnostic variables will be discussed in terms of their suitability for use in low resource-settings. For the full discussion where all diagnostic variables and technological principles are discussed, please be referred to [54].

**The Skin Pinch Test:** It was found that a combination of dehydration and malnutrition would make this test not useful, as it is performed currently. More data should be gathered on the prevalence of dehydration (due to gastroenteritis) combined with severe malnutrition (or marasmus or kwashiorkor) to see how much this would limit the reliability of the skin pinch test. The expectation is that the combined prevalence would be too high, as diarrhoea often results in malnutrition (and vice versa). The physiology behind ST and its relation to dehydration should also be better understood to be able to validate this marker as a proper diagnostic variable, as it seems that no real consensus has been found on the underlying physiology.

**Capillary Refill Time:** CRT is often regarded as an indicator for cutaneous perfusion, which can be directly related to dehydration. Still it is believed that environmental and physiological factors of influence make CRT more complex than just that. It is known that ambient-, core-, and skin-temperature all affect CRT, and so might other factors. It is believed that CRT could be a complex conjunction of, for instance, perfusion, blood viscosity, blood pressure, blood volume, heart rate, surrounding tissue elasticity, temperature, compression force, vasoconstriction, and so on. It is believed that the exact underlying mechanism behind CRT is yet to be established. When using CRT as a quantitative measurement, the exact capillary refill process should thus be better understood.

Below a review of the same selection of technological principles as in section 2.2 will be conducted, by testing these principles with the following key requirements:

- **Performance** *(weight: 5)*, should be significantly higher compared to current standard methods.
- **Bill of Materials** *(weight: 5)*, should be cheap to produce in order to keep selling price low for low-resource settings. The aim for Bill of Materials is less than $10,- (based on requirement from supervisor).
- **User-friendliness** *(weight: 3)*, aim is to keep the use of the device just as easy as the use of current standard methods like the skin pinch test and capillary refill time. Aim is that 15 seconds should be the maximum duration of a single measurement. A simple diagnostic outcome of one of the three conventional degrees of dehydration should be the outcome: no dehydration, some dehydration or severe dehydration.
- **Hygiene** *(weight: 3)*, since all methods of interest are already non-invasive, they are generally considered sufficiently safe for the patient. The risk of hygiene is than the remaining point of distinction regarding safety. Risk of spread of infections should for instance be minimal.
- **Patient comfort** *(weight: 2)*, the device should be comfortable for neonates as a starting point.
- **Durability (robustness)** *(weight: 2)*, device should be able to survive in the harsh environment of rural low-resource settings. It should have a minimal lifespan of 2 years.
- **Disposables** *(weight: 2)*, the need for disposables or consumables should be avoided, to prevent risk of misuse of disposables or CHW's running out of stock due to poor logistic facilities for restocking in low-resource settings.

The weights represent the importance of each requirement, and will be used to determine the final score for the suitability of each technological principle in the multi-criteria analysis as follows (eq. 2.1):

$$\text{Weighted Score Technological Principle} = \sum_{i=1}^{n} \left( \frac{\text{Score Criterion } (n) * \text{Weight Criterion } (n)}{\sum_{i=1}^{n} (\text{Weight Criterion } (n))} \right) \tag{2.1}$$

$n$ = number of criteria.

| Criteria | Weight criteria | Bioelectrical impedance analysis | US measurement of the IVC & Aorta | US measurement of the IVC collapse | Camera based digital CRT | Camera based Digital Skin Turgor | Skin temperature profile sensor | Near-Infrared spectroscopy of the skin | Photo-plethysmography of Capillary Refill Time |
|---|---|---|---|---|---|---|---|---|---|
| Performance | 5 | 2 | 4 | 1 | 3 | 3 | 1 | 1 | 4 |
| Bill Of Materials | 5 | 5 | 1 | 1 | 3 | 4 | 1 | 5 | 5 |
| User-friendliness | 3 | 4 | 1 | 1 | 3 | 4 | 5 | 5 | 4 |
| Hygiene | 3 | 3 | 3 | 3 | 4 | 4 | 5 | 4 | 4 |
| Patient comfort | 2 | 5 | 5 | 5 | 4 | 3 | 5 | 5 | 4 |
| Durability | 2 | 5 | 3 | 3 | 4 | 4 | 5 | 5 | 4 |
| Disposables | 2 | 3 | 3 | 3 | 5 | 5 | 5 | 4 | 4 |
| **Final weighted score** | | **3.7** | **2.7** | **2.0** | **3.5** | **3.8** | **3.2** | **3.9** | **4.2** |

Table 2.3: Multi-Criteria Analysis of technologies included in this literature study.

- **Camera based Digital Skin Turgor**

  *Performance*: ST is noted as one of the best clinical diagnostic variables [72], Although it is still subjected to substantial amount of examiner variability. The challenges of influence of external factors, subjectivity and training still exist in the camera based Digital Skin Turgor (DST) prototype of Kieser [53]. Pinch time and force is still executed manually, which could cause variability. Also the reliability of ST in malnourished children is doubtful [64], and this factor is not mitigated in the prototype. Also, since ST is mainly determined by extracellular water content of the dermis, it is possibly also influenced by external factors (taking a shower, sweating, body lotions, etc.). Yet, an experiment on the diagnostic performance of the concept showed relatively high diagnostic performance [53] (see table 2.2)). Another experiment should be done to indicate the influence of malnutrition (or loss of subcutaneous fat) and external water absorption of the skin. It would also be interesting to see if performance increases even further when the pinching process and data analysis are both automated, and therefore standardized. For now, because of the possibility that the significant influence from malnourishment might never be minimized in redesigns of DST, the score is **3**.

  *Bill Of Materials*: The used resources are a camera, illumination and a video-processing unit (again a Raspberry-Pi). Altogether the cost of this concept should be reasonable, although for automated video analysis, relatively high computing capacity might be necessary. Score: **4**.

  *User-friendliness*: The pinching procedure in this concept is not automated, and thus has to be carried out manually on the abdomen of the patient. Also the camera has to be placed correctly on the sternum

on an adequate distance and angle for a good shot. This requires a lot of actions for the user, as well as an expected low observer repeatability due to differences in test set-up and pinching time and force. Design alterations might mitigate these shortcomings. Score: **4**.

*Hygiene*: Apart from keeping the camera lens clean of any dirt and regular cleaning of the device in general, this concept needs minimal cleaning. If the device would be in direct skin-contact of the patient, some cleaning would formally be needed to prevent spreading infections. Score: **4**.

*Patient comfort*: This method is quite unobtrusive to the patient although the pinching procedure might cause some minor stress to very young and irritable patients (if mildly dehydrated). Score: **3**.

*Durability*: This concept does not house any moving particles and thus wear does not play a major role here. Yet, in any redesign where the pinching process might be automated, where moving parts would be essential, wear could play a slightly bigger role. Score: **4**.

*Disposables*: No disposables are needed for this concept in its current form. Score: **5**.

- **Near-Infrared spectroscopy of the skin**

  *Performance*: With this technology, one can estimate the water content (or more precisely its chromophore concentration) within a certain part of the body [77]. Although no data have been published yet on its diagnostic accuracy for dehydration assessment, it is known that the use of infrared spectrometry for skin hydration specific assessment is quite accurate [21]. The downside of the use of infrared-spectrometry is that the penetration of the light is only enough to measure skin-hydration. In many experiments which aim to detect skin-hydration, the assumption is made that the level of skin hydration is correlated to the level of total body dehydration (thus TBW). Although this is true physiologically (as total body dehydration influences interstitial fluids and ICW of the dermis), it is hypothesized that there are many more external factors that could also influence skin hydration, such as contact of the skin with fluids and lotions, ambient humidity, temperature and so on. Indeed, it is known that skin, the stratum corneum in particular, can absorb water (and other small molecules) from the environment [59]. Moreover, a sorption-desorption test was done when testing the prototype [77], where a high correlation between absorbed infra-red light and external absorption of water by the skin was found. An internet search was conducted to information that indicate any correlation between skin hydration and total body hydration, but no results have been found. Therefore more research should be done on the actual correlation of skin hydration to total body hydration. Thus, for now it will be assumed that there is no correlation, consequently assuming that skin hydration is a poor diagnostic variable for total body dehydration. In a personal conversation with Dr. Ir. K. Dellimore, one of the researchers at Philips in the study [77], this assumption was confirmed informally. An expected diagnostic performance score of **1** therefore would be appropriate.

  *Bill Of Materials*: Since the only resources needed next to a signal-processing unit are just two LED's and one photo-diode, this method can be made very cost-effective. Score: **5**.

  *User-friendliness*: This concept is very user friendly. The only action for the user to undertake is to place the probe on the skin of the patient. Score: **5**.

  *Hygiene*: Hygiene is not a big concern as long as the device is used upon intact skin. It would formally need some cleaning after each use on a sick patient to prevent spreading infectious diseases such as gastroenteritis. Score: **4**.

  *Patient comfort*: The patient is not expected to be under stress as a result of this method. Score: **5**.

  *Durability*: Small number of individual key-components and no moving parts, so wear plays a very minor role. Score: **5**.

  *Disposables*: This concept uses a reusable probe. It is not known whether motion artefact will influence the reading. If so, an adhesive probe might still be needed, which often requires disposable adhesive membranes to attach to the probe. Yet motion artefact might also be mitigated with proper design. Score: **4**.

- **Photo-plethysmography of Capillary Refill Time**

*Performance*: CRT is a recurring subject, mostly because of its theoretical potential in diagnostic performance. Photoplethysmographic (PPG) recording of this biomarker is therefore another principle that sounds promising. Theoretically, PPG could measure CRT a lot more accurately and cost-effective compared to the earlier discussed DCRT, with possibly less influence from ambient light and skin pigmentation. As the use of a certain wavelength (such as 420 nm blue light, which was used in a study by E. Kviesis-Kipge et.al. [55]) and backscattered light measurement only has a penetration depth to the dermis of the skin, without measuring any other pulsating signals from underneath the dermis. If that could be achieved, this method might have the best signal-to-noise ratio for recording CRT, as the way CRT is assessed right now with the naked eye also solely reflects refill of the capillaries in the dermis, which causes the white-to-pink colour change of the skin (or nail-bed in highly pigmented patients). Another anticipated benefit of using one specific wavelength of light, instead of the mixture of wavelengths as used in DCRT, is that the photo-detector used for this application could have a peak-sensitivity specified to that wavelength. This would already filter out noise from for instance ambient light wavelengths. Since the absorption of a specific wavelength by blood can be extracted by subtracting the static DC-component from the higher frequency AC-component which is caused by blood volume changes in the piece of tissue of interest (in this case the dermis), capillary refill can be very accurately measured and quantified. This has been proven in several studies into the use of PPG for CRT assessment [55][56]. CRT would still be affected by skin temperature. Too deal with this, algorithms have been developed to adjust the readings with regard to simultaneously measured skin temperature using appropriate sensors [14], based on regression models developed by several studies [17][42]. Surface temperature of the extremities is also considered to be a diagnostic variable for dehydration degree, as seen in table 2.1. That is convenient, as combining these signs might increase the effective diagnostic performance of a diagnostic tool.
At this stage no published data has been found on diagnostic performance of existing PPG-CRT concepts for dehydration assessment. Yet, it is highly expected due to the benefits described above that it would utilize the full potential of CRT as a diagnostic sign for dehydration, which is already considered by some researchers as the best individual sign, due to PPG's sensory accuracy and mitigation of confounding factors such as skin-pigmentation and temperature if used in conjunction with the right temperature sensors. The fact that literature on a number of concepts exploiting this principle has been found, supports this expectation [14][61][60][65][55][25][51][56]. It is known that PPG is prone to motion artefact, which requires robust designs for a stable sensor placement on the body. Even for this problem, there are published algorithms that sensitively detect unreliable measurements using just the PPG signal, for instance due to insufficient pressure, low perfusion signals and motion artefacts [51]. Besides CRT, the PPG signal derived from capillary blood dynamics can contain much more information, such as pulse rate, pulse quality (or blood pressure), respiration rate, vasomotor activity, vasoconstrictor waves, Trabe Hering Mayer waves and thermoregulation [71] [16]. One of the best known applications of PPG when using red in combination with infra-red light sources is pulse-oximetry, where even blood-oxygen levels can be derived from the PPG signals. PPG is therefore very versatile, since its signal houses a bulk of information, potentially relevant for dehydration assessment.
In conclusion, despite the absence of published data on diagnostic performance, it can be said that with some extra research and development efforts, it is very likely that this principle will result in a high diagnostic performance, when used solely for children under the age of five. Main reasons are the mitigation of the known confounding factors, the relative sensory accuracy of PPG for CRT, and the information that is acquired from PPG (and skin-temperature sensors) that can form a combination of parallel (or serial) tests, which together can boost sensitivity or specificity if needed [80]. A score for the expected diagnostic performance of **4** therefore seems to be appropriate.

*Bill Of Materials*: All that is needed next to a small signal processing unit is at least 1 LED (wavelength to be determined) and at least 1 photo-diode. In addition for this application: a system that is capable of standardizing the amount and time of pressure applied (either automated by a simple mechatronic system, passively controlled by linear compression springs, or guidance by force-feedback to the user for instance), and a temperature sensor to adjust the signal to skin-temperature. Score: **5**.

*User-friendliness*: If the blanching process is automated or intuitively guided, and the time needed to get reliable data is sufficiently short, the user-friendliness of this concept is estimated to be quite good. Especially when the quality of the reading is automatically validated. Due to some minor usage complexity that is expected with the blanching process, the chosen score is **4**.

*Hygiene*: As long as the device is used on intact skin, hygiene is expected to play a very minor role. Some cleaning would officially be required after each use on a sick patient. Score: **4**.

*Patient comfort*: Apart from the moderate pressure applied on the skin of the patient, the use of this concept is not expected to introduce any stress to the patient. Still, some dehydrated patients might be very irritable, therefore the score is **4**.

*Durability*: The influence of wear on durability depends on the use of moving parts. Otherwise wear will play no significant role. It is expected that ideally the blanching process is controlled (actively or passively), which would need some moving parts, therefore the score is **4**.

*Disposables*: Ideally this concept would consist of a reusable (possibly handheld) probe. It is unclear at the moment if this is possible, due to the potentially significant motion artefact introduced by relative motion of the examiner. It could be the case that adhesive probes are the most optimal solution for this, which are often (partially) disposable. There are existing PPG solutions that are integrated in finger-clips, wearables such as smartwatches and in mobile phones, which all don't use disposables. This topic should be investigated in follow-up studies. Score: **4**.

## 2.4. Conclusion

Based on the MCA, it can be concluded that *Camera based Digital Skin Turgor* (DST), *Near Infrared Spectroscopy of the Skin* (NIRS) and Photo-Plethysmography of Capillary Refill Time (PPG-CRT) have the highest scores based on their performance and suitability for (rural) low-resource settings. Yet, the criteria *Performance* and *Bill-of-Materials* should not merely be considered the most important. These criteria should be considered absolutely critical for any diagnostic method or tool to be successful in low-resource settings. With that in mind, NIRS should be disqualified from this list due to its expected low-diagnostic performance. BIA would than count as the third most suitable method, but as with NIRS its expected performance is also considered to be too low for now. DCRT could then be considered the third best tool/method from the MCA, as neither expected performance and bill of materials are very low. Both DCRT and PPG-CRT are based on the same biomarker (CRT), yet PPG-CRT is expected to measure CRT more accurately. Therefore it is considered that any more research into DCRT would be redundant, at least until the legitimacy of PPG-CRT would be invalidated for any reason. In conclusion, PPG-CRT and DST are therefore considered the most suitable principles, as these have the best combination of performance and general fitness for dehydration assessment in low-resource settings.

Of all the biomarkers that can be assessed non-invasive, outside of lab-settings and instantly (spot-check, thus excluding all tests based on the acquisition of body-fluids), ST and CRT scored the highest in diagnostic performance as far as known. This supports the conclusion that PPG-CRT and DST would be most suitable, as these technological principles are then based on the best diagnostically performing biomarkers.

It has to be kept in mind that, at the moment of writing, none of the included methods (both current standard methods and technologies in development, excluding the fluid-sample collection methods) perform well enough to be suitable as individual diagnostic tools for dehydration. Therefore more efforts in research and development are needed, in order to further optimize these methods. Likely, a combination of PPG-CRT and DST in one diagnostic device would draw the best diagnostic performance

### 2.4.1. Recommendations for further research

A number of steps still need to be taken before any such diagnostic tool can be implemented successfully. These steps regard improving *diagnostic performance*, *understanding the biomarkers* and their relation to total-body hydration level, knowing what the impact of such a diagnostic device will be in terms of *reduced child-mortality and reduced cost*, and understanding the *needs and desires of the users* of the tool. In the following recommendations the focus is on DST and PPG-CRT, as these principles were concluded to currently carry most potential to be successful.

In order to optimize *diagnostic performance* to the maximum performance one would be able to get from these biomarkers, it is key to know the influence from any external factors such as temperature and humidity to be able to minimise their influence, or to generate a multi-variate regression model based on the influence of these factors. It is therefore recommended to perform a data-collection and analysis study in order to see any correlations between these confounding factors and the biomarker of interest. To be able to perform

such a study, the appropriate equipment for gathering this kind of data has to be used, which meets the right criteria. Also the right criteria need to be investigated, such as for instance light emitter wavelength for PPG-CRT or pinch-force for DST. It would require the development of prototypes of any appropriate measurement equipment is not yet commercially available. Another promising way of optimizing diagnostic performance in terms of sensitivity and specificity is to combine PPG-CRT and DST in later design stages, in a way that both test act as parallel or serial tests during a single diagnostic measurement [80].

It was also noticed that the understanding of the underlying *mechanics of CRT and ST* are not very well defined, and sometimes the literature is somewhat inconsistent on this matter. A recommendation is to investigate the exact mechanics that determine CRT and ST, and especially how dehydration exactly plays a role in the variations of these biomarkers. These mechanics should include an exact physiological and anatomical explanation of these biomarkers. An example would be to build an analytical model of the process, making it possible to simulate the behaviour of these biomarkers. This knowledge should help with the interpretation data-study (first recommendation), and help with the mitigation of all confounding factors.

The assumption where this study is based on is that improving the process and results of assessing the severity of dehydration would have a significant positive impact on the *reduction of child mortality and cost of treatment* for dehydration. This assumption originates from two facts: that child mortality due to dehydration is still high, while global authorities have been investing in improved hygiene and sanitation, and increased availability of treatment resources. The other fact is that diagnostic tests are proven to be very unreliable, even though they are key in the decision making process for choosing the appropriate treatment for the patient. It suggests that improving diagnosis would be a remaining step to drastically reduce mortality, but this argumentation cannot yet be considered as proof of this assumption. A quantitative and qualitative data collection study, based on interviews with Community Health Workers and doctors in the field, should be performed to gather the right data that should shed light on the question where the main bottlenecks in reducing child mortality due to dehydration exist. If this data would prove that wrong diagnosis of dehydration is actually a cause of mortality, it would also confirm the assumption of the high added value of any diagnostic device for dehydration assessment.

In addition, the question that has to be kept in mind is whether or not such a tool will ultimately be the *solution for this problem*, and if objectifying assessment (with technology) will result in higher credibility for the health-worker. It is absolutely necessary to have a clear understanding of the criteria of such an innovation, based on the needs of the local community health workers. It is therefore recommended to collaborate with local researchers, engineers, designers, clinicians and community health workers (users) in order to make a product that will be successful in terms of user-acceptance and adoption.

# 3

# Validation Experiment

The next phase of this assignment consisted of an experiment, which aims to validate the predictive characteristics of both *skin turgor* and *capillary refill time*. The results of this experiment would give insight into the usefulness of these diagnostic variables for assessing dehydration, and it would serve as a pilot study for future dehydration studies. In this phase of exploring the topic of assessing dehydration, it was chosen to do a relatively small scale lab-experiment rather than going to the field (rural low-resource settings). Arguments for this are that getting approval to perform biomedical experiments abroad, especially on young and sick children, is a very time-consuming process and it would cause too much delay for the progression of this graduation assignment. So instead it was chosen to do an internal lab-experiment first. The main approach was to create a comparable experimental condition where significant changes in hydration state of the human body should be accomplished. While dehydration progresses, measurements with dedicated equipment that could record relevant data for ST and CRT would be taken for analysis. The expected outcome of this experiment would obviously be a clear trend of parameter changes over the course of progressing dehydration, from which ideally a good predictive model should be created using regression analysis.

In this chapter the preparation, execution and analysis of the experiment is discussed, starting with the research question. From there the approach, overall experimental design and prototyping phase are discussed. The chapter will close with the explanation, analysis and discussion of the results, and finally the conclusion and recommendation for further continuation of this assignment.

## 3.1. Research Question

The main objective is to validate whether or not there is any relation between the parameters of interest (CRT and ST) and the degree of dehydration, and how any other external factors my have influence on these parameters of interest. A secondary objective is to test the included experimental equipment, whether off-the-shelve or prototype, for suitability of use in future experiments, as well as the overall experimental protocol. The learnings of this experiment should therefore be translated into recommendations for future experiment protocols and equipment requirements.

Based on the main objective, the *research question* is:

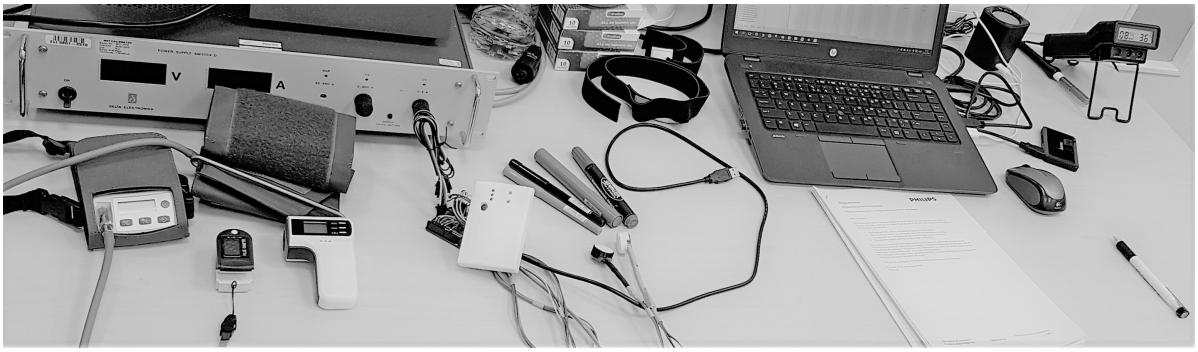

*"Does progressing dehydration significantly increase capillary refill time and significantly decrease skin turgor, when these variables are measured objectively using digital methods?"*

This research question will now be broken down into two main *experimental hypotheses*:

- It is predicted that digitally measured *capillary refill time* is *proportionally* related to the severity of dehydration.
- It is predicted that digitally measured *skin turgor* is *inversely* related to the severity of dehydration.

## 3.2. Approach

This experiment was conducted by stimulating loss of fluid through sweating at volunteering subjects, whilst denying access to rehydration for a considerable amount of time. This approach would ensure an accelerated fluid output with zero fluid input, and this will eventually lead to dehydration. The approach also consists of taking measurements of ST and CRT and other external factors of influence over the course of the experiment as the subject loses more and more of its total body water. Once all the measurements were made, data will be processed and statistically analysed using Matlab. In this section, the choice of this approach will be further clarified.

### 3.2.1. Internal lab experiment

As explained before, time and resources were limited, so a large scale child study in the field was not an option within the scope of this assignment. Although it would eventually be preferred to perform such a field study, meaning collecting data with functional prototypes from already dehydrated children under the age of five in low-resource settings. This is considered to be the best way to gather representative data, as it would be difficult to otherwise reach children that are dehydrated for testing the technological principle. It is important to eventually test a device on dehydrated children, because testing on dehydrated adults could draw different results as their normal body water content differs from young children. It is also known for instance that CRT characteristics change over age, and moreover CRT is much more consistent to dehydration in young children compared to adults [69]. It is also trivial that biomechanical properties of the skin, and therefore also ST, change over age.

Yet before performing this study, it is important to have any proof-of-principle ready, showing that there is a clear relation between dehydration and the parameters of CRT and ST. Otherwise any medical ethical committee would not approve such a child study. Hence, the internal lab experiment should lead to this proof-of-principle.

### 3.2.2. Dehydration by profuse sweating

Stimulating diarrhoea to cause dehydration with the subjects is obviously impractical, and therefore other routes to stimulate dehydration should be used. It was found that in earlier experiments where dehydration needed to be stimulated, it was done by physical exercise (sometimes in a warm environment [53][77][18]. This causes the body to warm up, and to dissipate the abundant heat the sweating mechanism is put into effect. Tonicity of dehydration due to profuse sweating is most often hypertonic[31], in contrast to diarrhoeal dehydration which is most often isotonic as explained in section 1.1.3. Yet, in that same section it was also explained that according to WHO tonicity of dehydration does not make a difference in assessing dehydration. Therefore profuse sweating as a stimulant of dehydration is considered to be an appropriate substitute for diarrhoea.

### 3.2.3. Variables

The main *independent variable* for this experiment is *the percentage loss of body mass*, which is currently defined as the golden standard for dehydration assessment. The main *dependent variables* are CRT and ST as measured with experimental equipment which will be defined in section 3.3. In addition, a few identified parameters of influence will also be measured: Core temperature, skin temperature, ambient temperature and ambient relative humidity. These parameters will assessed as independent variables that influence the dependent variables, and in a *multivariate regression analysis* their influence should be quantified.

For a better understanding of both the dependent variables CRT and ST, these variables have been studied a bit more in depth to get a better understanding of what is actually measured and what actually causes the

changes.

Capillary Refill Time

Using CRT as a diagnostic measurement involves the visual inspection of the pink colour returning after compressing the skin with moderate pressure for a few seconds. This process of compressing the skin results in the distal capillaries of the dermis being emptied of blood, hence the lighter colour shortly after releasing the pressure. The return of the pink colour is the process of blood refilling these capillaries, which can thus be visually inspected. The speed of this process is mainly defined by peripheral perfusion.

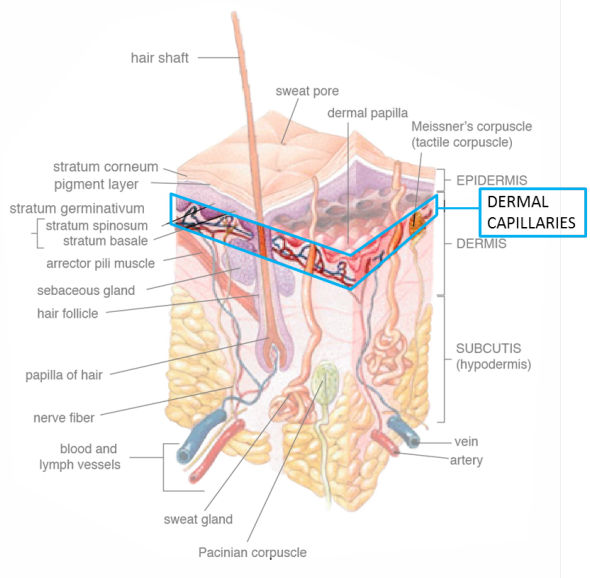


Figure 3.1: CRT is defined by blood volume changes in the dermal capillaries

Physiologically the mechanism behind peripheral perfusion, and thus CRT, is very complex and also not very well defined. It is known that it depends on a couple of factors, such as: the main determinants of capillary blood flow (such as driving pressure, arteriolar tone and hemorheology) and capillary patency (the density of capillaries in a certain area. It has to be noted that no publications have been found that support the theory that variations in peripheral perfusion cause differences in speed of the capillaries refilling with blood, and would therefore be related to CRT. [65]

In this assignment the accepted line of reasoning is that dehydration eventually causes blood volume to drop, which is well known. This lowered blood volume then would affect both blood pressure and arterial tone, as the body responds with vasoconstriction to concentrate the blood to the vital organs in cases of shortage of blood volume. This causes reduced peripheral perfusion of the skin.

In terms of the preferred body location to perform this test there is no universal agreement, although different body locations do provide different standard values for CRT [65]. Some examples of suggested body locations in literature are:

- Fingertips
  - Index finger [55]
  - Little finger [55]
  - Thumb (suggested by WHO) [65]
  - Finger pulp [73]
  - Nail bed [73]
- Chest (on the sternum) [65]
- Midpoint of the forehead [65]

- Heel [65]
- Palm [65]
- lip mucosa [73]
- Big toe (suggested by WHO) [65]
- Kneecap (suggested by WHO) [65]
- Forearm (suggested by WHO) [65]

Based on few studies, most paediatric health workers prefer to use the *chest* for CRT testing ($\frac{2}{3}$), or the *fingertip* ( $\frac{1}{3}$ ) [65]. It is found that measuring from the *fingertip* can be more difficult compared to the *head* or the *chest* due to movement of the child [65]. In addition, measurements from the *forehead* and *chest* have shown to be more consistent compared to other sites. It has to be noted that the areas of the chest and the head are priorities in the case of blood-volume depletion. In cases of dehydration it therefore could be the reason why these sites react differently to dehydration compared to for instance the fingertips, which are low priority. In highly pigmented individuals (which obviously make up the majority in Sub-Saharan Africa) a body site where pigment levels are relatively low is obviously preferred, since pigment blocks the view on the pink colour change of the capillaries refilling. CHW's are therefore often restricted to using the *nail bed* in these settings. Otherwise the *head* and *chest* would thus be preferred. The use of the chest has also been suggested by Prof. dr. Sidarto Bambang Oetomo in a face to face interview (see appendix B, since the presence of the sternum directly under the skin provides a nice solid and consistent structure for counter-pressure in the compression phase, which should be beneficial for CRT testing. The same is true for the forehead.

Currently known (external) factors, other than perfusion related factors or subjectivity, that can have influence on the characteristics of CRT are:

- *Age*: Age has a significant effect on normal levels of CRT, although is can also be seen that consistency of normal CRT in children under the age of 5 is the highest of all age groups [69]. It is therefore hypothesized that CRT is best used as a diagnostic variable in young children due to relatively similar inter-individual baseline for normal CRT. In this group of age, it is also concluded that age doesn't cause any additional variations.
- *Ambient temperature*: It has been found that CRT decreased 1.2% for every degree (Celsius) rise in ambient temperature (in adults) [17]. This temperature can have effect on peripheral perfusion and skin surface temperature, which might explain this behaviour (as a mechanism to conserve body heat by allowing less "warm" blood to come near the colder surface of the body).
- *Skin surface temperature*: A significant increase in CRT of .21 seconds per degree reduction of skin-temperature has been found [42]. This could be explained by the same reasoning as with *ambient temperature*, but the effect is much bigger here as temperature differences in the skin would have a more direct effect on peripheral perfusion, hence the stronger resulting variability.
- *Core temperature*: A decrease of 5% CRT for every increased degree of tympanic (or core) temperature (in adults) [17]. This can be explained similarly, as with higher core temperatures more heat needs to be dissipated through the peripheral capillary system. This therefore increases peripheral perfusion, and therefore shortens CRT.
- *Pressure application*: Several parameters influence the compression of the skin: the applied force, the contact surface area, and the amount of time the skin is compressed. There is no universal agreement on the amount of force and time needed for optimal compression, but the main accepted instruction is "moderate pressure for 3 to 7 seconds" [65]. It was also found the less pressure (just enough to blanch the skin) results in shorter CRT but also less variability between measurements [67].

Skin Turgor

Skin turgor assessment involves performing the skin pinch test, which consists of pulling a part of the skin of the subject up with the thumb and index-finger, which stretches the skin upwards. At a point where the skin is fully stretched, without causing pain for the patient, the skin is released. It is than visually inspected how long the skin takes to fully recoil to its original position. The slower this process is, the more dehydrated

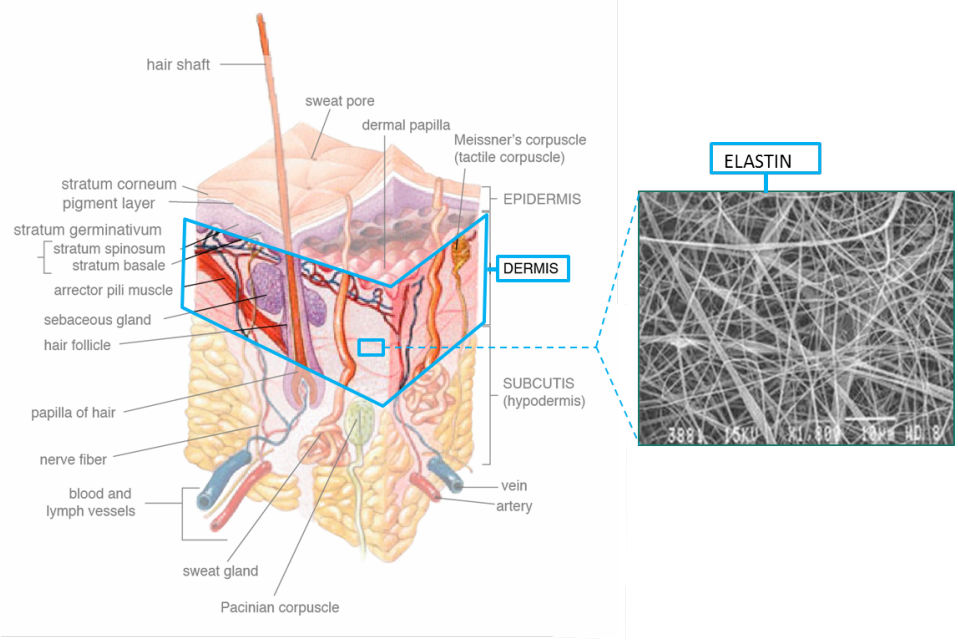


Figure 3.2: ST is defined by state of the elastin proteins in the dermis

the patient. This is a test that is very often performed (according to interviews with CHW's and clinicians, see appendices B and A, even with elderly.

Physiologically there is also some debate about the underlying mechanism of variations in ST. The name "Skin Turgor" implies the balloon-like rigidity of cells, which would be caused by rise in hydrostatic pressure inside the cell [38]. Loss of ST would therefore mean loss of intracellular water, and would therefore result in more "floppy" skin. Loss of ST is also often regarded simply as loss of elasticity of the skin, or in other terms the loss of ability of the skin to return to its original shape after deformation.

These two explanations don't seem to capture the essence of the variable ST, according to Dorrington et al. [38]. ST would primarily rely on the integrity of the rubber-like state of the *elastin fibres in the dermis of the skin*. Elastin fibres are proteins that are found in many tissues that under normal circumstances should have elastic properties, such as skin, arteries, the lungs or cartilage. The two known factors that can have influence on the state of these elastic proteins are *temperature* and the presence of *water*. Temperature needs to be high enough to preserve thermal motion of the chain molecules, while water acts as a lubricant for the motion. If water in the dermis would become deficient, these proteins transit from a rubber-like state into static glass, which can be over a thousand times more rigid [38]. As the elastic fibres, which consist of elastin, are found in the *extracellular matrix* [59], the change of ST due to dehydration would eventually be subject to loss of *extracellular water*.

It is now clear that short term loss of ST due to dehydration is linked to the rubber-like state of these elastic fibres. Yet it is also already stated in section 2.2 that malnutrition also affects the outcome of assessing ST, which can be explained by loss of subcutaneous fat (fat-tissue in the hypodermis, which is inferior to the dermis). This fat-tissue obviously contributes to the observable elastic response of the skin to stretching, and it is clear that with the skin pinch test this contribution disturbs the outcome of the test due to the large amount of skin that is pulled up. A method where ST is assessed by focussing on the dermis part of the skin, with minimal influence from the hypodermis would be ideal. In fact, the epidermis (the most superficial layer of the skin, just superior to the dermis) also would contribute to this test. It is known that the epidermis, even though when among its functions is to be a water-resistant barrier, will absorb water when immersed in (non-salty) water [59]. This causes some swelling of the epidermis, which might have slight influence on the mechanical property of the skin. It can for instance happing during a shower, or when lotion is applied to the skin. It can therefore in the end be hypothesized that the use of ST as a diagnostic variable would be most optimal with a penetration depth in the skin that is focussed to the dermis, with minimal influence from changing mechanical properties of the hypodermis and the epidermis.

It is well known that elasticity of the skin decreases when the body is ageing, which is partly due to decreasing production of elastin. Therefore age is also considered as a factor that significantly influences ST.

In terms of body location, no universal standard has been defined. It is known that on neonates, often de lateral abdomen is used (see B). It is assumed that location is not a very important factor, as long as the skin is somewhat mobile and the build-up of sub-cutaneous fat is minimal in that area, for example the back of the hand. The fore-arm had also been suggested for ST testing [37].

Altogether the identified factors other than dehydration that influence ST are:

- *Age*: as elastin becomes less available in the skin at older age.
- *Skin temperature*: As elastin reacts to its surrounding temperature. This could therefore also be indirectly be influenced by *core-temperature* and *ambient temperature*.
- *Subcutaneous fat*: as discussed, absent (or abundant) fat tissue in the hypodermis causes variations in skin recoil time when assessing ST using the skin pinch test. It is regarded that the skin pinch test is not reliable anymore with extremely malnourished children. In addition, oedema, kwashiorkor, marasmus or other skin conditions all have influence on the reliability of this test. [64].
- *Pinch*: Although no literature has been found that proves this point, it is assumed that inconsistencies in the pinching process might cause unwanted variability. For instance the amount of skin that is pinched, how far the skin is pulled up or how much pressure is exerted on the skin between the thumb and index finger could all contribute to variations in skin recoil time.

## 3.3. Equipment

Based on the conclusion of the literature study, a choice has to be made on the most appropriate equipment to use for this experiment for both ST and CRT.

### 3.3.1. Capillary Refill Time - Photoplethysmography

In the search for a PPG sensor that can be used as a sensor for capillary refill time, a few decisions have to be made on various features that this specific device needs to comply to based on the knowledge gathered in section 3.2.3.

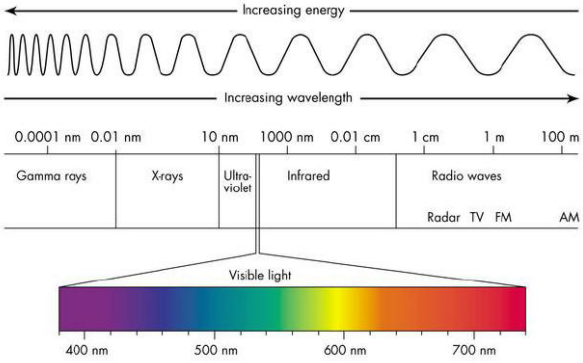


Figure 3.3: The electromagnetic spectrum, showing the location of green wavelengths within this spectrum. Source: `http://lumenistics.com/what-is-full-spectrum-lighting/`

#### Sensor type: Reflective Green Light PPG

A penetration depth of the sensor that is focussed on the dermal capillaries, as these capillaries make up the colour change that is observed when testing the CRT. Deeper penetrating signals would also pick up absorption by arterial blood, which causes extra noise due to its pulsation. For this reason *reflective* PPG would be preferred over *transmissive* PPG, with the additional benefit that reflective PPG can practically be applied anywhere on the skin. Transmissive PPG is on the other hand only restricted to body locations that are small enough to allow the (red or infrared) light to pass through, such as a finger, toe or earlobe.

It has been found that *green light reflective PPG* (with a wavelength of approximately 500nm to 600nm) would

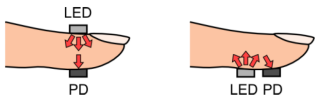


Figure 3.4: [74] In transmissive PPG the photo-detector is placed opposite to the source, while in reflective PPG the detector is placed next to the source.

be the most optimal type of light, for a number of reasons. In earlier CRT-PPG concepts it was found that opposed to red light (640nm) and infrared light (950nm), reflective green light PPG (520nm) would produce statistically the most significant data in experiments of CRT measurements on warm and cold skin (remember the external factors influencing CRT) [25]. Green light PPG for pulse monitoring has also been suggested

due to its increased depth of modulation (the ratio of the pulsatile component due to blood volume variations to the mean intensity of reflected light) compared to red and infra-red [45] [34]. It is hypothesized that this high modulation would also result in high CRT-related variations compared to the mean, which should result in an improved signal-to-noise ratio. In figure 3.5 the modulations over a range of wavelengths are plotted, while interestingly it seems to correlate well with the plot of absorption coefficients in the same figure. This observation suggests that the increased absorption coefficient of blood and bloodless tissue is mainly caused by increased absorption of light by the blood in comparison to bloodless tissue, as increased modulation means that a larger ratio of the absorbed light is due to absorption by blood, which is convenient for CRT measurement. This assumption is confirmed in other papers [74]. It can be clearly observed that there is a large peak of modulation within the band of 500nm to 600nm, which corresponds well to green light. The practical consequence of this increased modulation to the PPG signal is visualized in figure 3.6, where a significantly better signal-to-noise ratio can be clearly seen.

It has to be noted that red and infra-red have been more conventional ranges of light since these are used

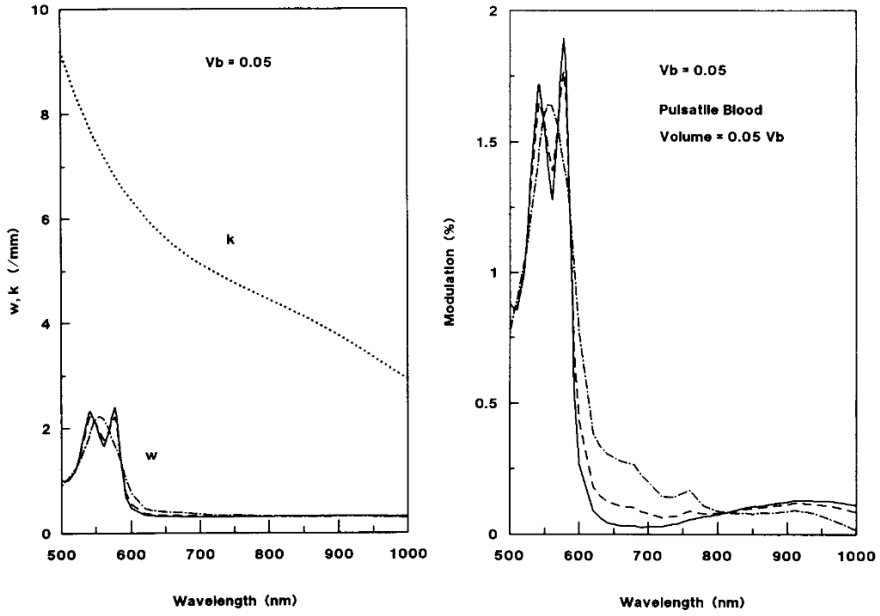


Figure 3.5: [34] The first plot shows the scattering coefficients (k) and absorption coefficients for blood and bloodless tissue (w) over a range of light wavelengths, while the plot on the right shows reflectance modulations for the pulsatile component over same range of wavelengths.

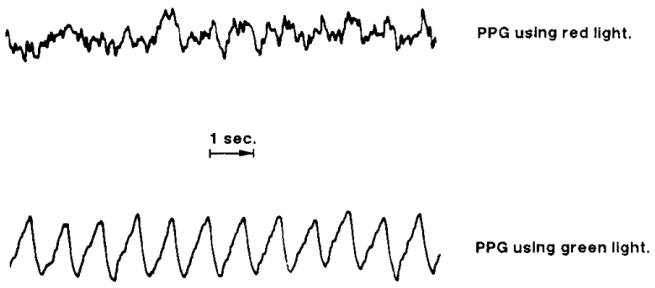


Figure 3.6: [34] Reflectance pulsations measured on the anterior surface of a lower leg, comparing the pulsatile (AC) components.

in pulse-oximetry because of their high penetration depth and their different absorption coefficients with oxyhaemoglobin and deoxygenated haemoglobin. Green light is known to have a much less deep penetration depth into the skin compared to red or infra-red, which is visualized in figure 3.7. Looking at image 3.8, which plots all the penetration depths of light over a large range of wavelengths into human skin, confirms that green light has a lower penetration depth, which is approximately 1mm to 1.5mm at wavelengths between 500nm and 600nm. Note that these penetration depths regard a "one-direction" situation, which is useful for determining the irradiation dose in photothermal and photodynamic therapy of various diseases

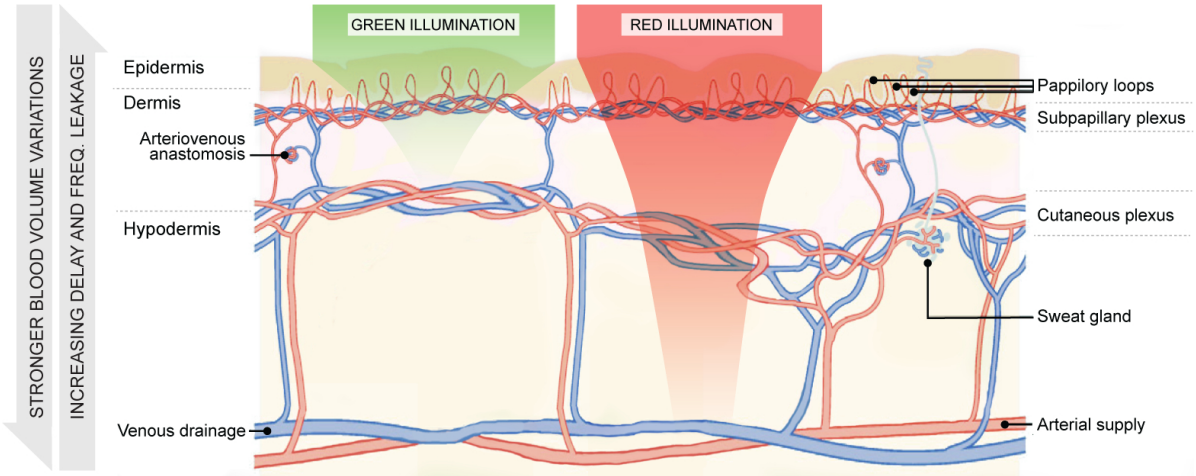


Figure 3.7: [62] Visualisation of penetration depths of green and red light reflective PPG.

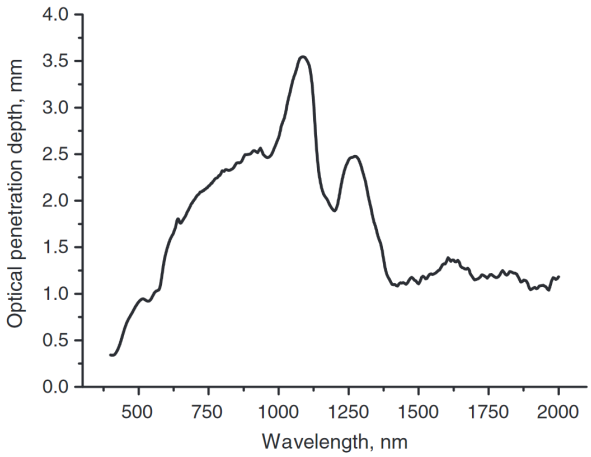


Figure 3.8: [23] A plot of all optical penetration depths of light into the human skin over a range of wavelengths of the electromagnetic spectrum (400nm to 2000nm).

[23]. Reflective PPG on the other hand relies on the reflected light that is sensed by the photo-detector, which would then be more of a "two-direction" situation. Calculating the penetration depth of reflective PPG is a complex process involving scattering, reflection, absorption and distance between the light source and photo-detector, and could also differ with skin pigmentation. Since no clear model for defining penetration depth of green reflective PPG has been found it is assumed that taking a third of the normal penetration depth as shown in figure 3.8 is assumed to be a good estimate. This is based on taking half of the penetration depth due to the round trip that photons have to travel before being detected by the PPG sensor, including a safety margin since the travel of photons from the light source to the photo-detector might not be a very straight path due to scattering. It is therefore assumed that a penetration depth for reflective green light PPG of $\frac{1}{3}$mm to $\frac{3}{4}$mm is a good estimation.

The three main layers of the skin have a different thickness [23], which can vary somewhat between subjects and body locations:

- Epidermis: *100 $\mu m$*
- Dermis: *1 mm - 4 mm*
- Hypodermis: *1 mm - 6 mm*

Recalling that for CRT measurement it is key to have a penetration depth that only measures the capillary blood volume changes in the dermis, the penetration depth should be at least 100 $\mu$m in order to surpass the

non-vascular epidermis. The penetration depth should not surpass the dermis, as the dermal capillaries are of interest here. The minimal thickness of the dermis is 1 mm, so in total the maximum penetration depth of the PPG light should be 1.1mm. This all corresponds well with the earlier defined penetration depth of green light PPG, and the visualisation in figure 3.7.

It can be concluded that green light reflective PPG is the most optimal choice for CRT measurements, due to its optimal modulation, SNR and penetration depth.

#### Compression: consistent force, time and contact surface

One factor that causes variability when assessing CRT, is the compression phase. More specifically, the pressure (a combination of force and contact area between the compressing object and the subject's skin) and the total time of compression are factors that cause variability.

Currently, there is no universal agreement on the optimal duration of the compression phase. Studies have shown that shorter compression can lead to shorter CRT, but no significant differences have been found between durations of 3 seconds and 7 seconds [65]. For this reason, a compression duration of *5 seconds* is chosen as the standard, leaving a 2 second error margin both ways. This is regarded sufficient for the CRT-PPG method, and would even allow manual compression in terms of timing.

In terms of applied force, there are no strict guidelines. Guidelines indicate that a "moderate" pressure should be applied [65], which should be just enough to cause blanching in the fingernail of the *examiner* [15]. Studies have shown significant differences in CRT when different amounts of force are applied during compression [19], but this does not indicate an optimal amount of pressure. Another finding states that lighter amounts of pressure eventually result in less variability [65]. This is wanted as any cause of variability other than dehydration should be mitigated. With this in mind, the amount of force should be determined by analysing the PPG waveform signal during compression. Knowing that in essence the function of the compression is to empty the dermal capillaries, it is defined that the optimal compression force is the minimum amount of force needed for the pulsatile component of the measured PPG waveform to become unobservable. This would namely mean that that part of the skin is not being perfused, and capillaries are therefore being emptied by the externally applied pressure.

For a clear distinction of the compression phase with the pre- and post compression phase (the CRT phase), it is key that the force should applied and released very promptly. If the force is for instance released slowly (for instance when it takes 0.5 seconds), it might have effect on the characteristics of the capillary refilling process. The transient response of the person (or actuator) applying the force should therefore have a very high response time, with a very rapid transient response. The steady state should ideally be reached within a few milliseconds.

In terms of optimal area of the contact surface embedding the PPG sensor, no guidelines or literature has been found that give an indication. Reasons for this might be that CRT testing is often done manually using the finger of the examiner, of which the surface area can of course not be controlled. As a starting point, it is taken that the surface area of the probe should be similar of that of an adult human index-finger. The most important requirement would however be that the contact surface area is consistent in every measurement to prevent variations due to this contact area.

Concluding the requirements for the compression appliance should thus be that the *duration* should be 5 seconds, the *force* should be just high enough to make the pulsing component of the PPG signal disappear, and the *surface area* of the probe should be similar to that of an adult human finger. For a consistent force, either electronic feedback is needed based on readings from a force sensor, or a mechanical spring-system needs to be set in place that guarantees a fixed amount of force applied to the skin during the compression phase when the device is used.

#### Parameters of interest that can be derived from the PPG signal

When assessing CRT using a PPG sensor as described in the previous paragraphs, there are several ways to do this analytically. Visually, CRT would be defined as the moment when the colour of the skin has return to its original "pinkness", or when it is at the same level again as the surrounding skin. With PPG, a lot more parameters can be drawn from the recorded signal. It has to be experimentally derived which parameters are in closest correlation with dehydration. A quick recap of the key components of the PPG-signal: the AC-component, which consists of the "high" frequency pulsating waveform (in rest approximately 1 Hz),

which is on top of the DC-offset, which is the low-frequency, more static, component of the PPG signal. The DC-component change in the seconds after the compression phase should consist of the capillary refilling process as observed visually when conducting the manual CRT test.

A clear distinction has to be made between the different phases of measuring CRT: the *pre-compression phase* for recording a reference before compressing, the *compression phase* which consists of 5 seconds of pressure on the skin, and the *Capillary Refill phase* (CR phase)which records the capillary refill process after release of pressure.

The proposed parameters are summarized in this section:

- Time of when the signal of the CR phase reaches the initial DC level from the pre-compression phase [55]:
  * IF $f_{[DC]}(t_{[CR\,phase]}) \approx f_{[DC]}(t_{[pre\,compression]})$,
    $t_{[CR\,phase]} - t_{[start\,CR\,phase]}$
    (time when DC is back at its initial level)

- Time of reaching the maximum DC level after the compression phase [55]:
  * $f'_{[DC]}(t) \approx 0$
    (when DC reaches a peak)

    AND

  * $f''_{[DC]}(t) << 0$
    (When DC decelerates)

- Time of reaching a stable, horizontal DC-offset after releasing pressure :
  * $f'_{[DC]}(t) \approx 0$
    (when DC reaches a peak)

    AND

  * $f''_{[DC]}(t) << 0$
    (When DC stops accelerating or decelerating)

- Time between the maximum DC level of the capillary refill process to the initial DC-offset [55]:
  * $t_{[DC\,CRT=DC\,initial]} - t_{[DC\,max]}$
    (Time difference)

- Exponential model of Capillary Refill Process [56]:
  * $\hat{y} = y(0) - A * e^{\frac{t}{T}}$
    (An exponential model that should be fitted on the data, with $\hat{y}$ = the fitted model, $y(0)$ = starting value of CRT, $A$ = steady state value, $t$ = x-axis value [time], $T$ = exponent parameter defining rapidness of exponential growth.)

- In an existing (patented) concept of a hydration sensor using PPG, other features are extracted from the PPG signal without using CRT [60]. These features could be extracted from the *AC-component* in the *pre-compression phase*:
  – Magnitude and frequency of the *primary harmonic* of the waveform, which is the *pulse quality* and *heart rate*.

- *Root Mean Square* (RMS) value of the waveform.
- *Maximum derivative* values of the waveform, f'(t) and f"(t).
- *Systolic peak-to-peak value* (prior minimum to maximum) of a pulse.
- *Crest factor*, or in other words the *systolic peak-to-peak* to *RMS* ratio).
- *Peak to Average Power Ratio* (PAPR) (crest factor$^2$)

Since this is a quite extensive list of parameters, which would all require a different algorithm to be extracted from the data, a choice of the key parameter to investigate has to be made for this experiment. This will eventually depend on the characteristics of the data that the PPG equipment of choice will acquire, such as the DC-component, modulation, or resolution.

It can however already be concluded that all of these parameters have a shared requirement for the PPG sensor of choice: the *"raw" PPG signal* has to be used in order to analyse the DC-component of the signal, or the unamplified AC-component. Usually, PPG is merely used to assess the AC-component (such as in pulse-oximetry). The AC-component is usually just a small percentage of the full signal strength. For this reason, in more conventional equipment, the signal is band-pass filtered, in order to filter out the DC-component and any high-frequency noise. The remaining AC-component is than amplified as such that the resolution is optimal, since the amplitude of the AC-component could vary over time or between subjects. Therefore the amplification of the system is actively adjustable. This is sometimes also done by actively adjusting the brightness of the light-source.

It is thus key to look for a PPG probe that is capable of returning a PPG-signal which is not high-pass filtered, in order to conserve the DC-component. Also the amplification of the signal needs to be static (non-adjusting), as well as the intensity of the light-source.

#### Additional measurements: Reference PPG & Temperature

Since it is known that *core-temperature*, *skin-temperature* and *ambient-temperature* all possibly contribute to variations in CRT, it should be able to measure these parameters simultaneously while recording CRT. Recording these parameters should give insight into the magnitude of their influence on CRT. Ideally, ambient temperature is kept at a constant level to prevent any variation due to this factor, but core-temperature and body-temperature are difficult to keep at a constant when the subject is exercising in a warm environment. Therefore these parameters should be measured, ideally simultaneously as measuring CRT, otherwise subsequently using dedicated equipment.

In order to compare the CRT signal as recorded by the PPG device, it should be compared using a *reference PPG signal*, recorded nearby the body location where CRT is measured. This should ideally be a normal PPG waveform, without any influence of the CRT process. The main benefit of using this reference PPG signal is to be able to cancel out any unwanted variations or drifts that can be seen on both PPG signals, such as the high frequency pulses or low frequency drifts such as Trabe Hering Mayer waves (which are small low-frequency variations in blood-pressure). This reference signal would therefore enable a filtered CRT signal, with a clean trend-line showing the unaffected capillary refilling process.

#### Body locations: Fingertip, Chest, Forehead

As discussed, the areas of the *chest* (on the sternum) and the *forehead* are of main interest, due to their profound advantages which are discussed in section 3.2.3. It is hypothesized that skin pigmentation levels would be less of an issue when using PPG, although it is known that melanin also absorbs a large part of green light. Still this should not be much of a problem, as it would only have influence on the signal-to-noise ratio, but not so much on the characteristics of the CRT curve. The tip of the index finger should also be measured, for purposes of possibly integrating any final concept device into existing pulse-oximetry clips. The requirement here is therefore that the used PPG device should be able to measure these three sites.

#### Used equipment

In the search of a PPG device that satisfied all these requirements (green reflective PPG that delivers "raw" data, able to guarantee a consistent amount of pressure at a consistent duration at every compression phase, measure the different kinds of temperature and a reference PPG signal, and is able to be used on different parts of the body), none of the currently available (experimental) PPG equipment lived up to these essential requirements. Therefore it was decided that a proof-of-principle device needed to be prototyped that fully complied to these requirements. A detailed prototyping report can be found in section 3.4.

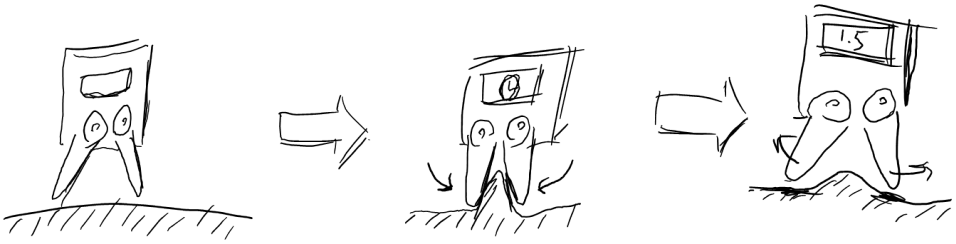


(a) An embodiment where two arms effectuate a pinching process. The subsequent recoil movement is measured with the same arms.

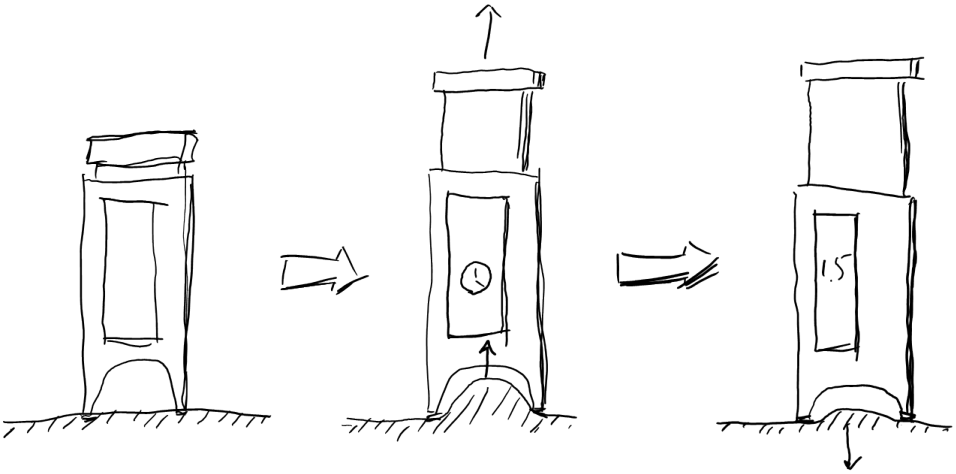


(b) An embodiment where a negative pressure is applied on a section of the skin, pulling the skin up. Release of the negative pressure causes recoil, which is then measured.

Figure 3.9: Idea sketches on how to measure ST.

### 3.3.2. Skin Turgor - Cutometer

Same as with the equipment that would be dedicated for CRT measurement, a number of required features specific to equipment use for skin-turgor assessment would be defined. 3.2.3.

#### Sensor & actuator type: undefined

In the conclusion of the literature study in section 2.4, the DCRT prototype developed by Kieser et al. [53] was considered the most suitable methods together with PPG-CRT. Here a camera was used to record the skin-pinch test for retrospective analysis. Yet, in contrast to PPG-CRT, the type of sensor was not specifically noted as the best option for ST measuring. 3D image might for instance improve sensory accuracy of any concept for ST. Next to optical sensing, ultrasound distance sensing would also be an option [32], or even a way where displacement of the skin could be sensed by mechanical (displacement) sensors (figure 3.9a).

Sensing is not the only factor that still has a lot of design options available, since for mechanical property measurements some form of actuation is also necessary. In the prototype of Kieser et al. [53] it still consisted of a manually performed skin pinch. As described in section 3.2.3 one of the assumed factors of unwanted variability is the pinching process, so it is believed that this process should ideally be automated in order to make it more consistent between measurements. Ways of actuation would then not be limited to a pinching process, but could also be effected using suction [32], like the Cutometer in appendix C [2]. In such a device also different ways of sensing skin movement are possible, such as ultrasound distance measurement, or air displacement. Applying torsion to the skin could also be a potential method, or vibrational perturbations.

#### Sensory penetration depth: dermis

Regardless of the type of sensor, the sensory depth of penetration in order for the device to make the right measurement should be focussed on the dermis. As described in section 3.2.3 the visco-elastic properties of the dermis are the properties of interest when addressing ST. Measuring the epidermis and the hypodermis should therefore be minimized. In practice, this means that a very specific amount of skin should be actu-

ated: too little and the influence from the epidermis would be too great, but too much and the influence from the hypodermis would be too great, although in the latter case the influence of the epidermis would be minimalized. Although depth of penetration is clear based on the thickness of the skin layers (see section 3.3.1), the appropriate amount of skin to address highly depends on the type of actuation.

In this experiment the short term hydration changes are expected to cause changes in the dermis, and the sweating would possibly cause changes in the epidermis (due to absorption). The hypodermis on the other hand is not expected to undergo drastic changes within the short amount of time, so for the sake of trying to detect a trend line of ST changes with progressing dehydration a larger penetration depth would be preferred over a smaller penetration depth.

#### Additional measurements: Temperature

Measuring temperature parameters should be done for similar reasons as with PPG-CRT (section 3.3.1). In this case, skin-temperature is expected to be the main cause of unwanted variability compared to core-temperature and ambient-temperature. Still these temperatures are also still considered, as no dedicated skin-temperature device has been used in this experiment, which means skin-temperature measurements could be inaccurate.

#### Body locations: Back of the hand, fore-arm, chest

To be more specific, the following locations will be addressed for ST assessment: the first dorsal interosseous (between the thumb and index finger), the anterior fore-arm, and the medial chest sternum level. These locations are chosen due to their relatively thin hypodermis (at least for the back of the hand), and mobility (the skin is relatively loose an can be easily pulled up. It is important for each iteration to address exactly the same spot, so at the first iteration the spot should be marked. In the end the device should thus be able to work on all of these body locations.

#### Used equipment

It was suggested by contacts from within Philips Research to use the *Cutometer* for ST measurements, of which the brochure can be found in appendix C [2]. It is currently considered to be the standard for measuring "*visco-elasticity*" of the skin, and is mainly used in cosmetic research. Yet, the working principle resembles the skin-pinch test quite well, while it can sense skin deformation with a high sensitivity.

The working principle is quite simple, yet elegant. See figure 3.10 for a visualisation of the working principle. The Cutometer probe is a cylindrical probe with a hollow chamber inside. The probe is placed on a section of the skin of interest. The tip of the probe is suspended by a spring system that effectuates a stable pressure on the skin, to minimise motion artefact. Negative pressure can be applied on the chamber, according to a programmable sequence of negative pressure inputs (up to 500 mbar). Negative pressure pulls the skin up inside the chamber. The perpendicular displacement of the skin is then sensed by a light beam, which is reflected by a set of mirrors inside the probe. The higher the skin is pulled, the more it will block the light beam. Consequently less light will fall upon the photo-detector, by which the displacement of the skin up in the chamber can be measured with a resolution of 1 $\mu$m and at a sampling rate of 100Hz. The application of negative pressure and normal (ambient) pressure can be sequenced as such that it simulated a serie of very well controlled skin-pinch tests, by pulling the skin up for a few seconds (negative pressure), and allowing it to recoil for a few seconds (normal pressure).

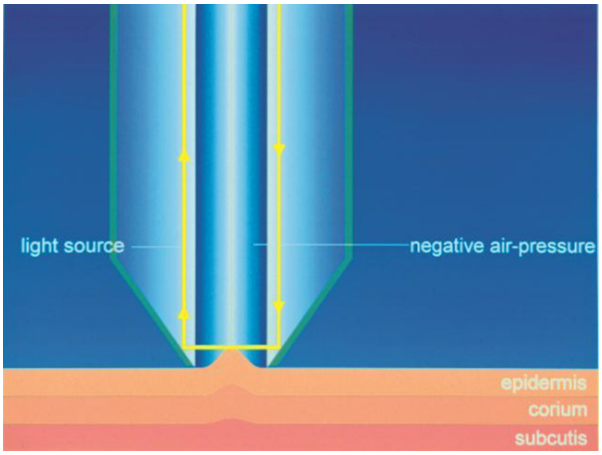


Figure 3.10: Working principle of the Cutometer. Source: `http://www.courage-khazaka.de/index.php/en/products/scientific/140-cutometer`

A very convenient option with the Cutometer for this particular application is that the aperture size of the air chamber can be modified between 2 mm and 8 mm in diameter. A wider aperture would give a deeper measurement of the skin.

Another point of convenience of using the Cutometer is that the software package automatically translates the raw data of the skin-displacement to 19 different parameters that all in their own way are related

to the elastic or viscous response of the skin to the perturbations. These parameters are considered to be "*semi-scientific*", as they don't return any values in engineering terms, such as Young's-modulus. Yet, these parameters are expected to be very useful as they are expected to show a trend with progressing dehydration. Below is the list of parameters that are expected to be most significant for this experiment:

- *Q1 (=QE/Q0)*
  - This value decreases as the elastic recovery of the skin after release of the vacuum also decreases in velocity, so it is directly related to skin elasticity.
  - It is expected to be inversely related to dehydration
- *Q2 (=QE/Q0)*
  - This value decreases as the viscolelastic recovery of the skin after release of the vacuuem also decreases in velocity, so it is directly related to skin viscous-elasticity.
  - It is expected to be inversely related to dehydration
- *Q3 ((=QE+QR)/Q0)*
  - Combined the two parameters given above, so if both Q1 and Q2 show significant effect from dehydration Q3 might be even better related.
  - It is expected to be inversely related to dehydration

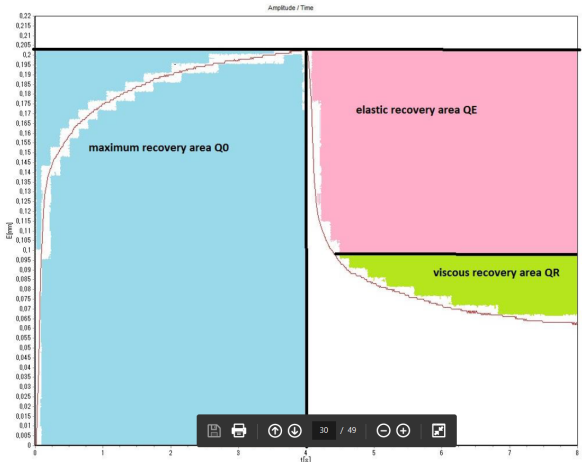


Figure 3.11: Plot of typical Cutometer data, indicating Q-parameters. Source: Cutometer manual.

- *F1* (area below recovery line, above recovery value after recovery period which is fixed)
  - Closely related to Q3, smaller values should be read when the skin retracts more slowly.
  - It is expected to be directly related to dehydration
- *F0* (area above vacuum line, under value when vacuum is released)
  - The more elastic the skin, the closer to 0 the value should be.
  - It is expected to be directly related to dehydration

- *R0* (*Uf*, maximum "stretch" or "passive behaviour" of the skin to the vacuum)
  - The displacement of the skin in response to the vacuum is another measure of the "elasticity" of the skin, but based on applied force instead of force release. Could be a bit dependent on the individual subject's skin characteristics.
  - Relation to dehydration is expected to be inverse
- *R2* (*Ua/Uf*, gross elasticity, the higher the value the more elastic the curve)
  - According to the manufacturer a very important parameter, as it indicates gross elasticity. It is the ability of the skin to return to its original position within a certain amount of time, expressed as a

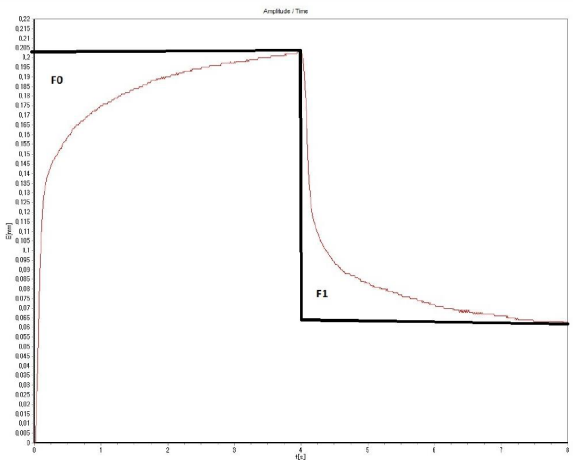


Figure 3.12: Plot of typical Cutometer data, indicating F-parameters. Source: Cutometer manual.

ratio of the total displacement in when the vacuum was on. It is related to the skin turgor test in the sense that it measures not the speed but the ability of the skin to recoil.

– Expected to be inversely related to dehydration.

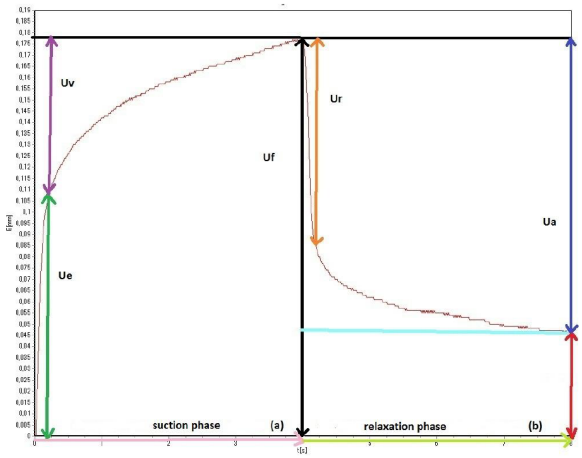


Figure 3.13: Plot of typical Cutometer data, indicating the arguments for defining the F-parameters. Source: Cutometer manual.

The full list of parameters can be found on the second page of appendix C [2].

In collaboration with the manufacturer of the Cutometer, the following sequence has been programmed for this experiment:

- A "square wave" will be used for negative pressure control inside the air chamber (a on/off sequence). The "on-time" will be 4 seconds in order to let the skin fully stretch out before release (under negative pressure), and the "off-time" will be 5 seconds to assure that the skin gets enough time to "fully" recoil (under normal pressure). This on/off sequence is repeated 3 times per go for better accuracy.
- An aperture size of 8 mm is chosen in order to have a maximum depth of measurement. It is assumed that this is large enough to fully measure the mechanical response of the dermis, while minimising influence from the epidermis. It is not known if this aperture will also cause influence from the hypodermis on the reading, but since the contribution of the hypodermis is expected to be constant throughout the experiment, the expectation is that it will not cause any significant noise intra-individually.
- The negative pressure during the "on-time" will be at 350 mbar. Lower pressures would cause the displacement of the skin to go beyond the sensory limitations of the probe at the chosen aperture size.

## 3.4. Prototyping

It is already established that a PPG prototype will have to be developed for the purpose of conducting this experiment, since no existing device has been found that satisfies the needs for this experiment. In this section the development of the PPG-CRT prototype is reported. The design of the prototype is based on the established requirements from section 3.3.1. The development phase starts with a more condense and complete list of requirements, which is described in section 3.4.1.

### 3.4.1. Requirements

**Technical requirements:**

1. PPG probe should at least consist of 1 LED with an *emission peak-wavelength of between 500 nm and 600 nm* (green light).
2. The photo detector should be placed adjacent to the LED, in order to detect *reflected* photons.
3. At least 2 PPG probes should be used near each other, one for measuring CRT and one as a *reference*.
4. For consistency of the compression process, the CRT PPG sensor should be placed in series with a *force sensor*.
5. The PPG sensors should return a *"raw" signal*. This means that the signal should not be high-pass filtered in order to conserve the DC-component, and signal amplification should be constant and adequate to return a voltage that is suitable for the Analogue-to-Digital converter (ADC) of choice.
6. The most suitable *sampling rate* for PPG signals has been defined to be at least 30Hz in order to get a smooth PPG waveform (determined in consulting sessions with developers with experience in PPG experiments). Any significant high frequency noise above 15Hz should be filtered out using a low-pass filter, hence a Nyquist frequency of $2 + 15Hz = 30Hz$.
7. The *resolution* of the ADC should be high enough to show a distinctive pulse in the PPG signal of at least 10 ADC-levels on top of the DC-component. This is chosen since if the pulse is clearly visible, so will also probably be the capillary refilling process without any significant quantization error. A 12-bit ADC (with possible ADC-values that can vary from 0 to 4095) is considered to be sufficient for this application.
8. The following *data* should be stored either on a PC or any other external storage device for retrospective analysis using Matlab or Excel. Data should therefore exist of numeric values, which should directly represent the ADC-reading. Data that should be stored per column are (but should not be limited to):
    - A *timestamp* per data sample in *milliseconds*
    - Raw PPG data for *CRT* analysis (ADC-value)
    - Raw PPG data from the *reference* probe (ADC-value)
    - *Force reading* from the force sensor (ADC-value)
9. In the pre-compression phase and capillary refill phase, the pressure that the PPG probe exerts to the skin should be *minimal and constant*. Minimal pressure is defined as the pressure where a pulse is clearly visible in the PPG signal, while the contact is tight enough to minimise any motion artefact.
10. In the compression phase, any force that is exerted to the CRT-probe should not interfere with the reference probe. The reason is to keep this signal free of *artefacts*, so that it can be used to cancel out unwanted features from the CRT signal.
11. The CRT probe should be able to withstand external *forces* up to 20N (including a 100% safety margin), while the force sensor should be able to measure forces up to 10N. Reason is that 10N is considered to be sufficient force to blanch the skin.

**Use:**

1. In this first embodiment of the prototype it was chosen to apply force *manually* on the PPG probe. To keep the compression phase consistent, the device should feature an interface that provides feedback to the user on the force and timing of the compression, based on the reading of the force sensor. It is assumed this would be sufficient, as *very minor* variability in compression force would not have a significant effect on CRT.

2. The PPG probe that is in contact with the skin of the subject should not consist of any toxic materials, and should be made *water-proof* to prevent shorts due to sweat.

3. The format of the data should be easily convertible for use with *Excel or Matlab*.

4. All signals should be able to be plotted in real time. The main benefit of this would be for the examiner to check whether all the sensors are placed correctly. For the PPG probes this would mean that a pulse is clearly visible.

### 3.4.2. Concepts

In appendix D a series of concept sketches can be seen. These are some results of an ideation session for different answers on the question: "*How can you compress the skin with a very consistent force and release force very promptly?*" It was chosen to avoid the use of electronic actuators for now to save time of prototyping. It is also considered that a final concept should eventually be able to work without the use of actuators if possible, as this would increase the cost drastically. This experiment is therefore simultaneously a test of using manual compression for CRT measurement.

The main types of embodiment found in appendix D are *hand-held probes* or *probes that are fixated to the body* (either using straps, adhesives, or finger-clips). There are also 2 ways of controlling the amount of force defined: using active feedback to the user using a interface with input from a force sensor, or using a spring-system that makes it practically impossible to overshoot a certain compression force. The latter method uses *Hooke's law* ($F = -k * x$), which states that at a certain constant deformation of a linear compression spring from its natural length, the spring will exert a constant force. If the compression of the spring is blocked from a certain point of displacement, this system will assure a constant force.

For this experiment, it has been chosen to use a probe that is fixated to the body, on which manual force can be exerted provided with visual feedback on the amount and duration of force. The reasons for this choice are:

- At the moment there are very few hand-held devices that use PPG sensors. It is therefore unknown whether such a hand-held device would provide a signal that is free of motion artefact due to the movement of the hand of the examiner relative to the skin of the subject. Spring systems would dampen these motion artefacts, but were considered too time-consuming to develop for this pilot-experiment, as well as too uncertain to work in preventing motion artefact. Therefore, the safe method was chosen, being a PPG probe that is fixated to the skin. Ideally the probes would be fixated to the skin using adhesives, since it is assumed that adhesives provide a very stable fixation to the skin of the subject, while at the same time practically exerting no pressure on the skin during the pre-compression phase and capillary refill phase, which is considered most optimal for an undisturbed capillary refilling process. Adhesives are on the other hand probably not possible in a final concept of the PPG device, due to the necessity of disposables (the adhesive membranes can often just be used once). Yet for this experiment they are used for the sake of proving the principle with this prototype. Also, using a clip for fixating the probe would limit the use of the probe to small body parts such as the finger, toe and earlobe. Yet, it was already determined that the main body sites of interest would be the index-finger, sternum and forehead. Therefore the use of a clip would not be possible.

- It was also chosen to use a manual force application which would be controlled by visual feedback using LED's which give information on the adequateness of the amount of force, and when the five second duration of the compression phase has passed. This consideration was made since it would either way (for all compression methods) be necessary to include a force sensor to monitor the applied force. It was also considered already a major improvement to the blanching process to provide feedback whether the applied force is within the allowed range, and to give feedback on when to release the pressure. Any remaining variations in applied force (duration) were considered to be of minimal influence to CRT. Also, using a spring mechanism to control the applied pressure would take more development time, would make the probe more bulky.

Development time was an issue, due to the limited options of periods in which the lab could be used for this experiment.

### 3.4.3. Design

Components
The key components necessary for this prototype are the following:

- 1 micro-controller for signal processing
- 2 PPG sensors, preferably off-the-shelve
- 1 sensor for force feedback
- 1 module for data-storage
- Housing for the data-collection unit and for the PPG-probes
- 5 LED's for user feedback (4 for force feedback, 1 for feedback on compression duration).
- 1 Pushbutton for resetting the device

Each of these components and their integration will be discussed in this section.

**The Micro-controller:** For this prototype it is needed to connect all the sensors and modules into one system and convert all the analogue output signals from the sensors into digital data which can be used for retrospective numeric analysis after storing it. To accomplish such a data collection functionality, a micro-controller is needed. This micro-controller would function as the "brain" of the prototype, and would assemble all separate modules into one product.

There are many different microprocessors available on the market that are suitable for this project. Yet it was chosen to work with Arduino. Arduino builds a variety of single-board micro-processors, and open-sources its hardware and software. This makes it very easy to work with, as there are plenty of example codes available online for use with a large variety of digital and analogue components. The micro-controllers are also relatively easy to programme, making them attractive for designers, artists and students to use in their projects. Also due to lack of experience using any other platform for micro-controllers, and since the task of the controller would be relatively easy (collect and store data), Arduino would be the first choice for this project.

For this project, the main requirement to the micro-controller is that it has a high-resolution ADC. Sampling rate should be at least 30 Hz, but this is easily achieved with any micro-controller. Since there are no other critical criteria to the micro-controller, eventually the *Arduino ZERO* was chosen as the most suitable option. The Arduino ZERO has a similar footprint as the Arduino UNO (which is the most popular model), but has a few relevant benefits to this project such as a higher clock-speed (which leads to a faster possible sampling rate) and more importantly a four times higher ADC resolution (12-bit, compared to the 10-bit of the UNO). In accordance with the team at Philips Research this would become therefore the choice for this prototype.

**PPG Sensors:** In the search for a green light PPG sensor, the Pulse Sensor Amplified came up as a good option (`http://pulsesensor.com`). It is a plug-and-play component (connections: 3.3V in, GND, and Analog Signal Out), consisting of a PCB containing reflective green-light PPG components (green LED, and a photo-diode) and integrated filtering an amplification components (see figure 3.14). The PCB is about 16 mm in diameter, and is therefore considered to be very suitable for use with CRT measurement.


Figure 3.14: Front view of the Pulse Sensor.

The circuit of the Pulse Sensor is designed as such that a highly amplified and filtered PPG signal comes out, with voltage values between 0V an 3.3V or 5.0V, depending on the power source. In the

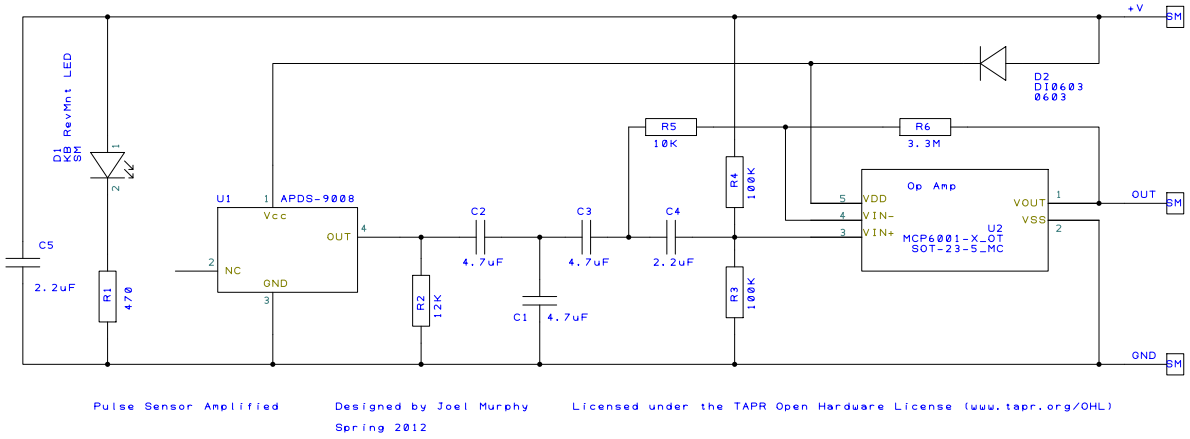


Figure 3.15: Electronic schematic of the used *Pulse Sensor Amplified*. Source: `http://pulsesensor.com/pages/open-hardware`

schematic (figure 3.18) it can be seen that the output signal of the photo-diode (APDS-9008) is first high-pass filtered, before the remaining AC-component is amplified using an operational amplifier. The output signal is a very smooth, high SNR and high amplitude pulse-wave, which is very useful for heart-rate monitoring. Yet in this case the DC-component is of interest. To extract the "raw" PPG signal which includes the DC-component, the circuit has to be probed directly at the output connection of the photo-diode (see figure 3.16a, the orange wire). This method was suggested by the developers of the Pulse Sensor. Testing the signal, it seems that the photodiode already filters out high frequency noise and amplifies the signal based on the input voltage. This can be explained as the photo-diode has a power-source connection ($V_{cc}$), which would be used to power the amplification of the output signal of the photo-diode. Thanks to this small hack, this output signal can therefore be used as-is for this prototype.

To finish off the pulse sensor, hot glue was used on the back for insulation, protecting the cables from mechanical stress and for creating a flat surface to later on adhere to the embodiment of the probe (see figure 3.16b). Also, a plastic adhesive film is placed on the sensitive side to protect the probe from dirt and debris, whilst also insulating it.

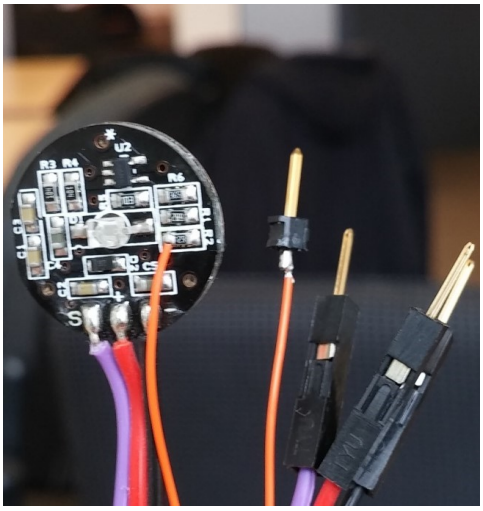

(a) Rear view of the Pulse Sensor, including extra tab for raw-PPG signal.

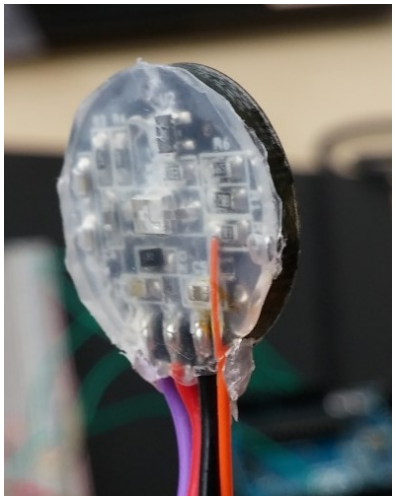

(b) Rear view of the Pulse Sensor, with insulation.

Figure 3.16: Probing and finishing the Pulse Sensor.

**Force sensor:** A *Force Sensitive Resistor* (FSR) is used for force sensing, due to its extremely compact size which makes it easy to physically integrate into the PPG probe, and due to its ease of use. More specifically, the *Interlink Electronics FSR 402* was used due to its size (see the datasheet in appendix E [6]. These FSR's are basically variable resistors that vary their resistance from high to low when applied pressure to their sensitive region increases. When interfaced with another resistor in a *voltage divider* set-up, the voltage between these two resistors can be used as a signal that is proportional to the applied force.

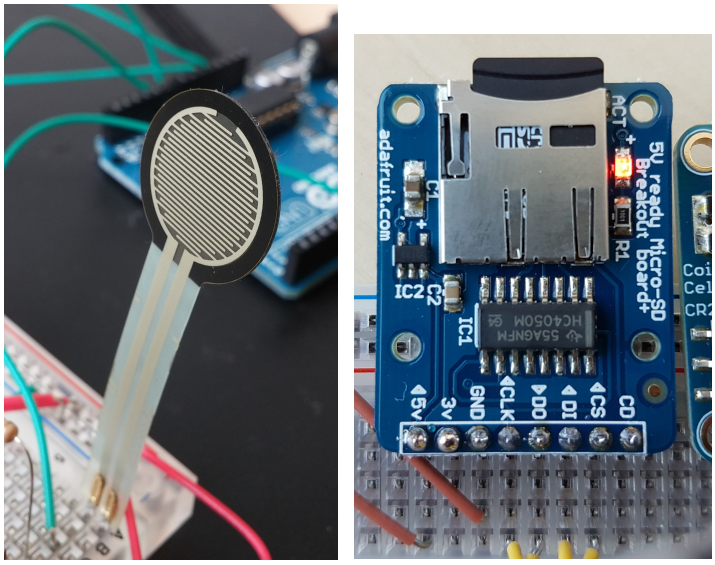


(a) An FSR connected to a bread-board.

(b) Micro-SD module.

Figure 3.17: More components to be integrated in the prototype.

**Data storage:** Data storage could either be done using the serial connection with a PC, or using a data storage module that can be connected to the Arduino. Data storage on a PC was a cumbersome process using the Arduino ZERO, so it was therefore chosen to use the *Adafruit 5V ready Micro-SD Breakout board+* instead. This module can be easily connected to the Arduino board directly, and example codes and libraries for writing data to the SD card are readily available on the internet. Data can be easily stored in .txt files, with values separated by tabs. When the SD card is inserted to a SD-card reader that is connected to a PC, these files can be directly imported into Excel-sheets and Matlab matrices (.mat files). Because of its ease of operation, and the additional benefit that the prototype could store data as a stand-alone device without the need of a PC, this Micro-SD module would be the most optimal choice for data storage.

**Housing, LED's & pushbutton:** Furthermore, 4 conventional 5 mm LED's are used to provide visual feedback to the user on the correctness of the amount of force exerted to the probe: 1 green LED in the middle, and on each side a red LED. The red LED's will light up if the force is either too high or too low, while the green LED indicate that the force is within the predefined boundaries. Another green LED placed on a different location is to signal that the device is turned on, but no pressure is put on the PPG probe. Another green LED is used that blinks during the compression phase, and stops blinking after 5 seconds to indicate that the duration of the compression phase has passed. This is feedback to the user to release pressure immediately. The blinking process is initiated when the sensed force by the FSR exceeds a certain threshold.

The housing of the prototype will consist of a 3D-printed case (PLA) for the data collection unit, and probe casings which house the PPG (and force) sensor. This housing should be able to distribute the pressure evenly over the FSR for a more accurate force reading.

A push-button is interfaced with the reset-line of the Arduino board, in case it is necessary to reset the prototype. This could be necessary for instance when the timer needs to be set to zero, or when an error occurs.

Electrical design
The complete circuit diagram of the prototype is shown in figure 3.18.

- The output of both *pulse sensors* are connected to separate ADC ports of the Arduino. The signal outputs consist of a "raw" PPG signal from the added signal output, and the "amplified" AC PPG signal, which is the intended signal output of the Pulse Sensor. This signal is of interest as is could also be used for pulse-cancelling operations. Since the ADC of the Arduino ZERO can only read voltages between 0V and 3.3V the Pulse Sensors are fed by a 3.3V power input. The power source for the Pulse Sensors comes from a separate coin cell, not from the Arduino. The reason for this is that the other components that are connected to the Arduino (especially the Micro-SD module) drain a lot of the current from the Arduino. This resulted in a lot of noise on the PPG signal due to a very noisy power input from the Arduino. Therefore this problem was solved by using an external power source, which indeed resulted in a smoother signal.

- The FSR is interface as part of a voltage divider together with a 10KΩ resistor. A 10KΩ was chosen since it has a relatively good sensitivity curve to forces between 0N and 10N (see appendix E [6]).

- The LED's are directly connected to the digital outputs of the controller board. The states of these LED's can therefore be controlled by defining their states in the code for the Arduino. These LED states are directly connected to the output of the FSR.

- The Micro-SD module is fed by a 5V power input directly from the Arduino, and is interfaced using the SPI port on the Arduino. The SPI protocol consists of a *Data-In* line for data to be written to the card, a *Data-Out* line to read data from the SD-card, and a *Chip-Select* line to enable the communication between the slave (SD-module) and the master (the Arduino).

- The reset button is interfaced between the reset pin and ground. When the button is pushed, it establishes a connection which pulls the reset pin to ground. This is a signal to an integrated function of the Arduino to restart the board.

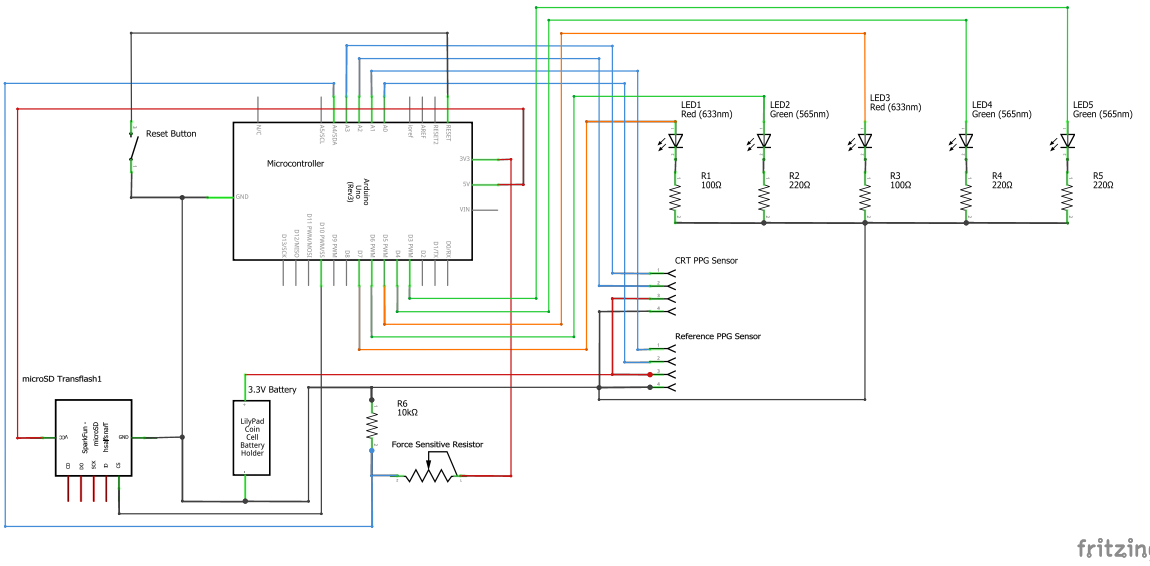


Figure 3.18: Complete electronic schematic of the PPG prototype. Note that the actual micro-controller used in the prototype is an Arduino ZERO, and that the micro-SD module is connected to the Arduino's SPI-lines, which are not shown in this diagram.

Coding
Programming the Arduino was done using the IDE software. This software can be used to write sketches (scripts with tasks for the Arduino), and can then be uploaded to the Arduino board after it is automatically converted to C++ code. The full sketch can be found in appendix F.

It basically consists mainly of a loop (void loop) that keeps running while the Arduino board is powered, with a speed of about 30 iterations per second. During each iteration of the loop, the sensor inputs from the ADC's are read and send to the PC for plotting the values. Also, every loop a time-stamp is defined for that iteration based on the amount if milliseconds since the loop started, which is when the prototype was turned on. The sensor data and timestamp is stored to the SD-card every loop to a .txt file in a new line of data at every iteration. In addition, based on input from the FSR, the state of the LED's is determined at every iteration of the loop for force feedback to the user.

The signals are stored mainly as their raw ADC values, only the raw PPG data is somewhat adjusted. The values are converted from the voltage output (0V-3.3V) of the photo-diode to ADC levels. As more photons are sensed by the photo-diode, a higher voltage output is the result and therefore a higher ADC-value. This would be inversely proportional to the blood volume changes in the dermis, as with higher blood-volumes more green light photons are absorbed by the blood. To make the stored "raw" PPG data directly proportional to the blood volume changes, each ADC reading of this signal is mirrored around 2048 (the middle of the range of ADC levels). This small adjustment makes the signal more intuitive to read.

Embodiment

A 3D printed case, consisting of 2 interlocking shells (figure 3.19), is used as a housing for the micro-controller and the PCB board on which all components are soldered. This is the main control unit, and also contains the LED's for visual feedback and the reset button. The probe consists of a 3D printed piece (figure 3.20) that

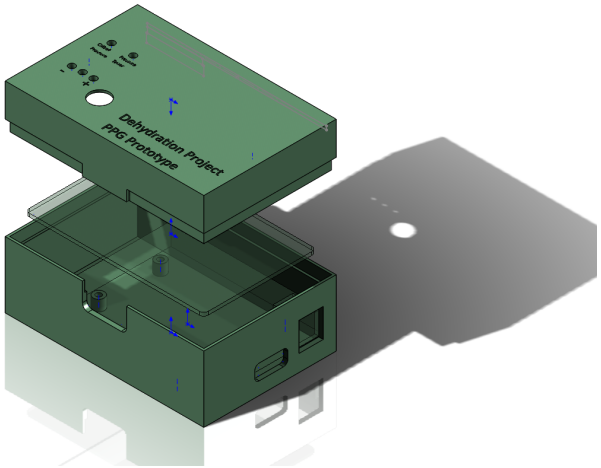


Figure 3.19: Solidworks model of the control unit housing.

serves as a cap that distributes the exerted force evenly over the probe. This is partly to reinforce the probe, and to improve the accuracy of the FSR in the CRT-probe. To assemble the probe, double coated foam tape

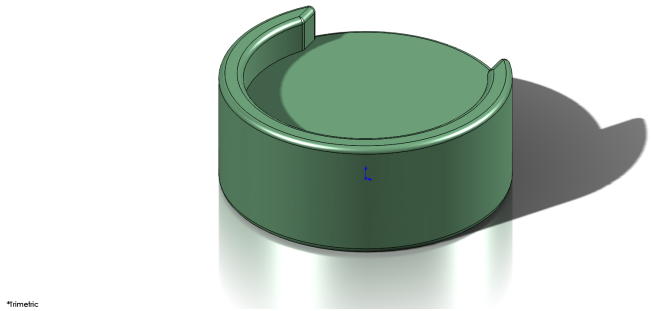


Figure 3.20: Solidworks model of the Probe piece.

was used to adhere the FSR to the 3D printed part. The same tape was used again to than adhere the Pulse

Sensor to the FSR. The foam should help to evenly distribute the load to the FSR. It should also act as a flexible mount, that should make the PPG probe somewhat compliant if the load on the probe is not perfectly in the middle or perpendicular. A little compliance would prevent bad contact with the skin. To close everything off and to water-proof the probe, hot glue was used for the edges between the components and the housing. The same steps are taken for the assembly of the reference probe, although the FSR is not integrated in this probe. See figure 3.22 for a look at the final realisation of the prototype. Finally, using two-component glue

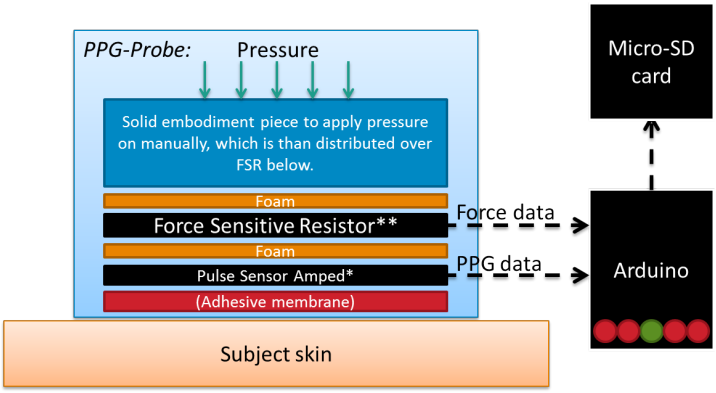


Figure 3.21: Schematic view of the CRT prototype (without the reference probe).

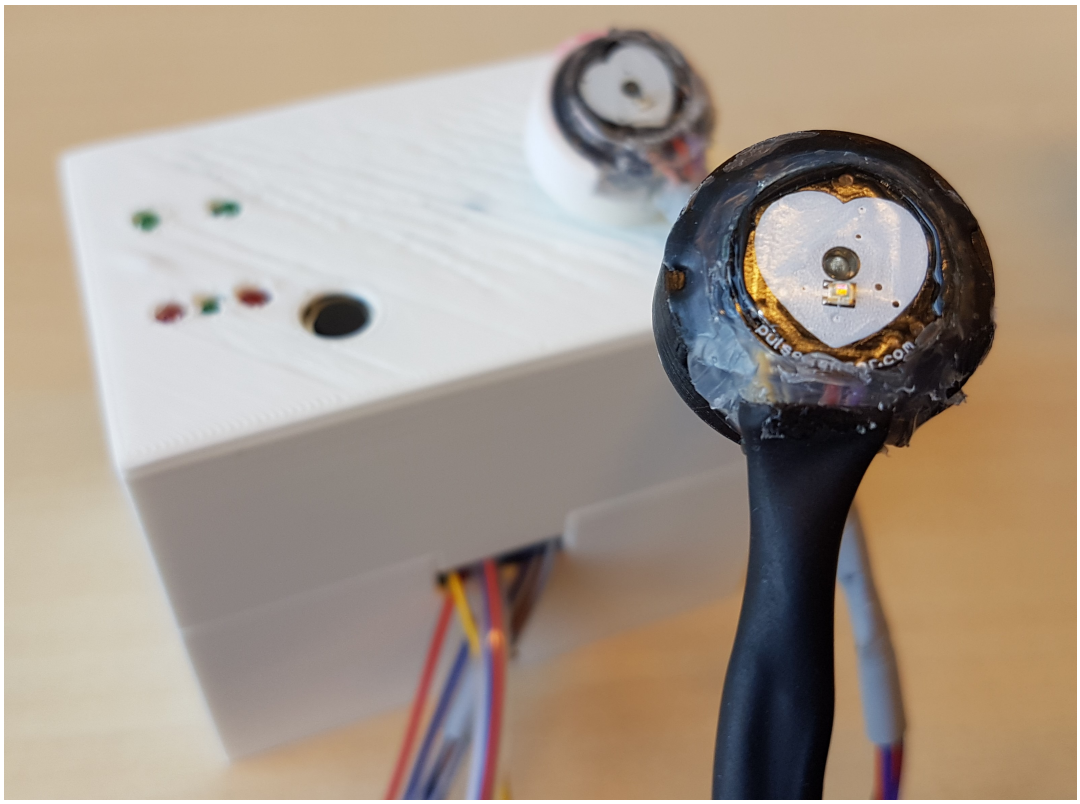

Figure 3.22: The final physical prototype.

the *hooks* component of a *Hook and loop fastener* (Velcro) is glued to the back of the probe. It was initially the case that double-coated adhesive film would be used with a hole in the middle to allow light to pass. As described earlier, this method of fixating the probes to the skin would be ideal for experimental reasons due to the negligible pressure during the capillary refill phase. As the experiment date had to be moved to an earlier time, the delivery of these adhesives would not be in time. Therefore, option B was chosen for now, which involved the use of straps.

The straps used consist of elastic material that sticks to the Velcro on the PPG probes. This velcro thus prevents the probes from moving around when applied on the skin. 4 straps were created for this experiment: 1 large strap that fits around the chest for measuring PPG at the sternum level, 1 smaller strap for the head, and 2 separate smaller ones for measuring at the finger (1 for each probe). The 2 larger straps are also wider to be able to fit 2 probes next to each other. A small cut along the strap between the attachment areas for the probes prevents influence from the compression of the CRT probe on the reference probe. The downside of using these straps is that a minor constant pressure on the probes is necessary to keep the probes fixated and to prevent motion artefacts due to slipping. Also, this constant pressure needs to be consistent at every measurement, even if the straps are removed in between measurements. To overcome this problem, the straps are adjusted to the size of the subject before every experiment. If the probe is tight enough, but doesn't cause the PPG AC-component to disappear due to blanching, the size of the straps are considered to be just fine. This fitting of the straps is also done using Velcro, so these Velcro contact points should not be taken apart until after the experiment to prevent differences in pressure at different measurement moments.

### 3.4.4. Validation

During development, a few tests had been performed to validate the working of the prototype. The main areas of focus were the calibration of the FSR and validating the use of the Pulse Sensor for CRT measurement.

Validating the Pulse Sensor

**Expectation:** Based on the knowledge of the blood fluid dynamics during the compression phase and capillary refill phase, the following expectation can be defined in terms of PPG signal behaviour during these phases. When the PPG-probe is placed on the skin, in this case on the finger, during the pre-compression phase a normal PPG wave-form is expected, consisting of a barely varying DC-component and a pulse wave-form on top of that. When pressure is applied on the sensor, the sensor transfers the pressure to the skin, which in turn compresses the dermal capillaries and empties them of any blood. The decrease of blood would result in less photons being absorbed by the blood, and therefore more protons being reflected into the photo-diode. As the signal value is mirrored by the Arduino, the expectation is that the plotted data would show a decreasing trend during the compression phase. Once the pressure is released, the capillaries start refilling with blood, which means over the course of a few seconds the amount of light that is absorbed would increase, which results in an decrease of reflected light over time which is plotted as an increasing trend in the PPG signal. This growth process should reach a steady state within a few seconds, which should be as approximately the same level as in the pre-compression phase. The growth process is expected to show approximately an exponential curve. This process is again visually explained in figure 3.23.

**Validation:** In figure 3.24 the plot of a sample of the validation runs with the sensor is shown. It is representative to most CRT tests performed on the pulp of the index finger with the Pulse Sensor. A clear distinction can be seen in the 3 different phases of the CRT measurement. The signal behaves very much as expected earlier. One notable observation is that the signal seems to hit an almost horizontal bottom quickly after starting the compression phase. This was not expected, but it is hypothesized that it could be explained by the capillaries being fully emptied rather quickly. The capillaries are unable to be emptied further, so with continued pressure the signal does not change much until the release of pressure. In this sample the capillary refill phase signal has a steady-state which is approximately the same as in the pre-compression phase. This is not always the case due to very low-frequency variations in the DC-component. These variations are hypothesized to be caused by the *Trabe Hering Mayer waves*. It is not expected that these slow trends in DC-values would have much of an effect on the CRT, but they should be easily filtered out by *detrending* or carefully *high-pass filtering* the signal if needed, without affecting the capillary refill trend.

One of the concerns was that usually the *current* output of a photo-diode is used instead of the *voltage* output in these applications. The reason is that current output of these photo-diodes is much more linear to sensed light intensity compared to voltage. For this reason, the current is often first converted into a voltage, using an operational amplifier. This is what is happens at the op-amp in figure 3.15 on the right side that outputs the amplified signal. Yet, surprisingly, the "raw" signal output tapped directly from the photo-diode already outputs a seemingly very linear signal compared to light intensity. When looking up the data-sheet of the *Avago APDS-9008 photo sensor*, it was made clear that this sensor is not a conventional photo-diode. The suggested current to voltage conversion would be done using an external resistor (and capacitor for noise filtering) that is connected from the sensor-output to ground. By converting the current to voltage using that method, the output of the sensor can be directly read with the ADC. Looking at figure 3.15, it can be seen that

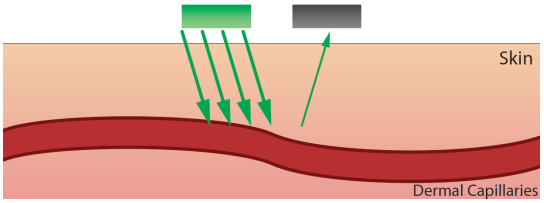


(a) When the PPG sensor is placed on the skin without substantial pressure that compresses the dermal capillaries, a normal PPG waveform will be observed.

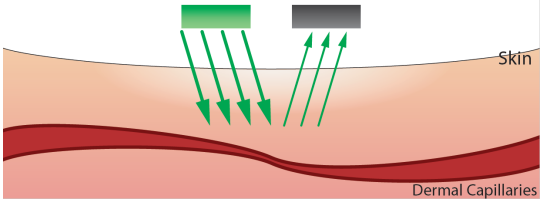


(b) A homogeneous pressure is applied on the skin by the PPG sensor, emptying the capillaries. Less blood is in the capillaries, so more photons are reflected into the photo-diode. The photo-diode outputs a stronger current.

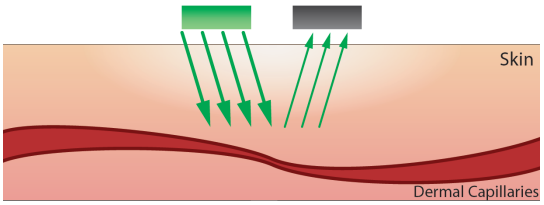


(c) The moment the pressure is released, the capillaries are still empty. Therefore many photons are still reflected into the photo-diode which returns a strong current. From this stage the capillaries start to refill.

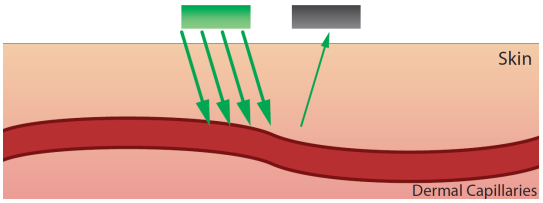


(d) After a few seconds the capillaries have fully refilled, so more light is absorbed by the blood and less is therefore reflected. A weaker current from the photo-diode is the result. the observed signal should be similar now as in figure 3.23a

Figure 3.23: A visualization of the process of the CRT test using PPG. The green block represents the green light source, and the black block represents the photo-diode.

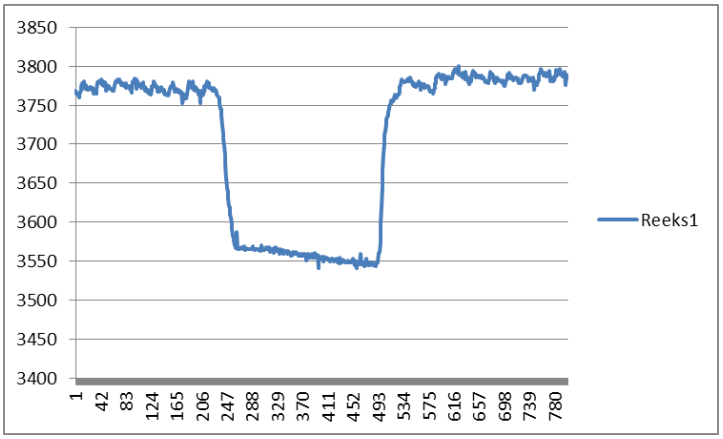


Figure 3.24: Observed CRT data from the Pulse Sensor

R2 is the load resistor, and c1 the capacitor that are connected to ground. It is not fully understood how this specific method of voltage-to-current actually works, but it does explain why the voltage output that is read using the ADC is linear to the light intensity. Also the fact the the voltage is able to range between 0V and 3.3V can be explained by the fact that the sensor has a power input of 3.3V, and in the datasheet it can be observed that the sensor houses an internal amplifier.

Calibrating the FSR

The data-sheet of the FSR (appendix E [6]) provides some expected force-to-voltage curves for different voltage-divider set-ups. In this case it was chosen to interface the FSR with a 10KΩ resistor. Since it is known that the response of FSR's can vary depending on many different factors (temperature, drift, force distribution, etc.), it was chosen to perform a quick calibration test. Another reason to perform this calibration is that when the FSR is integrated into the probe, the force might be differently transferred to the FSR.

The main set-up of this test was to take a variable weight (a bottle of water in this case), and measure the voltage response of the FSR when the load is exerted to it. The mass of the bottle is weighed using a *microbalance* with an accuracy of up to .01g, assuring a very precise amount of mass. The bottle with the exact amount of mass noted is placed on the PPG probe (with the FSR already integrated), and held in placed by hand for 10 seconds. This process is repeated for a number of masses between 0g and 2000g. The recorded ADC values are imported in an Excel-sheet for analysis, with the weight (in Newtons) to ADC-value curve in figure 3.26 as result.

In this figure the curve is clearly visible, although some drift is also visible which can be seen in the standard-deviation lines. It can also be seen that this drift decreases in its proportion relative to the actual amount of load when the load is bigger.


Figure 3.25: The mass of the bottle being determined using a micro-balance.

Now that the load to voltage curve has been established, the amount of force needed to blanch the skin has to be experimentally derived. This was done by placing the probe (with the integrated FSR) on the skin, and slowly manually increasing the pressure. At this stage a 12-bit ADC was used, so ADC levels from 0 to 4095 were possible. It was seen that using this probe, a quite substantial amount of force was needed to completely block the pulses, which is regarded here as the minimal amount of force to completely blanch the skin. It was seen in the finger-pulp that a the pulses stopped around approximately an ADC level of 3560. This value corresponds to a load of approximately 14N. Since the load will be applied manually, a certain margin of human error needs to be allowed. Therefore it was chosen to take a load of 15N as the aim, with a margin of 1N on both sides, to prevent that the load would ever be below the minimum of 14N during the compression

phase. The green feedback-LED would therefore be on if the load is between 14N and 16N. This corresponds to a 12-bit ADC value between 3560 and 3640.

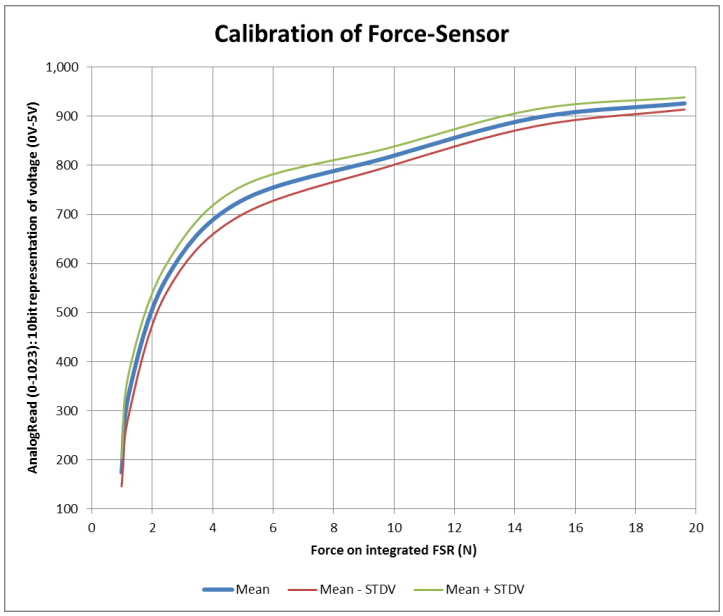


Figure 3.26: Weight to ADC-value curve for the used FSR.

## 3.5. Methods

In this section, the overall design of the experiment will be explained. First a few additional secondary pieces of equipment will be summarized. subsequently a detailed protocol will be described. Than an explanation will be given on how all the data is processed, after which the process of analysing the data will be explained.

### 3.5.1. Peripheral equipment, additional parameters & experimental setting

A few additional parameters will be measured during the experiment, both for safety monitoring reasons and to track any potential factors that could influence the main experimental variables during this experiment. The equipment needed to measure these variables are listed below among other kinds of peripheral equipment. Also an explanation of the experimental setting is given. For a more in depth explanation of why certain safety margins are chosen for some of these parameters, please see appendix G.

**Weighing scale:** To be able to analyse the main dependent variables, they have to be compared to an independent variable that represents the severity of dehydration. It has been established that loss of body weight is the golden standard for measuring the severity of dehydration. In fact, loss of body weight is the actual definition of the severity of dehydration. Since the subjects in this experiment are monitored from their euhydrated states as a starting point until they reach a certain level of dehydration within a short period of four hours (which is the maximum time per subject allowed by the ICBE, Philips Research's internal committee for biomedical experiments), short term loss of body weight is considered to be an excellent choice as the independent variable. This weighing scale measures in Kg's (so formally loss of body *mass* will be monitored instead of weight), with an accuracy of up to 1 decimal (like conventional digital weighing scales). This is considered accurate enough as the chosen *maximum allowed loss of body mass is 4%*, which can easily be measured with this scale. For more details on why exactly 4% has been chosen as the maximum allowed dehydration, please read appendix H.


Figure 3.27: The used weighing scale for this experiment.

**Infra-red thermometer:** The *HuBDIC Thermofinder FS-300 Non-Contact Infrared Thermometer* was use for measuring both *core-temperature* and *skin-surface temperature*. This CE-approved thermometer can measure these temperatures with a 0.1°C resolution. Core temperature is monitored for 2 reasons: risk mitigation and as a potential factor influencing the dependent variables. It is expected that the core temperature of the subject will rise, due to the warm ambient temperature during the experiment, and the physical exercise. It is considered safe if the core temperature stays within a ± 1°C offset from the starting core temperature (see appendix G). Core temperature will also be tracked, for later use in a multivariate regression analysis to learn about its influence on the two main dependent variables: ST and CRT. The core temperature is measured using the *core-temperature function* of the device, and is measured at the *tempel* (side of the head).

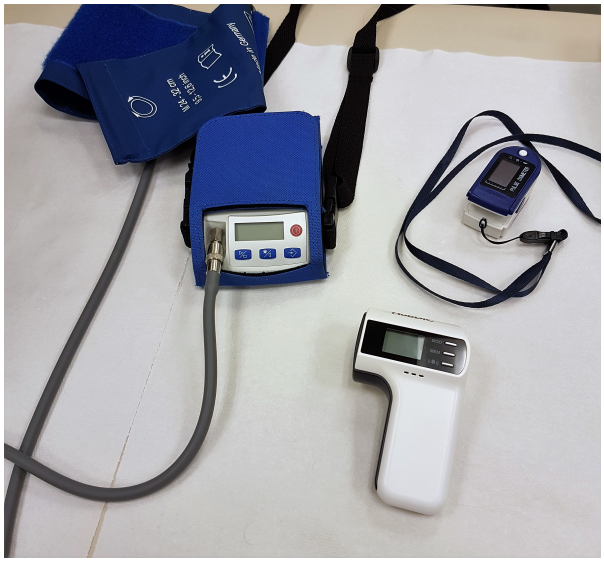

Figure 3.28: Several monitoring devices: A blood pressure monitor (top-left), a pulse-oximeter (top-right), and a thermometer for core- and object temperature (bottom).

The thermometer also has a function to measure object surface temperature, which is intended to be used to measure for instance the temperature of a bottle of milk after warming it up in the microwave. It is assumed that this function can also be used for skin-surface temperature reading, although this has not been indicated as intended use. Measuring skin-temperature on the hands and the chest clearly resulted in different temperature readings, which is expected as the extremities are known to be much colder compared to the chest, which suggests that this method is valid for measuring skin temperature. Since no other dedicated device was available within the lab that could measure skin temperature, this device was the final choice for skin surface temperature measurements.

**Digital thermometer & hygrometer:** It was also chosen to monitor *ambient temperature* and *ambient humidity*. The experiment is conducted in a *climate chamber*, where a constant temperature of 35°C and constant relative humidity of about 10% is maintained. A digital thermometer/hygrometer was used to monitor these parameters, mainly to check whether these parameters wouldn't drift too much from their set-points. The high temperature is used to stimulate sweating. 35°C was chosen as the set-point since this is the max-

Figure 3.29: Device for measuring ambient temperature and ambient relative humidity.

imum allowed setting for the climate chamber. The low relative humidity was chosen to increase the speed of evaporation of sweat from the surface of the body. It is known that the main cooling mechanism of sweat is the evaporation of sweat. It is also known that a lower-relative ambient humidity (relative since the maximum allowed evaporated water particles in the air depends highly on temperature) speeds up this evaporation process. The low ambient relative humidity is therefore a safety measure to prevent hyper-thermia. The *Wet-Bulb Temperature* theory was used to validate the safety of exercising in this combination of high

ambient-temperature and low relative ambient humidity. For a more detailed explanation of these chosen parameters, please see appendix I.

**Pulse Oximeter:** The CE-approved *Contec CMS50D Pulse Oximeter* (figure 3.28) was used to monitor $SpO_2$ (blood oxygen saturation) levels and *heart rate*. Heart rate monitored to determine if the subject should decrease its physical effort if it goes beyond its calculated maximum heart-rate, to prevent over-burdening the subjects. There is no expected risk of decreased $SpO_2$ levels, but they are still monitored as it is one of the main vital signs. If for any reason the $SpO_2$ level drops to below 95% (the generally accepted minimum of safe $SpO_2$ levels), the subject should rest.

**Blood pressure monitor:** A portable blood-pressure monitor (borrowed from a Philips Research employee) was used to regularly monitor blood pressure (figure 3.28). One of the main issues with dehydration is a decrease in blood-volume, which could lead to *hypovolaemia*. hypovolaemia can be monitored using a blood pressure monitor. For a more detailed explanation of the normal values of blood pressure, please see appendix G.

**Spinning bike:** A spinning bike was used as the main exercise equipment for the subjects. This device was chosen as a very constant amount of physical effort can be exerted, which can be adjusted to wish very easily. The main requirement for the type of exercise was that it should not be too high in effort to prevent overburden of the subject, and it should have a very constant level of subject power output to stimulate a very linear response of dehydration due the exercise. It was also the only low-effort cardio fitness device available within the vicinity of the climate chamber that could be easily moved into the chamber.

Figure 3.30: The spinning bike, placed inside the climate chamber.

**Laptop:** A laptop was used to plot the signals from the PPG-CRT prototype an the Cutometer, to store the data from these experimental devices, and to manually input any other parameters of interest into an Excel-sheet for retrospective analysis. All the data would be stored on this laptop in different folders per subject.

The laptop will also be used for retrospective data processing and analysis, using Excel and Matlab.

**Climate chamber:** For this experiment, the climate chamber was reserved for a full week. The climate chamber was a large chamber, which is regularly used for biomedical experiments where climate should be controlled closely. The parameters that could be controlled via a small control panel are ambient temperature and ambient relative humidity. For ambient temperature, the maximum allowed temperature is 35°C, and the minimum allowed relative humidity was 10%. Therefore, these exact numbers are also chosen as

the constant values for these parameters to stimulate fluid loss through sweating while preventing hyperthermia. Throughout the experiment, these parameters would always stay constant, in order to have as little influence as possible on variability of the measured dependent variables.

Figure 3.31: The interior of the climate chamber.

### 3.5.2. Protocol

A single pilot run has been conducted in the week before the experiment, where the responsible researcher has followed the steps below to test this protocol on himself. Based on found issues the protocol was adjusted appropriately. Volunteers were recruited internally using the flyer which can be seen in appendix K. This experiment was approved by the Internal Committee Biomedical Experiments (ICBE) of Philips Research, under the restriction that only 5 subjects were allowed to be included in this experiment, for each of which a maximum of four hours of participation time is allowed. All risks regarding the execution of this protocol and the use of the equipment have been identified and mitigated to an acceptable level. The risk analysis can be found in appendix J.

The *inclusion criteria* for selecting the volunteers were:

- Philips Research or PInS (Philips Innovation Services) employee
- Healthy volunteer
- Aged between 18 and 40 years old
- Signed informed consent

The *exclusion criteria* for excluding volunteers were:

- Over- or underweight
- Suffering chronic dehydration
- Any serious medical complaints or conditions
- Pregnancy
- Skin diseases
- Low toleration for high temperature environments

- If wearing lenses, unable to remove them during the experiment

Before the start of the experiment, the subject has read the information and provided the chance to ask questions, has read and signed the informed consent form, and has followed the preparation instructions properly. See appendices L and M for the information document and preparation instructions respectively.

1. For the subject to be well hydrated before the experiment, he/she should drink a large glass of water (500ml), 1 hour before measurement, as stated in the preparation instructions. Within one hour before the first measurement drinking and eating should be avoided. The reason for this is to have all fluids absorbed by the body before the first *hydration snap-shot* (explained in step 3) is taken. This should thus ensure a reliable first measurement, which is used as a reference for the *euhydrated state* of the subject.
   (a) As the subject cannot eat during the time-span of the experiment, he should be sure that he has sufficiently eaten well one hour before the experiment, as stated in the preparation instructions.
2. In order to get a "clean" measurement of the weight, subject should visit the toilet just before the measurement. Otherwise, the first measurement would be biased due to the weight of any remaining urine or excrement, while this extra weight does not contribute to body weight or hydration status.
   (a) It is assumed that any effect of build-up of urine in the bladder or excrement during the four hours of the experiment on the measurements can be neglected. If the subject, despite having visited the toilet before the experiment, still has to go, his/her weight should be measured right before and after the toilet visit, in order to take any loss of weight into account.
3. Subject enters the climate chamber and changes into appropriate cloths.
4. Measure the *hydration "snap-shot"*:
   The hydration snap-shot is performed every 15 minutes. It consists a very extensive series of measurements, and is therefore quite time-consuming. In order not to minimise the time that is taken for these measurements, and therefore to keep the subject exercising for as long as possible to further stimulate sweating, the hydration snap-shots are divided in two different versions: one for safety monitoring, and one for safety monitoring and taking all measurements using the experimental equipment. These different snap-shots are taken in turn, so the measuring CRT and ST actually happens after every 30 minutes of exercise.
   The steps taken for the hydration snap-shot are described below. Every measurement output is noted in a dedicated Excel-template, including the data from the experimental equipment for measuring CRT and ST.

**Safety monitoring measurements** (taken every 15 minutes):

1. Note the starting time of the hydration snap-shot.
   (a) The Excel-template has an integrated function that notes the time stamp of each value input in an adjacent cell, in order to track when all measurements are exactly taken.
2. Let the subject weigh him/herself on the scale.
   (a) Unless the subject objects, let him/her remove the shirt in order to get a clean body-mass measurement. Any weight from the shoes or shorts is neglected.
   (b) Note the weight
3. Take and note core temperature 3 times
4. Take and note value of heart rate, blood pressure (systolic and diastolic) and SpO2
5. Note the ambient temperature and ambient relative humidity.

**PPG-CRT Prototype measurement** (taken every 30 minutes):

1. Before taking the measurements, gently wipe the body-sites of interest of the subject clean.
   (a) Body sites of interest:
      i. Index-finger
      ii. Sternum
      iii. Mid-point of forehead
2. Measure the skin-temperature 3 times at each body-site of interest with the IR-skin thermometer and note all measurements. The Excel template will return a mean temperature value.
3. Place the probe on the skin of the subject, one body location of interest at a time.
4. Initiate the prototype (start recording the data)
5. Let the probe record the baseline PPG-signal
   (a) For at least 10 seconds
6. Apply the appropriate amount of force on the probe with the index finger, based on the feedback that the prototype provides.
   (a) 5 seconds (+/- 1 second), based on feedback of the prototype.
7. After pressure stage, quickly release index finger and let the PPG probe record for another 10 seconds.
8. repeat this process from step 6 at least 3 times per body location.
9. Place the probe on the next body site of interest and repeat from step 4
10. Copy, paste and save the gathered data in spreadsheet for retrospective analysis

**Cutometer measurement** (taken every 30 minutes):

1. Before taking the measurements, gently wipe the body-sites of interest of the subject clean.
   (a) Body sites of interest:
      i. Back of the hand
      ii. Fore arm
      iii. Chest
2. Measure the skin-temperature 3 times at each body-site of interest with the IR-skin thermometer and note all measurements. The Excel template will return a mean temperature value.
3. Place the probe on the skin of the subject, one body location of interest at a time.
4. Initiate the measurement (start recording the data)
5. Place the probe on the next body site of interest and repeat from step 3
6. Copy, paste and save the gathered data in spreadsheet for retrospective analysis

7. Subject sits on the spinning bike and begins the mild exercise.
   (a) The ambient temperature is held at a constant 35°C )highest possible setting of the climate chamber)
   (b) Ambient relative humidity at a constant 10% (lowest possible setting of climate chamber)
      i. For an overview of identified risks with prolonged times in these kind of high temperatures in combination with physical exercise, see appendix I.
   (c) The intensity of the physical exercise should be mild (heartrate aim is 60% of the subject's maximum heartrate, which is derived by subtracting the age of the subject from 220). The subject is free to change its effort during the experiment to his/her liking, and pauses are also allowed, as long as 4% loss of body weight is achieved.
   (d) Throughout this period, repeat the hydration snap-shot in step 4 every 15 minutes.
   (e) During the experiment, eating and drinking is prohibited for the subject.
8. When the subject has lost 4% body weight (= 2,8 litre of fluid lost in a healthy 70kg adult) as a result of dehydration, the last hydration snap-shot will be performed. 4% dehydration is chosen since WHO has defined a weight loss due to dehydration under 5% as no dehydration. When a 20% measurement error margin is applied we come to 4% as a limit, which is assumed to be enough if we want to observe usefulness of technological principles, as the assumption is that the used equipment for ST and CRT are very sensitive to changes in dehydration severity. The experiment is ended after the last snap-shot measurement, or earlier when:
   (a) The subject indicates to want to stop the experiment
   (b) The subject eats or drinks during the experiment
   (c) The monitored vital signs go outside of the predetermined boundaries.
   (d) After 4 hours

When the experiment has ended, the subject may exit the climate chamber. The subject should rehydrate appropriately, drinking at least the same amount of ORS as the amount of fluids lost due to dehydration over the next 4 hours. The first litre of ORS should be consumed within the vicinity of the researcher, in order for the researcher to make sure the subject is sufficiently rehydrated to leave. After drinking the first litre of ORS, the subject should be provided the rest of the ORS for further rehydration elsewhere (at home or in the office).

### 3.5.3. Data processing

PPG-CRT prototype
All data values that require manual input (such as the health monitoring parameters), are collected in an excel template (see appendix N for an example). Data from the PPG-CRT prototype are stored on the micro-SD card as a .txt file. The data are represented as a matrix, in which the columns represent the different data vectors and the rows represent samples. The data that are stored in this file are from column 1 to column 6: time-vector (ms), raw CRT PPG data (ADC), amplified CRT PPG data (ADC), raw reference PPG data (ADC), amplified reference PPG data (ADC), FSR reading (ADC).

To process the data, it first has to be cut into pieces. The data is stored as one single large matrix that contains all CRT tests per hydration snap-shot. First the data of the .txt file is imported to an Excel sheet for the first processing steps. First the data has to be cut and sorted per body location. This is easy, as before the first measurement per body location the device was reset which causes the time-vector to start again at 0. So now the data is successfully distributed per body location. It was already sorted per hydration snap-shot, with corresponding time stamps.
Now that the data is appropriately separated and sorted, it can be further processed using Matlab. Now there are 3 sets of data for each body location, each containing 3 CRT tests which also have to be separated. This separation can be done by looking at the force sensor values, for which a separate Matlab script was written (appendix O.1). The compression phase data can be extracted by selecting all data samples when the force reading is above a certain threshold. Since the force application and release happen very promptly, the force data makes very rapid changes between the three different phases, almost making up a square wave characteristic. Because of this, the data that comes after the extracted compression phase is considered to be the

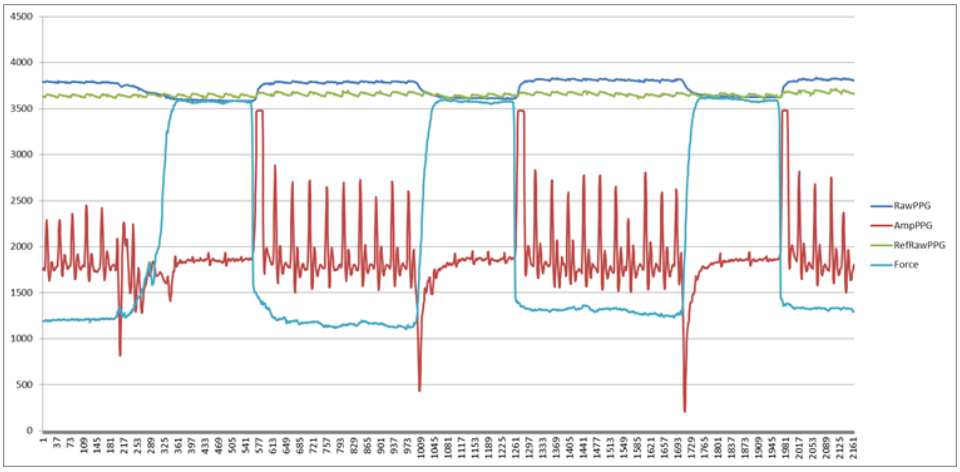


Figure 3.32: An example of a plot of raw PPG data, including the raw PPG data and amplified PPG data, and the reading from the force sensor.

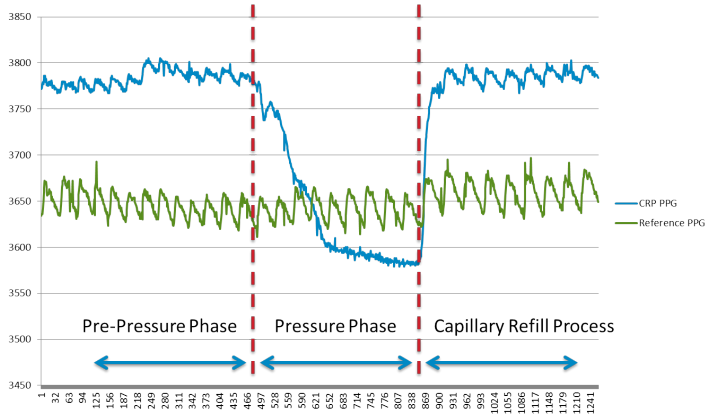


Figure 3.33: An isolated example of a typical CRT curve plot, together with the reference PPG signal. A clear distinction of test phases can be seen.

capillary refill phase of that CRT test, and at the same time the pre-compression phase of the next CRT test.

Now the data is ready for the final processing steps, to convert it into data that can be analysed. Before doing this, the most appropriate method has to be chosen. In section 3.3.1, a set of potentially useful parameters has already been defined, and it was concluded that the most appropriate parameter should be based on the characteristics of the data returned by the prototype. After going through all the potential parameters, an comparing them to the observed data, it was in the end chosen to use the exponential model of CRT [56], which looks like eq. 3.1:

$$\hat{y} = y(0) - A * e^{\frac{t}{T}} \tag{3.1}$$

This method was chosen due to the following reasons:

- comparing DC-levels of the capillary refill phase with the pre-compression phase would be unreliable due to the observed *Trabe Hering Mayer waves*.
- searching for a peak would cause very inconsistent results, as not every CRT test result shows peaks in the DC-component after refilling.
- The time it takes to reach a stable DC-value also would be unreliable due to variations such as the Trabe Hering Mayer waves and other artefacts.

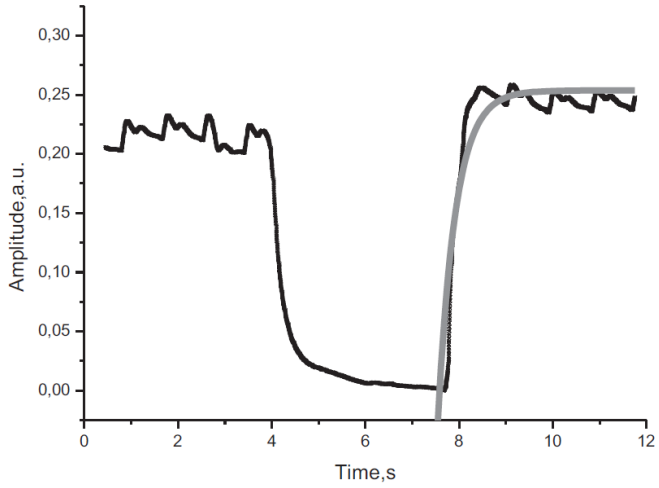


Figure 3.34: A plot of the result of a model-fitting principle for blue-light CRT PPG used by Kviesis et al. [56]

- The time difference between the DC-peak and the stable DC-offset would than automatically also not be usable.
- Almost all capillary refill data do represent a type of exponential growth line, with a horizontal asymptote. Using the exponential model, would therefore be the most optimal method. In the article where Kieser et al. describes this first draft of this exponential model, this method is also suggested to be the most optimal method for processing CRT data from PPG measurements into appropriate parameters for analysis, although the proposed model is not yet properly quantified [56]. This method would closely resemble a *parameter estimation* task for which model fitting algorithms would be the most preferred choice.

To most optimally use the model, and to be able to eventually derive a single parameter from it that can be used for analysis, the model has been slightly adjusted, see eq. 3.2.

$$\hat{y} = \mathbf{A} * (-e^{\frac{-x}{\mathbf{B}}} + 1) \tag{3.2}$$

The starting point of the model in eq. 3.2 is that the origin of the signal in the capillary refill phase starts at $y(0) = 0$. This is why the $y(0)$ term in eq. 3.1 is left out in eq. 3.2. Any script applying this model to the data should therefore first subtract the mean of the last few samples of the compression phase from the CRT data, in order to have the starting point of the CRT data at approximately $y(0) = 0$. It was chosen to take the mean of the last 10 samples to minimise the effects of noise on this subtraction.

The basis of this model, is that a power of the number $e$ is used. The reason for this is as the Capillary Refill Process is a natural, continues process, and therefore should be considered as continues growth.

More specific: it is assumed that the speed of blood refilling for each time-point, is inversely proportional to the volume of blood already in the capillaries in a continues time-domain, hence the natural exponential function $e^x$. The exponential function $e^x$ is flipped around the y-axis by making the exponent negative ($e^{-x}$), because than the function will approach an asymptote over time. The function is flipped around the x-axis by taking the negative of the exponential function ($-e^{-x}$) so that the function grows, instead of decreases. To have the function crossing the origin ($x = 0, y = 0$), and to have the base-asymptote on y=1, the whole function is moved up by y=1, hence the baseline of the model is $\hat{y}(x) = -e^{-x} + 1$.

The asymptote $A$ (the mean DC value of the PPG signal after the capillary refilling process) is manipulated by multiplying $\hat{y}(x)$ with $A$. The capillary refilling 'growth rate' is manipulated by dividing the exponent $x$ by an arbitrary parameter $B$. This $B$ parameter is key in analysing the Capillary Refilling Process changes, as this

parameter would become larger for a slower CRT.

To fit this model to the CRT data, a Matlab function was created using the *Curve Fitting* tool, using a custom equation (appendix O.2). This function is called by the script that applies this method to selected chunks of data (appendix O.4). The error function returns a plot of the fitted model (figure 3.35), along with the coefficient outputs, which are the estimated model parameters $A$ and $B$.

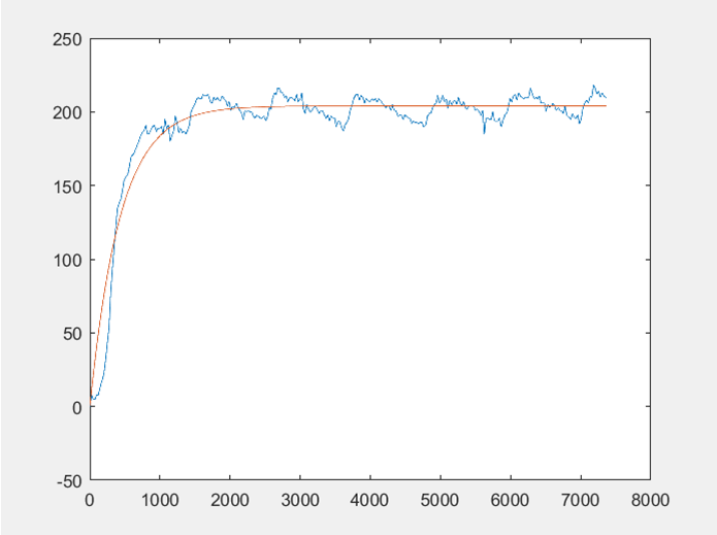


Figure 3.35: A plot of a CRT sample with the fitted exponential model.

It can be concluded that the model fitting algorithm has worked, although the fitted model is not very close to the actual dataset. It can be seen that the actual data shows a slight s-curve in the beginning. To overcome this issue, another curve fitting run is performed, with a slight alteration in the data. Instead of starting at the beginning of the capillary refill phase, the origin of the model should now be placed on the value of the data where the capillaries are halfway of refilling (so right at the point where $y(x) = A/2$). This indeed results in a better fit, as can be seen in figure 3.36, since taking away the bottom half of the s-curve, what remains is an exponential curve.

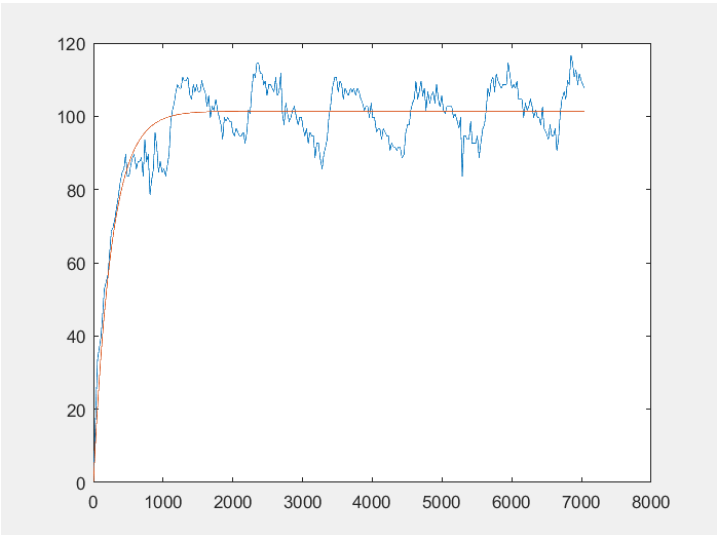


Figure 3.36: A plot of a CRT sample (starting halfway of refilling) with the fitted exponential model.

There is still some residual error due to the pulses in the signal, the AC-component. It is hypothesized that these pulses could actually have influence on the CRT. As can be seen in the plots, the measured CRT

here is quite fast, and could happen within the length of a pulse. The thought is that if the pressure is released in between pulses right before the minimum, CRT may be slower compared to a situation where pressure is released just before the peak of a pulse. The pulse might give a boost to the refilling process. Therefore it was decided that a "clean" capillary refill process is needed, without the influence of the pulses. For this, conveniently, the reference PPG signal has been used.

The reference PPG signal contains the same AC-component and other low-frequency artefacts that can also be found in the CRT PPG signal. If the reference signal is fitted upon the CRT signal, these unwanted shared variations can be cancelled from the CRT data in two ways: subtraction or division. First the reference signal has to be filtered to reduce noise, to prevent that the high-frequency noise of the reference signal is transferred on the CRT data when subtracting or dividing, on top of the already presenting high frequency noise. After trying a few filters, taking the 20th order Fourier series of the reference signal seemed to be sufficient for getting a smooth reference PPG waveform. (In hindsight, using the *filtfilt* function with a low-pass filter design would have formally been a more appropriate method for noise filtering.) The noiseless reference waveform is than fitted on the last few seconds of the CRT data, since the last seconds of the data most closely resemble the reference waveform which make the last seconds most suitable for the fitting process. The fitting algorithm is performed using a grid-search function (appendix O.4), which results in a fitted reference function as can be seen in figure 3.37.

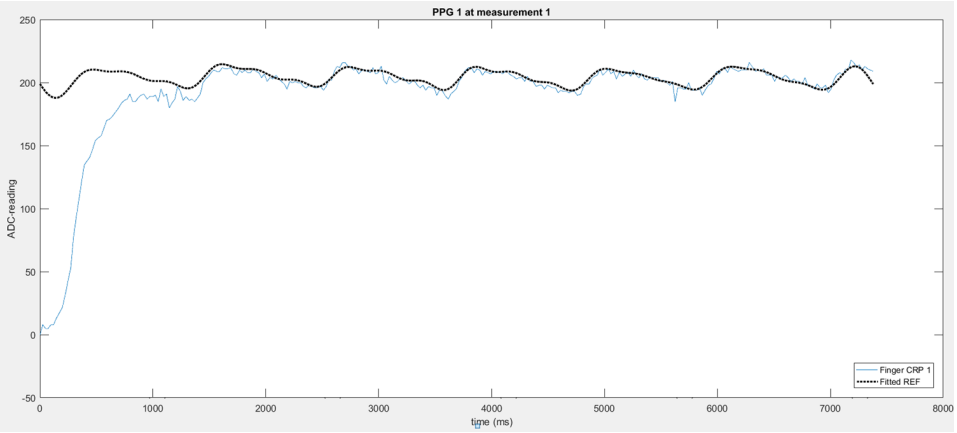


Figure 3.37: A plot of a CRT sample with a filtered reference signal fitted to it.

As explained before, the AC-component can now be cancelled by either subtracting the normalised reference data from the CRT data, or by dividing the CRT data by the fitted reference data, which automatically normalises the CRT curve to values between 0 and 1.

It is hard to determine which method would be better. The difference lies in how the pulses change during the capillary refill process: does magnitude of the pulses get any bigger in relation to the DC-growth, than division would be the most appropriate method. If the magnitude of the pulses stay constant, even during the growth of the capillary refill process, than subtraction would be the most appropriate. It is hypothesized that the latter explanation is the correct one, as it is believed that the pulse itself might be the driving force behind the capillary refill process. It is in fact the case that a beat of the hart pumps the blood around, and it is the same beat that causes the observed pulses on the PPG signal. Yet, as this explanation is merely hypothetical, both methods (subtraction and division) are used. In figures 3.38a and 3.38b at can be seen that it does not make a significant difference in the characteristics of the waveform, except that with the division method the curve is normalized. This normalization is fine, since it will not have effect on the $B$ parameter of the fitted exponential model, which is the main parameter of interest.

In the end, six different versions of the same sample are used for the estimation of the $B$ parameter of the exponential model. This should indicate which method of processing the data results in the best correlation of the $B$ parameter with dehydration.

### Cutometer data

The data from the Cutometer is exported as an Excel file per hydration snap-shot. The raw data consists of a time-vector column, and three columns containing the skin displacement values in mm for each body location. Also the parameter matrix is exported as an Excel sheet. This data doesn't need any further processing

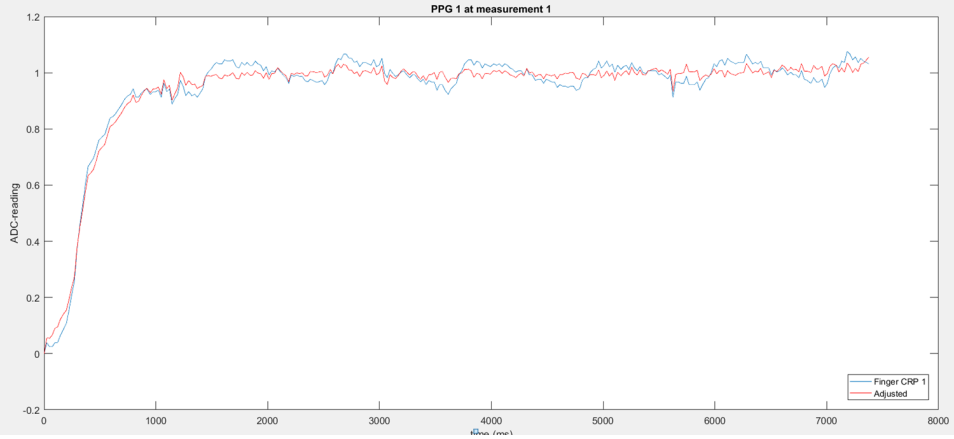


(a) Remaining CRT curve after subtracting the normalised reference data from it.

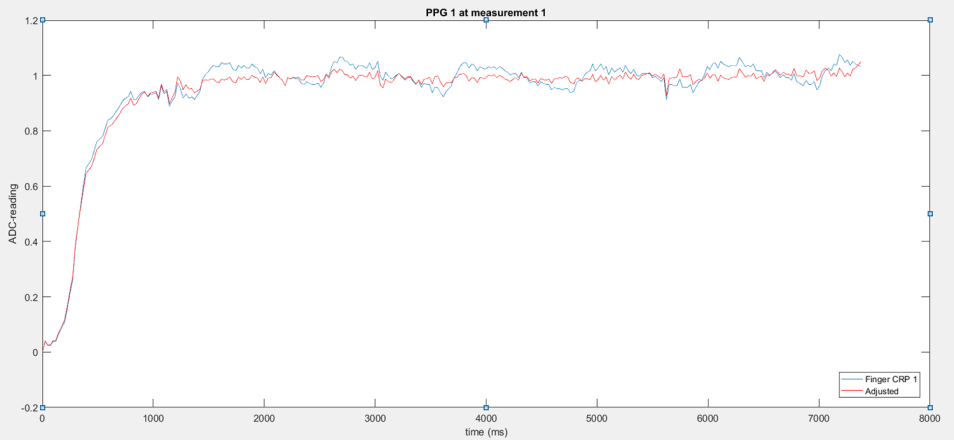


(b) Remaining CRT curve after being divided by the fitted reference data.

Figure 3.38: A comparison of the data after cancelling out the AC-component by either subtraction or division.

| | Original CRT data | CRT data / Reference data | CRT data - Reference data |
|---|---|---|---|
| Origin at start of capillary refill phase | $O$ | $O/R$ | $O-R$ |
| Origin halfway refilling process | $\frac{1}{2}O$ | $\frac{1}{2}O/R$ | $\frac{1}{2}O-R$ |

Table 3.1: All different versions per CRT sample, which will be included in the analysis.

as the Cutometer software already translates the raw data into very useful parameters. These parameters will be used as-is in the retrospective analysis.

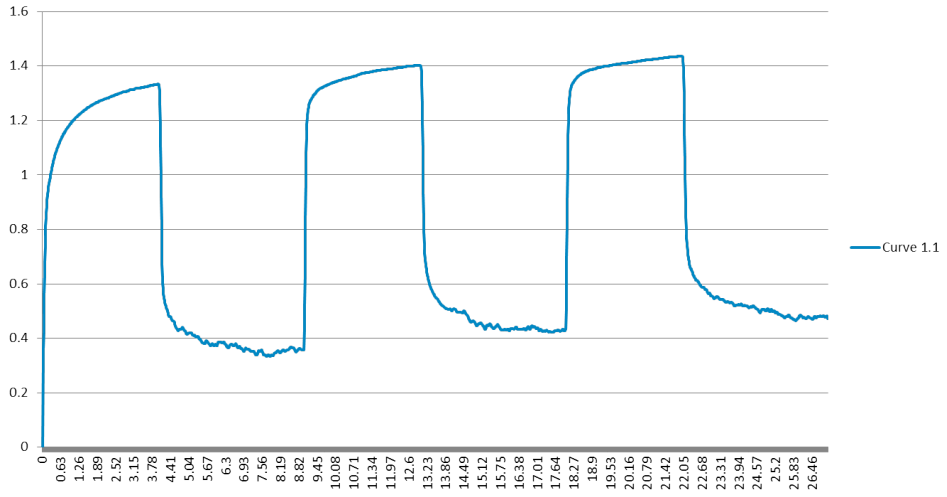


Figure 3.39: An example of a plot of raw Cutometer data

### 3.5.4. Data analysis

The parameters of interest from both the PPG prototype and the Cutometer were analysed using a regression analysis. The main point of interest is the influence of degree of dehydration (the independent variable) on the individual parameters of CRT and ST (the dependent variables). Yet, these individual dependent variables are, next to dehydration, also dependent on core-temperature, skin-temperature and/or ambient-temperature. Due to the theoretical dependency of the parameters on multiple variables at a time, a *multivariate regression analysis* will be conducted. A regression analysis is in this case proposed as the best option for assessing the data of interest for its predictive value for diagnosing dehydration.

The main principle of a regression analysis is to plot the position of each data point, with the value of the dependent variable (any CRT or ST related parameter = $P$) on the y-axis and the value of the independent variable (dehydration degree = $D$), in the case of a normal regression analysis. The next step is to create a linear model that fits best to this data (eq. 3.3). For this experiment it is not yet known if any relation between $D$ and $P$ is linear or non-linear, but since the amount of samples per subject will be relatively small (4 to 6), it is for now chosen that a linear regression analysis would be sufficient. With this small amount of samples per subject, using a non-linear model could also cause over-fitting, which should be avoided as it would not be representative as a predictive model.

$$\hat{y} = a + bx \tag{3.3}$$

The best fit is determined by optimizing $a$ and $b$ in eq. 3.3 until the *Sum of Squared Error* (SSE) is at its minimum. Error is defined as the difference between the regression model and the actual data at each sample (eq. 3.4).

$$e = y - \hat{y} \tag{3.4}$$

SSE (eq. 3.5) is the accumulated squared error of all data samples, and is therefore a measurement of the variance in the data which is not accounted for by the regression model (or unexplained variation).

$$SSE = \sum((y - \hat{y})^2) = \sum e^2 \tag{3.5}$$

With the regression analysis the variance that actually is accounted for by the model can also be derived, by calculating the accumulated difference between the mean of the actual data ($\bar{y}$) and the regression model at every sample (eq. 3.6). This is also called the Sum of Squares of the Regression variations (SSR), and can simply put be regarded as the explained variation.

$$SSR = \sum((\hat{y} - \bar{y})^2) \tag{3.6}$$

The total variation of the actual data (compared to the mean of all the data) can then also be derived (eq. 3.7). It is called the Sum of Squared Total variations (SST).

$$SST = \sum((y - \hat{y})^2) = SSE + SSR \tag{3.7}$$

Now the main thing to learn is how well this model can predict the dependent variable $P$ based on the independent variable $D$. This sounds contra-intuitive, because in the end it should be possible to predict $D$ based on $P$. Yet for the sake of formally conducting the regression analysis correctly, it should first be decided how well $D$ determines $P$. If the predictive relation is proven in one way, it should work similarly when turning the independent and dependent variables around. In fact, this way of working becomes more important when conducting a multivariate analysis, where two independent variables (Temperature $T$ and $D$) are investigated for their predictive characteristics toward $P$. If this relation is established and significant enough, $P$ (potentially in combination with $T$) should be able to be used in predicting $D$. The regression model in a multi-variate regression analysis with two independent variables becomes three dimensional as in eq. 3.8.

$$\hat{y} = a + bx + cz \tag{3.8}$$

The main statistical result that is of importance in this analysis is the *coefficient of determination* ($R^2$), which stands for the rate of variance that is explained by the regression model (eq. 3.9). So if $R^2$ is close to 1, it suggests that the regression model serves very well as a predictive model (within the group of samples that were analysed). If $R^2$ is closer to 0, is suggests a very poor predictive value of the model.

$$R^2 = SSR/SST = 1 - \frac{SSE}{SST} \tag{3.9}$$

This $R^2$ has to be interpreted with care when having a small amount of *Degrees Of Freedom* (DOF). DOF is the total amount of samples ($n$), minus the amount of predictive variables ($k$, which in the case of linear regression is equal to the amount of independent variables used) and minus 1 (eq. 3.10).

$$DOF = n - k - 1 \tag{3.10}$$

One can imagine a regression analysis where only 2 samples are used, to which a linear model has to be fitted using 1 predictive variable. A linear model through 2 data samples obviously has a SSE of 0, the same goes for a 3D model (with $k = 2$) through 3 data points. For both these examples DOF = 0, which means that the sample size is too small. A very low DOF therefore always results in an overestimated $R^2$, due to the lower SSE for small sample-sizes. DOF should at least be 1 in order to perform a regression analysis, although the statistical power of that analysis will still be very low, while $R^2$ is substantially overestimated. $R^2$ can thus be quite deceiving when not used with care.

Sometimes a low DOF is inevitable, which is the case in this experiment due to restrictions. For these situations, one can use the *adjusted* $R^2$ ($\bar{R}^2$), which is explained in eq. 3.11. $\bar{R}^2$ takes the DOF into account. So when adding meaningless (non-predictive) variables to the model, it decreases $\bar{R}^2$ due to the decreased DOF. Yet if the added variables seem to have some predictive properties regarding the dependent variable, $\bar{R}^2$ will also increase. In this analysis, $\bar{R}^2$ is therefore considered the most important result to take into account in the conclusion.

$$\bar{R}^2 = 1 - (1 - R^2)\frac{n-1}{n-k-1} = 1 - \frac{SSE}{SST} * \frac{n-1}{n-k-1} \tag{3.11}$$

For the regression analysis, the Matlab function *"fitlm"* has been used. This function fits a linear model to a data-set, and can be used to return any multi-variate regression analysis related results. For the full script of the regression analysis, please see appendix P.

$\bar{R}^2$ will eventually be calculated per snap-shot, per measurement, per body location, per subject. This will result in a quite large set of $\bar{R}^2$'s, instead of a single value to rely on. The reason for this is that for now an analysis should be made on which body-location and processing method is regarded to generate the best results. A mean figure for all subjects is not taken into account, as the subjects are adults. It is known that for CRT the normal values can vary a lot between adult individuals, and the same is assumed for ST. Therefore, all the results will be sorted as shown in tables 3.2 and 3.3.

| | **Subject 1** | | | | | | ... |
|---|---|---|---|---|---|---|---|
| Sample processing | Original CRT | | | Reference subtracted | | | ... |
| Body location | Finger | Chest | Head | Finger | Chest | Head | ... |
| Sample 1 | $\bar{R}^2_{o,f,1}$ | $\bar{R}^2_{o,c,1}$ | $\bar{R}^2_{o,h,1}$ | $\bar{R}^2_{-r,f,1}$ | $\bar{R}^2_{-r,c,1}$ | $\bar{R}^2_{-r,h,1}$ | ... |
| Sample 2 | $\bar{R}^2_{o,f,2}$ | $\bar{R}^2_{o,c,2}$ | $\bar{R}^2_{o,h,2}$ | $\bar{R}^2_{-r,f,2}$ | $\bar{R}^2_{-r,c,2}$ | $\bar{R}^2_{-r,h,2}$ | ... |
| Sample 3 | $\bar{R}^2_{o,f,3}$ | $\bar{R}^2_{o,c,3}$ | $\bar{R}^2_{o,h,3}$ | $\bar{R}^2_{-r,f,3}$ | $\bar{R}^2_{-r,c,3}$ | $\bar{R}^2_{-r,h,3}$ | ... |
| Mean | $\bar{R}^2_{o,f,m}$ | $\bar{R}^2_{o,c,m}$ | $\bar{R}^2_{o,h,m}$ | $\bar{R}^2_{-r,f,m}$ | $\bar{R}^2_{-r,c,m}$ | $\bar{R}^2_{-r,h,m}$ | ... |

Table 3.2: Data analysis structuring for PPG results.

| | **Subject 1** | | | **Subject 2** | | | ... |
|---|---|---|---|---|---|---|---|
| Body location | Hand | Arm | Chest | Hand | Arm | Chest | ... |
| Parameter $R0$ | $R0_{h,1}$ | $R0_{a,1}$ | $R0_{c,1}$ | $R0_{h,2}$ | $R0_{a,2}$ | $R0_{c,2}$ | ... |
| Parameter $R1$ | $R1_{h,1}$ | $R1_{a,1}$ | $R1_{c,1}$ | $R1_{h,2}$ | $R1_{a,2}$ | $R1_{c,2}$ | ... |
| ⋮ | ⋮ | ⋮ | ⋮ | ⋮ | ⋮ | ⋮ | |

Table 3.3: Data analysis structuring for Cutometer results.

The means and standard deviations of the $\bar{R}^2$'s from all subjects, sorted per parameter type and body-location, will eventually be plotted for a clear overview.

## 3.6. Results

In the next section the results of the experiment will be addressed and discussed, followed by the conclusion regarding the results of this experiment. Finally this chapter will be closed with a recommendation for next steps regarding the insights from this experiment.

### 3.6.1. Raw data

An example of manually noted data in a dedicated Excel template, other than the CRT or ST data, is shown in appendix N. Examples of the recorded CRT and ST data are shown in the tables below.

PPG data

In table 3.4 a sample of data as it is stored by the prototype is shown. This data will undergo the processing steps as is explained in section 3.5.3.

Cutometer data

In tables 3.5 and 3.6 a sample of data is shown, as it is returned by the Cutometer software. The parameters as shown in table 3.6 will directly be used as dependent variables for the regression analysis, and do not require further processing.

### 3.6.2. Processed data

For all processed data regarding CRT, ST and other parameters, please see appendix Q. In this section, a few samples are shown. Figure 3.40 shows the processed PPG data in the form of estimated parameters of the exponential model, plotted per iteration. For each iteration, the severity of dehydration grows. In figure 3.41

| | | | | | |
|---|---|---|---|---|---|
| 205 | 4054 | 56 | 4053 | 82 | 974 |
| 382 | 4050 | 66 | 4051 | 69 | 972 |
| 476 | 4047 | 65 | 4056 | 64 | 970 |
| 570 | 4055 | 82 | 4052 | 86 | 976 |
| 661 | 4051 | 78 | 4049 | 71 | 972 |
| 756 | 4050 | 60 | 4050 | 69 | 968 |
| 891 | 4050 | 81 | 4053 | 84 | 957 |
| 917 | 4052 | 69 | 4052 | 77 | 956 |
| 938 | 4050 | 87 | 4053 | 81 | 955 |
| 959 | 4050 | 75 | 4050 | 68 | 952 |
| 980 | 4051 | 74 | 4052 | 68 | 953 |
| 1001 | 4051 | 72 | 4052 | 66 | 951 |
| 1022 | 4036 | 55 | 4051 | 67 | 955 |
| 1043 | 4047 | 67 | 4051 | 63 | 939 |
| 1064 | 4053 | 70 | 4051 | 65 | 945 |
| 1085 | 4050 | 62 | 4053 | 59 | 943 |
| 1106 | 4053 | 67 | 4054 | 75 | 955 |
| 1127 | 4055 | 81 | 4052 | 77 | 950 |
| ⋮ | ⋮ | ⋮ | ⋮ | ⋮ | ⋮ |

Table 3.4: A sample of raw data from the PPG prototype, as it is stored in a .txt file on the micro-SD card. The columns represent (from left to right): time-vector (ms), raw CRT PPG data (ADC), amplified CRT PPG data (ADC), raw reference PPG data (ADC), amplified reference PPG data (ADC), FSR reading (ADC).

| | **Curve 1.1** | **Curve 1.2** | **Curve 1.3** |
|---|---|---|---|
| Time / s | 20160905_130602_000001.mpa | 20160905_130703_000001.mpa | 20160905_130758_000001.mpa |
| 0 | 0 | 0 | 0 |
| 0.01 | 0 | 0 | 0 |
| 0.02 | 0 | 0 | 0 |
| 0.03 | 0.314 | 0.591 | 0.8 |
| 0.04 | 0.364 | 0.665 | 0.873 |
| 0.05 | 0.422 | 0.75 | 0.955 |
| 0.06 | 0.49 | 0.843 | 1.044 |
| 0.07 | 0.565 | 0.941 | 1.137 |
| 0.08 | 0.629 | 1.017 | 1.207 |
| 0.09 | 0.685 | 1.076 | 1.261 |
| 0.1 | 0.735 | 1.125 | 1.304 |
| 0.11 | 0.777 | 1.164 | 1.338 |
| 0.12 | 0.813 | 1.194 | 1.365 |
| 0.13 | 0.841 | 1.217 | 1.387 |
| 0.14 | 0.864 | 1.235 | 1.406 |
| 0.15 | 0.883 | 1.25 | 1.421 |
| ⋮ | ⋮ | ⋮ | ⋮ |

Table 3.5: An example of raw Cutometer data (skin displacement in mm) as it is are stored in Excel, from a single measurement moment. The columns represent from left to right: Time(ms), the back of the hand, the fore arm, and the chest.

all parameters from the Cutometer have been plotted for a single subject based on measurements from the hand.

Additional processing steps taken

For the PPG prototype, a few extra steps for processing the data had to be taken. This was mainly due to the inconsistency of the characteristics of the CRT curve.

- The sampling time of the PPG prototype was typically approximately 35 ms per sample, which results in a sufficient sampling rate for PPG purposes. Yet, the sample time did show some instability, resulting

| | **Curve 1.1** | **Curve 1.2** | **Curve 1.3** |
|---|---|---|---|
| Results | 20160905_130602_000001.mpa | 20160905_130703_000001.mpa | 20160905_130758_000001.mpa |
| R0 | 1.334 | 1.699 | 2.195 |
| R1 | 0.357 | 0.093 | 0.045 |
| R2 | 0.7324 | 0.9453 | 0.9795 |
| R3 | 1.436 | 1.769 | 0 |
| R4 | 0.471 | 0.163 | 0.083 |
| R5 | 0.6925 | 0.9156 | 0.8957 |
| R6 | 0.815 | 0.5102 | 0.6833 |
| R7 | 0.3816 | 0.6062 | 0.5321 |
| R8 | 0.977 | 1.606 | 2.15 |
| R9 | 0.102 | 0.07 | -2.195 |
| | | | |
| F0 | 0.4671 | 0.3568 | 1.4559 |
| F1 | 0.225 | 0.2659 | 0.3778 |
| F2 | 0 | 0 | 0 |
| F3 | 0 | 0 | 0 |
| F4 | 0 | 0 | 0 |
| Q0 | 667 | 849.5 | 1097.5 |
| Q1 | 0.0296 | 0.0158 | 0.0429 |
| Q2 | 0.018 | -0.0018 | 0.0316 |
| Q3 | 0.0116 | 0.0177 | 0.0113 |

Table 3.6: An example of Cutometer parameters as they are stored in Excel, from a single measurement moment. The columns represent from left to right: the back of the hand, the fore arm, and the chest.

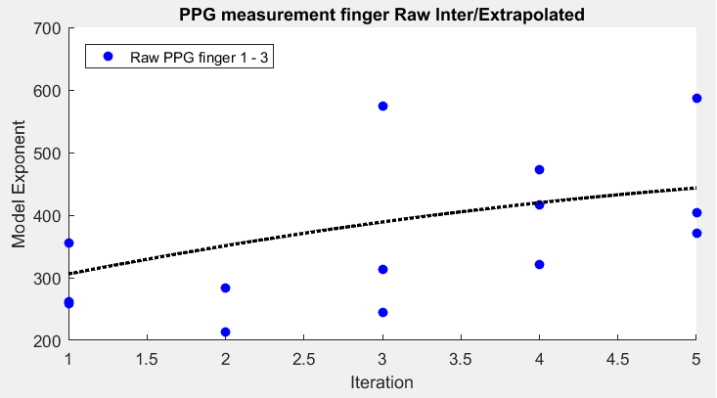


Figure 3.40: An example of a plot of all parameter outputs (Model exponents) from the pulp of the finger of a single subject, of which three are taken per iteration (hydration snap-shot). A non-linear regression line has been added, but can be neglected.

in variations of a few ms for every sample-time. This instability was mitigated by interpolating the data using the *"interp1"* function in Matlab, selecting the "linear interpolation" option. This also virtually increased the sample rate to 100Hz.

- Some CRT data vectors contained very substantial artefacts that mode processing of the data impossible. The script was adjusted to recognise these unexpected characteristics, and automatically exclude these samples from further processing. The main identifier of useless samples was a mean that was lower than the first few samples of the capillary refill process.
- Sometimes, these artefacts would only show a few seconds after the capillaries have already filled. To let the Matlab script include these, these artefacts were cut out of the data vector manually.
- Inter- and extrapolation functions of Matlab have been used in order to account for the excluded data samples from processing. In that way, the regression analysis could still be executed even though some samples were excluded.

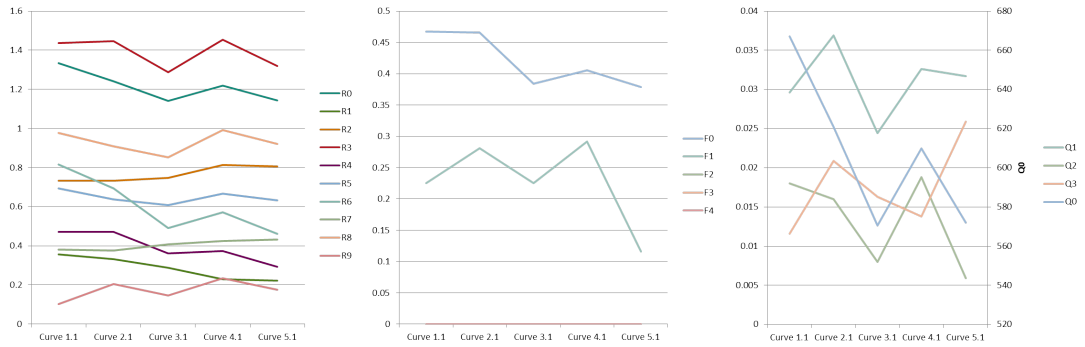


(a) R-parameters (b) F-parameters (c) Q-parameters

Figure 3.41: All cutometer parameters plotted per iteration. Data regards all measurements on the hand of a single subject.

### 3.6.3. Data analysis

All results of the regression analysis can be found in appendix R. The results are summarized in figures 3.42 to 3.47, in terms of means and standard deviations of the regression results ($\bar{R}^2$) of all subjects together.

In figures 3.42 to 3.44 the $\bar{R}^2$-plots are shown. The closer $\bar{R}^2$ is to 1, the better the parameters of interest which are described in the caption of each plot can be used for predicting dehydration. The plots are divided in body location per column (finger, chest and head, in that order). Shown per row are the consecutive measurements per snap-shot, as at every snap-shot 3 measurements are taken. The bottom row represents a mean of the raw data of those three samples, which is a way of averaging and filtering out noise. Per plot six lines represent the mean and standard deviations from all subjects, divided per sample processing method as shown in table 3.1. These 6 differently processed samples thus represent from left to right: the original sample ($O$), the sample with the origin half-way of the refill process ($\frac{1}{2}O$), the original sample with the AC-component filtered out by dividing it by the reference data ($O/R$) and with the half-way origin ($\frac{1}{2}O/R$), and the version with the AC-component filtered out by subtracting the reference data($O/R$), together with the half-way origin ($\frac{1}{2}O-R$). Each figure represents the regression analysis using different variables, where figure 3.42 represents the regression analysis of CRT vs. % loss of body mass, figure 3.43 represents the analysis of CRT vs. % loss of body mass and local skin temperature, and figure 3.44 represents the analysis of CRT vs. % loss of body mass and core temperature.

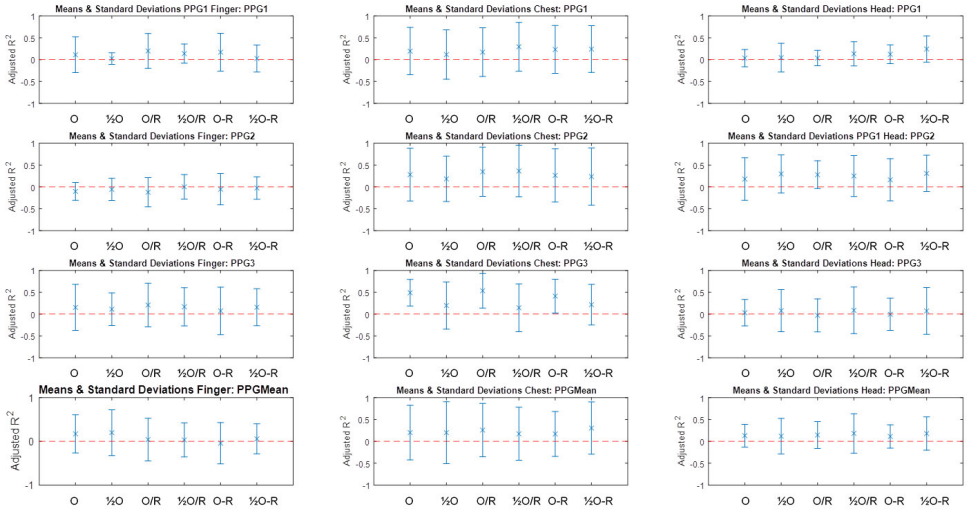


Figure 3.42: Regression analysis PPG-CRT: $\bar{R}^2$ of parameter $B$ vs. % loss of body mass.

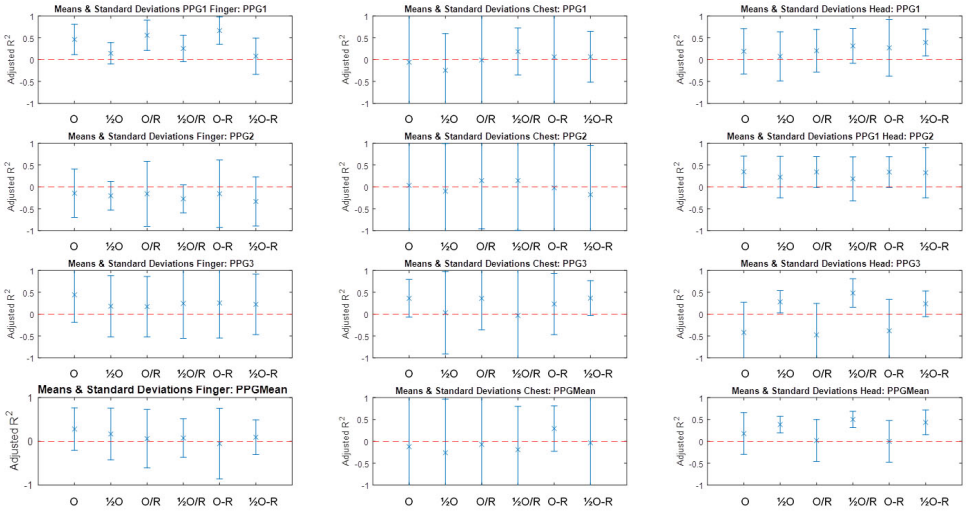


Figure 3.43: Multivariate regression analysis PPG-CRT: $\bar{R^2}$ of parameter $B$ vs. % loss of body mass & local skin surface temperature.

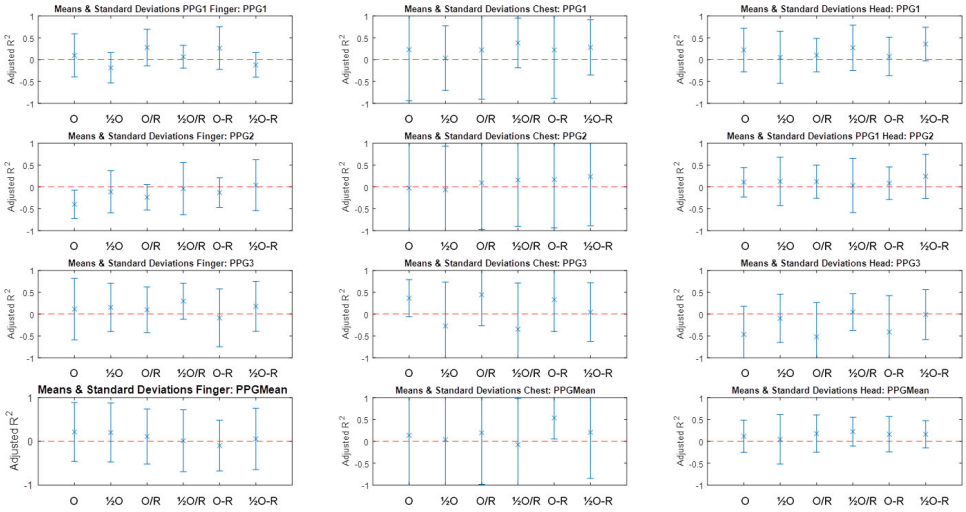


Figure 3.44: Multivariate regression analysis PPG-CRT: $\bar{R^2}$ of parameter $B$ vs. % loss of body mass & core temperature.

A similar way of plotting the results has been done for the results of the Cutometer, which can be seen in figures 3.45 to 3.47. These results are organised in different plots per body location (Hand, arm and chest, respectively), while every different plot illustrates the results per Cutometer parameter. Figure 3.45 represents the analysis results of all Cutometer parameters vs. % loss of body mass, while figure 3.46 represents the results of all Cutometer parameters vs. % loss of body mass combined with local skin surface temperature. Figure 3.47 represents the results of all Cutometer parameters vs. % loss of body mass combined with core temperature.

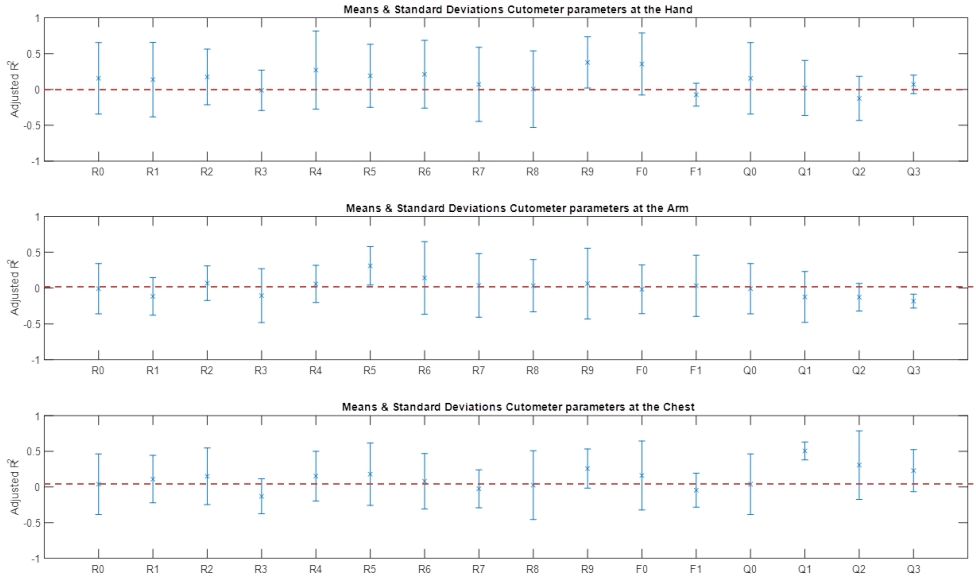


Figure 3.45: Regression analysis Cutometer: $\tilde{R^2}$ of all Cutometer parameters vs. % loss of body mass.

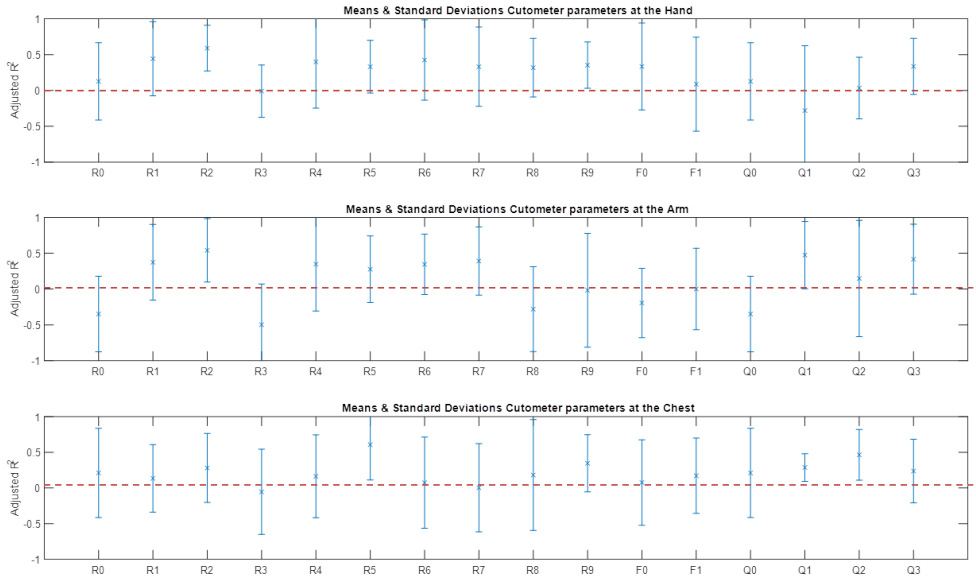


Figure 3.46: Multivariate regression analysis Cutometer: $\tilde{R^2}$ of all Cutometer parameters vs. % loss of body mass & local skin surface temperature.

### 3.6.4. Notable observations

- Due to the relatively low DOF, some $\tilde{R^2}$'s seem to have gone below 0, as can be seen in the result plots. This should be a result of adjusting these coefficients by DOF (eq. 3.11). Any $\tilde{R^2}$ below zero is therefore regarded as zero.
- In appendix R on the last page, a plot can be found that shows the regression analysis results of dehydration with core temperature. There seems to be a very good fit between these variables for most subjects. This can be explained by a number of reasons:

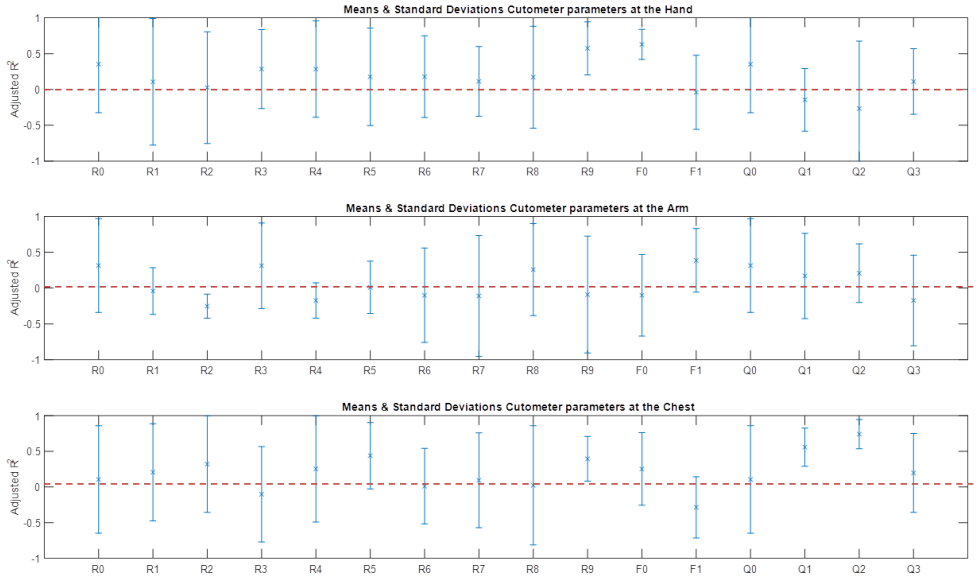


Figure 3.47: Multivariate regression analysis Cutometer: $\tilde{R^2}$ of all Cutometer parameters vs. % loss of body mass & core temperature.

  - Core temperature rises because it is affected by the sudden high ambient temperature in the lab. Core temperature gets raised gradually because of this.
  - Due to the prolonged exercise, core temperature rises over time.
  - Dehydration could also have some effect. It could be that dehydration reduces sweat-rate over time, which leads to less effective cooling of the body. Still, it is not believed that the rate of sweating gets reduced by a significant amount below 4% dehydration.
- For these reasons, despite the seemingly high $R^2$, core-temperature should not be considered a good diagnostic variable individually.

## 3.7. Limitations

Although it is believed that the way this experiment was conducted was to most optimal given the prior knowledge, the available resources and restrictions, there still were some considerable limitations to this experiment which have to be taken into account before interpreting the results. There were both limitations to the overall experimental design, as well as to the equipment, which will all be mentioned in this section.

**Experiment limitations**

- *The number of subjects*: The ICBE gave a restriction to only experiment on a maximum of five subjects in total. This eventually meant that only 4 dehydration subjects could be included, and only 1 control subject. This limits the statistical power of the acquired data.
- *The number of samples per subject*: There were only 4 to 6 hydration snap-shots per subject where the experimental equipment was used. The reason for this was the limited amount of time per subject (max. 4 hours as restricted by the ICBE), and the fact that taking many different measurements at a single hydration snap-shot with just 1 researcher in the room can be very time consuming. It would have been better if less measurement actions had to be taken during each hydration snap shot, so that more time is left for more hydration snap-shots. The low number of samples also was the reason for a very low DOF, which limits the amount of variables that can be used in a multivariate analysis and causes an unreliable coefficient of determination.
  Due to both the small number of subjects and the small sample size, the *p-value* for testing statistical significance of the data is not regarded in the analysis, as it can already be presumed that given the amount of samples, the statistical significance of the experiment should be rather low (meaning $p >$

0.05). Any observed (causal) relations in this experiment should therefore be considered nothing more than a suggestive insight for further research.

- *The maximum severity of dehydration*: The maximum allowed severity of dehydration was chosen to be 4%, to keep it safe. Yet, this relatively low degree of dehydration does have the disadvantage that the effects on CRT and ST could be very small. This could cause any effects to be unnoticeable, even when measured with the used equipment. It is hypothesized that any effects of dehydration would've been much more noticeable in a regression analysis when a dehydration of for instance 10% could have been achieved. It would on the other hand be difficult to increase the max. severity of dehydration, since within the 4 hour time-window the subjects rarely succeeded to reach the 4% limit. More time would've been needed, and combined with a more severe degree of dehydration this would be very straining on the subjects. Therefore it would be difficult to achieve higher levels of dehydration within a lab setting.
- *The age of the subjects*: The group of focus for this assignment is children under the age of five, and it has already been established that CRT and ST are affected differently by dehydration within this age group when compared to adults, as these diagnostic variables become less predictive in older age. The subjects were all between 20 and 25, which is significantly older than young children. This could have caused a lot of unexplainable biological variability between measurements.
- *The control group*: Only one subject was picked to play the role of the control group, due to the strict restriction in maximum allowed subjects. Ideally, the control group is the same size as the experimental group. Another limitation of this control group was that it consisted of the researcher himself. As measurements were conducted by himself, and had to be stored on the PC during this experiment run, there was no time to exercise in between these measurements. Ideally, the control subject would also have exercised, but in contrast to the other subjects the control subject would have gotten enough water to rehydrate.

**Equipment limitations**

- *PPG-CRT Prototype limitations*
  - *Timing of the measurements*: These measurements were relatively time-consuming, as every time the strap had to be attached to the subject, and a good skin contact had to be validated. Also, skin-temperature measurements had to be taken with other dedicated equipment, which caused extra time delays. Also, this resulted in skin- and core temperature measurements to be taken on a slightly different moment, causing time-difference between these measurements. Ideally, these measurements are taken simultaneously.
  - *Motion artefact*: In a number of data samples considerable artefacts have been found, most of which could be attributed to relative motion of the sensor in relation to the skin of the subject. Better ways of stabilizing the sensor should thus be found.
  - *Manual pressure*: The assumption before the start of the experiment was that manual pressure application with feedback from a FSR would result in a sufficiently consistent pressure application. Yet is showed to be quite difficult still to keep the compression force within the predefined boundaries, and some variation can be seen in the data recorded from the FSR. In addition, in hindsight it was found that a FSR is actually quite unsuitable to use for accurate force measurements, due to many significant variations in the sensory response of the component to force. Variations are for instance caused by temperature, force duration, humidity and many more factors. A more suitable and accurate sensor would be preferred.
  - *Pulse Sensor*: The Pulse Sensor showed to be very suitable for heart-rate monitoring, yet for this application there are some limitations to the component. Apart from the fact that a small hack had to be made in order to receive the un-amplified signal, the brightness of the led was relatively low compared to similar sensors. Also, the size of the photo-detector was small when compared to similar sensors. This could have caused a sub-optimal SNR. When calibrating the PPG probe for the minimum amount of force needed in order to blanch the skin, it was found that the force had to be quite substantial (at least 14N). The subjects notably experienced it as quite uncomfortable, let alone if this would have been applied to neonates. It is hypothesized that the reason behind this is due to the somewhat large and flat surface of the Pulse Sensor. It is believed that with a smaller contact area, less force has to be applied in order to blanch the skin. With a circular contact surface of the probe, the amount of force needed for a fixed amount of pressure increases exponentially

with an increasing diameter. Therefore a smaller surface area would maybe be preferred due to less force needed. It was also already established in literature that smaller compression forces result in more consistent CRT values [65].
Another observation of using this pulse sensor, was that the blanching process is not very optimal. When assessing the CRT by eye after blanching the skin using the Pulse Sensor surface, the observation was that the middle of the compressed area kept showing a red dot, which shows that apparently the blood in the capillaries is not fully pushed away, but rather pushed to the centre of the compressed area. This phenomenon is never observed when using the finger for compressing. The hypothesis is that the rigid, large flat surface of the probe causes stress accumulation on the skin around the edges of the probe, which pushes the capillary blood towards the centre rather than away from the centre 3.48. It is believed that this can be overcome by using a slightly domed probe, and ideally a slightly compliant material for the tip of the probe. This somewhat mimics the compression by a human finger, and should therefore be more optimal for CRT tests.

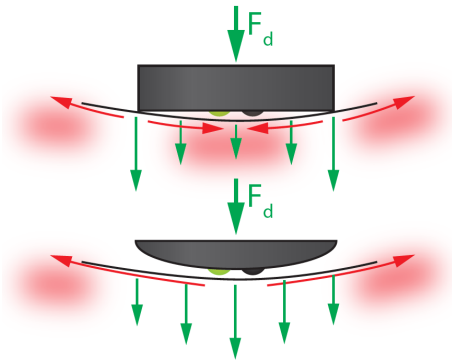


Figure 3.48: Force distribution of a flat surface vs. domed surface.

  - *Unstable sampling rate*: The used micro-controller (Arduino ZERO) didn't have a very stable sampling rate, which caused difficulties during signal processing. In future prototypes, the coding of the device should be made more efficient, whilst using a more powerful processor.
  - *Bad skin-contact on the chest*: Due to different shapes of the chest at the level of the sternum, the PPG-probe did not always make good skin-contact at the chest. This resulted in a lot of rejected samples, and overall bad signal quality. For this reason, the PPG samples taken from the chest should not be regarded as a reliable result.
  - *Inconvenient data storage*: As seen in section 3.6.2, the data is stored in such a way that it needs a lot of processing before it can be analysed. This resulted in a very time-consuming data processing phase after the experiment. In future devices, the data should be labelled more conveniently, so that it can more easily be sorted for automated processing using Matlab scripts, which saves a lot of time. Also, the points where there is a change between the three phases is quite ill-defined. This would be improved when automated compression is used.

- *Cutometer limitations*
  - *Aperture size*: As already established, the area where ST should be defined is at the dermis. For the Cutometer it is known that a larger aperture size causes a deeper penetration depth. Yet, it is ill-defined what the exact contribution of the skin layers are on the readings when using different aperture sized. There is a good chance that the used aperture size (8 mm) was either too small or too wide.
  - *Motion artefact*: On many measurements some motion artefact can be seen due to relative motion between the examiner and the skin of the subject, especially at the chest, since the hand or arm can easily be stabilized on a table surface. Sometimes the motion even caused loss of skin contact, which caused loss of negative pressure.
- *Skin surface temperature measurements*: Apart from the fact that time delays were caused as the skin-surface temperature had to be measured separately from the PPG and Cutometer measurements, instead of simultaneously, the use of this device for skin-temperature measurements is not the intended

use of this device. The object temperature function is mainly intended for other warm objects such as a warm bottle of milk. Therefore the reliability of these measurements cannot be guaranteed. Also, some variations can be seen in subsequent skin measurements.

## 3.8. Discussion

### 3.8.1. Results from the PPG-CRT Prototype

Looking at the overall results of the regression analysis, a lot of inconsistency in the data can be observed. Due to bad skin-contact, the measurements from the chest are considered to be unreliable, and are therefore neglected. Looking at the remaining results, the regression $\bar{R}^2$ coefficients of the single-variate regression analysis between degree of dehydration and the estimated parameter of the exponential model don't seem to show any significant predictive properties. When local skin-temperature is introduced as an independent variable, the $\bar{R}^2$ seem to benefit from it, especially the samples taken from the forehead which are processed using the "half-way" method. Also in the finger there seems to be some effect, yet this is rather inconsistent. This could be explained by the difficulties that existed with taking skin temperature from the index-finger. Other attempts at introducing other independent variables such as core temperature, or even core- and skin temperature simultaneously did not result in any improvements in $\bar{R}^2$.

Based on these results, CRT as measured with PPG would be most optimal when measured on the forehead, and should be adjusted by local skin temperature on the forehead in order to improve the diagnostic performance.

### 3.8.2. Results from the Cutometer

The same sort of inconsistency can be observed in the regression analysis of the parameters that were returned by the software of the Cutometer at each measurement. In the single-variate regression analysis where changes in each Cutometer parameter are compared with changes in degree of dehydration, the only parameter that seemingly shows a consistent and relatively significant coefficient of determination can be seen at the chest with parameter Q1, with an $\bar{R}^2$ of approximately 0.6. Q1 stands for the relative elastic recovery in relation to the total displacement of the skin during the "suction-phase", which is considered to be an representative parameter for ST. This strong $\bar{R}^2$ is therefore expected. Yet, looking at the individual trend-lines of the changing Q1 parameter over time (see appendix S), it can be seen that the trend lines move up in subjects 4 and 6, while the trend lines move down in subjects 2 and 3. It is a reminder that performing a regression analysis on measurements at individual subjects may indicate how well the regression model fits to data on individual level, but it does not mean it is thereby applicable to a larger population. These differences can be explained by the significant biological differences in mechanical properties of the skin in adults.

In a multivariate regression analysis where local skin temperature is introduced as an independent variable, it can also be seen that $\bar{R}^2$ is reduced for Q1 at the chest. On the other hand, Q2 (viscous recovery) at the chest, Q1 at the arm, and R2 (gross elasticity) at both the hand and the arm seem to be improved in terms of $\bar{R}^2$. R2 remarkably also shows a decreasing trend with increasing dehydration at every subject in both the hand and the arm (accept in the hand of subject 2). Observing all trend-lines of R2 in the chest, these also almost all of them show a decreasing trend, although the variability is much higher compared to the hand and the arm, which may be due to the larger motion artefact, which explains the lower $\bar{R}^2$. Altogether it can thus be said that R2, as a parameter representing gross skin elasticity, is showing expected behaviour in by far most cases.

When using core-temperature instead of skin-temperature in the multivariate regression analysis, the resulting $\bar{R}^2$'s change again. Now Q1 and Q2 in the chest show high $\bar{R}^2$ values again, along with R9 (representing tiring effects after repeated suction) and F0 (representing elastic and viscous response to negative pressure) in the hand. R9 indeed shows a consistent trend upwards with increasing dehydration for all subjects, although showing some variability as well. The effect of dehydration on tiring of repeated deformation of the skin has not been anticipated yet, but suggest rethinking the way ST could be assessed, such as looking at tiring of the skin after repeated perturbations.

## 3.9. Conclusion

For the Cutometer, the R2 parameter stands out as a diagnostic parameter for dehydration, especially when combined with local skin temperature. This parameter represents the gross elasticity of the skin (the total skin displacement during suction divided by the total skin recovery after release), and is regarded by the manu-

facturer of the Cutometer as a "very important parameter" (appendix C [2]). It suggests that skin elasticity measurements in combination with local skin surface temperature would be a possible diagnostic variable for dehydration assessment.

Regarding the CRT measurements which were made using the PPG prototype, it seemed that measurements on the forehead resulted in measurements that could in general be used best to predict dehydration, especially when combining the measurements with local skin temperature.

Apart from a few very specific outliers, the parameters which have been included in this regression analysis for both ST and CRT show very unexpected results overall, with not much predictive value or consistency among these results. Also with the outliers described above, none of them show a unanimous $\bar{R}^2$ that comes close to 1, meaning there is still a lot of variations which are not yet accounted for by any variable. Based on the results of this experiment, the experimental hypothesis can therefore not be confirmed yet.

It also has to be mentioned that are a number of significant limitations to the used equipment and the over experimental set-up. Especially the age-group of the participants and the range of dehydration are believed to have significantly contributed to variability in the results. If more severe dehydration was to be achieved, the contribution of unaccounted noise on the data would have probably been for less. It is also expected, based on literature, that children under the age of five would generate much more consistent and expected results. As for the equipment, also considerable limitations were identified, which should be addressed in any future studies.

## 3.10. Recommendations

Based on the insights that have been identified up to now, there are a few key recommendations that should be given away for any future research regarding this topic.

1. Based on the identified limitations of the used equipment in this experiment, a new set of prototypes should be developed as functional prototypes which are suitable for use as data-collection devices. Key should be that no user related variability should be allowed when using these prototypes, meaning all processes (including kinetic processes) should be automated. Prototypes should be developed based on CRT and ST, as these are still proven to have the best overall diagnostic performance. Yet, preferably more research should be conducted into more direct ways of measuring dehydration, such as directly measuring the water content of a large piece of tissue. Altogether a set of at least 3 prototypes should be developed, which could all be used by researchers for data-collection studies

2. The next step would then be to conduct a data-collection study, indeed using the set of prototypes which is suggested above for comparison. In this experiment a learning point was that measuring only a small number of up to 4% dehydrated adults will not generate any statistically significant results. A suggestion would therefore be perform a child study, where the effects of severe dehydration in children are measured using the different prototypes. It is obvious that conducting a similar lab test with actively stimulating dehydration in young children would ethically be an issue, and should therefore not be considered as a feasible next step. Performing data collection tests on children that already suffer from severe dehydration (due to diarrhoea) in a clinical setting would therefore be preferred. Yet, such patients are very rare to find in high-quality healthcare systems such as in the Netherlands, based on conversations with a neonatologist, see appendix B. It is therefore recommended to, after having done small validation tests with the prototypes, already go with the functional data-collection prototypes to low-resource settings, in areas where the prevalence of dehydration is known to be high. It is recommended to cooperate with local health-workers who cope with dehydrated children on a daily basis. These health workers could use these prototypes (one at a time) in parallel to their normal work-flow, on the condition that this extra action does not interfere with their normal work-flow in a damaging way. The data collected with the devices should be compared with the degree of dehydration, by letting the health worker monitor the weight gain of the patient. The initial degree of dehydration at the time of first contact with the patient can then be derived retroactively, by defining the weight of the patient when he/she is considered to be fully rehydrated.

   The collected data can then be analysed in a similar way using multivariate regression analysis. If needed, for instance when a lot of different parameters need to be analysed for their relation to different degrees of dehydration, *machine learning algorithms* would be a suggested method for defining a definitive predictive model for use in future diagnostic tools for dehydration assessment. This definitive predictive model should then not be limited to a single diagnostic variable with any confounding factors taken into account. The feasibility and diagnostic performance increase of using a combination of

diagnostic variables, such as CRT an ST, should thus also be investigated, as it is hypothesized that any combination of diagnostic variables would improve the performance of any eventual diagnostic tool.

# 4

# Prototype Redesign

Based on the recommendations given at the end of chapter 3, it was decided to spend the last month of this assignment on translating the insights and identified limitations into an improved PPG-CRT prototype. It was decided that the remaining time for this assignment would be too short to be able to build a set of functional prototypes and test all these prototypes in a dehydration study in low-resource settings, as was recommended in chapter 3. This prototype therefore is intended as a demonstrator, and a next step towards a prototype that would be suitable for use in the type of data-collection study which is mentioned in the same section. The intention is to also do a quick validation study which should prove the working principle of this prototype, or in other words, answering the question: *"Is this technological principle indeed capable of measuring expected differences in CRT?"*

It was chosen to go forward with the PPG-CRT prototype specifically for several reasons. First of all since there was already a lot of experience in prototyping using PPG from building the first prototype. In addition, CRT would in theory still be the most promising diagnostic variable to further investigate. ST on the other hand is also still promising, especially based on some of the findings from the conducted experiment. Yet, there are still a lot of unknowns regarding automated ST assessment. Questions such as how to effectuate the proper depth of measurement, how to actuate the deformation of the skin and how to sense the response of the skin are yet to be investigated. For all these unknowns, it would be best to initiate a whole new assignment, in order to make a substantiated design direction for the next prototype based on ST.

## 4.1. New list of requirements

Following the list of requirements in section 3.4.1, in this section a set of additional or substitute requirements will be defined.

**Physical and mechanical requirements:**

- The timing and the applied force during the compression phase should be automatically controlled by the prototype. Force application should ideally be controlled using feedback PID-control with an

accurate force sensor, to be able to cope with any perturbations. The set-point for the wanted force should be adjustable. The actuator itself should generate a force output that can be easily manipulated, and should have a fast response time. Steady state force output should be reached within 100 ms, while force release should happen instantly. The actuator should be able to exert forces up to 10N.

- The prototype should have integrated temperature sensors that measure local skin-surface temperature accurately during CRT testing, with a resolution of at least 0.1°C.
- Influence from motion artefact should be mitigated. This could be done by increasing the friction coefficient between the probe and the skin, by increasing the surface of the contact area by adding an extra stabilisation surface surrounding the PPG probe, or by mechanically dampening any motion perturbations through spring-systems.
- The probe used for compressing the skin and measuring the CRT data should have a diameter of not more than 10mm. Also should the probe be slightly domed, in order to more effectively blanch the dermal capillaries.
- The prototype should have an "initiate measurement" button, which starts an automated measurement protocol, as well as a reset button.
- The prototype should be designed to work on the chest at the level of the sternum, and/or on the forehead.

**Signal and data processing requirements:**

- A stable sampling rate of 100Hz should be achieved.
- Any noise on the PPG signal with frequencies higher than 15Hz should be filtered out using analogue filters.
- Data should only be stored when the measurement protocol is running (after pushing the initiate button).
- The prototype should have an integrated real time clock in order to give appropriate time-stamps to the measured data.
- All data vectors should be labelled appropriately in the first row.
- All data samples should be labelled by their corresponding measurement phase (phase 1, 2 or 3), in order to easily separate the data in terms of measurement phase.
- Per measurement, a new .csv file should be created, with the time-stamp as name.
- An error protocol should be integrated that recognises any anticipated issues with the software, which controls an error LED.
- LED's should indicate the progression of the measurement protocol.
- A serial connection with a pc should be possible to plot the data in real time, both when measuring and when not measuring. Through this serial connection, information on measurement progression should also be printed on screen.

## 4.2. Concepts

Before translating the list of requirements into a tangible device, an ideation and conceptualization phase had to be conducted in order to come to a well substantiated prototype design.

### 4.2.1. Ideation: How-to's

In this section the ideation phase is documented by means of dealing with five key *how-to* questions. These questions are answered with idea sketches for future prototypes. In this section, all idea sketches per question are illustrated and explained.

How to stabilize the probe to the skin to minimize the motion artefact, while applying minimal pressure to the skin (Pre- & Post-compression phase)?

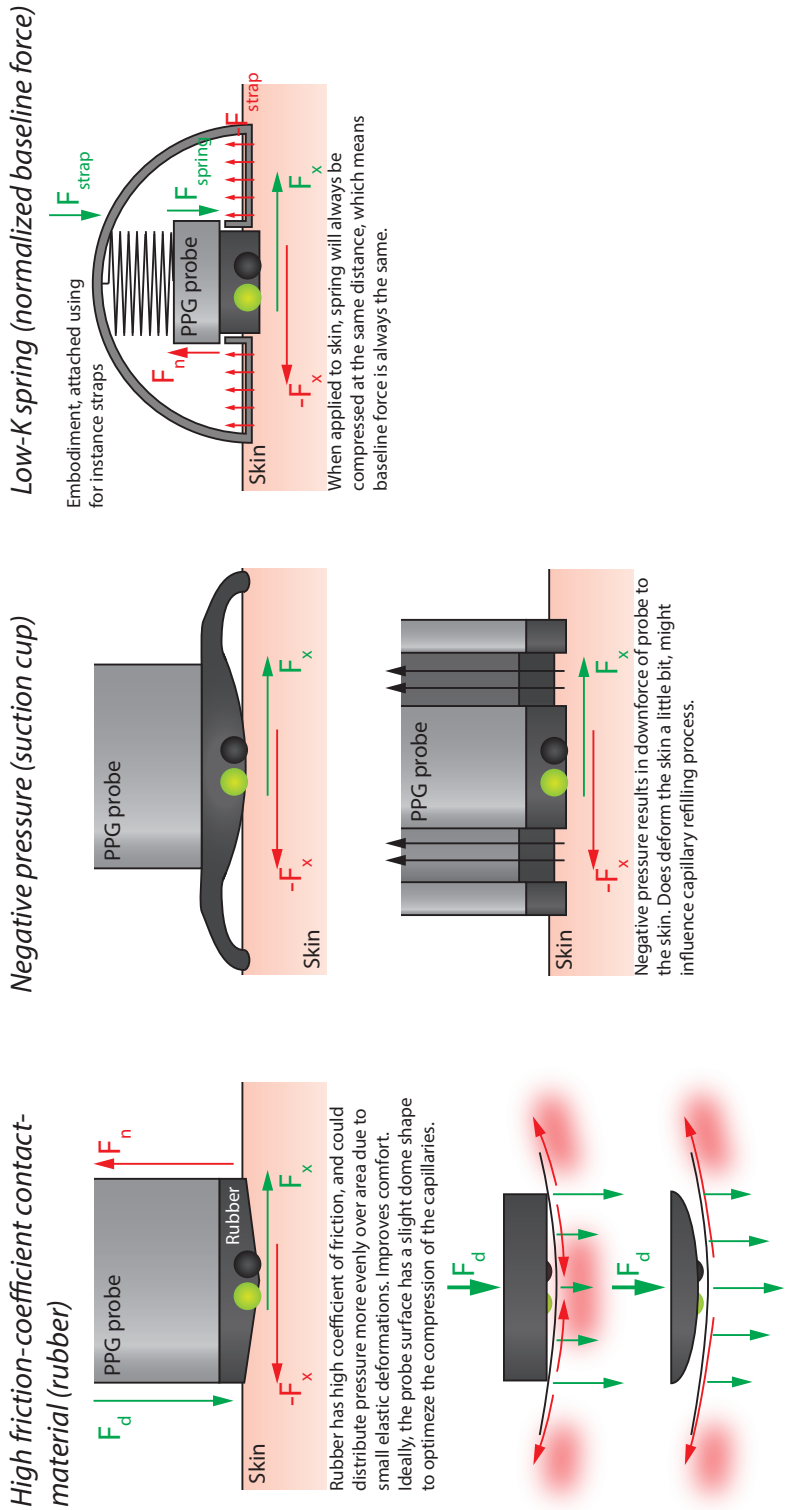

# How to apply a controlled amount of force on the skin for a controlled amount of time?

*Manual compression with feedback*

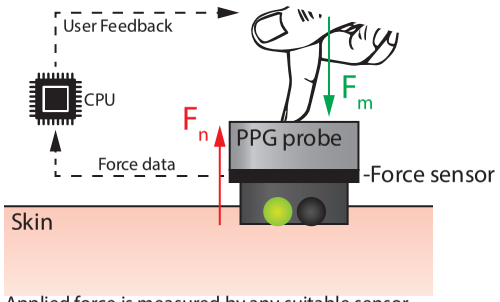


Applied force is measured by any suitable sensor. Force data from sensor provides feedback to use on the correctness and time of the compression.

*Manual compression with mechanical (passive) force control*

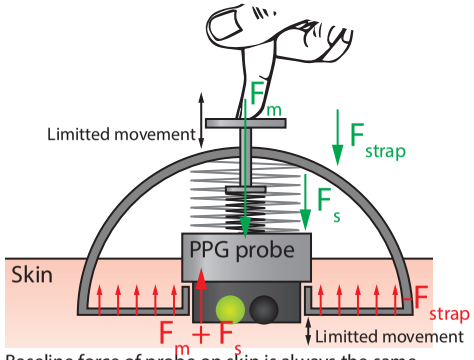


Baseline force of probe on skin is always the same due to the big spring and the limitted relative displacement of the probe. Compression is actuated manually by pushing the press button all the way down. The small spring will ensure a standard force everytime the button is pushed. Still needs feedback for time (switch in circuit?).

*Automated compression*

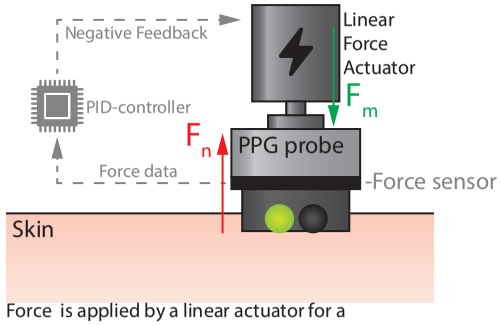


Force is applied by a linear actuator for a standardized amount of time. Amount of force is accurately controlled, could be supported by a force-sensor feedback-loop. A more sophisticated version might also use PPG-waveform as an input signal for the feedback loop (should be flat).

# How to determine local skin temperature accurately within 10 seconds?

*Average T from multiple sensors*

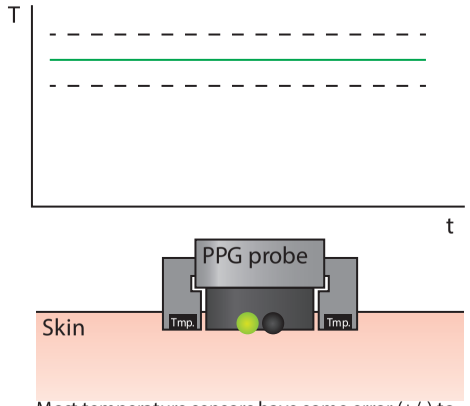


Most temperature sensors have some error (+/-) to the actual temperature. By using 2 or more sensors closely around the measurement site, you can take the mean measurement of those sensors to minimise the error.

*Predictive curve for slow-response sensors*

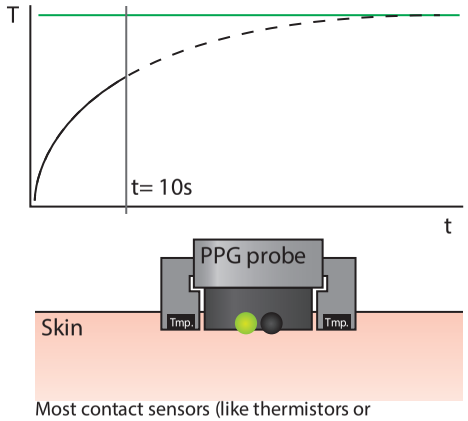


Most contact sensors (like thermistors or semiconductor sensors) have a certain stepresponse to rapid temperature changes, which sometimes takes much longer than 10 seconds to reach a steady state reading. To take this into accound one can extrapolate the initial curve to estimate the asymptote. This might increase error of the sensor, and does require some computational power from the device.

*Use non-contact IR sensors*

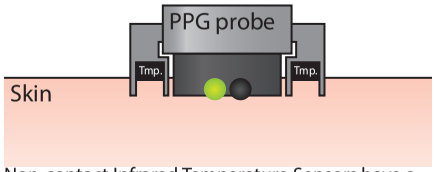


Non-contact Infrared Temperature Sensors have a very fast response, and are easy to implement. They are a bit less accurate than most contact sensors (+/- 0.1°C, between 30°C & 40°C) and are a bit more costly. They are easy to implement, and can also measure ambient temperatuer in parallel.

# How to make a tool that fits all sizes (finger, chest, head), without having effect on the pressure that is exerted to the probe?

### *Head & Chest: Use large contact area for attaching the probe*

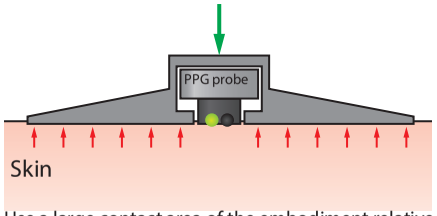


Use a large contact area of the embodiment relative to the compression piston area (containing the PPG probe). This spreads out the downforce (to keep the device in place, straps could be used). Contact area could be made slightly flexible. Reaction force of compression piston needs to be taken into account

### *Finger: large contact area surrounding the PPG probe*

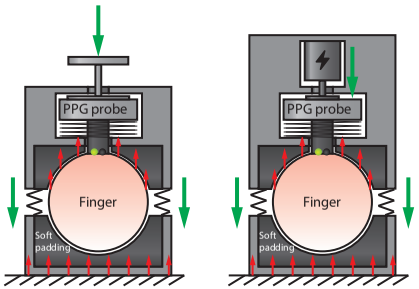


Use a clip or "cigar-cutter" like design to clamp the finger with a standardized, continuesly low pressure. The probe piston can be pressurized manually (external) or by an actuator (internally). In the last case a thoughtful consideration between clamp & piston area, as well as clamp & piston force has to be made as such that clamp and piston are of minimum influence to each other.

### *Finger: Active force standardization*

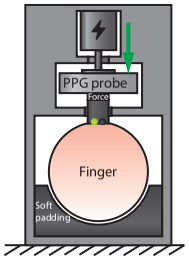


Instead of using passive springs for force normalization, a linear actuator is used with a very linear force controll over the total reach of its travel. Maximum travel should also be higher to make the probe fit all sizes of fingers. A high quality force sensor would probably be key in this design, as well as a fast responding, accurately controllable linear actuator for both position and force. Will increase cost.

# How to make a lay-out for the PPG-probe (Led('s) and photodetector(s)) that is optimal for capillary refill time measurement?

## *Standard off-the-shelve emittor-detector set-up (Osram)*

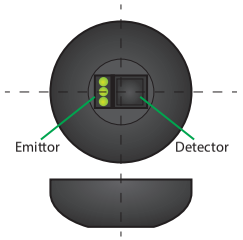


The standard Osram SFH 7051 BioMon sensor module can be used in its standard lay-out. Between the emittor (green-LED) and detector a barrier is placed to minimise optical cross-talk. It is a proven set-up for heartrate monitoring, and can be integrated relatively easy. It is though a one-directional measurement, and the module itself has a flat (non-domed) surface. A transparent domed cap could be placed over the sensor, with a light barrier to prevent optical cross-talk, to make the probe domed again.

## *Circular lay-out*

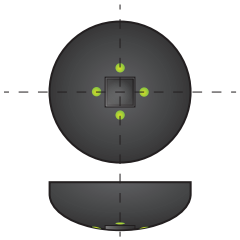

A circular lay-out would enable to record capillary refill from multiple angles, especially when used sequentially. This might give a more accurate recording of capillary refill, as this is assumed to be a "circular" process. The transparant protective cap on the detector would be domed for an optimal compression of the capillaries.

## *Adittional reference PPG-sensor*

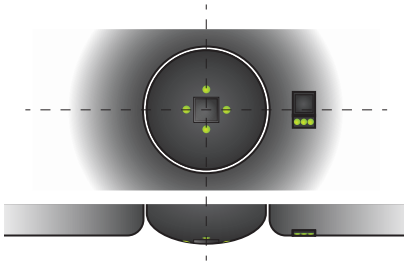

The surface surrounding the compression piston (non-compressing surface) should also house a PPG sensor as a reference. This reference PPG waveform could (among other things) be used to filter out the pulsatile component of the Capillary Refill signal. It should be investigated wether or not this improves accuracy of the overall method. The pressure on this PPG sensor should be constant and there should be no optical crosstalk between this sensor and the piston LED's.

### 4.2.2. Conceptualization

The ideas that have been sketched in section 4.2.1, will now be converged into 3 main concepts. These 3 concepts are illustrated in this section.

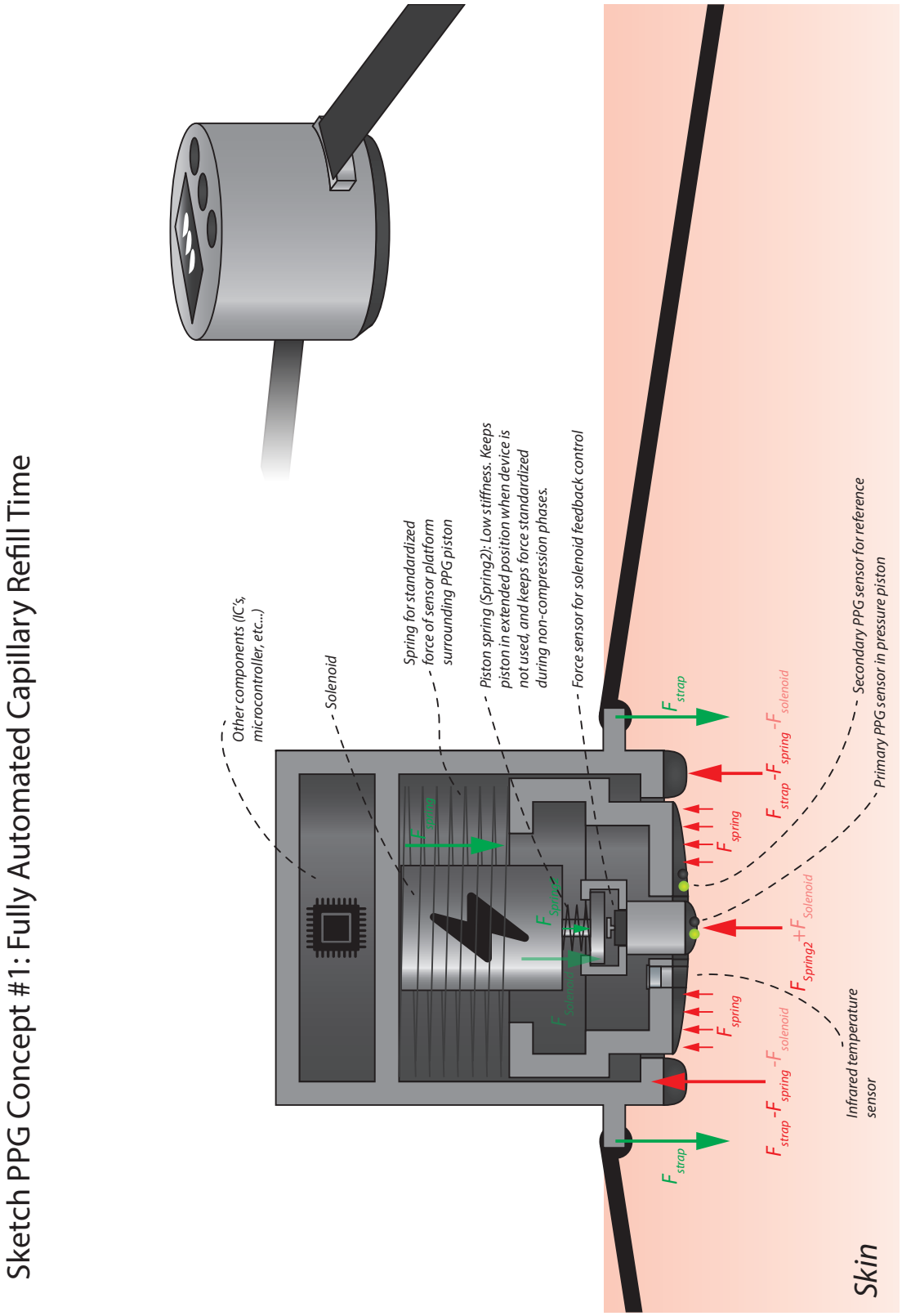

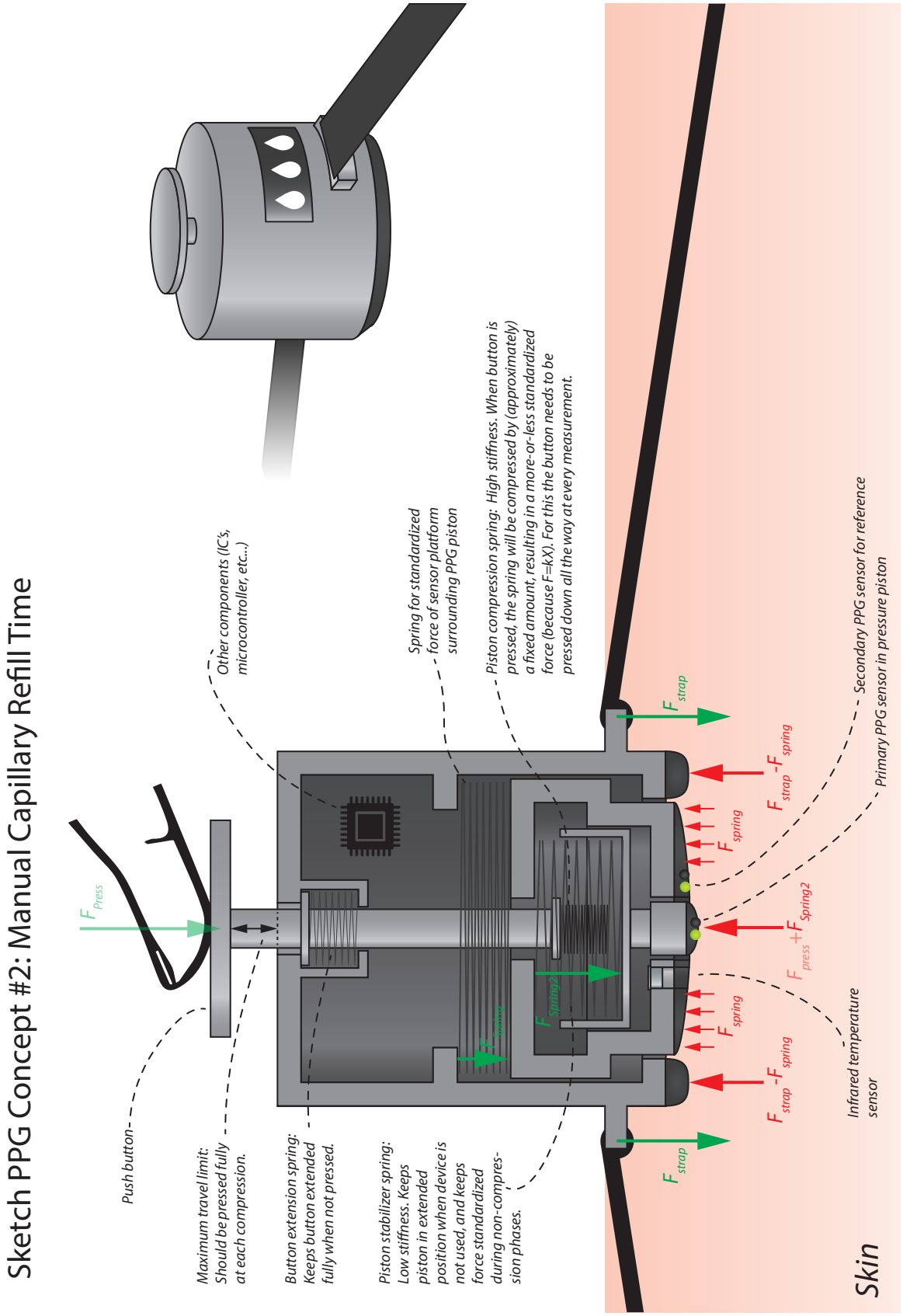
Sketch PPG Concept #2: Manual Capillary Refill Time
Push button
Maximum travel limit: Should be pressed fully at each compression.
Button extension spring: Keeps button extended fully when not pressed.
Piston stabilizer spring: Low stiffness. Keeps piston in extended position when device is not used, and keeps force standardized during non-compression phases.
Other components (IC's, microcontroller, etc...)
Spring for standardized force of sensor platform surrounding PPG piston
Piston compression spring: High stiffness. When button is pressed, the spring will be compressed by (approximately) a fixed amount, resulting in a more-or-less standardized force (because F=kX). For this the button needs to be pressed down all the way at every measurement.
Secondary PPG sensor for reference
Primary PPG sensor in pressure piston
Infrared temperature sensor
Skin
F Press
F Spring
F Spring2
F strap
F spring
F strap -F spring
F press +F Spring2

# Sketch PPG Concept #3: Finger + Chest simultaneous Capillary Refill Time

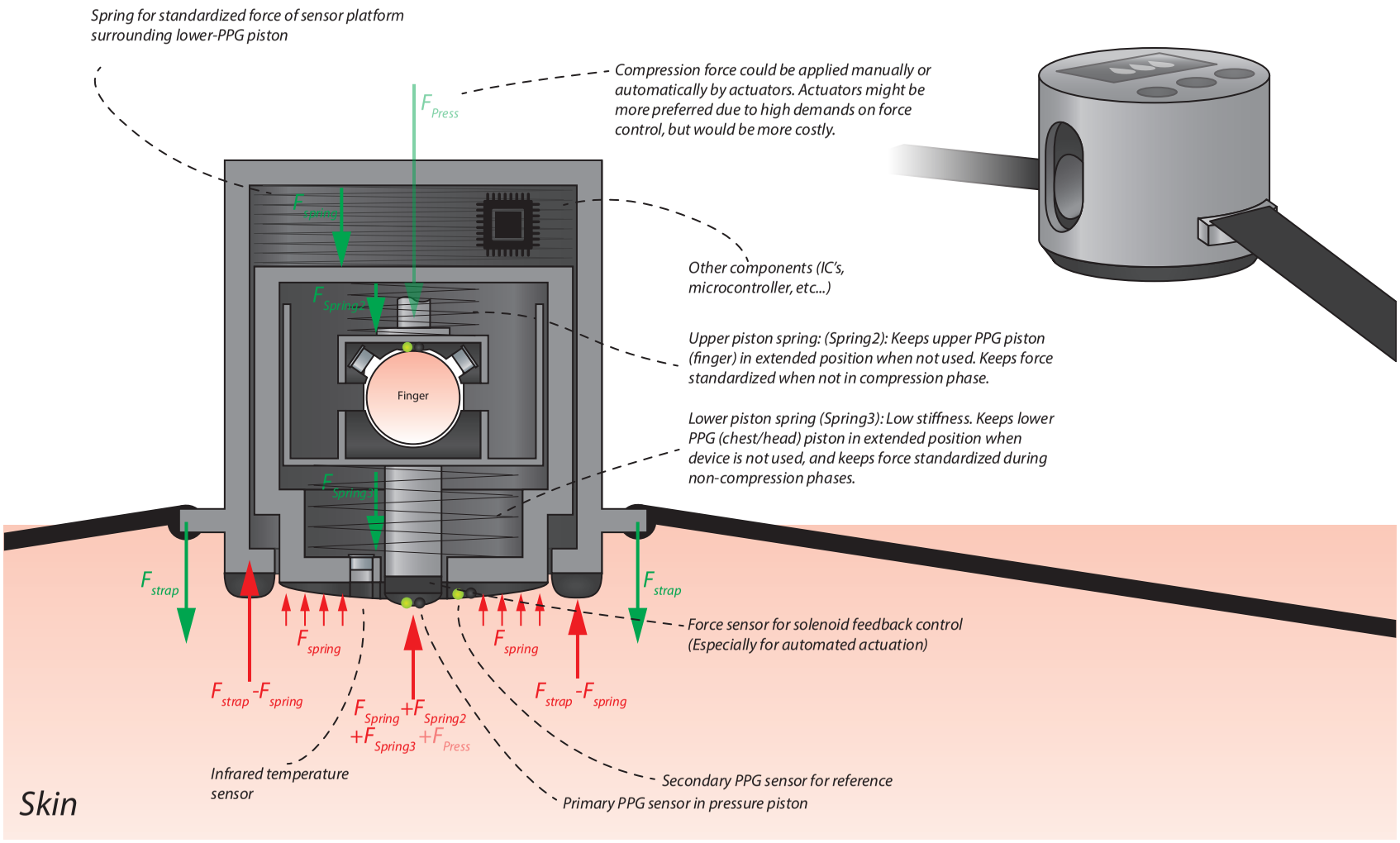

### 4.2.3. Concept choice for Prototype #2

From the concepts shown in section 4.2.2, a few main features are brought together in a final design for the prototype. Below a first sketch is given.

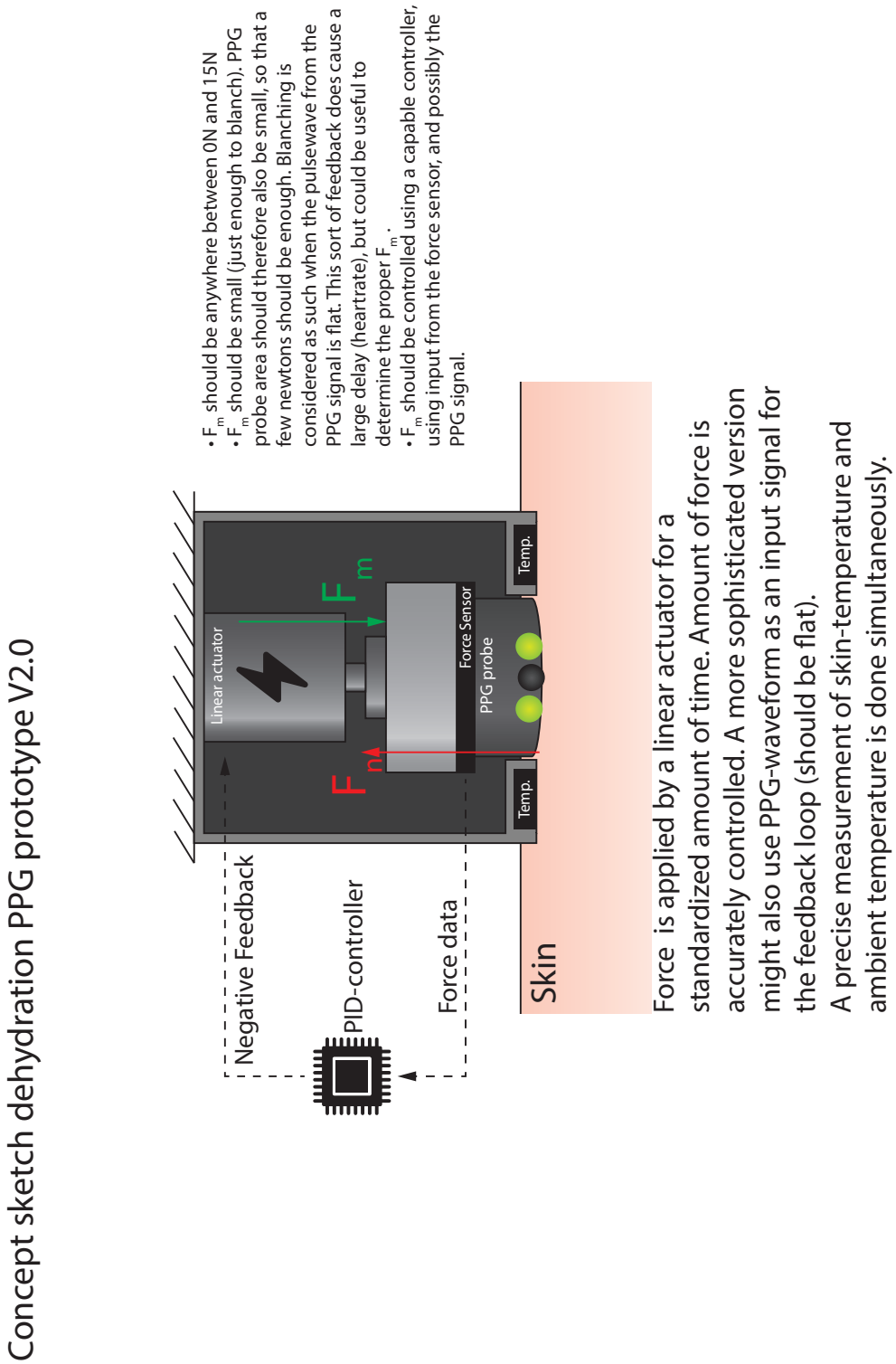


It has been chosen to use a linear actuator for applying a controlled amount of force on the skin during the blanching process. That does not mean that using springs for controlling the amount of exerted force

cannot be used as in concept #2, but for purposes of quickly prototyping a highly accurate device in terms of force application, it was chosen to use an actuator. A relatively cheap actuator could be used, as long as it is interfaced with a highly accurate force sensor to provide force feedback through a PID-controller. In figure 4.1 a final version of the working principle is visualized in the form of an FBD.

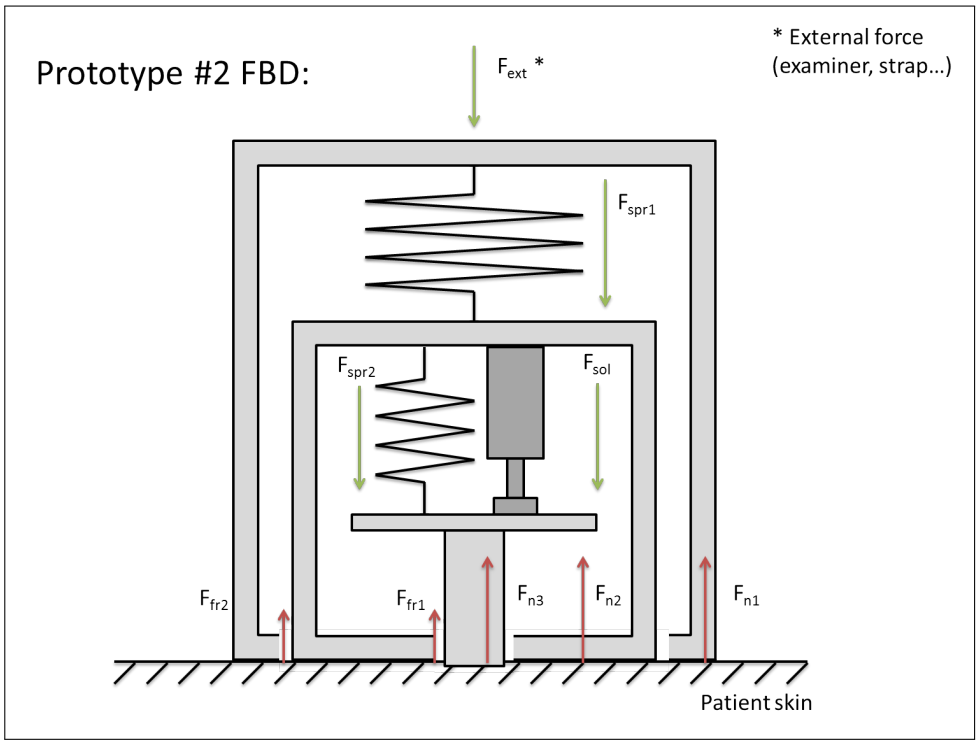


Figure 4.1: A conceptual FBD of Prototype #2

In line with the concept sketches in section 4.2.2, it is finally chosen to use a *telescope* design: the small-surface PPG-piston is surrounded by a larger piston, which houses additional PPG and temperature sensors, which is in turn surrounded by an outer cylinder. This means that there are 3 contact surfaces with the skin which can move relative to each other. Smallest piston, the CRT-PPG piston, is there for the reason of blanching the skin whenever the actuator (the solenoid) exerts force ($F_{sol}$) to it. Whenever the actuator is at rest, the downforce of $F_{spr2}$ will cause a slight downforce which ensures a good skin-contact. The down-force is small enough to allow blood in the dermal capillaries to pulsate, meaning that it will have minimal effect on CRT. Any effect that this downforce still introduces will be consistent, as $F_{spr2}$ is always approximately the same. This is ensured as the CRT-PPG piston is always pressed into the larger piston until the same depth (causing a consistent compression of SPR2), since when the device is pushed upon the skin the surfaces of the CRT-PPG piston and the larger piston are always aligned. Similar is the mechanism that keeps the larger piston level with the outer housing. $F_{spr1}$ always pushes the larger piston down with the same amount of force as that spring is always compressed to the same level. SPR1 should press the larger piston lightly against the skin to ensure good skin contact with the sensors, and it should ensure a consistent amount of downforce in all situations. Since the force that is needed to keep the probe in place is exerted to the outer part of the housing ($F_{ext}$), this force can be high and may vary, as force variations will never result in significant differences in compression length of the springs. Any abundant force (greater than the reaction force of both compression springs) on the outer part of the housing is thus completely counteracted by this outer-part, without effecting the inner pistons which contain the sensors. For this reason, this external force may be applied by a strap that keeps the probe in place, or it could be applied by the human examiner (the user) that manually keeps the probe in place.

In this prototype it has thus been chosen to control the amount of force that the device exerts on the skin during pre-compression and capillary refill phase in a passive manner using compression springs. This downforce should be minimal, and the spring-constants (k) of both linear compression springs should be as low as possible in order to keep the force constant even when the shape of the part of the body the probe is placed on differs slightly. These springs are also expected to absorb any motion artefacts in the axial direc-

tions, which should prevent motion artefact in the signal.

During the compression phase on the other hand the actuator exerts actively controlled force to blanch the skin. This force exerted by the actuator plus the force of the spring $F_{spr2}$ should not be greater than $F_{spr1}$, as that would result in the larger piston being pushed away from the skin. $F_{spr1}$ should thus be sufficiently high to prevent this, but since the contact surface area of the larger piston is significantly larger than that of the smaller CRT-piston, $F_{spr1}$ is allowed to be much higher than $F_{spr2} + F_{sol}$, as a larger area results in smaller pressure on the skin. Pressure is considered key here: the down-force may be high, but as long as the surface area is large and therefore the pressure is low, this force would not interfere with capillary blood flow. friction between the moving parts, $F_{fr1}$ & $F_{fr2}$, should be kept minimal, and should be considered when choosing the material of this prototype.

It is chosen to anchor the actuator to the large piston, instead of the outer housing as is seen in concept 1 in section 4.2.2. The reason is to keep the same offset for the actuator at every measurement, as the displacement of the larger piston may vary between subjects of body locations. It is important to keep the displacement of the piston relatively minimal, due to non-linearities of the actuator in relation to armature-displacement, which is further explained in section 4.3.1. If the actuator would be anchored to the outer cylinder, the force exerted by the actuator would admittedly have less effect on $F_{n2}$, which would be beneficial for preventing artefacts on the signals of the sensors in the larger piston. Yet due to the high dependency of the actuator on armature displacement, and the limited throw of the actuator armature, it was considered best to anchor the actuator to the larger piston to minimise variations in armature displacement.

## 4.3. Design

### 4.3.1. Main Components

Before starting on the materialization of the prototype, an overall architecture was first defined as shown in figure 4.2. In general, the prototype should consist of a powerful micro-controller as the central processing unit of the prototype. This micro-controller should be able to convert incoming digital and analogue data (from the force sensor, PPG sensors, temperature sensors and the real time clock) into numerical values which can be stored on the Micro-SD card. In addition, the force sensor data is used as input for the PI-control loop which controls the force output of the linear actuator (the solenoid). Based on this architecture a list of main components is made, which will all be discussed in this section.

#### PPG Module

In this new prototype, it is chosen to stick with green light reflective PPG. Yet, to be able to comply with the requirements from section 4.1, the PPG module should be much smaller compared to the previously chosen module. Also, in order to optimize the SNR, a larger photo-diode (PD) surface is preferred. This would increase the sensitivity of the sensor towards the reflected green light, as it would absorb more light and therefore produce a larger current. A higher intensity of the green-light emitter (the LED) would also increase the SNR. In search for a suitable PPG module, which involved interviews with PPG-experts at Philips Research, the *Osram BioMon Sensor SFH 7051* was chosen (figure 4.3).

This PPG module was chosen since it has long been a trusted module by Philips Research Employees for prototyping reasons. It was also the only module that was found that fully relies on green-light reflective PPG, as it houses 3 very bright green LEDs. Combined these 3 LEDs would be a very high intensity light source, which combined with the larger PD would result in an optimal SNR. The package outline is also very small (just 4.7mm * 2.5mm * 0.9mm), which gives the design freedom of making PPG probe with a small surface area. If the surface diameter of the probe should not exceed 10mm, this PPG module would even leave space for a probe edge with a fillet (a rounded edge), which is considered a good alternative to a slightly domed probe. A fully domed probe surface would on the other hand not be possible with this "flat surfaced" module, since close skin contact is required in order to prevent optical cross-talk (when the emitted light is reflected directly from the

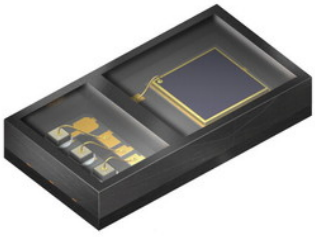

Figure 4.3: The Osram BioMon Sensor SFH 7051. Source: http://www.osram-os.com/osram_os/en/products/product-catalog/infrared-emitters%2c-detectors-andsensors/optical-sensors/health-monitoring-sensors/sfh-7051/index.jsp

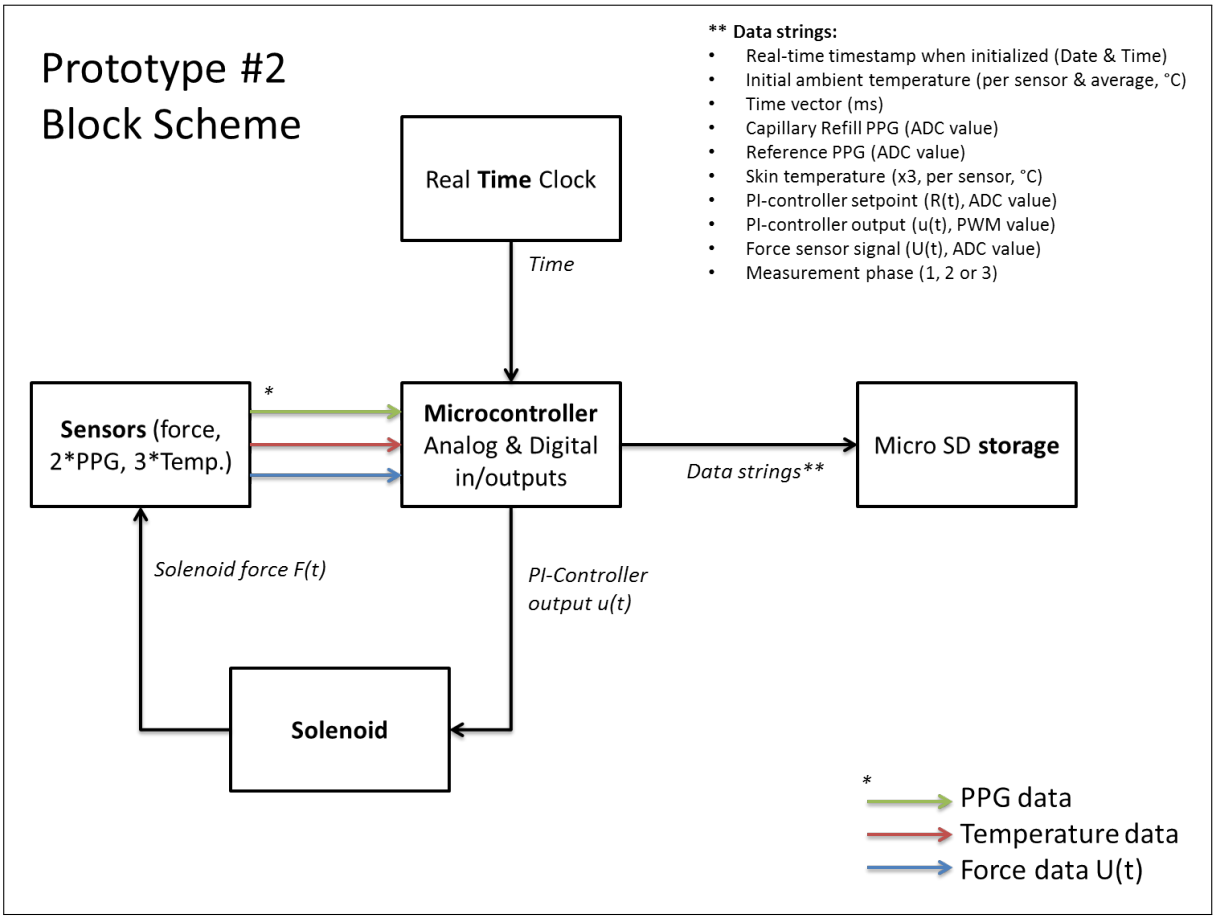


Figure 4.2: A block-diagram of the overall architecture of the prototype.

surface of the skin onto the PD, without first penetrating the epidermis), which would increase noise. The PPG module features a barrier between the LEDs and the PD to prevent this with good skin contact.

The small package of this PPG module is mainly as this is a very "passive" component, consisting of merely 3 LEDs and a PD, and 8 solder pads for connecting each of these components. This also means that the signal current from the PD still has to be filtered, amplified and converted to voltage in order to be used as an input signal for the ADC. With the PPG module from the first prototype, this circuitry was already integrated into the module. This module requires custom circuitry for these applications, which does provide more freedom of signal processing (one can now choose an optimal filter and amplification). More information on the chosen method of interfacing the PD output will be explained in section 4.3.2. For the full data-sheet of the PPG module of choice, please see appendix T [9].

### Force Actuator

For this prototype, an electromechanical linear actuator was needed in order to automate the blanching process. The main requirements for this actuator are that its force output should be variable, and that its response to the input current should be as good as instant. In search for an appropriate actuator, the *solenoid* came up as a very good option. Its main benefits are ease of integration, ease of control, instant response to input current, its low price and relatively small dimensions, making it very suitable for integrating it into a hand-held device. Typical uses of solenoids usually involve pinball levers, locks, switches and valves.

Figure 4.4: The used 9-24 VDC electromechanical solenoid. Source: `https://www.adafruit.com/products/413`

A solenoid is a very simple component, basically consisting of an inductive coil with a steel or iron rod in the centre. To put it in simple terms: when a current is flowing through the coil, it is known that it creates a condensed magnetic field in the centre of the coil. This coil functions as an electromagnet to the rod in the centre of the coil, and is therefore able to push the rod away from the centre. The electromechanical solenoid therefore functions as a sort of pneumatic/hydrolic cylinder (but than without using gas or fluids), which can either produce a push or pull reaction of the armature to an applied current. The higher the current flowing through the coil, the higher the output force. The output force of the solenoid can therefore be controlled in a similar way as by controlling the speed/torque of a DC-motor. One can vary the current or voltage to control the force output. Yet, the micro-controller (the Arduino DUE, also explained in this section) can only supply up to 5V. Therefore an external power-source other than the micro-controller should be used, which can deliver a supply voltage of 9V to 24V, and a current of about 250mA (based on the technical details provided by the supplier). For now, a 12V wall-adaptor with a maximum current draw of 1.5A would suffice to generate sufficient force.

To be able to vary the force output of the solenoid with the 12V power input, a *Pulse-Width-Modulated* (PWM) input signal will be used to control the delivery of this input current. The PWM output signal of an Arduino is a very fast on-off sequence, which repeatedly outputs either a 0V or a 3.3V output signal from one of the digital output pins with a frequency of at least 500Hz. The controller can vary the *duty cycle* of the PWM signal, which stands for the proportion of the "on-time" in relation of the "off-time" during every cycle. So a duty cycle of 0% means that the signal is constantly 0V, a duty cycle of 100% will be a signal that is constantly 3.3V, and a duty cycle of 50% will be a pure square wave that switches between 0V and 3.3V 500 times per second, with the on vs off time being equal. PWM signals are often used to power DC-motors, for which the duty cycle stands for the average amount of voltage supplied to the motor. The PWM output signal can be used in combination with a high-speed transistor, which is used as a switch controlled by the PWM signal to either open or close the circuit of the solenoid with the 12V power supply. Therefore in this case the average voltage supply to the solenoid can be varied between 0V and 12V. So the higher the duty cycle, the higher the output force of the solenoid. Vibrations due to the PWM signal are negligible, due to the high frequency of the signal and the inertia of the armature of the solenoid. A schematic of this circuit can be seen in figure 4.15 in section 4.3.2.

One disadvantage of using a solenoid for as an force actuator is the influence of the position of the rod with respect to the centre of the coil to the output force (next to flowing current in the coil). In general, it means that the further the push-rod is pushed out of the coil, the higher the output force is (see figure 4.5). This dependence on position is also non-linear. This makes it somewhat more difficult to control the force output of the solenoid. One way of solving this issue is to control the solenoid force output using a PID-controller, with a very accurate force sensor in the feedback loop. Key is to make the embodiment design of the PPG probe as such that the position of the armature varies very minimally when the prototype is used, so that it stays within the range of maximum force outputs needed for blanching the skin. On the other hand, it was found that the output force increases drastically when the position of the armature reaches 0mm (which means fully extruded on the push-side of the solenoid), which causes oscillations at the PID-controller. Therefore full extrusion should also be avoided by clever probe design.

#### Force Sensor

As explained earlier, a feedback control loop is needed in order to produce a consistent compression force using the Solenoid. In the feedback loop, an accurate force sensor needs to be integrated, as the exerted force will be based on the reading of this force sensor.

In the first prototype, a FSR was used for (discrete) visual force feedback. the FSR is a fine choice when cost and size are key differentiators, although it is known that these sensors should not be used for high-accuracy force measurements. In the data sheet of the used FSR (appendix E [6]), it can be seen that that the force repeatability is +/- 2%, the force sensitivity range starts at 0.2N (in a validation test it was even found that it only starts at approximately 1N as can be seen in figure 3.26), and that the sensor is influenced by temperature, humidity and hysteresis (10%, which is the difference in force readings between inclining and declining forces). Also, in a voltage divider set-up, the sensitivity is very non-linear (as can be seen in figure 3.26) and varies a lot in general under a constant load.

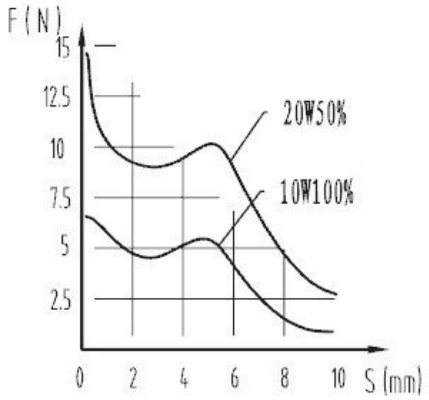


Figure 4.5: The dependence of the output force on the position of the rod, for the used 9-24 VDC electromechanical solenoid. Source: `https://www.adafruit.com/products/413`

When using a digital controller, the accuracy of the actuator directly relies on the accuracy of the used sensor. Also a fast response time, a near-zero lower-limit sensitivity range and low hysteresis are important, as these factors may cause instability of the feedback control system. This is in this digital control loop much more important compared to the discrete visual feedback provided to the user in the previous prototype, as humans are inherently less accurate actuators compared to electromechanical actuators. It can therefore be concluded that a more accurate force sensor is necessary in the new prototype.

In search for a more accurate force sensor, other types of FSRs were considered. The previous type was a *shunt-mode* FSR, which is cheaper and less accurate. Thru-mode FSRs have a more accurate sensitivity, and are also somewhat higher cost. These sensors are equally compact, and are therefore sometimes used in some medical devices for haptic feedback. Yet, the same limitations of humidity and temperature drift still exist here. In general, even in the case of a well-designed mechanical system, the resistance accuracy of any FSR is limited to about 10% [10]. A more accurate option could be a *single point load cell*, which has total error of 0.0064% at a constant room temperature [11]. Yet, with 60 grams and dimensions of 110mm * 33mm * 10mm, this load cell is considered to0 bulky for a small handheld sized measurement probe. Therefore, it was in the end chosen to use the *Honeywell FSG010WNPB* piezo electric strain gauge, which is with 9mm * 8mm * 12.7mm is much smaller. This sensor has a very good linear response to force (+/- 0.5%) and a very good repeatability (+/- 0.2%), based on the data-sheet provided in appendix U [4]. Also, it has a sensitivity range of 0N to 10N, which means it is sensitive to very small amounts of force (smaller than the minimum 1N needed for the previously used FSR). This fine balance in size and accuracy make this sensor the optimal choice as a feedback sensor to use in combination with the solenoid.

Figure 4.6: The Honeywell FSG-series Force Sensor. Source: the data-sheet (appendix U [4])

The sensor has 2 output pins, which under zero load provide an output voltage of half the supply voltage. The Vo+ output voltage increases when the load increases, while the Vo- output voltage decreases when the load increases. The difference of these two voltages (Vo+ - Vo-) is linear to the load. To appropriately integrate the sensor into the circuit these output voltages have to be amplified using a difference amplifier, which will amplify the output difference to a voltage that can be read by the ADC. This will be further explained in section 4.3.2 (see figure 4.14).

### Temperature Sensor

The main requirements for the temperature sensor are accuracy and response time. Most contact-based sensors, such as conventional thermistors and thermocouples, sense temperature based on heat transfer to their sensitive part. This transfer of energy takes time, based on thermal conductivity of the material of interest (skin). This results in exponential response curves to temperature changes. Ideally, the sensor can instantly sense the temperature of any object instantly with high accuracy. An internal contact suggested the use of the *Melexis MLX90615 Non-contact Infra-Red Thermometer*. This is a digital, compact sensor, with an accuracy of better than +/- 0.1°C between 30°C and 40°C, as stated in the data-sheet (appendix V [7]). It also has a very high readout resolution of 0.02°C, as this is not an analogue device. The object-temperature is measured by sensing the infra-red radiation emitted by the object, which can be done from a distance. As this relies on radiation rather than conductive heat transfer, the response time to heat changes is instant. An additional benefit is that these sensors can measure ambient temperature as well as object temperature in parallel. They are also intended to use in body-temperature related applications such as with home healthcare devices, ear-/fever thermometers, and continues body temperature monitoring. Given these features, this sensor was considered the optimal choice for this prototype. The main objective of these sensors is to measure the exact skin surface temperature at the exact body location where CRT is measured with the prototype. Yet, this is physically impossible, one can only place the temperature sensor in the vicinity of the PPG sensor that is measuring the CRT signal. Therefore it was chosen to place three temperature sensors in a circular pattern closely around the PPG sensor that measures CRT. It is assumed that taking the mean of the measured temperatures would be a sufficient approximation of the skin temperature that is directly under the PPG sensor in the middle.

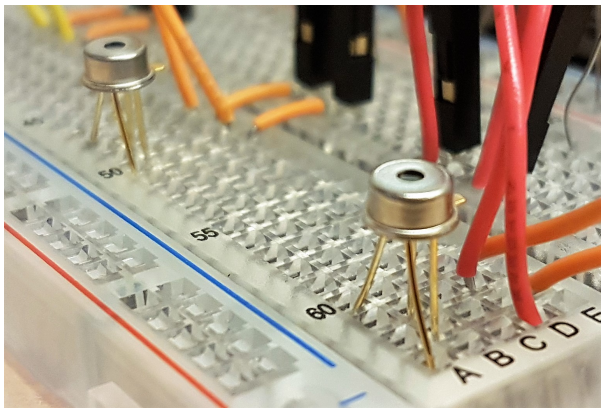


Figure 4.7: Two Melexis MLX90615 Non-contact Infra-Red Thermometers, connected through a breadboard during the test-phase.

### Real Time Clock Module

One of the problems that were faced when using the previous prototype was the very inconvenient way of storing and labelling the data. The sensor data was stored in very long columns of data samples, each column representing a different parameter (as can be seen in table 3.4). This meant that a lot of steps had to be taken in the data pre-processing phase, since these huge columns of data had to be cut into different measurements, and subsequently measurement phases (as explained in section 3.5.3), which was a very time-consuming process. One way of already organising the data per individual measurement, is making sure that data is only stored when the measurement protocol is running, and that the data for each measurement is stored in separated files. The most convenient way of automatically organising these files per measurement (without the need of any user input), is storing each data-file under the name of their time stamp (the exact time [HH:MM:SS] when the measurement was initiated). User input for organising the measurement was not wanted due to the lack of an interface for input, and to save time during each measurement. It is only up to the user to take note of the point of time when each measurement was taken, to further organise the files per subject manually.

Since most Arduino boards do not have an integrated Real Time Clock (RTC), it was chosen to integrate a RTC breakout-board into the prototype (see figure 4.8). This module can keep time, even without supply

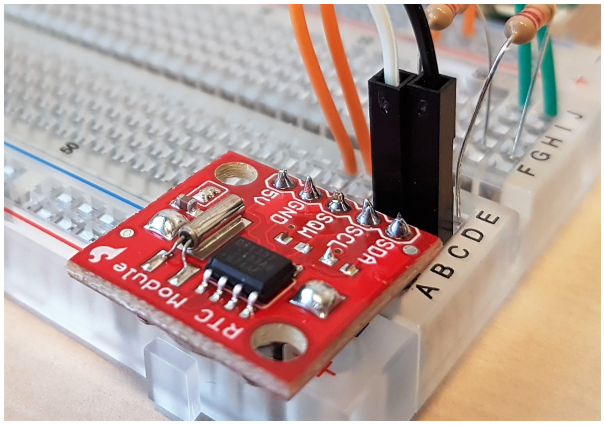


Figure 4.8: The used RTC module, that houses the Maxim Integrated DS1307 RTC IC.

voltage, due to the on-board lithium coin-cell. When called by the micro-controller, it will return a digital signal that indicated the year, month and day, as well as the time in hours, minutes and seconds. The module had to be adjusted slightly, as the operating voltage of the module is 5V and the used Arduino Micro-controller has an operating voltage of 3.3V. For this reason, the internal pull-up resistors of the RTC had to be removed and replaced by 3.3V pull-up resistors (see figure 4.9 in section 4.3.2).

#### Data Storage Module

The same type of data storage as in the previous prototype is used (see section 3.4.3), which was the *Adafruit 5V ready Micro-SD Breakout board+*. It was found that the high current that this module draws during operation can create noise on the signal, since the Arduino micro-controller can only supply a limited amount of current. Therefore an external power source (the wall-adaptor) is used for this module (see figure 4.9).

Also, the coding has been slightly adapted to only store the data during a measurement protocol, to appropriately label the data-columns and measurement phases, and moreover to store the data in .CSV format which means that the data can be directly opened using Excel or Matlab, without first converting the .TXT data using Excel which was the case in the previous prototype. More details about coding will be discussed in section 4.3.3.

#### Micro-Controller

The main requirements for the new micro-controller of choice would still be that the minimum ADC-resolution would have to be 12-bit, and that the programming interface for the micro-controller would be Arduino IDE (due to available experience with programming micro controllers). New requirements would be a higher clock-speed, to enable higher and more stable sampling rates, and more ADC and digital I/O pins to facilitate the high number of components. In addition to an improved sampling frequency for data collection, the higher clock-speed should also facilitate the use of the micro-controller as a PID-controller for the solenoid, which requires computational capacity.

To meet these requirements, the *Arduino DUE* was chosen as the micro-controller for this project. Its CPU features a clock-speed of 84MHz, which is much higher than the 48MHz of the ZERO which was used before [3]. The board also houses 54 digital input/output pins (of which 12 can produce a PWM output), which is considered more than enough. It also houses 12 ADC inputs, which is also considered enough to connect all analogue sensors. Also, it can be programmed using the same Arduino coding interface which was used before (Arduino IDE), which was preferable given the time that was still available to build this prototype.

### 4.3.2. Electrical design

The prototype would consist of two main parts: The *Control Unit* (CU) and the *Probe*. The probe houses all the sensors (the PPG modules, temperature sensors and force sensor), the solenoid for force actuation, as well as all components needed for amplification and active filtering of all the analogue signals. The CU houses the Arduino, the control interface (buttons and state-LEDs), the on/off switch, the Micro-SD module, the RTC module, supply power and USB cable connections, and some extra passive Resistor-Capacitor filters

(RC-filters) for incoming analogue signals. The CU is the part that will be used directly on the skin of the subject. The probe and CU are in connection through a data/power cable. In this section a detailed description of the electrical design will be given through schematics and a brief explanation. For convenience, the total circuit schematic of the prototype is cut into 5 separate circuit schematics, which are displayed in figures 4.9, 4.10, 4.11, 4.14 and 4.15.

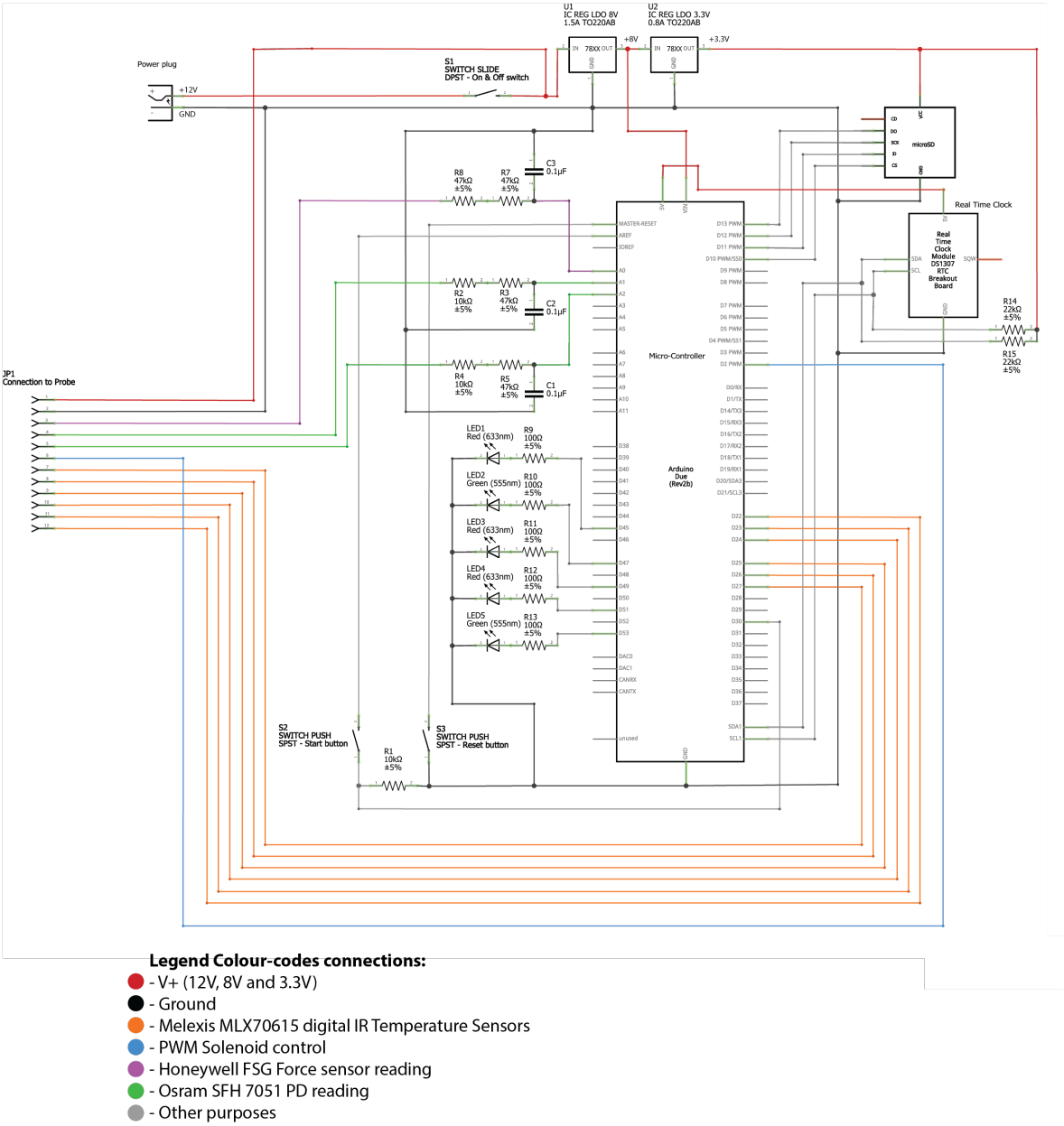


Figure 4.9: Circuit diagram of all components inside the CU

All components inside the *CU* are represented in *the schematic in figure 4.9.* In each of the schematics a colour code is used for all connection, which correspond to a certain component or supply voltage which is indicated in the legend. Power is supplied by a 12V wall adapter and can be switched on or off using a DPST on-off switch. The 12V power supply is directly supplied to the probe. Voltage regulators reduce the power supply to 8.0V for powering the Arduino, and 3.3V for powering the Micro-SD module. 2 push-buttons are integrated for either resetting the device (in case of any unexpected errors) and for initiating the measurement

protocol. The measurement protocol consists of 5 seconds pre-compression phase (phase 1), 5 seconds compression phase (phase 2) and 10 seconds CRT phase (phase 3). Since this process is fully automated, LEDs are used to provide feedback to the user regarding the current phase of the measurement protocol: 2 red LEDs and 1 green LED. The first red LED lights up during phase 1, the second red LED during phase 2 and the green LED during phase 3. There are two additional LEDs: a green one for indicating that the device is turned on and ready for initiating the measurement, and a red one that blinks whenever an error or inconsistency is identified by the micro-controller. The green LED also blinks a few times when a measurement protocol has finished.

3 RC-filters are also included as low-pass filters for the incoming analogue signals: the CRT-PPG signal, the reference PPG signal and the force sensor signal. These filters practically work as a sort of voltage divider, where the impedance of the resistor is static and the impedance of the capacitor gets lower with increased signal frequencies. This causes high frequencies to "leak" to ground, while low frequencies are passed through to the ADC. The output signals of the sensors are already low-pass filtered using active-filtering (with operational-amplifiers), which will be discussed later on (figures 4.11 and 4.15). Any high-frequency noise from electromagnetic interference picked up inside the probe after amplification of the signal or in the data-cable to the CU are filtered out by the RC-filters. These filters are especially necessary because of the strong and high-frequency electromagnetic field (high frequency due to the PWM signal) generated by the solenoid, which may otherwise be highly visible during the compression phase. The cut-off frequencies for filtering these analogue signals are defined as the conventional $f_{3dB}$, which is the minimal frequency where the gain is -3dB, which is about half of the power before filtering. Defining the right resistance (R) and capacitance (C) for a wanted $f_{3dB}$ can be done using the formula in eq. 4.1:

$$f_{3dB} = \frac{1}{2\pi RC} \tag{4.1}$$

Defining the correct $f_{3dB}$ for each analogue signal depends on the sampling rate of the ADC and the characteristic of each signal. Since it was chosen to use a stable sampling rate of 100Hz any frequency in the signal above the *Nyquist-frequency* (half of the sampling frequency, $\frac{1}{2}f_s$), which is *50Hz*, would cause *aliasing*. Aliasing is the phenomenon where signal frequencies higher than $\frac{1}{2}f_s$, would seemingly show different (lower) frequencies after sampling the analogue signal to a discrete-time signal by the ADC. Therefore any $f_{3dB}$ higher than 50Hz is considered useless. It should ideally even be a bit lower to minimise aliasing, since no filter is ideal. Simple RC-filters as used in this example are first-order low-pass filters, which means that after the $f_{3dB}$ point the slope of the bode-plot of the filter is approximately $-20dB/decade$.

For the force sensor (purple), given the available capacitors and resistors, a RC-filter set-up has been chosen with the following combination of resistance (in $k\Omega$) and capacitance (in $\mu F$):

$$f_{3dB,\,\text{force}} = \frac{1}{2\pi * 43k\Omega * 0.1\mu F} \approx 37Hz \tag{4.2}$$

This is considered to be sufficiently low to filter out high frequency noise and prevent aliasing, while conserving a fast response time of the force sensor for an adequate feedback loop for the PID-controller. As already stated in section 3.4.1, a minimum suitable $f_{3dB}$ for the PPG signals (green) would be 15Hz. Given the available resistors and capacitors, the following RC-filter was used:

$$f_{3dB,\,\text{PPG}} = \frac{1}{2\pi * 57k\Omega * 0.1\mu F} \approx 28Hz \tag{4.3}$$

This is considered good enough to conserve all pulsating (AC) and static (DC) components from the PPG signal, while preventing aliasing and filtering out high-frequency noise from electromagnetic interference. Any remaining high-frequency noise that is picked up at the ADC for both PPG and force signals is considered to be noise generated at the ADC. Any such noise should be filtered digitally in the retrospective analysis.

Other connections to/from the probe (at JP1, on the left of the schematic) include the digital SMBus connections to the three temperature sensors (in orange), the PWM signal for controlling the force output of the

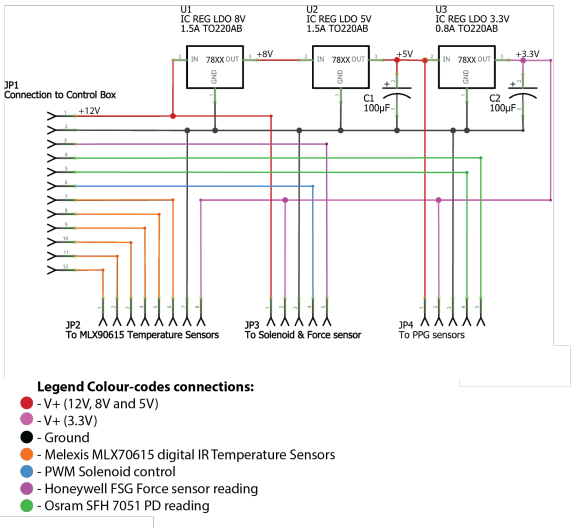


Figure 4.10: Circuit diagram of probe at entry level. Main functions are routing of signal connections, and regulating various voltage levels for different components.

solenoid (blue), ground (black) and power supply (12V, red).

In figure 4.10 the cable-connections between the probe and CU are displayed on the entry level of the probe (*JP1*). It shows how the data connections are routed to the appropriate parts of the probe, and how the supply voltage is regulated by separate voltage regulators (*U*1, *U*2 and *U*3) into a 12V, 5V and 3.3V supply voltage. Different voltage levels are needed as different components require different supply voltages. Capacitors *C*1 and *C*2 are integrated to smoothen any imperfections in the consistency of the supply voltages. This is especially important for the LEDs inside the PPG modules, as any imperfections in the brightness of these LEDs will be picked up by the photo-diode as noise. The connections of *JP2* lead to the temperature sensors (in figure 4.14), which consists of 6 digital SMBus data connections (2 per sensor, SCL and SDA), a ground and a 3.3V power supply. *JP3* leads to the solenoid/force sensor system which is part of the PID feedback-system (in figure 4.15). It consists of a 12V power supply for the solenoid, a 3.3V power supply for all other components, a ground connection, a 3.3V PWM signal input (blue) which controls the force output of the solenoid, and the amplified analogue force sensor output (purple) from the feedback loop of the controller. *JP4* leads to the PPG circuit, which is composed of 2 PPG modules (CRT and reference) and a trans-impedance amplifier (figure 4.11). The connections include a 5V and 3.3V power supply, a ground connection, and the 2 amplified analogue PPG sensor outputs.

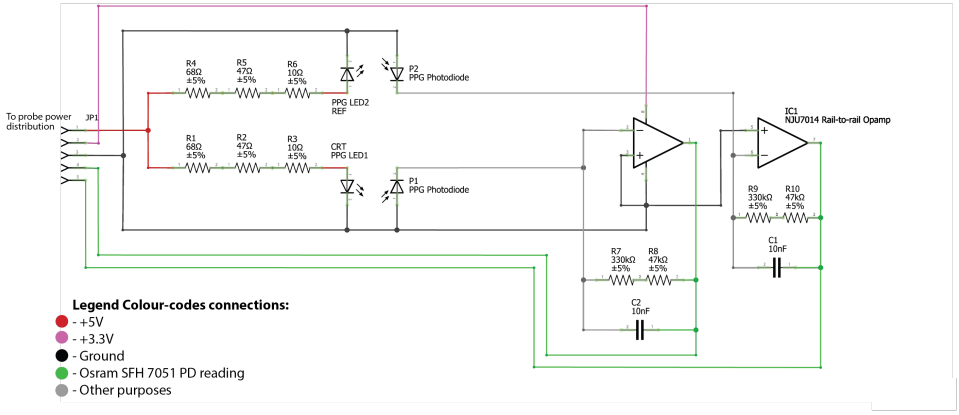


Figure 4.11: Circuit diagram for both Osram SFH 7051 reflective PPG sensors, which are interfaced with a NJU7014 rail-to-rail transimpedance amplifier for current to voltage conversion.

In figure 4.11 one can see the design of the PPG circuit. The LEDs and PDs (P1 and P2) are integrated into two separate PPG modules (Osram SFH 7051 reflective PPG sensors), one for recording the CRT signal and one for recording the reference signal. In compliance to the data-sheet of this module (in appendix T [9]) the LEDs should be powered with a forward voltage of 3.2V, and a forward current of 15mA when all 3 LEDs are used or 25mA when just a single LED is used. Yet it was chosen to use just 1 LED per module, and power it with 3.2V (so a voltage drop accross the resistors of 1.8V is needed) and 15mA, which is achieved (approximately) by using the resistors that are connected in series with the LEDs (eq. 4.4).

$$I = \frac{U}{R} = \frac{U_{supply} - U_{LED}}{R_{1,4} + R_{2,5} + R_{3,6}} = \frac{5.0V - 3.2V}{125\Omega} = 14.4mA \approx 15mA \tag{4.4}$$

According to an application note of the manufacturer [5], the SNR should increase with a higher current (and thus light intensity). Therefore, in order to increase the SNR all three LEDs were chosen to be used at 15mA at first. Yet, it was found during the testing phase that the intensity of the reflected light into the PD was too high, as the PD seemed to saturate. In practice, this meant that the signal amplitude was cut-off above a certain value. The actual cause of this saturation has not been practically studied, but the phenomenon may be explained by the fact that a photo-diode may be modelled by an equivalent circuit that houses (among other things) an ideal current source and a resistor in series [63]. This series resistance is ideally zero, but usually ranges from $10\Omega$ to $1k\Omega$, and is a determinant for non-linear response of the photo-current from the diode to the light intensity. Usually the generated current is very linear, while the voltage level is less linear to the light intensity. Given the combination of non-linear voltage response to absorbed light by the PD and the series resistance, with Ohm's law ($I = \frac{U}{R}$) the non-linear current output of the PD can thus be explained. Also, it has already been established that in practice all PDs have a certain saturation point at which current doesn't increase anymore when light intensity increases [63].

To be able to use the full range of the PD (until its saturation point) it was empirically found that using 1 LED at the lower current level (14.4mA) would result in the most optimal signal strength without saturating the PD.

Now it is established that the (negative!) current output of the PD is linear to light intensity striking the sensory surface of the PD, this small current output needs to be converted to a voltage value within the range of 0V - 3.3V, in order to use this voltage output for the ADC in the micro-controller. A conventional way of doing this is to use a *transimpedance amplifier* (TIA), which can also be seen at the operational amplifiers (Opamps) in figure 4.11. A typical example of a TIA is illustrated in figure 4.12.

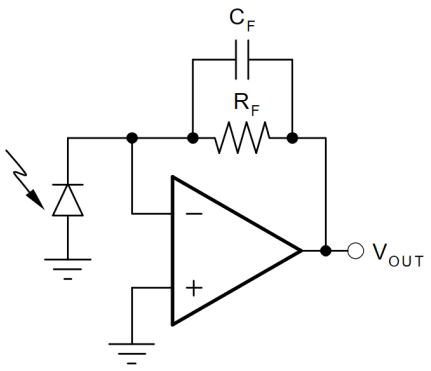


Figure 4.12: A typical photo-diode transimpedance amplifier [78]

A TIA is implemented by integrating an opamp with a feedback resistor ($R_F$) and a feedback capacitor ($C_F$) to the inverting input (-). The cathode of the PD is also connected to the inverting input. the non-inverting input (+) is connected to ground. The rule of any opamp is that it will always try to equalize the inputs at the inverting and non-inverting side. The non-inverting input is connected to ground, which means that the opamp will always try to neutralize the inverting input. So when the PD generates a negative current on the

inverting input (), the opamp will output a (positive) voltage ($V_{out}$) that through the feedback loop tries to compensate the negative current. $R_F$ is key in this feedback loop, as its resistance directly determines the gain of the amplified signal at $V_{out}$, and it is also key in converting the current signal at the inverting input to a voltage signal at $V_{out}$. Based on Ohm's law, the rule for calculating $V_{out}$ with a given input current from the PD at the inverting input ($-I_{PD}$) and a given feedback resistance $R_F$ is given in eq. 4.5 (if $C_F$ is not taken into account, and only true for low-frequency input).

$$V_{out} = -I_{PD} * R_F \tag{4.5}$$

This equation does not exactly add-up in practice, since most Opamps dissipate some power. The value of $R_F$ thus still has to be determined empirically. The output voltage $V_{out}$ will be directly (after being filtered again at a low-pass RC-filter as in figure 4.9) into the ADC. Since the ADC can only read voltages between 0V and 3.3V, $V_{out}$ should ideally be able to exploit this whole range. Opamps often tend to saturate close to their rails, they usually only use about 80% of the range of supply voltages. In this case the supply voltages are 3.3V at the $V_{DD}$ pin and ground (0V) at the $V_{SS}$ pin. To fully use this voltage range, a rail-to-rail opamp is used, the *JRC NJU7014* to be exact (data-sheet can be found in appendix W [8]). During tests for determining the right $R_F$ for the optimal $V_{out}$, it was found that it should be $377k\Omega$.

The problem with TIAs is that they are prone to oscillate [78]. Even very small high-frequency noise on the output signal of the PD can cause the system to become unstable. The main reason for this is the nature of the PD, which can be modelled as an ideal current source, with a resistor ($R_D$) and capacitor ($C_D$) in parallel (see figure 4.13).

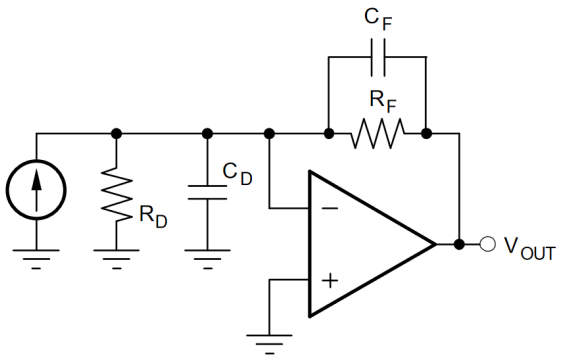


Figure 4.13: A TIA with a PD modeled with ideal elements (current source, parallel resistor and parallel capacitor) [78]

To put it in relatively simple terms: this $C_D$ in combination with $R_F$ creates a passive RC-filter in the feedback loop. The $R_FC_D$-filter will filter high frequencies out of the feedback loop, which causes the system to act as an open-loop system above these frequencies, and an open-loop opamp is inherently unstable. Another way of explaining it: the has a frequency response determined by its Gain-Bandwitdh-Product (GBP). GBP is determined by the voltage gain ($A_V$) and the bandwidth ($f_B$), with the GBP being constant for every opamp (see eq. 4.6).

$$GBW = A_V * f_B \tag{4.6}$$

It is known from the data-sheet that the NJU7014 opamp has a GBP of 200000kHz. $A_V$, and therefore the feedback resistance $R_F$, determine the $f_B$ of the opamp. So with an open-loop amplifier the $A_V$ is infinite, and thus the $f_B = 0$. $F_B$ therefore stands for the $f_{3dB}$ of the opamp, and is the point after which the frequency response of the opamp ($A_O$) transits into a $-20dB/decade$ slope. The RC-filter in the feedback system also has its own frequency response ($A_F$), of which the $f_{3dB}$ can be calculated like eq. 4.1. Since this RC-filter is placed in the feedback loop of the opamp, the nett-frequency response is inverted ($\frac{1}{A_F}$), which means the slope of the response is $+20dB/decade$ after the $f_{3dB}$ point. The phase shift in lower frequencies

(within the opamp bandwidth) is -180 degrees since the response of the TIA is inverting. After the $f_{3dB}$ point of the opamp frequency response, the phase-shift will move -90 degrees. After the $f_{3dB}$ point of the feedback frequency response, the phase shift will move another -90 degrees, adding up to -360 degrees in total [24]. A phase shift of -360 means that there is positive feedback, which is not ideal since the TIA is configured to work with negative feedback. This introduces a *pole* at a certain high-frequency, which will be at the point where the frequency response lines of the opamp ($A_O$) and the feedback system ($\frac{1}{A_F}$) intercept. At this interception point, the pole, the combination of the opamp and feedback systems will generate a unity gain, as explained with eq. 4.7.

$$A_O = \frac{1}{A_F} \Longrightarrow A_O A_F = 1 \tag{4.7}$$

Positive feedback in combination with unity gain will lead to a situation where the response of the total system will become unstable and starts oscillating at the frequency of this pole. The pole frequency ($f_P$) can be determined when the GBW, the $R_F$ and the $C_F$ are known. From the datasheet of the PPG module it can be derived that the capacitance of the PD ($C_D$) at zero reverse voltage is 15pF. The $f_P$ can be derived as in eq. 4.8 [78].

$$f_p \approx \sqrt{\frac{GBW}{2\pi * R_F * C_D}} = \sqrt{\frac{200000}{2\pi * 377k\Omega * 15pF}} \approx 75kHz \tag{4.8}$$

Now it is known that the system would become unstable at 75kHz if not compensated. That is where $C_F$ comes into play. $C_F$ turns the TIA into an active filter, since high frequencies can now bypass $R_F$ through $C_F$ with a very low impedance. This causes these high frequencies to be amplified at unity gain, and since the amplitude of these high frequencies coming from the PD are very small they can be neglected. This will flatten the frequency response of the feedback system, causing the phase shift to move up 90 degrees, preventing a phase-shift of -360 degrees. It is key that the $C_F$ is chose as such, that the point where the frequency response flattens before $f_P$. The conventional formula for determining the minimal capacitance for $C_F$ is stated in eq. 4.9 [78].

$$C_F = \frac{1}{4\pi R_F GBW}\left[1 + \sqrt{1 + 8\pi R_F C_D GBW}\right] \approx 6.7pF \tag{4.9}$$

Yet, this way of determining $C_F$ is mainly useful whenever conservation of bandwidth is a key factor. This is for instance the case with pulse-oximetry, where red and infra-red LEDs emit light into the PD in very fast pulses. A large bandwidth would be needed here, as these high-frequency light pulses would otherwise be filtered, which would distort or even neutralize the signal from the PD.

In this prototype, no pulsating LEDs are used. Instead, the LEDs emit green light continuously during measurement. Because of this, there are no high-frequency components in the signal of interest, other than noise. For this reason, it is chosen to minimise the bandwidth of the TIA in order to filter out any high frequency noise, by choosing a much larger feedback capacitor than the one defined in eq. 4.9.

Sources of noise for the PPG signal could originate, apart from electromagnetic interference, from ambient light striking the photo-diode in the PPG module. The influence of ambient light should be blocked physically as much as possible. Although continues light sources such as daylight are not believed to have much influence on the characteristics of the CRT-curve, high-frequency flickering light sources such as dimmed LED lights and TL-light can cause high-frequency noise on the PPG signal. The lowest frequencies exist in low-frequency TL-light, which flickers at a frequency of 100Hz to 120Hz. The bandwidth of the TIA should be chosen as such that these frequencies are filtered out.

Since a relatively large $C_F$ will be chosen in order to achieve this, $C_D$ and GBW can be neglected, as the $f_{3dB}$ will be much lower than the $f_B$ of the opamp (which can easily be assumed is well above 1kHz). For this reason, the TIA can now be approached as an active low-pass filter, which is established using eq. 4.10.

$$f_{3dB} = \frac{1}{2\pi R_F C_F} \tag{4.10}$$

For this set-up, one of the available capacitors had a capacitance of *10nF*. Integrating this as $C_F$ the following active filter is established.

$$f_{3dB} = \frac{1}{2\pi * 377k\Omega * 10nF} \approx 42.2Hz \tag{4.11}$$

This cut-off frequency is considered well below the maximum of 100Hz in order to filter out all high frequency noise, and well above the minimum of 15Hz (as established earlier). Since this frequency is also much lower than $F_P$ as defined in eq. 4.8, the system is also stable. The output signal $V_{out}$ is now ready to be fed into the ADC, after low-pass filtering once more as described earlier at figure 4.9.

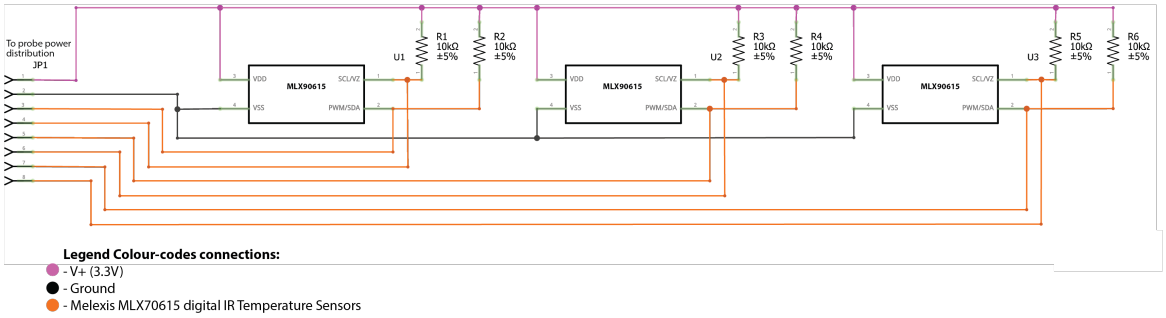


Figure 4.14: Circuit diagram for the three digital Melexis MLX70615 IR Temperature sensors.

Figure 4.14 shows the circuit schematic for the three MLX70615 temperature sensors. These sensors are fed by a 3.3V supply voltage. These sensors output a digital signal, which carries information on object and ambient temperature. The sensor works with a 2 wires protocol for data transfer: an SDA connection and an SCL connection. The SCL wire is used as the clock for the communication between the Arduino and the sensor. The SDA wire is the data output of the sensor. Both SDA and SCL connections are connected to a pre-programmed digital in-/output pin of the Arduino (as in figure 4.9), and a pull-up resistor. The pull-up resistor functions to clearly distinguish between a low data output (0V) and a high data output (3.3V). Without the pull-up resistor the digital highs will float anywhere around 1.6V, which can cause confusion at the digital input of the Arduino.

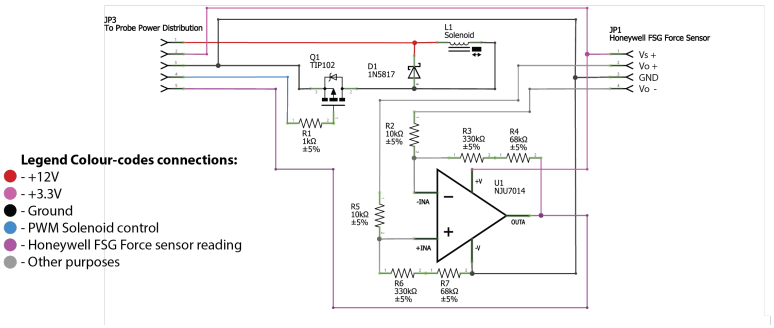


Figure 4.15: Circuit diagram for both the Force Sensor and the Solenoid.

In figure 4.15 the actuator and feedback sensor circuit is illustrated. A 3.3V supply is used to power the opamp (NJU7014 rail-to-rail opamp, the same one as used in figure 4.11) and the force sensor. The 12V power supply is used to power the solenoid. 12V power supply circuit to the solenoid is controlled by the PWM signal (blue), which is used to quickly open and close the circuit using the TIP102 transistor.

As described in section 4.3.1, this PWM signal therefore controls the force output of the solenoid, as a large *duty-cycle* will result in a high output force, and a zero duty cycle will completely stop the current from flowing and results in a zero (active) actuator force. The duty-cycle of the PWM signal is calculated by the Arduino, which serves as the controller in the PID feedback-control system. More about this control loop will be discussed later on.

A part of the solenoid circuit is the Schottky diode (D1). This diode is very important, as it serves as a *flyback diode*. When a current flows from +12V through the coil of the solenoid to ground, it bypasses the diode, as the diode only allows current in 1 direction. A characteristic of an inductor (the coil), is that it doesn't like sudden changes in current flow. This can be explained by the fact that the coil creates a magnetic field when a current flows through it. This magnetic field stores a lot of energy. When the current is stopped suddenly, it will naturally cause the magnetic field to disappear as well. Based on *Faraday's law of induction*, any fast changing magnetic field will cause a current to flow at the inductor. Therefore, when the positive current through the coil is abruptly stopped, which causes a huge spike in negative voltage due to the negative potential that is created by the changing magnetic field. This is thus the process of converting the stored energy in the magnetic field back to electrical energy. The problem with this voltage spike is that it can do major damage to the circuit or even create arcs across air gaps, when not dealt with appropriately.

The flyback diode creates an extra loop in the circuit, through which the generated flyback current can flow when the circuit is opened at the transistor. The current flows through this diode back to the positive terminal of the solenoid until all energy is dissipated in the solenoid (in kinetic energy or heat). What makes this diode additionally important in this circuit is that abrupt changes in current happen constantly when the solenoid is activated, due to the fast opening and closing nature of the PWM controlled transistor. The flyback diode should therefore be able to conduct high levels of current for at least 5 seconds (the duration of the compression phase).

The force sensor, as part of the feedback loop of the PID-controller, will sense the force exerted by the solenoid and feed the resulting signal back into the controller. As already explained in section 4.3.1, the force sensor outputs two signals: Vo+ and Vo-. At zero load on the sensor both outputs are equal: both are half the supply voltage, which in this case is 1.66V which is approximately half of the supply voltage of 3.3V. When the load increases, the voltage output of Vo+ increases somewhat and the voltage output of Vo- decreases somewhat, which causes a difference between the outputs. This difference is linear to the load that is applied on the armature of the sensor. During the testing phase, it was found that the voltage difference never really goes beyond 50 to 100 millivolts, which is considered too small to be used for the 12-bit ADC while having a good resolution. The output signals of the force sensor will have to be amplified using a *difference amplifier*.

For this application, the same opamp is used as in figure 4.11, mainly because of its rail-to-rail output range. This is important since it is key for the feedback sensor to have a linear response over the range of forces that it should measure. Not using a rail-to-rail opamp (which is fed single-sided [+3.3V & 0V, instead of +3.3V & -3.3V], as is the case here) would result in the the opamp becoming saturated at minimal load situations, making the response of the amplifier very non-linear to the input signal in these situations.

As was explained earlier, the opamp will always try to equalize the voltages at both inputs. In figure 4.15 it can be seen that the Vo(+) output of the sensor is connected to the non-inverting input (+) of the opamp, and Vo(-) is connected to the inverting input (-) of the opamp. The output voltage $V_{out}$ is fed back to the inverting input through resistors R3+R4. This configuration of the opamp makes it a difference amplifier, as $V_{out}$ increases when Vo(+) increases or Vo(-) decreases. Given that $R2 = R5 = R_A$ and $R3 + R4 = R6 + R7 = R_B$, the voltage gain of the difference in input voltage can be defined using eq. 4.12.

$$V_{out} = \frac{R_B}{R_A}(Vo(+) - Vo(-)) \tag{4.12}$$

provided the measured voltage difference that come out of the force sensor under normal use with the solenoid (50mV to 100mV), it was found that a gain of 40 should be sufficient to come to an output signal of the opamp that stays between 0V and 3.3V. Therefore, the following configuration was chosen:

$$V_{out} = \frac{330k\Omega + 68k\Omega}{10k\Omega}(Vo(+) - Vo(-)) \approx 40 * (Vo(+) - Vo(-)) \tag{4.13}$$

The output of the opamp is low-pass filtered for reducing any high-frequency noise in the signal using the RC-filter as illustrated in figure 4.9. This output signal can be used as input for the ADC, which will be used for the controller operations.

To be able to actively control the force output of the solenoid it was chosen to use a PID (Proportional, Integral, Derivative) controller. In this prototype, the Arduino DUE is the controller, the solenoid is the plant, and the force sensor provides is the feedback. The PID controller is used for its robustness, as it is hard to anticipate the behaviour of the highly non-linear solenoid. Due to its simplicity it is also the perfect controller

for the relatively easy task that it has to fulfil, namely keeping a constant force on the sensor. A PID controller operates by calculating at every sample the difference between the measured force sensor output $U(t)$ (feedback signal) and the desired amount of force output $R(t)$ (the *set-point*, or *reference*). This difference makes up the *error* $e(t)$. Since the sampling rate of this prototype is 100Hz, this also means that the PID controller has a sampling rate of 100Hz (100 iterations per second). Every time $e$ is determined, the controller will calculate the appropriate response to get $e$ to become 0 as fast as possible. That is where the *proportional*, *integral* and *derivative* operations of the PID controller come into play.

**P:** The *proportional* operation of the controller determines the controller output directly based on $e$. The output is calculated using the operation in eq. 4.14. The magnitude of the response of this operation is determined by constant $K_P$, which has to be defined heuristically. The higher $K_P$ the faster the response of the controller to any error, although a higher $K_P$ may also cause oscillations or even instability of the controller. This operation alone will never drive the system to a zero-error steady state, because a non-zero error is needed to drive it. It will therefore approach a zero error only until a certain level. The best way to think of it intuitively is by picturing a spring hanging from a sealing which should pull a mass upwards to its normal length when it's not excited. With a non-zero mass this will of course never happen, because the spring has to be stretched at least a little bit in order to apply an upwards force to the mass. Hence the steady state error of this operation.

$$U_P(t) = K_P e(t) \tag{4.14}$$

**I:** The *integral* operation of the controller takes care of the steady state error. In eq. 4.15 it can be seen that this operation accumulates all error values from t=0 until the present time to determine the controller output. If well designed (meaning the optimal $K_I$ is chosen), this term will adjust its output as long as the error is non-zero. It thus actively creates a compensation output component (or bias) for the shortcoming of the proportional term.

$$U_I(t) = K_I \int_0^t e(\tau)d\tau \tag{4.15}$$

**D:** The *derivative* component acts as a damping term. Whenever the error changes very rapidly, this term will try to slow it down, as can be seen in eq. 4.16. This term will smoothen the response of the controller, and reduce overshoot.

$$U_D(t) = K_D \frac{de(t)}{dt} \tag{4.16}$$

The outcome of each operation is added up to form the response of the controller to a certain error. The gains (K) determine the magnitude of the contribution of each operation, and should be determined heuristically by experimenting. In practice the D-component is rarely used and neither will it be used in this controller, since during tests the P and I components already established a fast response without too much overshoot. This means therefore that $K_D = 0$. Therefore the resulting controller is a PI-controller as only the proportional and derivative components are used, of which the formula is stated in eq. 4.17. A side-note to this system is that the PWM output of the controller ($U_{PWM}(t)$) has a resolution of 8-bits. This means that the output can take on integer values from 0 (0% duty-cycle) to 255 (100% duty-cycle). A block scheme of the total system is illustrated in figure 4.16.

$$U_{PWM}(t) = K_P e(t) + K_I \int_0^t e(\tau)d\tau \tag{4.17}$$

To describe the system as a closed loop transfer function G(s), first the components (signals and subsystems) of the system have to be transformed into the Laplace-domain. This Laplace transform enables to easily define the transfer function of the total system G(s). The (simplified) system in Laplace transform is illustrated in figure 4.17.

The transfer function of the system can be derived by the following steps. first of all the transfer function in Laplace transform of the total system can be defined by dividing output by input:

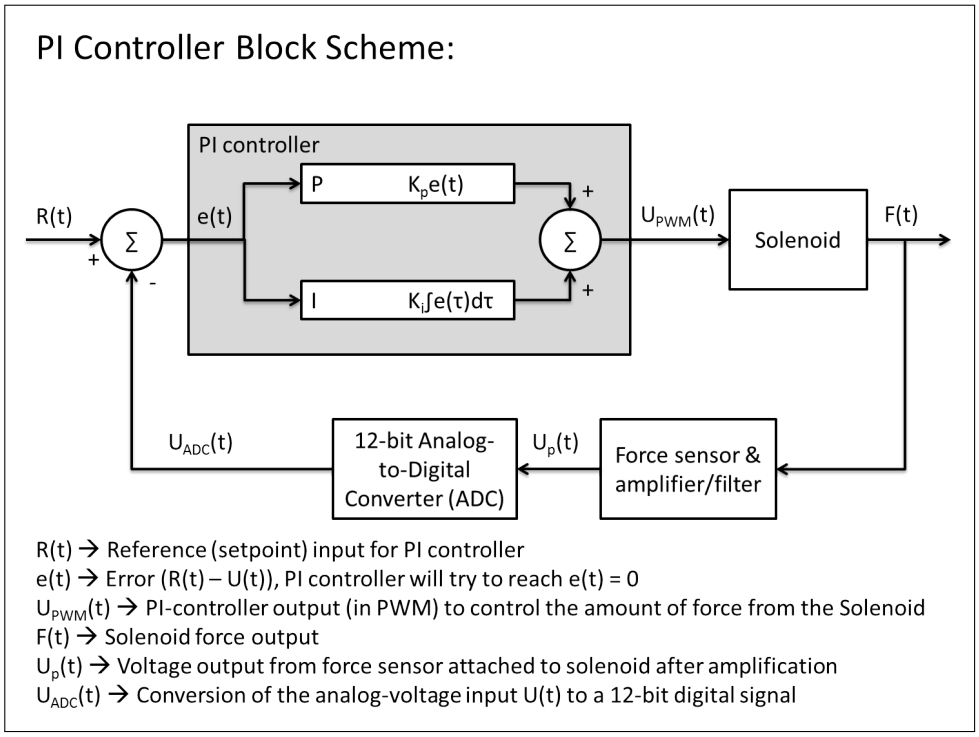


Figure 4.16: A block-diagram for the feedback-loop of the PI-controller.

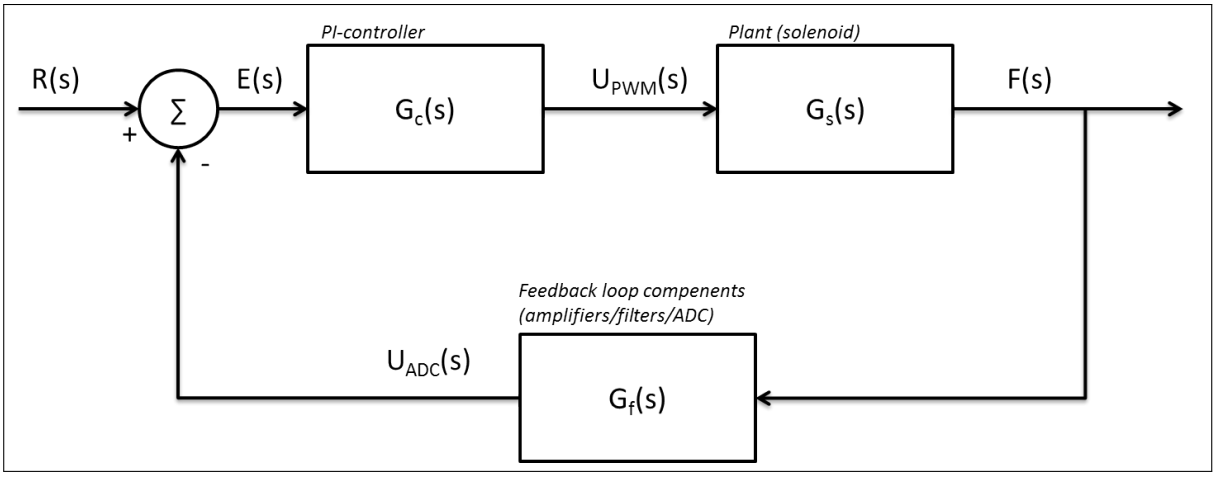


Figure 4.17: PI-controller simplified and in Laplace form.

$$G(s) = \frac{F(s)}{R(s)} \tag{4.18}$$

The output can be defined as follows:

$$F(s) = E(s) * G_c(s) * G_s(s) \tag{4.19}$$

The error can be defined as follows:

$$E(s) = R(s) - F(s) * G_f(s) \tag{4.20}$$

The reference can then be established from eq. 4.20:

$$R(s) = E(s) + F(s) * G_f(s) \tag{4.21}$$

When substituting F(s) it becomes:

$$R(s) = E(s) + E(s) * G_c(s) * G_s(s) * G_f(s) \tag{4.22}$$

When F(s) and R(s) are substituted in eq. 4.18, it becomes:

$$G(s) = \frac{E(s) * G_c(s) * G_s(s)}{E(s) + E(s) * G_c(s) * G_s(s) * G_f(s)} = \frac{G_c(s) * G_s(s)}{1 + G_c(s) * G_s(s) * G_f(s)} \tag{4.23}$$

Eq. 4.23 thus describes, as expected, a transfer function of a closed loop system with negative feedback. $G_c(s)G_s(s)$ describes the open loop gain, while $1 + G_c(s)G_s(s)G_f(s)$ describes the loop gain. The individual transfer functions of the components of G(s) can also be described by a transfer function. For $G_c(s)$ the Laplace transform of eq. 4.17 is taken, which is derived as follows:

$$U_{PWM}(s) = \left(K_P + \frac{K_I}{s}\right) E(s) \tag{4.24}$$

$$G_c(s) = \frac{U_{PWM}(s)}{E(s)} = K_P + \frac{K_I}{s} \tag{4.25}$$

As expected, the transfer function $G_c(s)$ of the PI controller in eq, 4.25 consists of a pure gain component $K_P$ and an integrator component $\frac{K_I}{s}$ for input $Es$ and output $U_{PWM}(s)$. The transfer function for the solenoid, $G_s(s)$, can be defined as follows:

$$G_s(s) = \frac{F(s)}{U_{PWM}(s)} \tag{4.26}$$

The behaviour of this transfer function is not known exactly. It is known that the output force of the solenoid is linearly proportional to its PWM input, when the position of the armature is fixed. Yet the further the armature of the solenoid is extruded from the coil, the higher the output force at a constant PWM input. This behaviour is also quite non-linear, as can be seen in figure 4.5. The solenoid that is used in this prototype has also been gauged for its force output vs. different 12V PWM duty cycles and different armature positions. The results are illustrated in figure 4.18. In this figure it can also be seen that different armature positions at 0 current already cause different force outputs. This is due to the internal spring of the solenoid, which keeps the armature extended. The function for this is to maintain skin contact of the PPG-piston outside the compression phase, to maintain a good PPG signal. This spring therefore adds an extra variable to the determination of the force-output. This graph also shows the response of the measured force to a PWM input when the duty-cycle is increasing and when the duty-cycle is decreasing. The fact that a substantial difference can be seen between equal PWM duty-cycles when they are either increasing or decreasing suggests that the system is influenced by hysteresis at either the solenoid or the force sensor (or both). Not data is found regarding hysteresis of either component. It is assumed that this observed hysteresis is mainly a characteristic of the solenoid, since it is known that the force sensor has a very good repeatability (0.2% margin) and linearity (0.5%) (appendix U [4]).

All these characteristics of the solenoid together make that the behaviour of the solenoid is quite ill-defined. This relatively unpredictable behaviour of the plant is the main reason that feedback control is needed to keep a consistent output force during compression and correct for any unexpected behaviours of the plant, by using a high-quality force sensor.

The transfer function of $G_f(s)$ in the feedback loop, which includes the force sensor, amplifier, filter, and ADC, can be described as in eq. 4.27.

$$G_f(s) = \frac{U_{ADC}(s)}{F(s)} \tag{4.27}$$

The feedback loop consists of a force sensor, which converts force (N) to a voltage signal (V), an amplifier, a low-pass filter to filter out any external high-frequency noise, and a 12-bit ADC. The $U_{PWM}(t)$ signal drives the force F(t) (in Newton) exerted by the solenoid on the force-sensor. This sensor has a sensitivity of 3.6mV/Vin/N, and as we have an input voltage of 3.3V the effective sensitivity is 11.88mV/N. This is than amplified with a gain of 40 to 475.2mV/N. In terms of 12-bit digital ADC-steps this “digital sensitivity” is thus 590 steps/N for $U_{ADC}(t)$ . $G_f(s)$ can therefore be interpreted as (approximately) a pure gain, which produces a ADC value of 590 per Newton increase in force.

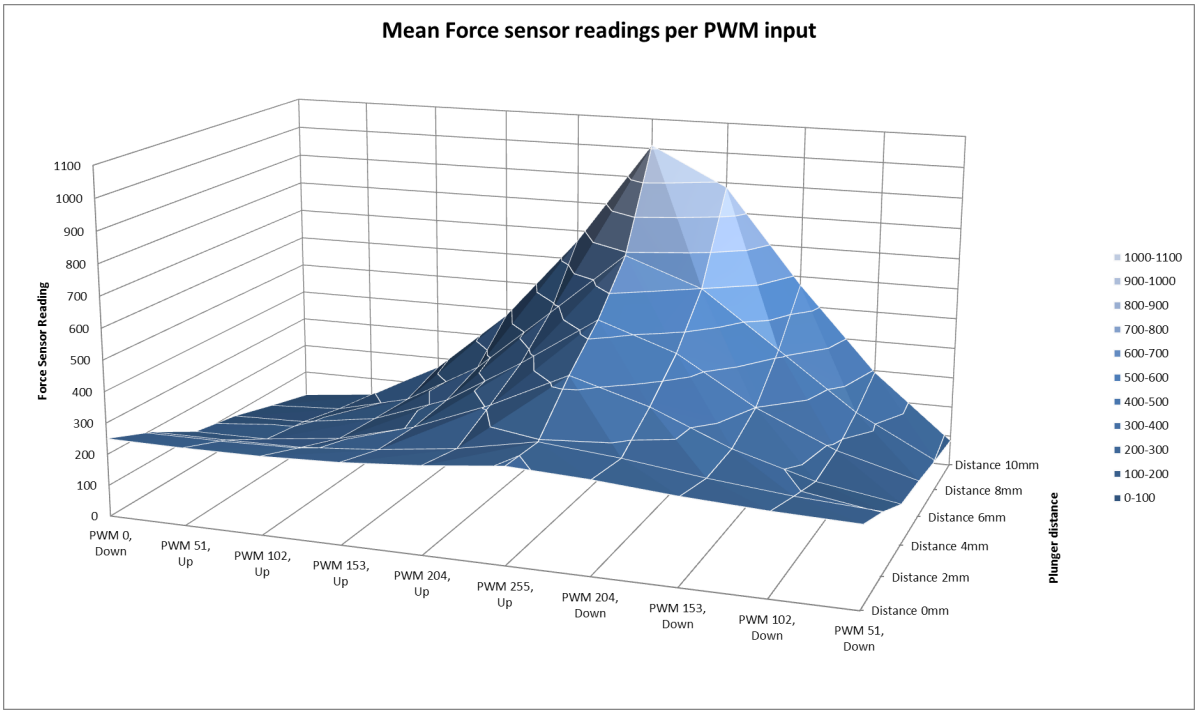


Figure 4.18: Force output of the solenoid for different armature positions and PWM inputs. Force sensor readings have been amplified during this test with K=20 instead of K=40 (as in eq. 4.13), hence the somewhat low ADC values.

$$G_f(s) = K = \frac{U_{ADC}(s)}{F(s)} = 590 \tag{4.28}$$

Now that the full system is defined, the PI-controller needs to be tuned appropriately. This means that $K_P$ and $K_I$ are tuned as such that the response of the actuator to a changing set-point is as fast as possible while preventing oscillations and overshoot of the force as much as possible. A PID algorithm that is developed for Arduino boards specifically is used, and can be seen in appendix X. The tuning process can only be performed heuristically. The Ziegler-Nichols method was used for defining the starting values of $K_P$ and $K_I$. The test set-up is shown in figure 4.19. The final values of the gains would be: $K_P = 0.25$ and $K_I = 20$. The step response of the system is shown in figure 4.20. The system responds relatively quick, and is able to reach a steady state within 100ms to 200ms. After determining the optimal gains, stability was tested at differing positions of the armature. The system remains stable at all times, except when the armature comes close to being fully extended (which increases the responsiveness of the solenoid to current). Also when the armature is more retracted, it changes the maximum amount of output force that can be achieved (at a 100% duty cycle). It confirms that the position of the solenoid should not change too much during compression to stay within the area where the solenoid is able to generate the desired force. Also it means that the solenoid armature should not come close to full extension, since the steep change in generated force at a constant current causes the PI-controller to become unstable and oscillate when the armature is near full extension.

### 4.3.3. Coding

In this section a concise explanation of the main protocol and functions of the script that is used for programming the Arduino DUE will be given. The code used to programme the Arduino is based on the requirements that were defined in section 4.1. For the complete sketch, please see appendix X.

Once the prototype is powered, a loop starts running that collects data from each of the sensors, and sends it through the USB-connection to a PC whenever one is connected to the prototype. Using Arduino IDE, one can see the sensor outputs and current time in real-time, which is useful for checking the signals when measuring. Any error messages are also displayed through this connection. The loop also checks whether or not the start-button is pushed at each iteration.

Whenever this button is pushed, it initiates the *measurement protocol*, which is a separate function from

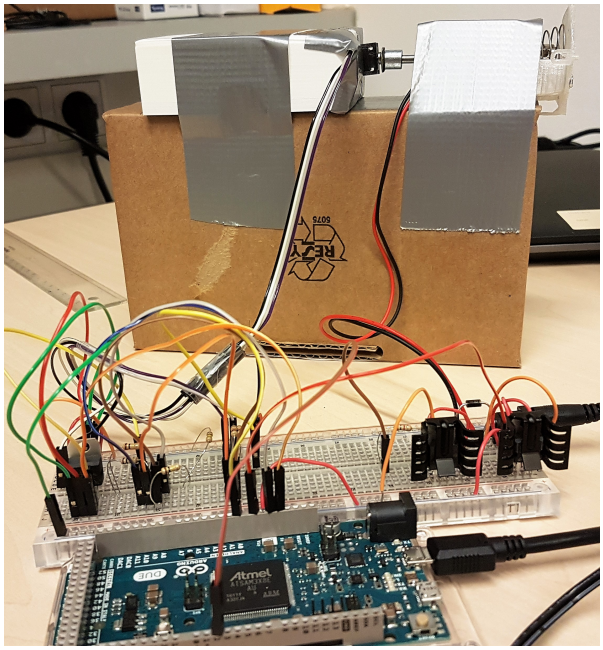

Figure 4.19: Test set-up to heuristically determine the appropriate gains for the PI-controller.

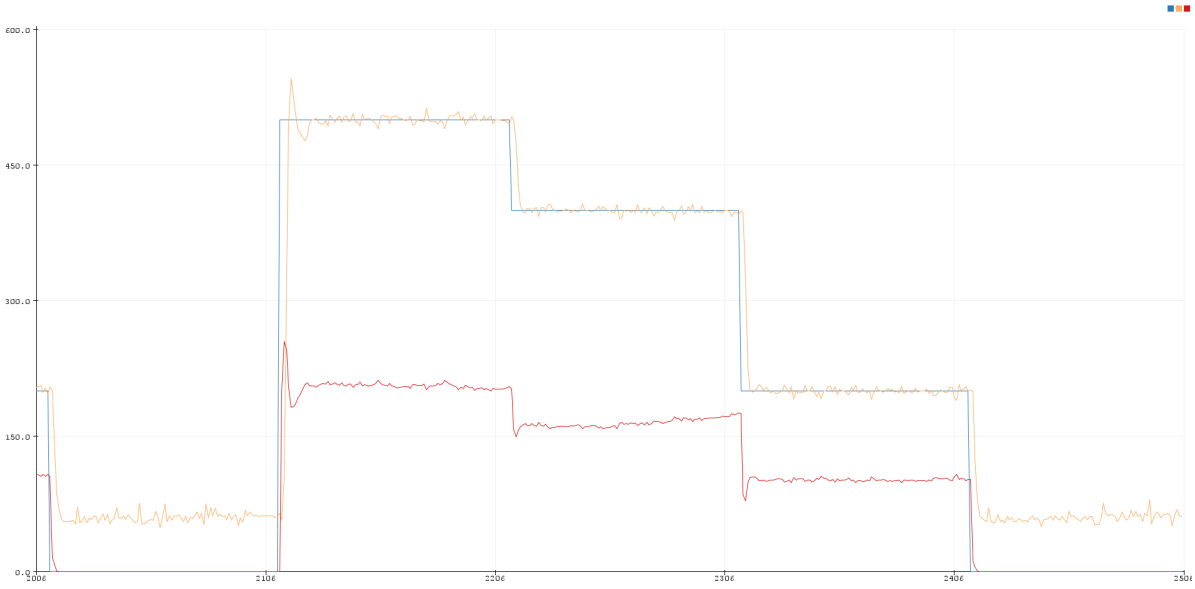


Figure 4.20: Step response of the system. The blue line is the set-point, the red-line is the PWM-output of the controller, and the yellow line is the output force of the solenoid. The y-axis represents the ADC-value.

the normal loop (void-loop). When the protocol starts, it first opens a new .CSV file on the SD-card, and names it after the current time. This file is not closed until the end of the measurement protocol. The first row of the data-file is written, which consists of the labels of the data, current ambient temperature, and exact time and date according to the RTC.

When this initiation phase is finished, a for-loop is started which should iterate through all sensor measurements with a rate of exactly 100Hz. To ensure this, an if-statement is introduced which selects the right points in time to create a new sample, based time count of the *millis()* function of the Arduino, which returns the amount of milliseconds since a certain code has been running at every loop-iteration. Another if-statement than decides the measurement phase. As explained before, the phases consist of a 5-second pre-compression phase (phase 1), a 5 second compression phase (phase 2) and a 10 second capillary-refill phase (phase 3). In phases 1 and 3 the PID set-point is 0, meaning that no force is actively exerted to the

skin by the solenoid. In phase 2 (the compression phase) the PID set-point is set to 1500, meaning that the controller will work to exert the right amount of force with the solenoid to get the force sensor ADC to this value. This set-point has been experimentally defined by looking at the minimal amount of force needed on the skin to block the pulsation of the dermal capillaries, since this is considered to be enough to fully blanch the skin. As was defined in section 4.3.2 the force sensor ADC level increases by 590 steps at every newton increase in force. The set-point of 1500 therefore corresponds to a compression force of approximately *2.55N*. During this protocol, all relevant data is stored on the SD-card as displayed in table 4.1. Next to the labelling of each data column in the top row, also each measurement phase is labelled. This enables a much easier, faster, and more accurate pre-processing method for organising the data per measurement phase compared to the previous prototype. In this prototype, measurement phases were separated by an analysing the force-sensor data, which is much more time consuming, computationally demanding and inaccurate. During the measurement, all data can still be printed in real-time on-screen through a USB-connection, in order for the user to monitor the signals. Each measurement phase also turns on a corresponding LED for user feedback on the progress. When the measurement protocol has finished (after 20 seconds in total), the "ready" LED blinks and the .CSV file is closed. The SD-card can be inserted into any PC for retrospective analysis.

In addition to the measurement function, the algorithm also includes an error function. This function sends an error message to the PC through the serial connection, and blinks a red LED on the device. The error function is summoned in the following situations:

- If no SD-card is inserted into the device when the start-button is pushed.
- when a low sampling rate is noticed. A restart is required to solve this problem.
- If for any reason the prototype can't open a file to write the data to.

| Milliseconds | Reference PPG Signal (0 - 4095) | CRT PPG Signal (0 - 4095) | Skin Temperature 1 (°C) | Skin Temperature 2 (°C) | Skin Temperature 3 (°C) | Solenoid PID Setpoint (Reference R) | Solenoid PID Input (Force Sensor Data, 0 - 4095) | Solenoid PID Output (PWM, 0 - 255) | Measurement Phase | Ambient Temperature (°C, Sensors 1, 2, and 3): | 30.48 | 32.46 | 29.68 | Average Ambient Temperature (°C): | 30.87 | Time Stamp (DD/MM/YYYY-HH:MM:SS): | 14/2/2017-11:13:48 |
|---|---|---|---|---|---|---|---|---|---|---|---|---|---|---|---|---|---|
| 0 | 3256 | 3321 | 33.22 | 34.86 | 33.44 | 0 | 175 | 0 | Phase 1 | | | | | | | | |
| 10 | 3283 | 3333 | 33.22 | 34.86 | 33.44 | 0 | 175 | 0 | Phase 1 | | | | | | | | |
| 20 | 3286 | 3337 | 33.22 | 34.94 | 33.44 | 0 | 173 | 0 | Phase 1 | | | | | | | | |
| 30 | 3288 | 3340 | 33.22 | 34.94 | 33.44 | 0 | 170 | 0 | Phase 1 | | | | | | | | |
| 40 | 3289 | 3339 | 33.22 | 34.94 | 33.44 | 0 | 170 | 0 | Phase 1 | | | | | | | | |
| 50 | 3290 | 3341 | 33.22 | 34.94 | 33.44 | 0 | 172 | 0 | Phase 1 | | | | | | | | |
| 60 | 3289 | 3339 | 33.22 | 34.94 | 33.44 | 0 | 172 | 0 | Phase 1 | | | | | | | | |
| 70 | 3289 | 3339 | 33.32 | 34.94 | 33.44 | 0 | 176 | 0 | Phase 1 | | | | | | | | |
| 80 | 3303 | 3337 | 33.32 | 34.94 | 33.44 | 0 | 173 | 0 | Phase 1 | | | | | | | | |
| 90 | 3290 | 3339 | 33.32 | 34.94 | 33.44 | 0 | 172 | 0 | Phase 1 | | | | | | | | |
| 100 | 3290 | 3338 | 33.32 | 34.94 | 33.44 | 0 | 171 | 0 | Phase 1 | | | | | | | | |
| 110 | 3293 | 3339 | 33.32 | 34.94 | 33.44 | 0 | 173 | 0 | Phase 1 | | | | | | | | |
| 120 | 3289 | 3335 | 33.32 | 34.94 | 33.44 | 0 | 170 | 0 | Phase 1 | | | | | | | | |
| 130 | 3288 | 3339 | 33.32 | 34.94 | 33.44 | 0 | 172 | 0 | Phase 1 | | | | | | | | |
| 140 | 3288 | 3340 | 33.32 | 34.94 | 33.44 | 0 | 171 | 0 | Phase 1 | | | | | | | | |
| 150 | 3295 | 3342 | 33.32 | 34.94 | 33.44 | 0 | 172 | 0 | Phase 1 | | | | | | | | |
| 160 | 3290 | 3339 | 33.32 | 34.94 | 33.44 | 0 | 174 | 0 | Phase 1 | | | | | | | | |
| 170 | 3292 | 3341 | 33.32 | 34.94 | 33.48 | 0 | 172 | 0 | Phase 1 | | | | | | | | |
| 180 | 3290 | 3340 | 33.32 | 34.94 | 33.48 | 0 | 172 | 0 | Phase 1 | | | | | | | | |
| 190 | 3273 | 3329 | 33.32 | 34.94 | 33.48 | 0 | 174 | 0 | Phase 1 | | | | | | | | |
| 200 | 3301 | 3345 | 33.32 | 34.94 | 33.48 | 0 | 171 | 0 | Phase 1 | | | | | | | | |
| 210 | 3301 | 3346 | 33.32 | 34.94 | 33.48 | 0 | 164 | 0 | Phase 1 | | | | | | | | |
| 220 | 3293 | 3341 | 33.32 | 34.94 | 33.48 | 0 | 177 | 0 | Phase 1 | | | | | | | | |
| 230 | 3294 | 3346 | 33.32 | 34.94 | 33.48 | 0 | 167 | 0 | Phase 1 | | | | | | | | |
| 240 | 3285 | 3338 | 33.32 | 34.94 | 33.48 | 0 | 169 | 0 | Phase 1 | | | | | | | | |
| 250 | 3291 | 3341 | 33.32 | 34.94 | 33.48 | 0 | 178 | 0 | Phase 1 | | | | | | | | |
| 260 | 3292 | 3341 | 33.32 | 34.94 | 33.48 | 0 | 171 | 0 | Phase 1 | | | | | | | | |
| 270 | 3291 | 3341 | 33.28 | 34.94 | 33.48 | 0 | 169 | 0 | Phase 1 | | | | | | | | |
| 290 | 3265 | 3331 | 33.28 | 34.94 | 33.48 | 0 | 174 | 0 | Phase 1 | | | | | | | | |
| 300 | 3299 | 3344 | 33.28 | 34.94 | 33.48 | 0 | 175 | 0 | Phase 1 | | | | | | | | |
| 310 | 3296 | 3346 | 33.28 | 34.94 | 33.48 | 0 | 170 | 0 | Phase 1 | | | | | | | | |
| 320 | 3297 | 3346 | 33.28 | 34.94 | 33.48 | 0 | 172 | 0 | Phase 1 | | | | | | | | |
| 330 | 3299 | 3347 | 33.28 | 34.94 | 33.48 | 0 | 168 | 0 | Phase 1 | | | | | | | | |
| 340 | 3296 | 3346 | 33.28 | 34.94 | 33.48 | 0 | 171 | 0 | Phase 1 | | | | | | | | |
| 350 | 3296 | 3343 | 33.28 | 34.94 | 33.48 | 0 | 171 | 0 | Phase 1 | | | | | | | | |
| 360 | 3295 | 3342 | 33.28 | 34.94 | 33.48 | 0 | 173 | 0 | Phase 1 | | | | | | | | |
| 370 | 3294 | 3344 | 33.28 | 34.94 | 33.48 | 0 | 172 | 0 | Phase 1 | | | | | | | | |
| 380 | 3299 | 3347 | 33.28 | 34.94 | 33.44 | 0 | 173 | 0 | Phase 1 | | | | | | | | |
| 390 | 3292 | 3342 | 33.28 | 34.94 | 33.44 | 0 | 174 | 0 | Phase 1 | | | | | | | | |
| 400 | 3292 | 3342 | 33.28 | 34.94 | 33.44 | 0 | 172 | 0 | Phase 1 | | | | | | | | |
| 410 | 3288 | 3341 | 33.28 | 34.94 | 33.44 | 0 | 176 | 0 | Phase 1 | | | | | | | | |
| 420 | 3293 | 3341 | 33.28 | 34.94 | 33.44 | 0 | 174 | 0 | Phase 1 | | | | | | | | |
| 430 | 3291 | 3340 | 33.28 | 34.94 | 33.44 | 0 | 170 | 0 | Phase 1 | | | | | | | | |
| 440 | 3285 | 3340 | 33.28 | 34.94 | 33.44 | 0 | 174 | 0 | Phase 1 | | | | | | | | |
| 450 | 3288 | 3340 | 33.28 | 34.94 | 33.44 | 0 | 173 | 0 | Phase 1 | | | | | | | | |
| 460 | 3288 | 3338 | 33.28 | 34.94 | 33.44 | 0 | 173 | 0 | Phase 1 | | | | | | | | |
| 470 | 3288 | 3340 | 33.28 | 34.94 | 33.44 | 0 | 174 | 0 | Phase 1 | | | | | | | | |
| 480 | 3288 | 3338 | 33.28 | 34.94 | 33.44 | 0 | 173 | 0 | Phase 1 | | | | | | | | |
| 490 | 3286 | 3340 | 33.28 | 34.94 | 33.44 | 0 | 173 | 0 | Phase 1 | | | | | | | | |
| 500 | 3290 | 3341 | 33.28 | 34.94 | 33.44 | 0 | 168 | 0 | Phase 1 | | | | | | | | |
| 510 | 3285 | 3339 | 33.28 | 34.94 | 33.44 | 0 | 175 | 0 | Phase 1 | | | | | | | | |
| . | . | . | . | . | . | . | . | . | . | | | | | | | | |
| . | . | . | . | . | . | . | . | . | . | | | | | | | | |
| . | . | . | . | . | . | . | . | . | . | | | | | | | | |

Table 4.1: A sample of the first few entries in a .csv file, as stored by the prototype.

### 4.3.4. Embodiment

For technical documentation regarding the mechanical parts of the prototype, please see appendix AB. These drawings have been used for communicating the design to the prototyping assistants.

This section will be building further upon the concept chosen in section 4.2.3, of which a conceptual sketch was illustrated in 4.1 in the form of a free-body-diagram (FBD). The FBD is repeated in this section in 4.22. Given the components of choice (see section 4.3.1), a detailed prototype design will be further elaborated in this section.

Figure 4.21: A picture of the final prototype, showing the probe and the control unit.

#### Probe embodiment

In this section the details design of the probe will be further specified. It has been chosen to optimise the design for use on the chest. The main reason for this is that it is assumed that mild forces on the chest of a neonate causes less stress to the subject compared to use on the forehead. Also, as stated by Prof. dr. Sidarto Bambang Oetomo (see appendix B), the chest is believed to be most optimal place for CRT assessment, due to its minimal motion and support of the sternum. It was also already established that measuring CRT on the chest would probably result in the most consistent CRT values.

**Mechanical design:** As already discussed in section 4.2.3, springs will be used to ensure good skin contact of the sensors and to ensure a consistent amount of downforce. These springs should also minimise the effect of any variations of external force on the probe that keep the probe against the skin of the subject. The configuration of these springs can be seen in 4.23, where a section view of the probe reveals the internals. SPR2 of the FBD in figure 4.22 can be seen in figure 4.23 just between the solenoid and the aluminium sheet that supports the solenoid. SPR2 exerts a very minimal force to the PPG piston, which ensures good skin contact and approximately equal compression forces during every measurement. SPR1 makes sure to exert

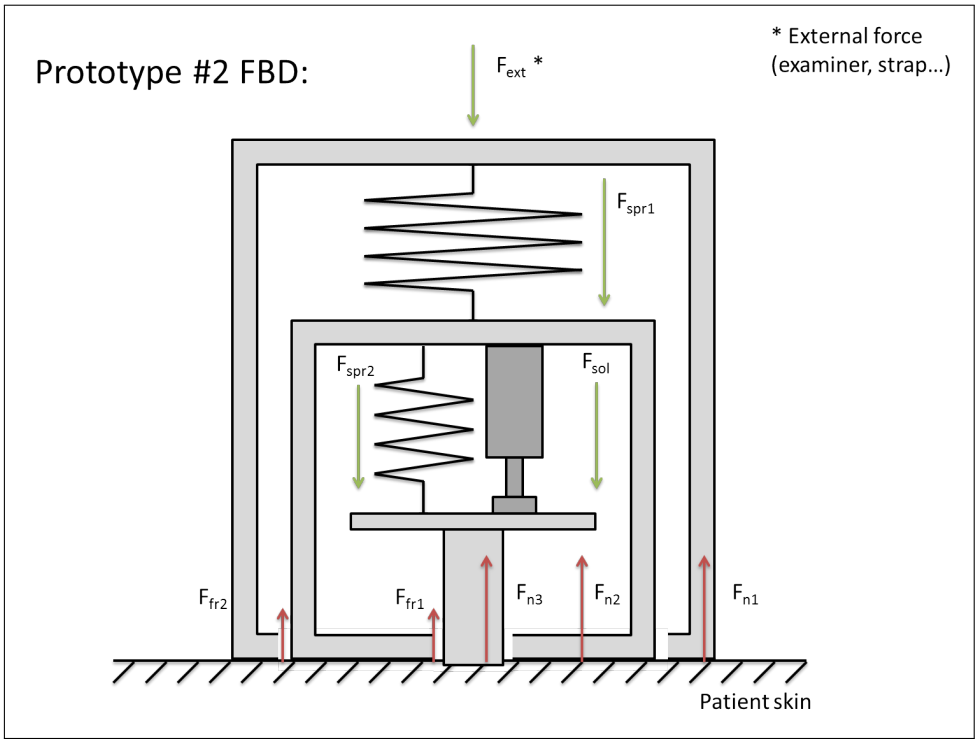


Figure 4.22: A conceptual FBD of Prototype #2

a force directly to the large piston. The function of this force is also to ensure good skin contact with sensors in this segment, but the exerted force should also be always larger than the exerted force of the solenoid and SPR2 added-up. This should ensure good skin contact of the sensors in the larger piston, even during the compression phase which causes counteracting forces on the larger piston because of the solenoid.

It was already established that the active output force of the solenoid would be about 2.55N. The compression force of SPR1 should therefore during use be larger than 2.55N. To build in a decent safety factor, it has been chosen to use an $F_{spr1}$ of 10N. This force is justified since the contact surface of the large piston is relatively large, which decreases the overall pressure caused by this force. It is believed that the actual driver behind blanching the skin is applying homogeneous pressure to the skin that exerts the blood fluid pressure inside the capillaries. To put it into perspective, the contact surface area of the PPG piston ($r = 4mm$) is $\pi(4)^2 = 50.26mm^2$, while the contact surface area of the large piston ($r = 25mm$) is $\pi(25)^2 - 50.26 = 1913.24mm^2$ (neglecting the holes of the temperature sensors). This is a difference in surface area with a factor 38. The overall pressure that the large piston exerts to the skin as a result of $F_{spr1}$ is therefore $5226.7N/m^2$, while the pressure of the PPG piston during compression is $50736.2N/m^2$. The latter pressure was considered the minimum pressure needed to blanch the skin, and since the normal pressure of the large piston is over a factor 10 smaller, it is considered to be sufficiently small to be unobtrusive to the blood-dynamics of the skin.

It is expected that the large piston, due to differences in anthropometric characteristics of the chest in children between 0 and 5 years old, would be subjected to the some variation in terms of relative displacement in the outer cylinder. It is assumed that this displacement variation is not more than +/-2.5mm from the normal displacement (when the large piston surface is level with the outer cylinder surface. It is chosen that a variation in $F_{spr1}$ of +/- 0.5N is allowed. Therefore, the maximum spring stiffness (K) that can be allowed for SPR1 would be $0.5N/0.0025m = 200N/m$. This means that, in order to get to a $F_{spr1}$ of 10N, the spring should be compressed by 50mm under normal use circumstances. A spring was provided by *Tevams* (see appendix Y), with a length of 110mm. Therefore, to get to a $F_{spr1}$ of 10N, the spring SPR1 should be compressed to 60mm, as can be seen in figure 4.23. For SPR2 the spring that was enclosed with the solenoid was used. The force of this spring is considered less critical, as long as it was small enough to allow the capillaries to refill during the CRT-phase.

Since the housing parts that should be able to move in relation to each other (the outer cylinder, the large piston and the PPG piston) are very prone to friction, these parts were made with the help of the Prototyping

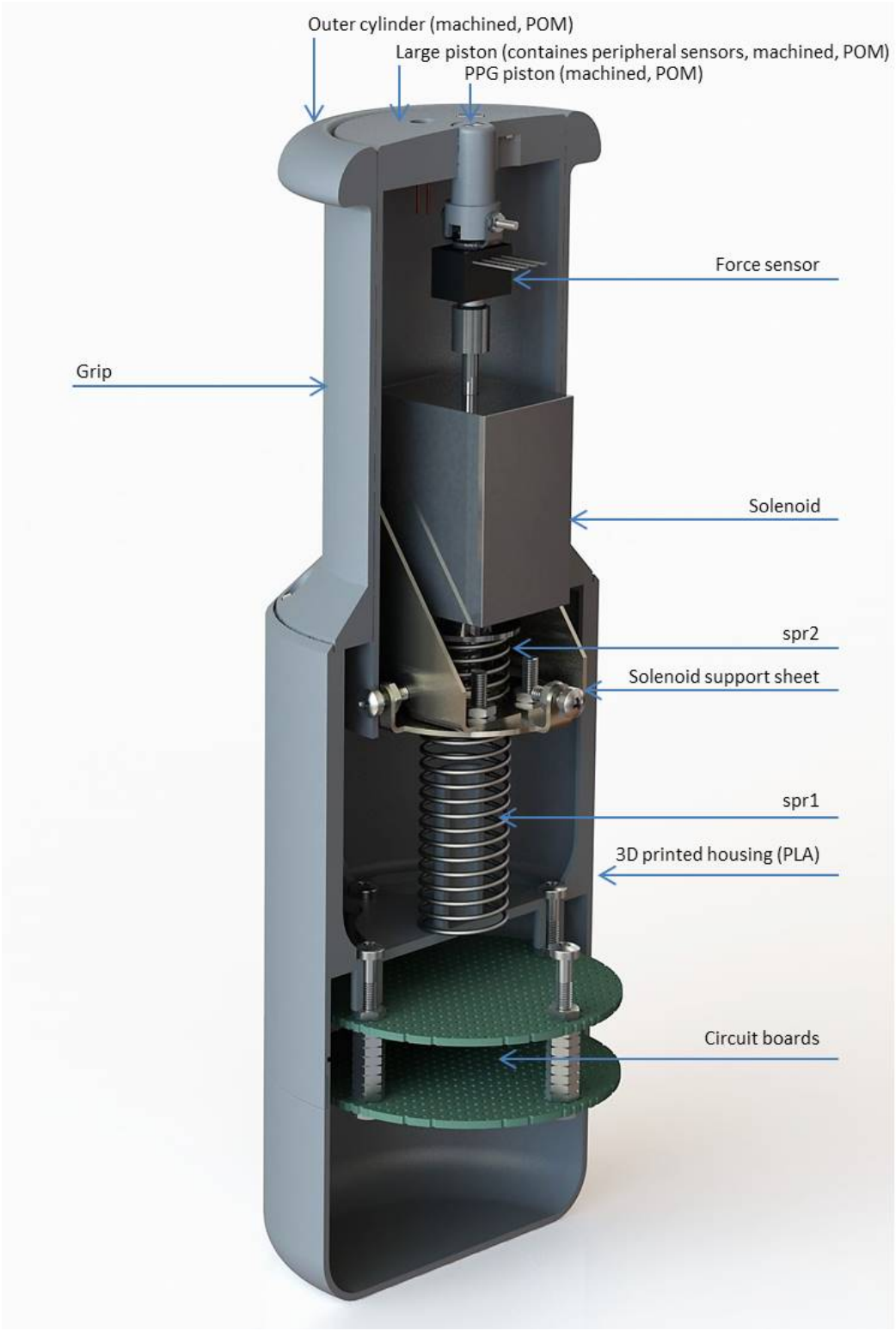


Figure 4.23: Render of the PPG probe, with a view of the internal lay-out.

Services Department at Philips Research. These components were machined out of blocks of *polyoxymethylene* (POM). This material is known for its outstanding mechanical properties, and is also considered biocompatible (FDA-approved). It is often used for high-performance applications such as gears, bushings, but also for instance for zippers. Due to its low friction coefficient, it is a very suitable material for parts that

Figure 4.24: Render of the PPG probe in exploded view.

should be able to slide over each other, such as with these parts [1]. It also has a very good water resistance. The prototype builders ensured that the movement of these parts relative to each other would be as friction-less as possible. All other parts of the housing would be 3D-printed, using Polylactic Acid (PLA) since this is

the standard material to print with at Philips Research.

The aluminium sheet bended solenoid support parts were produced by laser-cutting the parts. The prototype assistants would bend them into the right shape. The attachment of the force sensor to both the solenoid armature and the PPG piston is done by double-sided foam tape (figure 4.25). The forces on this part are only compressive forces and no tensile forces (under normal use), and due to the very small tolerances of both the solenoid and PPG piston to transversal movement, forces other than axial forces are expected to be minimal. Therefore adhesive tape is considered sufficient to fixate the sensor. The foam inside the tape also facilitates some minor damping of the forces on the sensor. This should dampen out large impact spikes in the force sensor signal due to fast force changes.

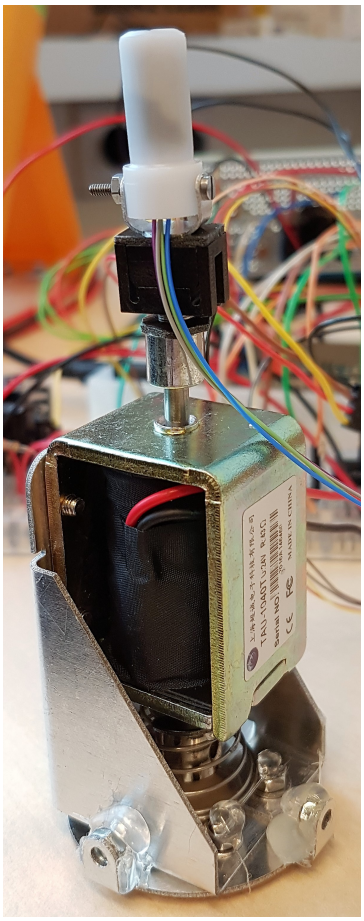

Figure 4.25: Assembly of the solenoid (attached to support sheet), force sensor and PPG piston.

**PPG sensor integration:** The Osram PPG modules were integrated into the device as shown in figure 4.27. The important thing was that the sensors were level with the surface of the probe. If the module would be placed below the surface, skin contact would be lost which would result in optical cross-talk and therefore a weak signal. Placing the module higher than the surface would cause irregularities in applied pressure (stress accumulations in the skin around the edges of the PPG modules), which could affect CRT.

To integrate the modules, help was sought again at the Prototyping Services Department. To successfully anchor the tiny modules, they were first carefully soldered onto a 8-pin header. To strengthen the junction, and to insulate the soldered connection, epoxy glue was applied between the header and the PPG module. The 8-pin connection (see figure 4.26) could be used to connect the module to the printed circuit board (PCB) by wire. The beam-like shape of the header also made it possible to fixate the sensor in the sensor holes using two-component glue.

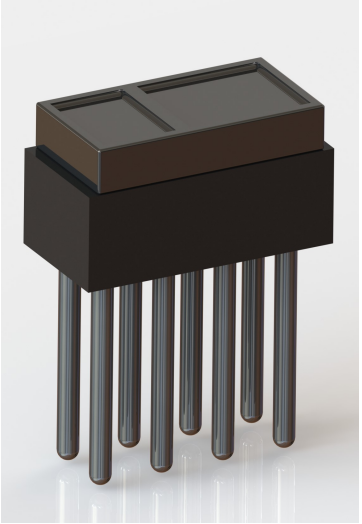

Figure 4.26: Render of the PPG sensor, soldered on top of a small header.

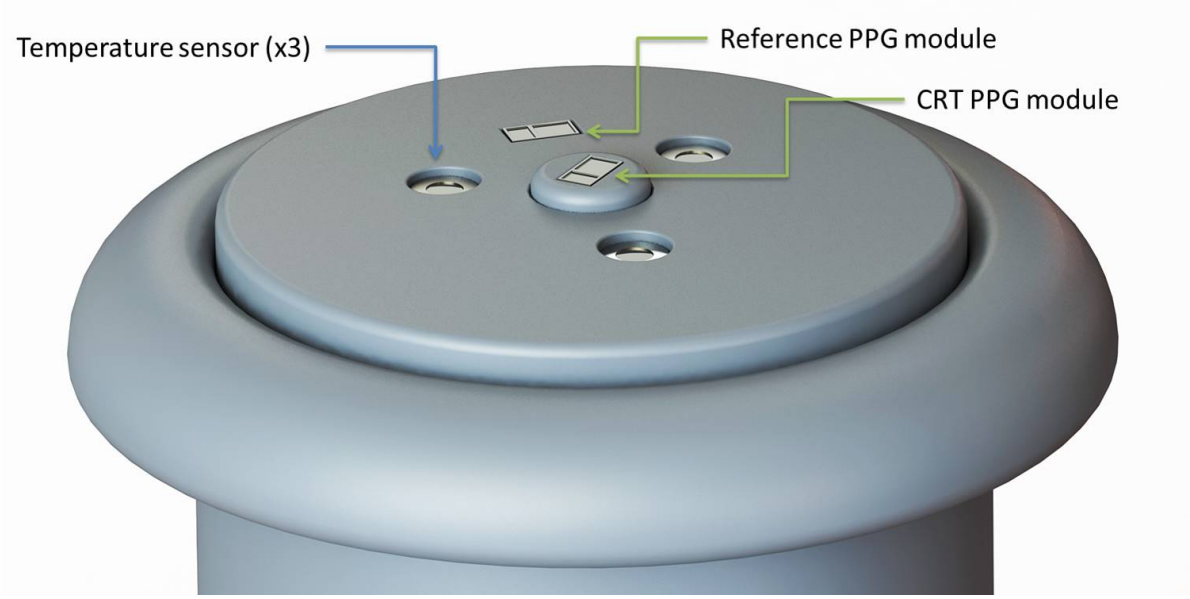


Figure 4.27: Render of the sensor-surfaces of the PPG probe, showing all sensors recording PPG and temperature data.

**Temperature sensor integration:** The temperature sensors were integrated into the probe using the same kind of glue. With these sensors, a precise distance from the probe surface was critical. These temperature sensors are non-contact, so preferable skin-contact is avoided. On the other hand, the sensors have a sensitive field-of-view (f.o.v.) of about 105°C. That means that if the sensor would be recessed too far under the probe surface, parts of its f.o.v. would be obstructed, reducing accuracy of the sensor. Depth of these sensors is therefore defined using the metrics as illustrated in figure 4.28. Sensor depth is defined as the distance from the lower tab of the sensor can, to the surface of the probe. It can be calculated that the maximum sensor depth in order to keep full f.o.v. would be 3.13mm, so rounded a depth of 3mm is chosen.

**Circuit boards:** All components that are part of the circuits in figures 4.10, 4.11, 4.14 and 4.15 (except for the sensors and solenoid) are soldered on the PCB's, which can be seen in the bottom of figure 4.23 and in figure 4.29. All amplification of analogue signals happen here, to prevent amplification of noise being picked-up on the way to the CU.

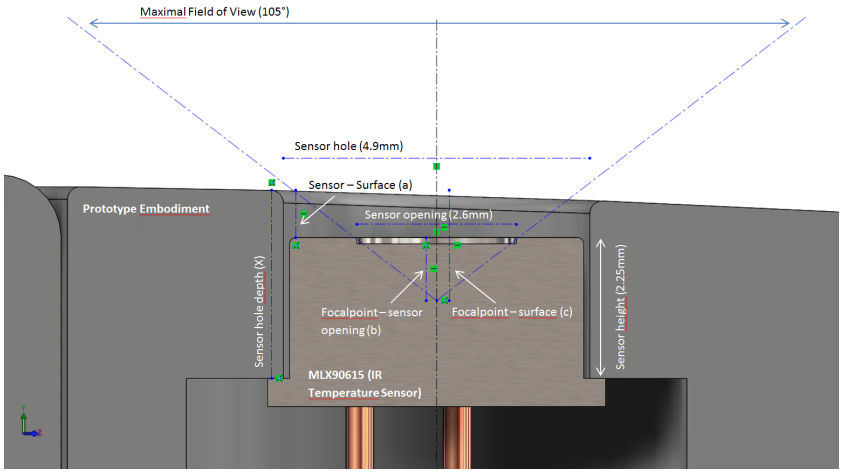


Figure 4.28: Section view of the temperature sensor, as it is integrated in the probe, including some metrics for defining sensor hole depth.

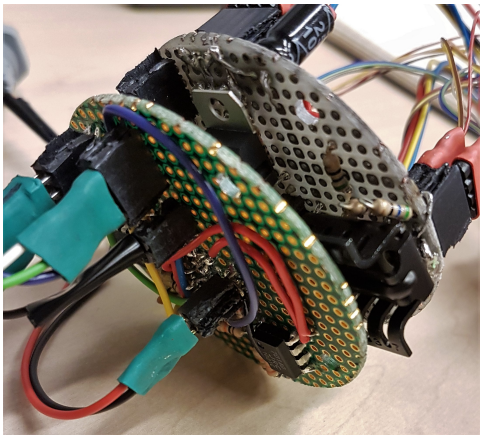

Figure 4.29: PCB's in the probe containing voltage regulation, signal amplification and filtering.

### Control Unit

The control unit consists of a 3D printed housing, which is basically a box made out of 2 shells. In one shell the Arduino is screwed in, while in the other shell a PCB containing all other circuitry is screwed in. Holes are made in the box in order to panel-mount the buttons, the power switch and to have an opening for cables (power supply, usb and connection to the probe) and for the micro-SD card. A snap-fit connection was integrated to keep the two housing shells together, although a tie-wrap was needed to ensure a robust fix.

## 4.4. Validation

Now that the new prototype has been built and is functional, it has to be validated. The measured PPG signal as measured from the chest looks quite typical for CRT, as can be seen in figure 4.31. Yet, to prove that this prototype actually does measure CRT, an expected variation due to a known independent variable should be demonstrated. It was considered that another dehydration experiment would for this application be a bit exorbitant. Therefore, a more easily controllable independent variable has been chosen of which its influence on CRT is already established: *ambient temperature*.

The research question of this short validation experiment is therefore:

*"Will a substantial increase in ambient temperature significantly shorten the CRT as measured with the new CRT-PPG prototype?"*

To be more specific about the dependent variable, a shorter CRT would result in a lower $B$ parameter as output of the exponential model.

Figure 4.30: Side of the CU, presenting the power switch and the micro-SD slot.

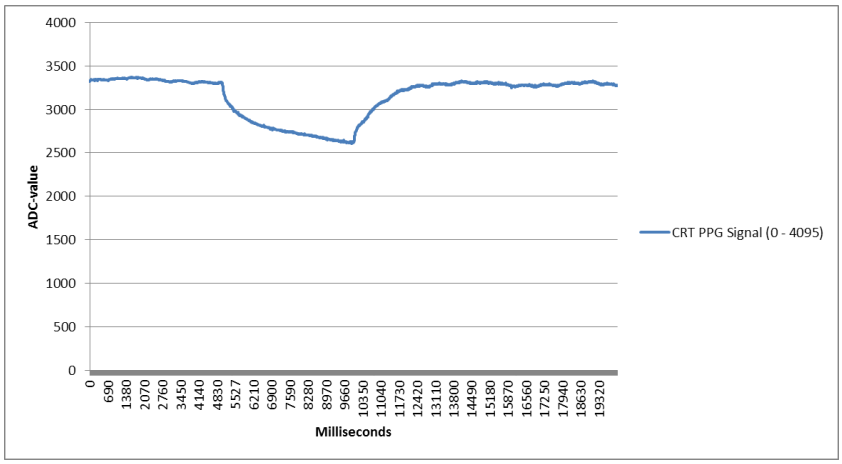


Figure 4.31: Typical CRT PPG signal measured from the chest, with a clearly distinguishable pre-compression phase, compression phase and capillary refill phase.

The protocol of this experiment is relatively simple:

- Take two rooms where a different ambient temperature is kept: approximately 10°C in one room (the cold room) and approximately 20°C in the other room (the warm room).
- Stay at least 15 minutes in the cold room, before taking at least 6 measurements with the prototype from the midpoint of the sternum.
- Repeat the last step in the warm room.
- While performing this experiment, no drinks or any mild physical excitement is allowed, in order to mitigate any other external influences.
- Repeat this protocol at least 3 times on different days.

The data is processed with an updated Matlab script, which can be found in appendices Z and AA. This script follows similar steps as in the first prototype, fitting the same exponential function, yet more efficiently due to the better data labelling by the software in the prototype. Also, now only the original capillary refill data is used for the curve-fitting (instead of cancelling out the AC-component). The reasons are the fact that in the previous experiment it did not consistently improve the signal, and since it is expected that the effect of these temperature differences will be significant enough to detect it on the original data. Also has it been identified that in general the AC-component is much smaller in relation to DC-level changes due to the CRT

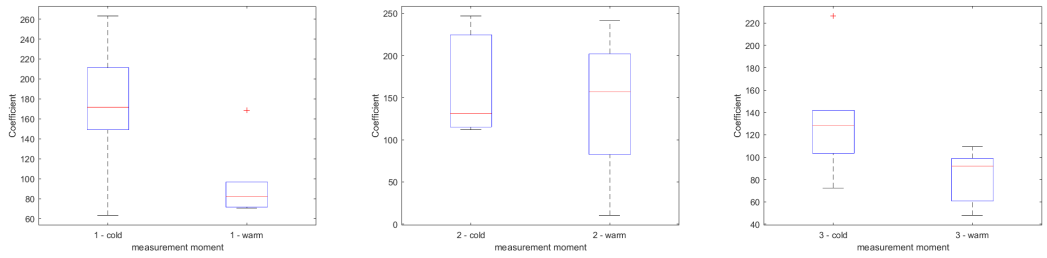


(a) Boxplot results day 1 (b) Boxplot results day 2 (c) Boxplot results day 3

Figure 4.32: All results after processing the data for each day, grouped per ambient temperature.

process, when it is compared to the PPG data of the previous prototype. It suggests that with this prototype the CRT signal may by default be less influenced by the AC-component, which suggests that cancelling out the AC-component may be unnecessary. All the data is filtered using the *filtfilt* function, to prevent any influence from high-frequency noise from the ADC.

After processing all the data, and having all the CRT data converted into an estimated $B$ parameter, the following boxplots in figure 4.32 can be regarded as a good summary of the parameters. It already seems like the measurements in the warm room return a lower parameter $B$, which is expected.

In figure 4.33 the effects plot can be found, which compares the mean of all parameters from the cold room to the parameters of the warm room, of all days. A clear difference can be seen.

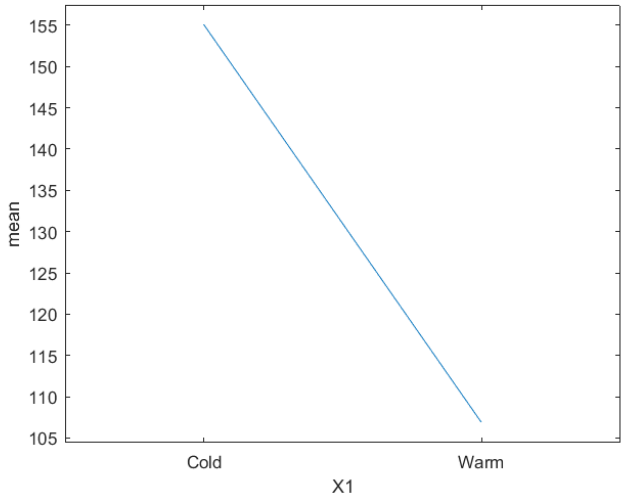


Figure 4.33: The main effects plot of different temperatures on CRT parameter.

To further back up the observation of temperature having substantial effect on the CRT by the prototype, a *one-way ANOVA* was performed using the *anovan* function in Matlab. In figure 4.34 the resulting ANOVA table can be seen.

**Analysis of Variance**

| Source | Sum Sq. | d.f. | Mean Sq. | F | Prob>F |
|---|---|---|---|---|---|
| X1 | 20920.4 | 1 | 20920.4 | 6.15 | 0.0182 |
| Error | 115630.9 | 34 | 3400.9 | | |
| Total | 136551.3 | 35 | | | |

Constrained (Type III) sums of squares.

Figure 4.34: ANOVA table.

It is chosen to abide by a maximum p-level of .05 for assessing statistical significance. From the ANOVA,

it can be concluded that the effect of ambient temperature on the CRT parameter $B$ is significant, $F(1,35) = 6.15$, $p < .05$.

### 4.4.1. limitations of prototype #2

A few limitations to the prototype have been identified which should be addressed in later iterations of new prototypes using PPG to measure CRT.

- In general the PID controlled force output performed quite good, especially when used on the chest with support of the rigid sternum. Yet when the prototype is used on softer body-locations (like the palm of the hand) or when a subject has more subcutaneous fat, the controller can become unstable and starts oscillating. This is believed to be a result of the non-linear behaviour of the solenoid when the throw of the armature can vary more. At the time of building the prototype no solution to this problem was found, although now it seems that a *variable force solenoid* (or *proportional solenoid*) might be able to tackle this problem. This type of solenoid is specifically designed to react linearly to input current in terms of force output or throw. These solenoids are also specifically design for applications where throw or compression force need to be controllable. The solenoid that is used for this prototype was not dedicated for variable force control, but is more intended for on/off applications. The use of a proportional solenoid is therefore recommended in future designs, as it still includes all of the benefits of conventional solenoids. They will come at a slightly higher cost.

- It was found that 10N is still quite high as downforce for the large piston (form SPR1). Despite the large surface area of the piston, the downforce of 10N did blanch the skin, which could have significant effect on the CRT reading at the PPG piston. During the experiment the large piston was therefore never fully compressed, but the probe was hold very still instead to prevent motion artefact. 5N (or less) is believed to be enough, and should be considered for future designs.

- The prototype is still quite bulky. Large components such as the compression spring and solenoid make it difficult to make a very compact design, but especially PCB design improvements and general spatial rearranging of components should be able to lead to significant improvements in terms of size of the device.

- The ambient temperature readings of the integrated IR-temperature sensors are often quite far apart from each other, which suggest that these measurements can be quite inaccurate. It is believed that these sensors are much affected by temperature of the device, which by continued use can also become somewhat warmer (due to body temperature). Therefore these readings should not be relied on as accurate temperature readings. Ambient temperature sensors should be placed on other places of the device where they are less affected by heat from the human body, or from heat generating components such as the voltage regulators or the solenoid.

- The reference sensor signal was relatively bad due to the high downforce of the large piston. Another reason for a bad signal was motion artefact as result from the compression of the PPG piston. When this piston compresses the skin, it also pushes the skin down at the level of the reference sensor. A solution is to move the reference PPG sensor further away from the PPG piston.

- The RTC module in the control unit did not continue with keeping the time when the device was switched off. This problem was fixed by connecting the device to a PC and uploading the code again in order to reset the clock. This is assumed to be a malfunction of the RTC, and should be overcome by using a different RTC in future prototypes.

- redesigning future prototypes to be made cable-less would improve the overall user-friendliness of the device. This could be done by integrating the CU and the probe into one single unit, and to use a high-capacity lithium-ion battery instead of a wall-adapter. The integration of a small display on the device make the use of a laptop or PC for signal strength monitoring redundant. This could also be done by using a smart-phone with a Bluetooth connection.

## 4.5. Conclusion

A significantly improved prototype has been realized in the last phase of this assignment. Based on the learnings from the earlier experiment, the prototype has been designed to mitigate external influences, effectuate a very consistent compression phase and overall return a PPG signal with a better SNR and higher sample rate. The device can be used hand-held, and is therefore easier and quicker for taking measurements, especially now that the skin-temperature sensors have been integrated into the device. Also data storage is now performed much more conveniently, which results in a much more efficient retrospective data processing.

Having established a significant relationship of the parameter $B$ from the exponential model with ambient temperature, and looking at the overall characteristics of the CRT signal in 4.31, it can be concluded that the reading of the prototype is likely to be highly affected by capillary refill time. This conclusion suggests that this concept should be suitable for further investigations into the effect of dehydration on CRT.

# 5

# Conclusions & Recommendations

## 5.1. Conclusions

It has been stated clearly that child mortality due to dehydration is a severe problem, which accounts for a very large proportion of all child deaths in low resource settings, since diarrhoea is known to be the second biggest killer of (post-neonatal) children under the age of five. It has been identified that assessing dehydration is currently a problem, as can be derived from literature reviews and interviews with health workers in low-resource settings. Currently children suffering from diarrhoea are often diagnosed with an inaccurate severity of dehydration. This misdiagnosis causes preventable deaths, as underestimation leads to delayed treatment of the condition, which in turn leads to severe (fatal) dehydration. The problems with diagnosis also can contribute to unnecessary high cost of healthcare in low resource settings, as Oral Rehydration Salts (ORS) is often out of stock due to over-subscription, while this lack of ORS then leads to administration of the more expensive intravenous fluids to patients who would have been fine with only ORS. In addition, regardless of the actual diagnostic performance of the current standard tests for dehydration assessment, parents or guardians often seem to distrust the assessment of the community health worker. This distrust in turn also leads to over-subscription of treatment resources that the patient does not benefit from. Therefore, finding cost-effective solutions that could solve the problem of dehydration assessment would both be beneficial for reducing child mortality and for reducing cost of healthcare in low-resource settings.

It has been established that the three main factors that cause low diagnostic performance of current tests are: subjectivity, lack of training and external factors that influence the assessment. Currently the most reliable tests are the capillary refill time test and the skin-turgor test. To overcome the three main issues with these current tests, it is concluded that a tool should be developed that can automatically and objectively perform a (digital) analysis of one or both of these diagnostic variables, while mitigating the influence of any external factors. For capillary refill time specifically, photoplethysmography has been recommended as the most promising technological principle.

By means of a validation experiment these principles were tested using regression analyses, the results did not came out as expected for most parameters of interest. Skin elasticity (one of the potential representative parameters for skin turgor) did seem do decrease somewhat with increased dehydration, while for capillary refill time assessment using PPG seemed to be best related to dehydration when measured on the forehead. Measurements on the chest showed practical issues, although it is still hypothesized that CRT on the chest would be a good diagnostic variable, based on literature and an interview with a neonatologist. Yet by far most of the analysed parameters did not result in a model with any predictive value. Still it is hypothesized that these unexpected results are due to substantial limitations regarding the conducted experiment, which should be well considered in any future studies. The main limitations were: low number of subjects and low number of samples per subject, age of subjects was not representative to target group, and the severity of dehydration achieved during the experiment is considered too low as clinically 4% dehydration is not regarded as mild dehydration.

A part of the learnings from the experiment were translated into an improved version of the PPG pro-

totype. This prototype successfully took all requirements and learnings into account in its design. A small validation experiment was conducted to proof that the measured parameter is actually CRT, and not just arbitrary data that coincidently shows similar characteristics. A clear relation of the measured CRT parameter with ambient temperature has been demonstrated with this experiment, and thus it can be said with confidence that the prototype measures what it is meant to measure: capillary refill time. Yet, the variability is still too large for the concept to be used for diagnostic purposes. It is hypothesized that this remaining variability could be mitigated by further optimizing the design of the prototype.

## 5.2. Recommendations

Having demonstrated the proof-of-principle that the prototype can very likely be used for CRT measurements, it is recommended to continue investigating this principle for dehydration measurement. Yet, it is also recommended that further research should not just be limited to CRT and PPG. the recommendations for near future actions regarding this topic are presented below.

### 5.2.1. Remaining learning points

Apart from the things that have been learned during this assignment, there are still a lot of unknowns regarding the topic of measuring dehydration. The key unknowns are listed below:

- Assuming that both sensitivity and specificity of a final concept of a diagnostic tool would be 100%, what is the quantified added value in terms of reduced child mortality and the cost of treatment saved, if such a device would be implemented in low-resource settings?
- How could skin turgor be assessed with a tool, which ensures an adequate measurement depth to the dermis? What would be the most cost effective method?
- Skin turgor and capillary refill time are diagnostic variables that are indirectly related to hydration status. Would there be a method to directly measure the water content of the body accurately, which satisfies all requirements set for this tool? (non-invasive, point-of-care, low BOM, etc...)
- It is already established that a field study in low-resource areas is needed in order to collect the appropriate data which could contribute to a predictive model. Yet, before conducting such a study, a convincing proof-of-principle has to be demonstrated in order to be sure that conducting such a study is justified. Would the current PPG prototype be fit for data collection for prediction models of dehydration assessment? How could that be proven? How to conduct a validation experiment where severe degrees of dehydration can be measured in a controlled environment?
- Would a final concept of a diagnostic device for dehydration be based on a single diagnostic variable (including any additional sensors to account for confounding factors)? Or could sensitivity and specificity of the future diagnostic device be optimized by combining a couple of diagnostic variables (such as capillary refill time and skin turgor) and sensors into one device? In order to answer this question, the concepts have to be tested extensively to know their actual diagnostic performances, and a design study has to be performed to investigate how different methods such as capillary refill time and skin turgor could be combined into one device, which could be used in a single action.

### 5.2.2. Iterating through New Concepts

- Before putting all focus on CRT, diverge! As already established, eventually a set of at least three working prototypes should be achieved before conducting any large scale data collection study. The reason to have a set of prototypes is to be able to make a substantiated choice for a concept or combination of concepts that performs best in diagnosing dehydration.
- The current prototype for PPG should be further optimized in terms of performance, stability, design, use-case, safety and making it possible for the prototype to work off-grid (should work without the presence of power sockets). Also the use of mechanically controlled compression instead of electrical actuation should be further investigated.
- A conceptualization effort should be performed to come up with potential embodiments for a skin-turgor prototype. The objective assessment of skin-turgor has not been well investigated up to now, as there are still a lot of design directions open for further investigation.

- A method which is able to measure total body water content directly, or at least of a body part, should be investigated. ST and CRT are indirect estimators for dehydration, which means that influence from external factors can cause variability on the measurement. In a direct measurement of the total body water content this variability might be substantially lowered. A feasible technological principle for measuring this is yet to be identified.

### 5.2.3. Future Studies

In order to learn more about the fundamentals of the problem of dehydration due to diarrhoea, to validate the diagnostic performance of any future functional prototypes and to collect data to base predictive models upon, more studies should be conducted in the near future. A few important recommended studies are listed below.

- Surveys in the field with local community health workers, clinicians, neonatologists and other potential stake-holders. These surveys should be focussed on assembling a detailed list of requirements for any future final concept. Also, by asking the right questions and searching for relevant quantitative data, information should be gathered that give an idea of the quantified added value in terms of reduced child mortality and health care cost. Such data are key for putting together a viable business-case for any final concept.
- After having established a set of prototypes which all have been validated up to a certain level, a data collection study using these prototypes should be conducted. The main objective is to collect data which can be used to build a predictive model, which can either be done using (multivariate) regression analysis techniques, or machine learning algorithms in case the parameters of interest are very complex.
  - Such a study should be conducted in collaboration with local community health workers or clinicians who are able to collect data with the prototype next to their normal workflow. It is key that this person sees dehydrated patients on a daily basis and that this person is capable of taking the measurements in parallel to the normal workflow without the extra action being too intrusive. Different collaborating health workers would work as separate spokes in different areas, using different prototypes.
  - The collected data would only be meaningful if the actual amount of dehydration is known during that measurement. As these measurements will mainly be taken from patients who present themselves already (severely) dehydrated, without any medical history or knowledge on their exact baseline (euhydrated) body weight. This euhydrated body weight should therefore be determined in hindsight, when the patient is clinically defined as fully rehydrated. This also requires the health worker to keep the dehydrated patient in its vicinity, as short term body-weight change should be closely monitored, while taking the measurements with the prototype as the patient rehydrates over time.
  - When predictive models are derived from the collected data, the diagnostic performance (sensitivity & specificity) can automatically be derived from the data. Knowing the exact diagnostic performance should indicate which techniques are significantly better than current methods. Also, it would enable a study into the benefits and disadvantages of combining certain techniques into one tool [80].

## 5.3. Take-Home Message

Dehydration due to diarrhoea is a very severe danger for young children in low-resource settings. The ways that global health authorities try to tackle this problem, by deploying treatment resources and prevention measures, seems to be only part of the solution. Effective utilization of the treatment resources needs to be ensured, for which proper diagnosis of the severity of dehydration is believed to be a key factor. Digital ways of assessing capillary refill time and/or skin turgor (instead of the current manual methods) may in theory be very feasible for diagnosing the severity of dehydration, by decreasing the effects subjectivity, external influences and dependence on examiner training on the measurement. In practice however there are still significant limitations to these methods, which should be addressed in future designs of diagnostic devices using these methods. In parallel, more "direct" ways of measuring total body water content should also be explored. When a successful diagnostic device could be realized, it is expected that it could play a very significant role in preventing unnecessary child mortality due to diarrhoea. In addition, cost of healthcare could be

decreased due to more efficient use of available treatment resources. For the most deprived people that are living on this planet this would be a large step forward, towards a life without the fear of loosing their children to a easily treatable disease.

## Acknowledgement

I am thankful to Philips Research for giving me the chance and the means to conduct this project. I want to thank every individual at Philips (in Eindhoven and in Nairobi) who supported me with their expertise on specific technical issues, and in particular I want to thank Pavan Dadlani for his guidance as my supervisor at Philips. In addition, I want thank Jenny Dankelman for being my supervisor at the TU Delft, for always being available for feedback on my general proceedings.

# Bibliography


[1] Cambridge engineering selector. Cambridge, UK.

[2] The cutometer mpa 580: Brochure. http://www.courage-khazaka.de/images/phocadownload/Brochures/Brochure_MPA580.pdf. Accessed: 28/06/2016.

[3] Arduino due information webpage. https://www.arduino.cc/en/Main/arduinoBoardDue. Accessed: 04/03/2017.

[4] Installation instructions for fsg series force sensor. https://sensing.honeywell.com/fsg-series-force-sensor-install-50090349-a-en-final-13aug13.pdf. Accessed: 22/12/2016.

[5] Sfh 7051 biomon sensor application note. http://www.osram-os.com/Graphics/XPic9/00194555_0.pdf/BioMon%20Sensor%20SFH%207050.pdf. Accessed: 24/11/2016.

[6] Fsr 400 series data sheet. https://www.interlinkelectronics.com/datasheets/Datasheet_FSR.pdf. Accessed: 04/01/2017.

[7] Mlx90615ssg product information. https://www.melexis.com/en/product/mlx90615/digital-plug-play-infrared-thermometer-ultra-small-to-can. Accessed: 22/12/2016.

[8] Nju7014 datasheet. http://www.njr.com/semicon/PDF/NJU7014_NJU7015_NJU7016_E.pdf. Accessed: 19/12/2016.

[9] Sfh 7051 biomon sensor datasheet. http://www.osram-os.com/Graphics/XPic2/00219352_0.pdf/SFH%207051,%20Lead%20(Pb)%20Free%20Product%20-%20RoHS%20Compliant.pdf. Accessed: 19/12/2016.

[10] Fsr 101: Force sensing resistor theory and applications. http://www.sensitronics.com/pdf/Sensitronics_FSR_101.pdf. Accessed: 24/11/2016.

[11] Vishay model 1004 single point load cell datasheet. http://docs-europe.electrocomponents.com/webdocs/010f/0900766b8010f46a.pdf. Accessed: 24/11/2016.

[12] Who global health observatory data repository. http://apps.who.int/gho/data/node.home. Accessed: 04/03/2016.

[13] Diarrhoeal disease fact sheet. http://www.who.int/mediacentre/factsheets/fs330/en/, 2013. Accessed: 04/03/2016.

[14] V. Kalyani et al. A. Bordoley, R. Irwin. Digit: Automated, tempera- ture-calibrated measurement of capillary refill time. *MEAM-446-2012-06 Senior Design Project - Final Report*, pages 1–13, 2012. http://www.me.upenn.edu/senior-design/2012/papers/team06.pdf. Accessed: 31/03/2016.

[15] H Ait-Oufella, N Bige, PY Boelle, C Pichereau, M Alves, R Bertinchamp, JL Baudel, A Galbois, E Maury, and B Guidet. Capillary refill time exploration during septic shock. *Intensive care medicine*, 40(7):958–964, 2014.

[16] John Allen. Photoplethysmography and its application in clinical physiological measurement. *Physiological measurement*, 28(3):R1, 2007.

[17] Bronwyn Anderson, Anne-Maree Kelly, Debra Kerr, Megan Clooney, and Damien Jolley. Impact of patient and environmental factors on capillary refill time in adults. *The American journal of emergency medicine*, 26(1):62–65, 2008.

[18] Ida Andersson and Anders Hedvall. Relationships between skin properties and body water level. Master's thesis, KTH, School of Technology and Health (STH), Medical Engineering, 2013.

[19] Annaclara Ariander. The effect of pressure on capillary refill time. 2015.

[20] Ann Ashworth, E Claire Schofield, Sultana Khanum, and Alan Jackson. Guidelines for the inpatient treatment of severely malnourished children. 2003.

[21] Michael Attas, Mark Hewko, Jeri Payette, Trevor Posthumus, Michael Sowa, and Henry Mantsch. Visualization of cutaneous hemoglobin oxygenation and skin hydration using near-infrared spectroscopic imaging. *Skin Research and Technology*, 7(4):238–245, 2001.

[22] Stephanie Baron, Marie Courbebaisse, Eve M Lepicard, and Gerard Friedlander. Assessment of hydration status in a large population. *British Journal of Nutrition*, 113(01):147–158, 2015.

[23] AN Bashkatov, EA Genina, VI Kochubey, and VV Tuchin. Optical properties of human skin, subcutaneous and mucous tissues in the wavelength range from 400 to 2000 nm. *Journal of Physics D: Applied Physics*, 38(15):2543, 2005.

[24] Akshay Bhat. Stabilize your transimpedance amplifier. 2012.

[25] LL Blaxter, DE Morris, JA Crowe, C Henry, S Hill, D Sharkey, H Vyas, and BR Hayes-Gill. An automated quasi-continuous capillary refill timing device. *Physiological measurement*, 37(1):83, 2015.

[26] Lawrence H Brown, N Heramba Prasad, and Theodore W Whitley. Adverse lighting condition effects on the assessment of capillary refill. *The American journal of emergency medicine*, 12(1):46–47, 1994.

[27] Ashley Carmichael. Initial treatment of dehydration for severe acute malnutrition. `http://www.who.int/elena/titles/bbc/dehydration_sam/en/`, April 2011. Accessed: 05/01/2016.

[28] Lei Chen, Yunie Kim, and Karen A Santucci. Use of ultrasound measurement of the inferior vena cava diameter as an objective tool in the assessment of children with clinical dehydration. *Academic Emergency Medicine*, 14(10):841–845, 2007.

[29] Lei Chen, Allen Hsiao, Melissa Langhan, Antonio Riera, and Karen A Santucci. Use of bedside ultrasound to assess degree of dehydration in children with gastroenteritis. *Academic Emergency Medicine*, 17(10): 1042–1047, 2010.

[30] Samuel N Cheuvront, Brett R Ely, Robert W Kenefick, and Michael N Sawka. Biological variation and diagnostic accuracy of dehydration assessment markers. *The American journal of clinical nutrition*, 92 (3):565–573, 2010.

[31] Samuel N Cheuvront, Robert W Kenefick, Nisha Charkoudian, and Michael N Sawka. Physiologic basis for understanding quantitative dehydration assessment. *The American journal of clinical nutrition*, 97 (3):455–462, 2013.

[32] Eric Cohen-Solal, Yan S Shi, and Balasundara I Raju. Method and apparatus for determining hydration levels from skin turgor, March 29 2007. US Patent App. 12/294,640.

[33] James E Colletti, Kathleen M Brown, Ghazala Q Sharieff, Isabel A Barata, Paul Ishimine, ACEP Pediatric Emergency Medicine Committee, et al. The management of children with gastroenteritis and dehydration in the emergency department. *The Journal of emergency medicine*, 38(5):686–698, 2010.

[34] Weijia Cui, Lee E Ostrander, and Bok Y Lee. In vivo reflectance of blood and tissue as a function of light wavelength. *IEEE Transactions on Biomedical Engineering*, 37(6):632–639, 1990.

[35] Márcia Marília Gomes Dantas, Érika Dantas Medeiros Rocha, Naira Josele Neves Brito, Camila Xavier Alves, Mardone Cavalcante França, Maria das Graças Almeida, and José Brandao-Neto. Bioelectrical impedance vector analysis for evaluating zinc supplementation in prepubertal and healthy children. *Food & nutrition research*, 59, 2015.

[36] Cornelia de Vries Feyens and Cornelis PC de Jager. Decreased skin turgor. *New England Journal of Medicine*, 364(4):e6, 2011.

[37] Helen Doolittle and Matthew Sainsbury. Expert review examination of hydration status.

[38] KeithL Dorrington. Skin turgor: do we understand the clinical sign? *The Lancet*, 317(8214):264–266, 1981.

[39] Susannah Fleming, Peter Gill, Caroline Jones, James A Taylor, Ann Van den Bruel, Carl Heneghan, Nia Roberts, and Matthew Thompson. The diagnostic value of capillary refill time for detecting serious illness in children: A systematic review and meta-analysis. *PloS one*, 10(9):e0138155, 2015.

[40] Jeremy N Friedman, Ran D Goldman, Rajendu Srivastava, and Patricia C Parkin. Development of a clinical dehydration scale for use in children between 1 and 36 months of age. *The Journal of pediatrics*, 145(2):201–207, 2004.

[41] Ran D Goldman, Jeremy N Friedman, and Patricia C Parkin. Validation of the clinical dehydration scale for children with acute gastroenteritis. *Pediatrics*, 122(3):545–549, 2008.

[42] Marc H Gorelick, Kathy N Shaw, and M Douglas Baker. Effect of ambient temperature on capillary refill in healthy children. *Pediatrics*, 92(5):699–702, 1993.

[43] Marc H Gorelick, Kathy N Shaw, and Kathleen O Murphy. Validity and reliability of clinical signs in the diagnosis of dehydration in children. *Pediatrics*, 99(5):e6–e6, 1997.

[44] MARC H GORELICK, KATHY N SHAW, KATHLEEN O MURPHY, and M DOUGLAS BAKER. Effect of fever on capillary refill time. *Pediatric emergency care*, 13(5):305–307, 1997.

[45] MR Grubb, James Carpenter, John A Crowe, Jeremy Teoh, Neil Marlow, Carole Ward, Chantelle Mann, Don Sharkey, and Barrie R Hayes-Gill. Forehead reflectance photoplethysmography to monitor heart rate: preliminary results from neonatal patients. *Physiological measurement*, 35(5):881, 2014.

[46] Elizabeth J Haines, Gerardo C Chiricolo, Kresimir Aralica, William M Briggs, Robert Van Amerongen, Andrew Laudenbach, Kevin O'Rourke, and Lawrence Melniker. Derivation of a pediatric growth curve for inferior vena caval diameter in healthy pediatric patients: brief report of initial curve development. *Critical ultrasound journal*, 4(1):1–5, 2012.

[47] Nopporn Howteerakul, Nick Higginbotham, Sonia Freeman, and Michael J Dibley. Ors is never enough: physician rationales for altering standard treatment guidelines when managing childhood diarrhoea in thailand. *Social science & medicine*, 57(6):1031–1044, 2003.

[48] European Hydration Institute. Consequenses of dehydration. `http://www.europeanhydrationinstitute.org/consequences_of_dehydration.html?gclid=CIeShf2S0LgCFUi33godb0UAtA`, 2013. accessed: 12/04/2016.

[49] Joshua Jauregui, Daniel Nelson, Esther Choo, Branden Stearns, Adam C Levine, Otto Liebmann, and Sachita P Shah. The buddy (bedside ultrasound to detect dehydration in youth) study. *Crit Ultrasound J*, 6(1):15, 2014.

[50] Joshua Jauregui, Daniel Nelson, Esther Choo, Branden Stearns, Adam C Levine, Otto Liebmann, and Sachita P Shah. External validation and comparison of three pediatric clinical dehydration scales. *PloS one*, 9(5):e95739, 2014.

[51] Walter Karlen, Amelia Pickard, Jeremy Daniels, Arthur Kwizera, Charles Ibingira, Guy Dumont, and J Mark Ansermino. Automated validation of capillary refill time measurements using photoplethysmogram from a portable device for effective triage in children. In *Global Humanitarian Technology Conference (GHTC), 2011 IEEE*, pages 66–71. IEEE, 2011.

[52] W Ullah Khan and DW Sellen. Zinc supplementation in the management of diarrhoea: biological, behavioural and contextual rationale. `http://www.who.int/elena/titles/bbc/zinc_diarrhoea/en/`, April 2011. Accessed: 07/03/2016.

[53] Eduard Kieser, Kiran Dellimore, Cornie Scheffer, Cobus Visser, and Johan Smith. Development of diagnostic sensors for infant dehydration assessment using optical methods. In *Engineering in Medicine and Biology Society (EMBC), 2015 37th Annual International Conference of the IEEE*, pages 5537–5540. IEEE, 2015.

[54] Ruben H.J. Kox. Clinical assessment of dehydration among children in low-resource settings: Diagnostic performance and suitability of diagnostic variables and technologies. Literature study report, Delft University of Technology. January, 2017.

[55] E Kviesis-Kipge, E Curkste, J Spigulis, and D Gardovska. Optical studies of the capillary refill kinetics in fingertips. In *World Congress on Medical Physics and Biomedical Engineering, September 7-12, 2009, Munich, Germany*, pages 377–379. Springer, 2009.

[56] E Kviesis-Kipge, E Curkste, J Spigulis, and L Eihvalde. Real-time analysis of skin capillary-refill processes using blue led. In *SPIE Photonics Europe*, pages 771523–771523. International Society for Optics and Photonics, 2010.

[57] Adam C Levine, Sachita P Shah, Irenee Umulisa, Mark Munyaneza, B Richard, Jean Marie Dushimiyimana, Katrina Stegmann, Juvenal Musavuli, Protogene Ngabitsinze, Sara Stulac, et al. Ultrasound assessment of severe dehydration in children with diarrhea and vomiting. *Academic Emergency Medicine*, 17(10):1035–1041, 2010.

[58] Adam C Levine, Justin Glavis-Bloom, Payal Modi, Sabiha Nasrin, Soham Rege, Chieh Chu, Christopher H Schmid, and Nur H Alam. Empirically derived dehydration scoring and decision tree models for children with diarrhea: Assessment and internal validation in a prospective cohort study in dhaka, bangladesh. *Global Health: Science and Practice*, 3(3):405–418, 2015.

[59] Elaine Nicpon Marieb and Katja Hoehn. *Human anatomy & physiology*. Pearson Education, 2007.

[60] James Wright Mcpherson, James Steven Cunningham, Timothy G Prodanovich, and Peter Donald Gadsby. Systems and methods for measuring hydration in a human subject, October 29 2015. US Patent 20,150,305,674.

[61] Joanne L Messerges and George M Hutchinson. Method and apparatus for measuring capillary refill time and carrying out pulse oximetry with a single device, December 20 2011. US Patent 8,082,017.

[62] Andreia Vieira Moço, Sander Stuijk, and Gerard de Haan. Skin inhomogeneity as a source of error in remote ppg-imaging. *Biomedical Optics Express*, 7(11):4718–4733, 2016.

[63] OSI Optoelectronics. Photodiode characteristics and applications. *Retrieved October*, 10:2013, 2007.

[64] World Health Organization et al. The treatment of diarrhoea: a manual for physicians and other senior health workers. `http://apps.who.int/iris/bitstream/10665/43209/1/9241593180.pdf`, 2005. Accessed: 29/2/2016.

[65] Amelia Pickard, Walter Karlen, and J Mark Ansermino. Capillary refill time: is it still a useful clinical sign? *Anesthesia & Analgesia*, 113(1):120–123, 2011.

[66] Kimberly Pringle, Sachita P Shah, Irenee Umulisa, Richard B Mark Munyaneza, Jean Marie Dushimiyimana, Katrina Stegmann, Juvenal Musavuli, Protegene Ngabitsinze, Sara Stulac, and Adam C Levine. Comparing the accuracy of the three popular clinical dehydration scales in children with diarrhea. *Int J Emerg Med*, 4(1):58, 2011.

[67] Jose M Saavedra, Glenn D Harris, Song Li, and Laurence Finberg. Capillary refilling (skin turgor) in the assessment of dehydration. *American journal of diseases of children*, 145(3):296–298, 1991.

[68] Mathuram Santosham, Aruna Chandran, Sean Fitzwater, Christa Fischer-Walker, Abdullah H Baqui, and Robert Black. Progress and barriers for the control of diarrhoeal disease. *The Lancet*, 376(9734):63–67, 2010.

[69] David L Schriger and Larry Baraff. Defining normal capillary refill: variation with age, sex, and temperature. *Annals of emergency medicine*, 17(9):932–935, 1988.

[70] Itai Shavit, Rollin Brant, Cheri Nijssen-Jordan, Roger Galbraith, and David W Johnson. A novel imaging technique to measure capillary-refill time: improving diagnostic accuracy for dehydration in young children with gastroenteritis. *Pediatrics*, 118(6):2402–2408, 2006.

[71] Kirk H Shelley. Photoplethysmography: beyond the calculation of arterial oxygen saturation and heart rate. *Anesthesia & Analgesia*, 105(6):S31–S36, 2007.

[72] Michael J Steiner, Darren A DeWalt, and Julie S Byerley. Is this child dehydrated? *Jama*, 291(22):2746–2754, 2004.

[73] KS Strozik, CH Pieper, and Filip Cools. Capillary refilling time in newborns–optimal pressing time, sites of testing and normal values. *Acta paediatrica*, 87(3):310–312, 1998.

[74] Toshiyo Tamura, Yuka Maeda, Masaki Sekine, and Masaki Yoshida. Wearable photoplethysmographic sensors—past and present. *Electronics*, 3(2):282–302, 2014.

[75] David R Thomas, Todd R Cote, Larry Lawhorne, Steven A Levenson, Laurence Z Rubenstein, David A Smith, Richard G Stefanacci, Eric G Tangalos, John E Morley, and Dehydration Council. Understanding clinical dehydration and its treatment. *Journal of the American Medical Directors Association*, 9(5):292–301, 2008.

[76] Unicef et al. Diarrhoea: why children are still dying and what can be done. `http://www.unicef.org/media/files/Final_Diarrhoea_Report_October_2009_final.pdf`, 2010. Accessed: 17/2/2016.

[77] Cobus Visser, Cornie Scheffer, Kiran Dellimore, Eduard Kieser, and Johan Smith. Development of a diagnostic dehydration screening sensor based on infrared spectrometry. In *Engineering in Medicine and Biology Society (EMBC), 2015 37th Annual International Conference of the IEEE*, pages 1271–1274. IEEE, 2015.

[78] Tony Wang and Barry Erhman. Compensate transimpedance amplifiers intuitively. *Texas Instrument Application Report*, 1993.

[79] WHO. Oral rehydration salts: Production of the new ors. `http://www.who.int/maternal_child_adolescent/documents/fch_cah_06_1/en/`, 2006. Accessed: 21/03/2016.

[80] Xiao-Hua Zhou, Donna K McClish, and Nancy A Obuchowski. *Statistical methods in diagnostic medicine*, volume 569. John Wiley & Sons, 2009.